Translational examination of the orbitofrontal cortex and striatum in obsessive compulsive disorder

by

Sean Christopher Piantadosi

B.A., St. Mary's College of Maryland, 2010

Submitted to the Graduate Faculty of

the School of Medicine in partial fulfillment

of the requirements for the degree of

Doctor of Philosophy

University of Pittsburgh

2019

UNIVERSITY OF PITTSBURGH

SCHOOL OF MEDICINE

This dissertation was presented

by

Sean Christopher Piantadosi

It was defended on

April 17, 2019

and approved by

Anthony Grace, Professor, Department of Neuroscience, University of Pittsburgh

Sandra Kuhlman, Associate Professor, Department of Biological Sciences, Carnegie Mellon University

Byron Yu, Associate Professor, Departments of Electrical & Computer Engineering and Biomedical Engineering, Carnegie Mellon University

Yanhua Huang, Associate Professor, Department of Psychiatry, University of Pittsburgh

Bernardo Sabatini, Professor, Department of Neurobiology, Harvard Medical School

Dissertation Director: Susanne Ahmari, Assistant Professor, Department of Psychiatry, University of Pittsburgh

Translational examination of the orbitofrontal cortex and striatum in obsessive compulsive disorder

Sean Christopher Piantadosi, PhD

University of Pittsburgh, 2019

For decades a causal role for orbitofrontal cortex (OFC) and striatal dysfunction in obsessive compulsive disorder (OCD) has been hypothesized. Structural as well as functional MRI studies have implicated these regions and their interconnections in OCD pathogenesis, though their precise roles in encoding obsessive or compulsive symptoms are still an area of active investigation. Several lingering questions therefore remain. First, what are the molecular adaptations in the OFC and striatum that give rise to these structural and functional deficits in OCD? Second, how do activity patterns in these regions give rise to compulsive behavior, and how do treatments that reduce compulsive behavior affect these activity patterns? Using a translational approach, we have investigated each of these questions for the first time.

In Chapter 1, we have performed the first post-mortem analysis of OCD tissue looking at gene expression in the OFC and striatum. Targeting our analysis only to genes implicated in previous clinical and preclinical studies, we found that many genes critical for excitatory synapse function were reduced in the OFC of individuals with OCD. Several transcripts were also reduced across OFC and striatal brain regions, including *DLGAP3* (also known as *SAPAP3*), which has been previously linked to OCD via preclinical studies showing that *Sapap3*-knockout mice display a compulsive behavioral phenotype and cortico-striatal alterations. In Chapter 2, we examine the functional consequences of reduced cortico-striatal *Sapap3* expression on activity patterns of large groups of neurons in the OFC and central striatum using *Sapap3*-knockout (KO) mice and *in vivo*

calcium imaging. Finally, in Chapter 3 we examine the role of genetically distinct striatal cell types in producing compulsive behavior. These data directly test several long-standing hypotheses regarding OCD pathogenesis and shed new light on how compulsive behavior may be generated in the brain.

Table of Contents

List of Tables

List of Figures

Preface

Graduate school has simultaneously been one of the most challenging and most rewarding experiences of my life. I would like to take this opportunity to express my sincerest gratitude to the many individuals who helped me along the way. First and foremost, I would like to thank my mentor and dissertation advisor, Dr. Susanne Ahmari. I will be forever grateful that Susanne agreed to take me into her lab at the beginning of my third year of graduate school. Not only did she accept me into her growing research group with open arms, she also presented me the opportunity to add new techniques and skills to my repertoire that have significantly expanded my toolbox as a translational researcher. Throughout our years together Susanne demonstrated first-hand what it means to be a researcher of integrity and showed me how to be a mentor and to lead by example. I would also like to thank my thesis committee, Dr. Anthony Grace, Dr. Yanhua Huang, Dr. Sandra Kulhman, and Dr. Byron Yu, for their expertise, support, and guidance. Together they have helped mold me into the scientist I am today. I would also like to express my gratitude to Dr. Bernardo Sabatini for taking time out of his incredibly busy schedule to serve as my outside examiner. Your feedback and unique perspective has affected how I think about this work.

In addition to my committee, many other faculty members across the neuroscience community have been integral to my development. Within the Translational Neuroscience Program, Dr. David Lewis and Dr. Jill Glausier have been patient with me as I learned how to conduct post-mortem experiments and their rigor has been a huge influence on how I think about science. Drs. Matt MacDonald, John Enwright, and Dominique Arion have all been excellent teachers and collaborators. Dr. Marianne Seney and Dr. Ryan Logan, two amazing scientists who I have watched blossom into fantastic independent investigators, have always had their doors open

and been willing to provide feedback on both data and career related topics. I'd also like to thank my previous graduate mentor, Dr. Etienne Sibille, for helping facilitate my transition into Susanne's lab and for continuing to support my progress.

I'd like to express my appreciation for the transparency and honesty of the directors of the CNUP and the CNUP graduate program, Drs. Alan Sved, Peter Strick, Steve Meriney, and Brian Davis. We have had some extremely frank and honest discussions during which my concerns were heard and I was always treated as a peer. I would specifically like to thank Dr. Brian Davis for all his advice and guidance throughout my time in the CNUP.

The Ahmari lab has become my second family in Pittsburgh over the past few years. Without Dr. James Hyde's expertise in microscopy and handiness the calcium imaging work presented in this thesis would not have been possible. Further, James is one of the most patient and kind individuals I have ever met, and I am honored to consider him a friend. Dr. Elizabeth Manning's scientific rigor, attention to detail, and unbelievable work ethic have pushed me to work better and harder and serve as a model for how I will attempt to handle myself as a post-doc. Dr. Jesse Wood has been integral in implementing many of the analytic methods used in this thesis. Jesse has an unparalleled ability to explain (both visually and verbally) complicated topics and has always taken time out of his day to answer my extremely basic coding questions. His explanations and hands-on help have greatly improved my ability to work with and analyze my calcium imaging data. Fellow graduate students Jared Kopelman and Zoe LaPalombara are both brilliant, funny, kind, and extremely hard working. They have greatly contributed to a fun, collaborative, and productive lab environment. Many thanks to all the undergraduate students that have assisted me along the way and been patient with me as I learned how to be a mentor myself. Specifically, I would like to thank Brittany Chamberlain for her hard work and for pushing me as much as I

pushed her. It has been an honor to work with you and I am incredibly excited to see what your future holds.

I would never have made it this far if it wasn't for my amazing friends who have helped keep me sane and grounded throughout this entire process. Most notably, Matt Rich, Meredyth Wegener, Laura Rupprecht, Kevin Mastro, and Victoria Corbit have all been there for me when I needed, and I will cherish your friendships forever. Finally, thanks to my family, my Mom Mary Kane, my brother Patrick Piantadosi, my Dad Christopher Piantadosi, and my girlfriend Jordana Yahr. Your constant support has been integral in my ability to achieve this milestone. Thank you all.

1.0 Introduction

"An exciting challenge for neuroscience is to convert this emerging genetic information into useful biology: information about molecular pathways, identification of relevant cell types and circuits (which can be investigated with new technologies such as optogenetics) and an understanding of pathogenesis that can be exploited to develop treatments."

I distinctly remember reading the above quote by Dr. Steven E. Hyman (2013) as I was beginning graduate school and was motivated by the idea that we are at a critical juncture between the psychiatric clinic and the laboratory. Technological advances, both in terms of our ability to clinically recognize features of disease, and newfound genetic and optical tools for precise control of specific cells and circuits in model systems, have gotten us closer to realizing the dream of translational psychiatry (Licinio 2011). In this thesis, I will test whether there are changes in expression of glutamatergic genes in post-mortem brain tissue of patients who suffered from the devastating psychiatric illness, obsessive compulsive disorder. Taking a translational approach, I will then utilize a mouse lacking a gene critical for normal glutamatergic neurotransmission and investigate how this affects neural activity associated with compulsive behavior.

1.1 Obsessive Compulsive Disorder

1.1.1 Burden of OCD

Obsessive compulsive disorder (OCD) is a devastating, chronic psychiatric illness that has a lifetime prevalence of between 1-3% and affects an estimated 50 million people worldwide (Koran 2000). OCD is characterized by intrusive, recurrent thoughts (obsessions), and repetitive behaviors or repetitive mental acts (compulsions) that are often performed to reduce the anxiety associated with the obsessions (Pauls et al. 2014). An OCD patient's urge to engage in these persistent behavioral patterns results in a poorer overall quality of life, an impairment in academic and work functioning, and a decrement in interpersonal relationships relative to healthy individuals (Koran et al. 2007; Koran, Thienemann, and Davenport 1996). OCD often presents in childhood, with a peak of approximately 10 years of age. 40% of childhood onset OCD cases continue into adulthood (Stewart et al. 2004). Valid first-line treatment strategies for OCD include cognitive behavioral therapy (CBT) as well as treatment with selective serotonin reuptake inhibitors (SSRIs). Relative to treatment strategies used for other anxiety disorders and depression, SSRI administration for OCD is most efficacious at higher doses and a prolonged treatment course of between 8-12 weeks (Bloch et al. 2008; Koran et al. 2007; Pittenger and Bloch 2014). However, even with optimal treatment (often involving combined CBT and pharmacotherapy), many patients continue to experience substantial symptoms and remission is rare (Pittenger et al. 2005). Given its chronic nature and treatment refractory nature, it is no surprise that individuals with OCD are 10 times more likely to die by suicide than the general population (Fernández de la Cruz et al. 2017). Together, these data highlight the overwhelming burden individuals with OCD suffer

through on a daily basis, and the need to further investigate the mechanisms underlying OCD and its treatments.

1.1.2 Heritability of OCD

Family studies of OCD have consistently suggested that OCD is familial (Geller 2006; Pauls 2010). Further, there is an increased rate of childhood-onset OCD if a first-degree relative has been diagnosed with the disorder compared to healthy individuals (Nestadt et al. 2001; Hanna et al. 2005). While this evidence strongly suggests that OCD travels in families, it cannot provide information about whether the root cause is genetic or environmental. Twin studies, by contrast, are more useful in determining whether genetic factors are involved in OCD. Twin studies have consistently suggested a genetic component to OCD (Pauls 2010). Heritability estimates of OCD as well as obsessive-compulsive characteristics demonstrate that genetic factors explain between 27% to 47% of the phenotypic variance (Bolton et al. 2007; Pauls 2010; Tambs et al. 2009; van Grootheest et al. 2005). A recent meta-analysis of 14 published twin studies indicates that genetic variance, irrespective of symptom severity or sex, accounts for approximately 40% of the phenotypic variance of obsessive-compulsive behaviors, while shared environmental factors did not contribute to the variance significantly (Taylor 2011). Importantly, this study identified that non-shared environmental factors, potentially epigenetic or post-translational modifications, accounted for 51% of the phenotypic variance (higher than the estimate of genetic factors). In summary, ample data support the hypothesis that there is a genetic component to OCD, though they are likely not the sole trigger for the disorder.

1.1.3 Genetics of OCD: Developing role for the glutamatergic system

1.1.3.1 Candidate gene studies

Given that evidence suggests OCD is at least in part a genetic disorder, an active area of research over the past 30 years has been to uncover genes or genetic loci that are associated with OCD. Based on the involvement of monoaminergic signaling and serotonin in the treatment of OCD, with SSRIs continuing to be the most effective pharmacological treatment for OCD (Barr, Goodman, and Price 1993), as well as data suggesting that agonists of specific serotonin receptor subtypes can exacerbate OCD symptoms (Koran, Pallanti, and Quercioli 2001; Stern et al. 1998; Zohar et al. 1987), early candidate gene studies focused on monoaminergic genes. Interestingly, associations between the majority of these genes and OCD have been either weak or nonsignificant (see (Pauls 2010) for a detailed review), and none have been consistently replicated. Thus, researchers have turned to other potential pathways that may be playing a role in the development of OCD.

Recently, several promising findings have been made linking dysregulation of the excitatory neurotransmitter glutamate may be playing a role in OCD (Pittenger, Bloch, and Williams 2011). In 2006, two independent candidate gene studies identified associations between OCD and the glutamate transporter gene *SLC1A1* (Arnold et al. 2006; Dickel et al. 2006). Additional studies have replicated and elaborated on this finding in a number of independent cohorts (Samuels et al. 2011; Shugart et al. 2009; Stewart et al. 2007), and genetic linkage studies have further implicated the genomic region (chromosome 9p) containing the *SLC1A1* gene (Hanna et al. 2002). Expanding on this finding, Wendland and colleagues (2009) identified a haplotype of three linked single nucleotide polymorphisms (SNP) that were twice as prevalent in OCD patients as in controls. They then demonstrated that one specific SNP resulted in a 50% decrease in *SLC1A1*

mRNA expression in cell culture, suggesting that *SLC1A1* expression in OCD patients may be reduced, though this has not yet directly been tested. Together, these data point to a functional role of *SLC1A1* in OCD pathogenesis.

Other candidate gene studies have implicated several glutamate receptors. Several studies have examined the relationship of *GRIN2B*, which encodes the glutamate ionotropic NMDA receptor 2B. NMDA receptors, and GRIN2B in particular, are critical for normal glutamatergic transmission and NMDA-mediated plasticity (Cho et al. 2009). An early study identified a significant association with OCD and variants within the 3'UTR of *GRIN2B* (Arnold et al. 2004), although several studies looking at this same locus in other populations did not find the same association (Alonso et al. 2012; Liu et al. 2012). An additional study looking at a different SNP found that the T-allele of SNP rs1019385 was significantly associated with ordering and checking OCD subtypes (Kohlrausch et al. 2016), raising the possibility that individual OC phenotypes may have different genetic underpinnings (Pauls et al. 2014). Genes encoding another group of ionotropic glutamate receptors, kainate receptors (*GRIK*), have also been associated with OCD. Several markers in the *GRIK2* gene have been shown to be significantly associated with OCD, though the sample size of these studies is small (Delorme et al. 2004; Rajendram et al. 2017; Sampaio et al. 2011).

1.1.3.2 Genome-wide association studies

In addition to hypothesis driven candidate gene studies assessing the association of a select gene and OCD, unbiased genome analysis has been conducted in OCD through genome-wide association studies (GWASs). Although no single genetic locus has reached genome-wide significance in OCD GWAS as of yet (a fact generally believed to be due a lack of samples and insufficient power (Mattheisen et al. 2015)), the results of these experiments thus far have also

converged on glutamatergic signaling as a potential source of dysfunction in OCD. The first OCD GWAS, conducted by the International Obsessive-Compulsive Disorder Foundation Genetics Collaborative (IOCDF-GC), involved 1,465 cases, 5,557 ancestry matched controls, and 400 trios, and analyzed 469,410 autosomal SNPs. In this analysis two SNPs located in the *DLGAP1* (discs large-associated protein 1) gene showed the strongest association with OCD (Stewart et al. 2013). *DLGAP1* is a member of a family of post-synaptic density scaffolding proteins responsible for maintaining receptors at glutamatergic synapses (Rasmussen, Rasmussen, and Silahtaroglu 2017). A meta-analysis of all data from both case-control samples and trios identified a SNP near *FAIM2* (FAS apoptotic inhibitory molecule 2) as having the strongest association with OCD. Similar to *DLGAP1*, *Faim2* in rats is known to be expressed in the post-synaptic density and colocalizes with the glutamate receptor GluR2 (Schweitzer, Suter, and Taylor 2002).

In the second OCD GWAS, conducted by the OCD Collaborative Genetics Association Study (OCGAS), a new marker was identified on chromosome 9 near the *PTPRD* gene which was the most strongly associated with OCD (Mattheisen et al. 2015). PTPRD protein is a tyrosine phosphatase that is involved in the differentiation of glutamatergic synapses (Dunah et al. 2005; Woo et al. 2009; Takahashi and Craig 2013). It also interacts with SLITRK3, a post-synaptic adhesion molecule thought to regulate GABAergic synapse development (Takahashi et al. 2012), as well as SLITRK5 to regulate TrkB receptor trafficking (Song et al. 2015). Critically, despite examining entirely distinct populations, analysis of previously identified hit regions in the IOCDF-GC study found that 12 of the 15 strongest signals showed associations in the same direction in the OCGAS GWAS. Additionally, while the exact genomic regions of both *DLGAP1* and *GRIK2* identified in the IOCDF-GC were not identified in the OCGAS, two independent markers in each of these two genes were identified and were significantly associated with OCD, providing more

confidence that these genes may be relevant candidate genes for OCD (Mattheisen et al. 2015). Finally, a meta-analysis of the two studies has recently been completed and demonstrated that previously identified SNPs near *DLGAP1, PTPRD, GRIK2, and FAIM2* were all strongly associated with OCD, albeit not significantly (*p*-values between 4.2×10^{-6} to 7.2×10^{-3}). Further, meta-analysis revealed multiple SNPs in another ionotropic glutamate receptor gene *GRID2*, though future work must replicate this finding ((OCGAS) 2018). While in its early days, genome wide studies of OCD have repeatedly implicated glutamatergic genes in OCD. Additional increases in sample size will likely push these highly-implicated genes toward genome-wide significance, as well as reveal new genes that can be functionally evaluated.

1.1.3.3 Post-mortem analysis of OCD associated genes

Given the heritability of OCD (Pauls 2010), the reported substantial environmental influences that may result in epigenetic changes (Taylor 2011), and the strong evidence implicating dysfunctional glutamatergic neurotransmission in OCD (Fig.1-1) ((OCGAS) 2018), a logical question to ask is, are expression levels of these genes altered in OCD tissue?

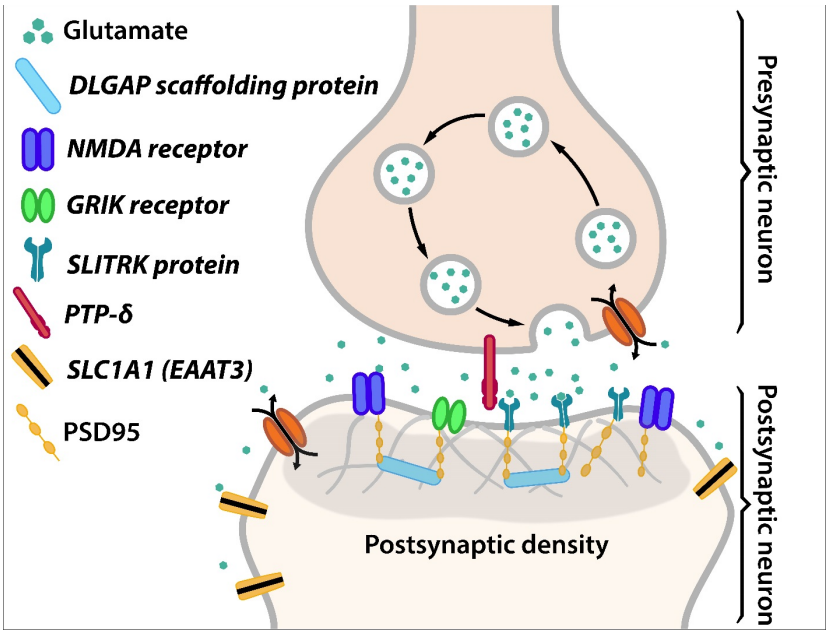

Figure 1-1. Schematic of glutamatergic synapse and OCD-linked proteins

Prototypical glutamatergic synapse, with a presynaptic axon terminal (top) releasing glutamate into the synaptic cleft. A dendritic spine on the post-synaptic neuron contains the postsynaptic density, which is enriched in synaptic proteins that regulate the excitatory postsynaptic response. Proteins in bold-italics have been genetically linked to OCD.

Surprisingly, only a single study to date has attempted to answer this question. Jaffe and colleagues (2014) investigated the genetic neuropathology of obsessive-compulsive symptoms across a range of disorders typified by compulsive behaviors. Using microarray analysis on tissue obtained from the dorsolateral prefrontal cortex (DLPFC), the authors identified dozens of genes that were differentially expressed between OCD/Obsessive compulsive personality disorder (OCPD)/Tic cases and controls. Gene set enrichment tests implicated several distinct biological pathways, though the glutamate system did not appear significantly affected. This could have been due to several factors, including the combining of several diagnoses together, the selection of the DLPFC, which has canonically not been considered a region involved in OCD pathogenesis (Menzies et al. 2008b; Pauls et al. 2014), as well as the difficulty in identifying significant

differential transcript expression with a small number of subjects when using a transcriptomic approach such as microarray. These data, while interesting, beg several questions. First, what are the regions most commonly linked to OCD pathogenesis? Second, is expression of glutamatergic genes relevant for signaling in these brain regions? And third, how does disruption of one or more of these associated genes alter activity levels in these regions?

1.1.4 Neural basis of OCD

Over the past 30 years, numerous improvements have been made in our ability to image the human brain, which has led to significant advances in our understanding of many major neurological and psychiatric disorders (Silbersweig and Rauch 2017). Relative to other psychiatric illnesses and across a variety of different task conditions OCD has demonstrated a high degree of concordance across imaging studies in the regions that are associated with the disorder (Chamberlain et al. 2005). Both anatomical as well as functional studies strongly implicate dysfunction in cortico-striatal circuitry, specifically within the affective cortico-basal ganglia loop (Menzies et al. 2008b; Graybiel and Rauch 2000) that consists of the orbitofrontal cortex (OFC) and direct glutamatergic projection to the caudate nucleus/dorsal striatum. These segregated cortico-striatal loops, which run in parallel and connect cortical regions basal ganglia outputs via the striatum (Alexander, DeLong, and Strick 1986), have been identified in primates and are each thought to subserve relatively independent functions that together help to coordinate the execution of a motor plan (Haber 2003, 2016; Haber et al. 1995). The “affective-loop”, so called because of the known function of the OFC in the flexible control of emotional and motivational aspects of behavior (Balleine, Leung, and Ostlund 2011; Chamberlain et al. 2005; Chamberlain et al. 2008; Gallagher, McMahan, and Schoenbaum 1999; Milad and Rauch 2007; Saxena et al. 1999), has

been hypothesized to lead to the development of more cognitively based habits that may form the basis for obsessions (Graybiel and Rauch 2000).

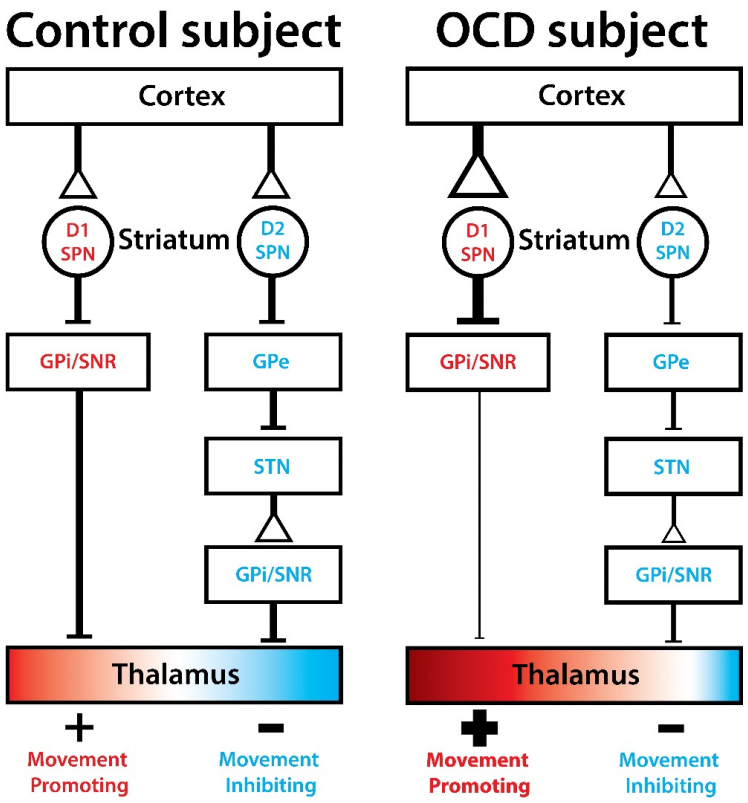

Figure 1-2. Frontocortico-striato-thalamo-cortical circuit dysfunction in OCD

Proposed dysfunction in frontocortico-striato-thalamo-cortical circuits in OCD. Control subjects (left) have balanced output from frontocortical regions (e.g. lOFC, ACC) through the basal ganglia, leading to appropriate behavioral selection. An OCD subject (right) has a bias toward activation of the direct pathway, mediated by dopamine D1-expressing (D1-) spiny projection neurons (SPNs) in the striatum. This activation is perpetuated in a feedback loop that results in overall thalamic disinhibition and possibly the engagement in compulsive behavior.

A typical conceptualization of frontostriatal circuitry entails a direct and indirect pathway that are comprised of dopamine D1-receptor expressing spiny projection neurons (D1-SPNs) and dopamine D2-receptor expressing spiny projection neurons (D2-SPNs) (Fig.1-2). In healthy control individuals (Fig.1-2 left), it is thought that the excitatory direct pathway is modulated by the indirect pathway's inhibitory function, allowing for appropriate behavioral selection. It has

been suggested that in OCD subjects an imbalance in direct and indirect pathway signaling leads to a bias toward the direct pathway (Fig.1-2 right), resulting in hyperactivity in the fronto-striatal loops (Pauls et al. 2014; Maia, Cooney, and Peterson 2008). This hyperactivity and direct pathway bias might drive obsessive and compulsive symptoms in multiple, non-mutually exclusive, ways. For example, disinhibition of the thalamus may decrease filtering of unwanted thoughts to emotion processing regions such as the OFC, leading to obsessive thoughts. At the same time, it is possible that hyperactivity in more motor fronto-striatal circuits may lead to the production of repetitive, compulsive behaviors. It is important to note, however, that these simplistic models are likely oversimplified, and cannot fully explain the heterogeneous nature of OCD. Further, key aspects of this model, chiefly the role of direct- and indirect-pathway projecting neurons in the striatum, cannot currently be directly tested in OCD patients.

Although many regions that are not part of cortico-striatal circuits have been implicated in OCD (see (Menzies et al. 2008b) for a full review), and recent studies have pushed to expand these canonical circuits to include additional limbic regions (Milad and Rauch 2012a; Wood and Ahmari 2015), the focus of this dissertation will be on the most well-replicated regions and circuit: the fronto-striatal circuit connecting the OFC and striatum.

1.1.5 Functional CSTC disruption in OFC and striatum of OCD subjects

Early studies used positron emission tomography (PET) to measure brain function via cerebral glucose metabolism demonstrated hypermetabolism (inferred as increased activity) in OCD subjects relative to controls within the OFC, both at rest and following provocation of OCD symptoms (Baxter et al. 1987; Baxter et al. 1988; Swedo et al. 1989; Rauch et al. 1994a). While not every study has found hypermetabolism in the OFC in OCD subjects (see (Saxena et al. 2001)),

a meta-analysis of PET studies found consistent evidence throughout the literature of hypermetabolism in both the OFC as well as the head of the caudate nucleus in OCD (Whiteside, Port, and Abramowitz 2004). Further support for the involvement of OFC and caudate hypermetabolism in OCD are data suggesting that successful pharmacological treatment normalizes hypermetabolism (Perani et al. 1995; Baxter et al. 1992; Saxena et al. 2003; Saxena et al. 1999; Rauch et al. 2002), though it is important to note that many OCD patients continue to experience significant symptoms even following optimal treatment (Pittenger and Bloch 2014).

In addition to PET scan studies, many functional magnetic resonance imaging (fMRI) studies of OCD have also implicated cortico-striatal circuits and the regions that comprise them. In symptom provocation tasks, several studies have found increased blood oxygen-level dependent (BOLD) signal in both the OFC and caudate, suggestive of increased levels of activity within these regions in OCD (Breiter et al. 1996; Adler et al. 2000a). A meta-analysis of case-control fMRI studies conducted by Menzies and colleagues (2008b) demonstrated consistent activation of orbitofronto-striatal regions in OCD, though consistent patterns of activation were also identified in other brain regions. It is important to note that while many studies suggest that the OFC is hyperactive in OCD across a variety of conditions, other studies indicate that it may be hypoactive (perhaps depending on the medial/lateral extent being imaged), with symptom severity scores inversely correlated with the function of the more medial OFC (Rauch et al. 2007a). These data highlight that more formal studies are necessary to fully tease apart consistent differences in activity in OFC subregions in OCD. Finally, resting state analysis of the connectivity between the OFC and the dorsal striatum has found evidence for increased connectivity that is positively correlated with overall symptom severity (Beucke et al. 2013; Harrison, Soriano-Mas, Pujol, Ortiz, Lopez-Sola, et al. 2009). Together, these data support the contention that fronto-striatal circuits

are involved in OCD, and specifically suggest that hyperactivity in OFC and the dorsal striatum (caudate) may be involved.

1.1.6 Neurochemical findings in cortico-striatal circuits in OCD

The main neurotransmitters in cortico-striatal circuits are glutamate and GABA, as well as neuromodulatory input via serotonin and dopamine (Haber 2016). Given the correlational evidence implicating changes in activity in these regions in OCD (Pauls et al. 2014; Menzies et al. 2008b), researchers have examined whether there are alterations specifically in glutamatergic or GABAergic signaling. Early studies examined levels of glutamate in the cerebrospinal fluid (CSF) of OCD patients and control subjects, demonstrating that CSF glutamate levels were elevated in OCD patients (Chakrabarty et al. 2005). A follow-up study replicated and expanded on this finding, demonstrating that in a larger group of subjects, glutamate and glycine (a co-agonist of glutamate receptors) levels were elevated in the CSF of OCD subjects (Bhattacharyya et al. 2009). While these data are suggestive of a general glutamate imbalance in the CNS of OCD subjects, CSF findings cannot be generalized to specific regions and circuits.

In order to make up for this deficiency and evaluate neurotransmitter concentrations in specific brains regions (though with significantly lower sensitivity and specificity) magnetic resonance spectroscopy (MRS) has been conducted in OCD subjects. MRS estimates the concentration of various small molecules in defined brain regions by detecting their distinct resonances within a magnetic field (Soares and Law 2009). While the technique isn't able to easily disambiguate glutamate from another amino acid, glutamine, a composite measure *Glx* can be compared between OCD and control subjects. Early MRS studies were indicative of glutamate dysregulation in OCD, finding that there were elevations in *Glx* in the caudate in pediatric patients

with OCD, and that this elevation was normalized after SSRI treatment (Moore et al. 1998; Rosenberg et al. 2000). Similarly, in unmedicated adult OCD patients, *Glx* levels were elevated in the OFC and levels correlated with OCD symptom severity (Whiteside et al. 2006). However, more recent studies have not replicated these findings (see (Pittenger, Bloch, and Williams 2011) for thorough review). Together, these data are suggestive of glutamatergic dysfunction, possibly in cortico-striatal brain regions, in OCD. However, how these abnormalities directly relate to the devastating symptoms of OCD (obsessions and compulsions) remains unknown.

1.2 Cortico-striatal dysfunction in OCD mouse models

As outlined in Chapter 1.1, there is ample evidence for cortico-striatal and possibly glutamatergic dysfunction in OCD. However, it is difficult if not impossible to test how this dysfunction causally contributes to compulsive behavior in humans. Using rodent models, researchers are able to directly evaluate the role of and interplay between 1) specific genes and their contribution to compulsive behavior, 2) particular circuits and how they mediate OCD-like symptoms, and 3) compounds that improve or exacerbate OCD symptoms and the regions and cell types on which they act. Despite these promising benefits, it is important to note that it is not possible to fully model a complex, heterogeneous disorder such as OCD in animals. Indeed, one of the eponymous symptoms of the disorder, obsessions, cannot be assessed in a rodent. Therefore, it is critical to thoroughly evaluate how findings from a model map back onto the disorder itself.

1.2.1 Transgenic mouse models of OCD-like behavior

Owing to the similarities in genetics and physiology between mice and humans, as well as the development of powerful tools to make genome editing easier with fewer off-target effects (Doyle et al. 2012), there has been a recent push to translate candidate genes identified in genetic studies of neuropsychiatric illnesses into mice (Donaldson et al. 2013). Indeed, several groups have recently independently generated mice that either underexpress (Zike et al. 2017; Gonzalez et al. 2017) or overexpress (Delgado-Acevedo et al. 2018) the most well-replicated OCD candidate gene, *SLC1A1* (Arnold et al. 2006; Porton et al. 2013; Samuels et al. 2011; Shugart et al. 2009; Stewart et al. 2007). These studies demonstrate that *SLC1A1* plays an important role in repetitive behavior (Zike et al. 2017), including grooming behavior, and that cortico-striatal circuits may be directly affected (Delgado-Acevedo et al. 2018). As additional genetic loci begin to consistently emerge from well-powered genetic studies of OCD, associated genes should be translated into rodent models for thorough mechanistic investigation.

While these hypothesis driven studies are critical to our growing understanding of the pathophysiology of OCD, we are still limited in well-replicated candidate genes or significant GWAS hits to test using this back-translational approach. Instead, serendipitous discovery of transgenic mice that model OCD-like behavior and exhibit cortico-striatal deficits have been used to understand the basic mechanisms underlying compulsive behavior (Burguiere et al. 2015; Nagarajan et al. 2018; Welch et al. 2007a; Shmelkov et al. 2010). These mice have varying levels of validity as OCD models, as defined by Chadman and colleagues (2009) (Table 1-1).

Table 1-1. Transgenic mouse models of OCD

Gene	Compulsive phenotype	Other behavioral phenotypes	Structural cortico-striatal alterations	Functional cortico-striatal alterations	*In vivo* cortico-striatal alterations	Predictive validity
Hoxb8	Compulsive grooming (Leads to skin lesions on body)	Anxiety-like behavior Social interaction deficits	Altered cortico-striatal synapse size	Cortico-striatal LTP alterations	N/A	Fluoxetine reverses behavioral deficits
Slitrk5	Compulsive grooming (Leads to facial lesions)	Anxiety-like behavior	Reduced expression of glutamate receptors in striatum	Impaired cortico-striatal neurotransmission in dorsal striatum	Increased OFC activity (FosB)	Fluoxetine reduces compulsive grooming behavior
Sapap3	Compulsive grooming (Leads to facial lesions)	Anxiety-like behavior	Change in expression of NMDA receptors in striatum Reduced cortico-striatal PSD thickness	Increased NMDA-mediated and reduced AMPA-mediated cortico-striatal neurotransmission in dorsal striatum	Baseline hyperactivity of central striatum Altered lOFC to central striatum signaling	Fluoxetine reduces compulsive grooming and anxiety-like behavior

1.2.1.1 *Hoxb8* mutant mice

One such mouse is the *Hoxb8* knockout (KO) mouse. These mice were generated in an attempt to understand the role of homeobox (Hox) genes on neurodevelopment, and surprisingly demonstrated a 100% penetrant compulsive grooming phenotype that led to the development of skin lesions (Greer and Capecchi 2002). Interestingly, expression of *Hoxb8* in wildtype mice was observed across a number of different brain regions, including the OFC and dorsal striatum (caudate/putamen). Intriguingly, a follow-up experiment characterized the origin of these *Hoxb8*-positive cells, finding that they give rise to brain microglia and that a bone marrow transplant from irradiated *Hoxb8* KOs was capable of reversing the compulsive grooming phenotype (Chen et al. 2010). More recently, dysfunction in cortical and striatal regions was directly assessed in *Hoxb8* KO mice, with alterations in post-synaptic density length and thickness of both symmetric

(inhibitory) and asymmetric (excitatory) synapses in both the OFC and striatum. Functionally, impaired striatal synaptic LTP was detected at cortico-striatal synapses (Nagarajan et al. 2018). Further, they demonstrated a slight anxiety-like phenotype in KOs and that the anxiety phenotype and the compulsive grooming phenotype could be reversed with chronic administration of the SSRI fluoxetine.

These data implicate both microglial dysfunction and an interaction with synaptic deficits in cortico-striatal signaling, which is especially interesting given that recent evidence suggests that Pediatric Autoimmune Neuropsychiatric Disorders Associated with Streptococcal Infection (PANDAS), which often presents with sudden onset obsessive and compulsive symptoms, has been associated with differential antibody binding in the striatum (Frick et al. 2018; Bernstein et al. 2010). Future research should further explore the potential link between immune function, cortico-striatal circuitry, and obsessive-compulsive symptoms.

1.2.1.2 *Slitrk5* mutant mice

Another serendipitous discovery involved the *Slitrk5* knockout mouse. Slitrk proteins are transmembrane proteins that serve as axon guidance proteins and are involved in both the development of excitatory and inhibitory synapses (Takahashi and Craig 2013; Takahashi et al. 2012). When *Slitrk5* is globally knocked out from a mouse, mice develop both an anxiety-like and a compulsive grooming phenotype that results in the development of facial lesions (Shmelkov et al. 2010). Much like *Hoxb8* mutants, the compulsive grooming phenotype was also reversed following treatment with the SSRI fluoxetine. Cortico-striatal alterations have also been observed in *Slitrk5* KOs, with an increase in baseline activation of the OFC as measured by expression of the immediate early gene FosB. Additionally, a reduction in the expression of several critical glutamate receptors (GluR1, GluR2, GluN2A, GluN2B) was also reduced in the striatum of KO

mice, which may represent a compensatory change in response to the OFC hyperactivity (Shmelkov et al. 2010).

Although direct links from *Slitrk5* to OCD have not yet been made, it is of note that the protein encoded by the most strongly associated GWAS hit for OCD, *PTPRD*, interacts directly with several different *Slitrk* family members, including *Slitrk5* to regulate TrkB receptors (Song et al. 2015). Further, *Slitrk1* has been linked to Tourette's syndrome, another disorder characterized by repetitive behaviors (Abelson, Kwan, et al. 2005; Proenca et al. 2011). Additional work is necessary to link Slitrks specifically to OCD, though preliminary unpublished evidence suggests the presence of rare non-synonymous mutations in *Slitrk5* in OCD subjects (Song et al. 2017).

1.2.1.3 *Sapap3/Dlgap3* mutant mice

Much like *Slitrk5*, another gene encoding a post-synaptic density protein that is enriched at cortico-striatal synapses, *Sapap3* (synonymous with *Dlgap3*) was also unexpectedly found to have a potential role in compulsive behavior. Welch (2007a) and colleagues noted that when *Sapap3* was globally knocked out, mice displayed anxiety-like behavior as well as a compulsive grooming phenotype that, similar to the *Hoxb8* and *Slitrk5* KOs, resulted in skin lesions. Again, both the anxiety-like phenotype as well as the compulsive grooming phenotype were reversed following fluoxetine administration. The phenotype was also localized to the medial striatum, with lentiviral rescue of wild-type *Sapap3* through the dorsal/ventral extent of the medial striatum normalizing both the compulsive grooming and anxiety-like phenotype. Further, functional characterization of cortico-striatal synapses demonstrated reduced fEPSP amplitudes in KO mice compared to controls, and a shift in the subunit composition of NMDA receptors to a more immature subtype (increased NR2B subunit expression). Critically, follow-up work demonstrated that this synaptic dysfunction is specific to cortico-striatal and not thalamo-striatal (Wan et al.

2014). Elegant work by Corbit and colleagues (Corbit et al. 2019) recently evaluated the main cortical inputs to the striatum that might be leading to these synaptic changes, finding that compared to inputs from lateral OFC (lOFC), inputs from secondary motor cortex (M2) were strengthened in KO mice.

Given these findings, there is substantial interest in whether *Sapap3* (more commonly referred to as *DLGAP3* in human literature) is associated with OCD. In a subset of OCD subjects, *DLGAP3* was associated with pathological grooming (pathological skin picking, trichotillomania, nail-biting) (Bienvenu et al. 2009a). Similarly, in OCD subjects with comorbid trichotillomania, multiple rare missense mutations were identified in *DLGAP3* (Zuchner et al. 2009), further cementing its association with pathological grooming and OCD. Additionally, SNPs in the gene encoding another DLGAP family member, *DLGAP1*, have been identified in two independent GWAS studies of OCD, though the associations have not reached genome-wide significance ((OCGAS) 2018; Stewart et al. 2013). Together, these data suggest an involvement of DLGAP proteins in compulsive grooming both in humans and in mice, though additional molecular studies are needed to demonstrate a clear link to OCD.

1.2.2 Optogenetic manipulation of cortico-striatal circuits

With correlational evidence of alterations in the activity of and connectivity between fronto-cortical and striatal regions in OCD (Pauls et al. 2014; Menzies et al. 2008b), and evidence of functional changes in cortico-striatal circuits in transgenic models that display a compulsive grooming phenotypes (Nagarajan et al. 2018; Shmelkov et al. 2010; Welch et al. 2007a), a logical question is how do these circuit specific alterations causally contribute to compulsive behavior. Over the past 5 years, due primarily in part to the advent and optimization of optogenetics for

controlling activity in defined circuits and cell types (Boyden et al. 2005; Deisseroth and Schnitzer 2013; Zhang, Wang, et al. 2007; Nagel et al. 2003), several studies have utilized optogenetics to investigate the neural circuits underlying OCD-like behaviors (see Appendix B /(Piantadosi and Ahmari 2015) for a thorough summary). Building off work demonstrating striatal dysfunction in *Sapap3* KO mice, Burguiere and colleagues (2013) demonstrated baseline hyperactivity of the principle striatal output neuron, spiny projection neurons (SPNs), in the central striatum of KO mice relative to wildtype mice. Further, they found that selective stimulation of projections from the lOFC cell bodies, or their terminals in the central striatum could normalize the compulsive grooming phenotype. Interestingly, it appeared that selective stimulation of these lOFC terminals, somewhat paradoxically, reduced activity in the central striatum. A possible mechanism for this reduction was a synchronization of striatal fast spiking interneurons (FSIs), which exert profound feed-forward inhibition onto nearby SPNs despite only comprising of 1-3% of all striatal cells (Berke 2011, 2008; Gage et al. 2010; Owen, Berke, and Kreitzer 2018). These data highlight not only a critical role for a specific cortico-striatal circuit in controlling compulsive behavior, but also suggest specific dysfunction in genetically defined striatal cell types may be contributing.

Further cementing a role for cortico-striatal hyperactivity in perseverative behavior, Ahmari et al. (2013) demonstrated that chronic stimulation of projections from the medial OFC (mOFC) to ventromedial striatum (VMS) of wildtype mice could induce a progressive and persistent increase in grooming. This increase in grooming was also correlated with a potentiation of mOFC to VMS evoked firing rates, both of which were normalized following fluoxetine treatment. Together, these data demonstrate that cortico-striatal circuit activity is involved in pathological grooming, though the precise activity patterns within these regions and the cell types that underlie this activity are currently unknown.

1.2.3 Using *in vivo* single-photon calcium imaging to investigate neural circuits

The optogenetic strategies described above, while providing a causal link between compulsive and repetitive behavior within specific neural circuits, utilize non-physiological stimulation parameters to perturb the cells within these circuits. Given that the coordination and execution of complex behavioral patterns relies on precise timing of neural activity from multiple cell types, it is critical to be able to assess the dynamics of specific cell populations of interest *in vivo*. Only within this context can the impact of stimulation be truly interpreted.

Multiple techniques are available for monitoring neural activity *in vivo*. In order to adequately assess the neural underpinnings of compulsive behavior, we required a method that meets three specific criteria:

1. *Simultaneous recording of hundreds of genetically distinct neurons in deep brain structures.*
2. *Free range of motion to engage in spontaneous behaviors (e.g. grooming).*
3. *Ability to accurately track neurons within and across sessions.*

Traditional methods to assess large-scale neural activity have utilized *in vivo* electrophysiology, which directly records the electrical potentials of individual or groups of cells (Hubel and Wiesel 2009; Grace and Bunney 1983; Buzsaki 2004). Electrophysiological techniques have unparalleled temporal specificity, allowing for precise correlation of neural activity with a behavior of interest. Further, estimation of action potential timing and number is far superior with electrophysiological measures than with any other current technique. However, currently available electrophysiological techniques that also permit a free range of motion for a mouse typically only produce on the order of dozens of cells recorded simultaneously. Additionally, the spatial location of these individual neurons is very challenging to ascertain, making tracking the same cell across the development of a behavior extremely challenging. Finally, while it has been used to great effect

(Kravitz, Owen, and Kreitzer 2013; Cardin et al. 2010; Cohen et al. 2012), it is often a laborious and low-yield procedure to combine optogenetics and electrophysiology to tag specific genetically defined populations of neurons, especially when the cell population is sparse.

An alternative to electrophysiological recordings of neuronal activity is imaging of intracellular calcium fluctuations that occur during heightened periods of neural activity (Berridge, Bootman, and Roderick 2003; Grienberger and Konnerth 2012). Several methods for recording calcium signals exist, but all rely on the expression of genetically encoded calcium indicators (GECIs) and an image sensor to read the fluorescence signal. Significant GECI development has produced fluorophores with excellent signal to noise, though the relation of calcium signal *in vivo* to spiking activity is still an active area of investigation (Akerboom et al. 2012; Chen et al. 2013; Pnevmatikakis et al. 2016; Vogelstein et al. 2010). One method of recording calcium signals *in vivo* is through two-photon calcium imaging, which provides access to thousands of simultaneously recorded neurons with limited background signal, as well as accurate spatial information for each cell (Svoboda and Yasuda 2006). However, recording from deep brain structures remains challenging with two-photon imaging, and for successful imaging mice must be head-fixed to a microscope, limiting the ability to assess naturalistic behaviors (Dombeck et al. 2007). Another commonly used method that has circumvented both the need for head fixation and limitation to superficial brain structures is fiber photometry, which records GECI signals through implanted lightweight fiber optics (Cui et al. 2014). However, this technique records bulk calcium signal with a complete lack of cellular resolution.

The recent development of lightweight miniature epifluorescence microscopes has proven to be the precise tool necessary to answer the questions in this dissertation (Ghosh et al. 2011). First, the issue of imaging deep brain structures has been solved through the addition of a gradient

refractive index (GRIN) lens that is implanted directly into the rodent brain above an area of interest. Second, a lightweight miniature microscope (~2g) is able to be carefully affixed to the rodent's head and can interface with the GRIN lens, allowing for mice to be freely moving during imaging (Resendez et al. 2016). Finally, the images produced, while significantly noisier than a two-photon recording, provides single-cell spatial resolution that can be accurately tracked across days (Sheintuch et al. 2017; Zhou et al. 2018). Combined, this tool allows us to specifically monitor sparse populations of neurons in deep brain structures that were previously inaccessible, and to understand how their activity contributes to normal and pathological behavioral states.

1.3 Goals of the current dissertation

The overarching goal of this thesis is to bridge a critical gap in our knowledge regarding preeminent hypotheses of OCD pathogenesis: glutamatergic dysfunction and functional abnormalities in fronto-striatal circuitry. First, I will test the hypothesis that glutamatergic genetic dysfunction is involved in OCD pathogenesis (Chapter 2). Using post-mortem tissue obtained from OCD subjects and matched comparison subjects, we will conduct the first post-mortem examination of the orbitofrontal cortex (OFC) and the striatum, the most commonly implicated brain regions in human imaging studies, looking specifically at excitatory and inhibitory transcripts, most of which have been previously genetically linked to OCD. Second, I will utilize a mouse (*Sapap3*-knockout) lacking a critical excitatory synaptic gene (*DLGAP3/SAPAP3*) that we demonstrate to be reduced in both cortex and striatum of OCD subjects and investigate the functional consequences of this reduction on activity in the OFC and striatum using *in vivo* miniature microscopy (Chapter 3). Finally, we will attempt to assess how genetically distinct

populations of striatal neurons individually contribute to compulsive behavior in *Sapap3*-knockout mice (Chapter 4). Together, these data will shed new light on the role of disrupted excitatory signaling in cortical and striatal regions in OCD, and how this disruption may contribute to compulsive behavior.

2.0 Decreases in excitatory synaptic gene expression in orbitofrontal cortex and striatum of subjects with obsessive compulsive disorder

Obsessive compulsive disorder (OCD) is a severe illness that affects 2-3% of people worldwide. OCD neuroimaging studies have consistently shown abnormal activity in brain regions involved in decision-making (orbitofrontal cortex [OFC]) and action selection (striatum). However, little is known regarding molecular changes that may contribute to abnormal function. We therefore examined expression of synaptic genes in post-mortem human brain samples of these regions from eight matched pairs of unaffected comparison and OCD subjects. Total grey matter tissue samples were obtained from medial OFC (BA11), lateral OFC (BA47), head of caudate, and nucleus accumbens core (NAc). Quantitative polymerase chain reaction (qPCR) was then performed on a panel of mRNA transcripts encoding proteins related to excitatory synaptic structure, excitatory synaptic receptors/transporters, and GABA synapses. Relative to unaffected comparison subjects, OCD subjects had significantly lower levels of several transcripts related to excitatory signaling in both cortical and striatal regions: *DLGAP3, DLGAP4, SLC1A1*. However, most transcripts encoding excitatory synaptic proteins were selectively lower in OFC of OCD subjects and unchanged in striatum. Composite transcript level measures supported these findings by revealing that reductions in transcripts encoding excitatory synaptic structure proteins and excitatory synaptic receptors/transporters occurred primarily in OFC of OCD subjects. In contrast, transcripts associated with inhibitory synaptic neurotransmission showed minor differences between groups. The observed decreased levels of multiple glutamatergic transcripts across both medial and lateral OFC may suggest an upstream causal event. Together, these data provide the

first evidence of molecular abnormalities in brain regions consistently implicated in OCD human imaging studies.

2.1 Introduction

Obsessive compulsive disorder (OCD) affects 2-3% of people worldwide, and has been identified by the World Health Organization (WHO) as a leading cause of illness related disability(Kessler et al. 2005) due to its chronic and relapsing course. The substantial societal burden of OCD–an estimated $10 billion annual cost in the U.S (Eaton et al. 2008)–stems in part from sub-optimal pharmacotherapeutic treatments. First-line monotherapy with selective serotonin reuptake inhibitors (SSRIs) leads to remission in only 10-20% of patients, with 25% failing to experience any symptom improvement (Bollini et al. 1999; Pigott and Seay 1999). Development of more effective treatments has been limited by a lack of knowledge regarding the molecular pathology of the disorder.

Neuroimaging studies have consistently identified cortical and striatal abnormalities in OCD (Graybiel and Rauch 2000). Specifically, structural MRI studies suggest that anatomical abnormalities in the orbitofrontal cortex (OFC) and striatum may contribute to OCD pathogenesis (Rotge et al. 2009a). Functional neuroimaging studies have also identified OFC and striatum as key loci of dysfunction in OCD, with most evidence suggesting hyperactivity in, and increased connectivity between, these regions (Pauls et al. 2014; Harrison, Soriano-Mas, Pujol, Ortiz, Lopez-Sola, et al. 2009; Fitzgerald et al. 2011a; Menzies et al. 2008a; Whiteside, Port, and Abramowitz 2004). Furthermore, hyperactivity in these critical regions is increased during symptom

provocation and decreased in response to successful SSRI therapy (Pauls et al. 2014; Rauch et al. 2002), suggesting this abnormal activity may be involved in OCD symptomatology. Further evidence for a causal relationship between activity in cortico-striatal circuits and OCD pathophysiology comes from studies indicating that deep brain stimulation of ventral striatal targets both relieves OCD symptoms and reverses cortico-striatal hyperactivity (Rauch et al. 2006; Bourne et al. 2012). Finally, a causal relationship between OFC-striatal activity and OCD-relevant behaviors has been demonstrated using rodent models and optogenetics (Ahmari et al. 2013; Burguiere et al. 2013). Thus, current knowledge regarding circuit level disruptions in OCD is consistent across multiple lines of evidence and highlights abnormalities in OFC and striatum.

Although the etiology of OCD is unknown, twin studies support a genetic contribution. A recent meta-analysis including 37 samples from 14 twin studies of obsessive-compulsive symptoms found that genetic factors accounted for 40% of the phenotypic variance; no significant contribution from shared environmental factors was noted (Taylor 2011). Unbiased genome-wide association studies (GWAS) indicate that genes encoding proteins found at or around excitatory synapses may account for this genetic contribution (Stewart et al. 2013; Mattheisen et al. 2015). Specifically, significant associations were observed with *DLGAP1* (discs large-associated protein 1), a post-synaptic density scaffolding protein family member, and *ISM1*, which is associated with expression of multiple genes related to glutamatergic signaling including members of the *DLGAP* family and glutamate receptors (Stewart et al. 2013). In a second OCD GWAS study, the most strongly associated marker was observed near the gene encoding *PTPRD* (protein tyrosine phosphatase delta), which promotes the differentiation of glutamatergic synapses (Takahashi and Craig 2013) and interacts with the post-synaptic adhesion molecule SLITRK3 (SLIT and NTRK-like protein 3) (Mattheisen et al. 2015). Excitatory synapse involvement is also supported by the

well-replicated finding of an association between OCD and *SLC1A1*, which encodes the primary neuronal glutamate transporter (Dickel et al. 2006; Arnold et al. 2006; Porton et al. 2013; Samuels et al. 2011; Shugart et al. 2009; Stewart et al. 2007; Zike et al. 2017). Finally, studies in transgenic mice also indicate that dysregulation of glutamatergic synapses may lead to OCD-relevant cortico-striatal dysfunction. Specifically, both *Sapap3* (also known as *Dlgap3*) and *Slitrk5* constitutive knockout mice display OCD-relevant compulsive grooming phenotypes and cortico-striatal hyperactivity that can be rescued with chronic fluoxetine treatment (Welch et al. 2007b; Burguiere et al. 2013; Shmelkov et al. 2010).

Because alterations in excitatory neurotransmission are commonly associated with homeostatic changes in inhibitory neurotransmission, prior work has also examined γ-amino butyric acid (GABA) signaling in OCD. A small literature in humans supports a possible role for GABA-ergic dysfunction by demonstrating decreased mPFC GABA levels via magnetic resonance spectroscopy in subjects with OCD (Simpson et al. 2012), and increased mPFC GABA levels following a single ketamine infusion (Rodriguez et al. 2015). In addition, transcranial magnetic stimulation (TMS)-based neurophysiological indices suggest dysregulated GABA-signaling in OCD patients (Richter et al. 2012). Tourette syndrome, which is highly comorbid with OCD(Du et al. 2010), has also been associated with reduced numbers of striatal GABAergic interneurons (both parvalbumin- and choline acetyltransferase-expressing subtypes (Kalanithi et al. 2005; Kataoka et al. 2010)). Preclinical evidence likewise supports a potential role for GABAergic alterations in repetitive behavior. For example, dysfunction in striatal parvalbumin positive interneurons has been linked to compulsive grooming behavior in *Sapap3* knockout mice (Burguiere et al. 2013). In addition, simulation of post-mortem findings from Tourette syndrome

in mice via ablation of parvalbumin positive interneurons in the dorsal striatum leads to an increase in stress-induced grooming and anxiety (Xu, Li, and Pittenger 2016).

Although the potential roles of glutamatergic and GABAergic signaling in OCD have been broadly investigated in human neuroimaging studies, only one prior study has directly explored the possible underlying molecular substrates of these signaling changes by quantifying gene expression in human post-mortem brain tissue (Jaffe et al. 2014). This study examined the dorsolateral prefrontal cortex (DLPFC) via microarray analyses in a group of subjects that had OCD, obsessive-compulsive personality disorder (OCPD), and/or tic disorder diagnoses. Although decreased parvalbumin levels (*PVALB*) were observed in OCD subjects compared to unaffected comparison subjects, gene set analyses did not reveal either glutamatergic or GABAergic neurotransmission as a top altered pathway. However, this study did not examine the OFC or striatum, which have been more commonly implicated in the OCD disease process (Breiter et al. 1996; Rauch, Savage, Alpert, Fischman, et al. 1997) than the DLPFC (Menzies et al. 2008b). To assess whether glutamatergic and/or GABAergic signaling is altered in these brain regions, we quantified the expression of 16 genes whose protein products are critical for normal excitatory and inhibitory neurotransmission (Table 2-1) in post-mortem tissue samples from the medial OFC, lateral OFC, caudate, and nucleus accumbens (NAc) of subjects with OCD and unaffected comparison subjects.

2.2 Methods

2.2.1 Human post-mortem subjects

Brain specimens (N=16) were obtained through the University of Pittsburgh Brain Tissue Donation Program during autopsies conducted by the Allegheny County Medical Examiner's Office (Pittsburgh, PA) after consent was given by next-of-kin. An independent panel of experienced clinicians examined clinical records, toxicology, psychological autopsy data, and structured interviews with family members to make consensus DSM-IV diagnoses. Unaffected comparison subjects underwent identical assessments and were determined to be free of any lifetime psychiatric illnesses. All procedures were approved by the University of Pittsburgh's Committee for the Oversight of Research and Clinical Training Involving Decedents and Institutional Review Board for Biomedical Research. To reduce biological variance, each subject with OCD (n=8) was matched for sex, and as closely as possible for age and RNA integrity number (RIN), with one unaffected comparison subject. Subject groups did not differ in mean age (t_{14} = 0.2, p = .83), post-mortem interval (PMI; t_{14} = 0.6, p = .54), brain pH (t_{14} = 1.6, p = .13), RNA ratio (t_{14} = 0.3, p = .75), or RIN (t_{14} = 0.2, p = .87), (Table 2-2).

2.2.2 Tissue collection and RNA extraction

Standardized amounts (50 mm3) of gray matter were collected via a cryostat from four separate brain regions identified cytoarchitectonically: medial orbitofrontal cortex (mOFC, BA11), lateral orbitofrontal cortex (lOFC, BA47), head of the caudate nucleus, and the nucleus accumbens core. RNA was extracted using an RNeasy Plus Mini kit (QIAGEN, Valencia, CA).

RIN values were obtained using the Agilent 2100 Bioanalyzer (Agilent Technologies, Santa Clara, CA). Each subject had a RIN value ≥ 7, indicative of high-quality, intact RNA.

2.2.3 Selection of transcripts for expression analysis

Using qPCR we examined the expression of 16 excitatory and inhibitory synaptic genes, the majority of which (11/16) have been genetically linked to OCD and OCD-related disorders (e.g. grooming disorders, skin picking, Tourette syndrome) (Table 2-1). Transcripts were broadly grouped into three categories based on the function of their protein product: 1) excitatory synaptic structure: contains transcripts in the DLGAP and SLITRK families, both of which have established roles in synapse formation and stabilization; 2) excitatory synaptic receptors and transporters: contains two transcripts encoding ionotropic glutamate receptors (GRIA1 and GRIN2B), the vesicular glutamate transporter SLC17A7, and the excitatory amino acid transporter SLC1A1; and 3) GABA synapse: contains the GABAergic synapse scaffolding protein GABARAP, two major GABA synthesizing enzymes (GAD1 and GAD2), two calcium binding proteins that characterize two functionally different classes of inhibitory interneurons found in the striatum and cortex (PVALB and CALB1), and the vesicular GABA transporter (SLC32A1).

2.2.4 Quantitative PCR (qPCR)

Complementary DNA (cDNA) was generated using 90ng of RNA per sample and qScript cDNA SuperMix (Quanta BioSciences, Gaithersburg, MD) following universal cycling conditions (65 to 59ºC touchdown and 40 cycles of 10s at 95ºC, 10s at 59ºC, and 10s at 72ºC). PCR products were amplified in triplicate on a Bio-Rad CFX96 Real-Time PCR system (Bio-Rad, Hercules,

California USA) using SYBR Green I nucleic acid gel stain. Subject pairs were run on the same qPCR plate to control for technical variance. Two housekeeping genes (β-Actin [*ACTB*] and Cyclophillin-A [*PPIA*]) were used to normalize target mRNA levels. Primer sequences for all housekeeping and target genes, as well as the transcript variants of each transcript amplified (identified using NCBI Primer-BLAST), can be found in Table 4. The difference in cycle threshold (dCT) for each target transcript was calculated by subtracting the geometric mean CT for the two reference genes (each run in triplicate) from the mean CT of the target transcript (mean of the three replicates). There were no significant differences in the geometric mean of CTs of the two housekeeping genes across all four brain regions (Fig.A-1). Because dCT represents the log2-transformed expression ratio of each target transcript to the reference genes, the relative level of the target transcript for each subject is reported as 2^{-dCT} (Vandesompele et al. 2002).

2.2.5 Statistical Analysis

To determine the OCD-associated expression patterns of transcripts, we employed a mixed-design analysis of covariance (ANCOVA). Brain region was considered a within-subjects variable with 4 levels (BA11, BA47, caudate nucleus, NAc), and OCD diagnosis was the between subjects factor. Main effects of OCD diagnosis and brain region, as well as the interaction between diagnosis and brain region, were tested using *F* tests for each individual transcript. Covariates included in each model were age, sex, PMI, and RIN. Data from all 8 subject pairs were analyzed in all regions unless noted in the text in cases of low transcript expression. In a minority of cases (6 total transcripts), data from the caudate and NAc of subject pair 8 were not collected due to low RNA yield (see Table 5 for detailed information about each transcript). If significant interactions were observed between diagnosis and brain region, post-hoc pairwise comparisons were conducted

using Sidak tests to control for overall type I error. Multiple comparison correction was conducted using the Benjamini-Hochberg procedure and a false discovery rate of 0.05 (Benjamini Y. 1995). For main effects and interactions, correction was made across 16 transcripts. For pairwise comparisons conducted only after a significant interaction, correction was made for 22 comparisons. For individual transcript comparisons, uncorrected *p*-values are reported in the main text and corrected *p*-values are reported in Table 7.

Composite scores of three groups of transcripts grouped broadly by the function of their encoded proteins (excitatory synaptic structure; excitatory synaptic receptors and transporters; GABA synapse) were computed. First, normalized (*Z* scored) expression levels were calculated for each transcript using ($Z = \frac{X-\mu}{\sigma}$), where μ is mean of expression ratios for the unaffected comparison subjects for a given transcript, σ is standard deviation of expression ratio for the unaffected comparison subjects for a given transcript, and *X* is the individual transcript measure from an unaffected comparison or OCD subject. Z-scores were then summed for all excitatory synaptic structure, excitatory synaptic receptors and transporters, and GABA synapse measures (see Table 2-1: Transcript grouping) within a given diagnostic group for each brain region. Post-hoc pairwise comparisons were conducted using Sidak tests to control for overall type I error. Multiple comparison adjustments were again made using the Benjamini-Hochberg analysis with a false discovery rate of 0.05. Both corrected and uncorrected comparisons are presented for composite scores in the main text, and full statistics can be found in Table 7.

Individual *t*-tests were performed with the Holm-Sidak multiple comparison correction and an alpha of 0.05 to analyze the effect of 1) antidepressants at time of death, 2) presence of benzodiazepines at time of death, 3) comorbid MDD diagnosis, and 4) presence of tobacco use at

time of death on expression of transcripts in OCD subjects (Fig.A-2-4). Statistical analyses were performed using SPSS (SPSS, Inc.; Chicago, IL).

2.3 Results

2.3.1 Effect of OCD diagnosis on expression of excitatory synaptic structure transcripts in cortical and striatal regions

Regional patterns of expression of excitatory structural transcripts implicated in OCD and grooming disorders were first examined (Fig.2-1). Several of these transcripts displayed lower expression in OCD subjects compared to unaffected comparison subjects selectively in OFC, and not striatum. First, although expression of the scaffolding protein transcript *DLGAP1* was unaffected by diagnosis ($F_{1,10} = 2.8$, $p = .13$) or region ($F_{3,30} = 1.8$, $p = .17$), the interaction between these two factors was significant ($F_{3,30} = 3.5$, $p = .03$). Post-hoc tests then revealed that mean *DLGAP1* levels were significantly lower in BA47 (-48%, $F_{1,10} = 5.1$, $p = .05$) but not different in BA11, caudate, and NAc ($p > .05$)] (Fig.2-1A). In addition, expression of another *DLGAP* family member, *DLGAP2*, significantly differed by diagnosis ($F_{1,10} = 34.4$, $p = .0001$) and brain region ($F_{3,30} = 3.5$, $p = .03$), with a significant interaction ($F_{3,30} = 5.4$, $p = .004$). Post-hoc pairwise comparisons of simple main effects showed lower *DLGAP2* in OCD subjects selectively in BA11 (-43%: $F_{1,10} = 27.7$, $p = .0004$) and BA47 (-41%: $F_{1,10} = 15.8$, $p = .003$) [expression was not significantly different in caudate/NAc ($p > .05$)] (Fig.2-1B). A third transcript, *SLITRK3* (Fig.2-1F), showed a similar pattern, with expression significantly affected by diagnosis ($F_{1,8} = 21.7$, $p = .002$), a trend towards a brain region effect ($F_{2,16} = 2.9$, $p = .08$), and an interaction between

diagnosis and brain region ($F_{2,16} = 4.2$, $p = .03$). Post-hoc contrasts indicated lower *SLITRK3* levels in BA11 (-42%: $F_{1,8} = 34.3$, $p = .0004$) and BA47 (-32%: $F_{1,8} = 7.8$, $p = .02$), but not in caudate (-24%: $F_{1,8} = 2.3$, $p = .17$; too low to detect in NAc).

Several excitatory synaptic structural transcripts also showed lower expression in both OFC and striatum of OCD subjects compared to unaffected comparison subjects. First, although ANCOVA revealed a significant effect of diagnosis on *DLGAP3* expression ($F_{1,10} = 7.0$, $p = .03$), there was no effect of brain region ($F_{3,30} = 1.9$, $p = .16$) or interaction between diagnosis and region ($F_{3,30} = 0.2$, $p = .90$) (Fig.2-1C). Similarly, levels of *DLGAP4* (Fig.2-1D) were lower in both OFC and striatum [significant effect of diagnosis ($F_{1,10} = 7.4$, $p = .02$) and brain region ($F_{3,30} = 3.3$, $p = .04$); no interaction ($F_{3,30} = 1.3$, $p = .30$)]. Notably, *SLITRK1* was the only excitatory synaptic structure transcript tested which showed no differences in expression related to diagnosis (Fig.2-1E) ($F_{1,8} = 3.0$, $p = .12$) or brain region ($F_{3,24} = 2.4$, $p = .09$), and no interaction between the two factors ($F_{3,24} = 1.0$, $p = .40$).

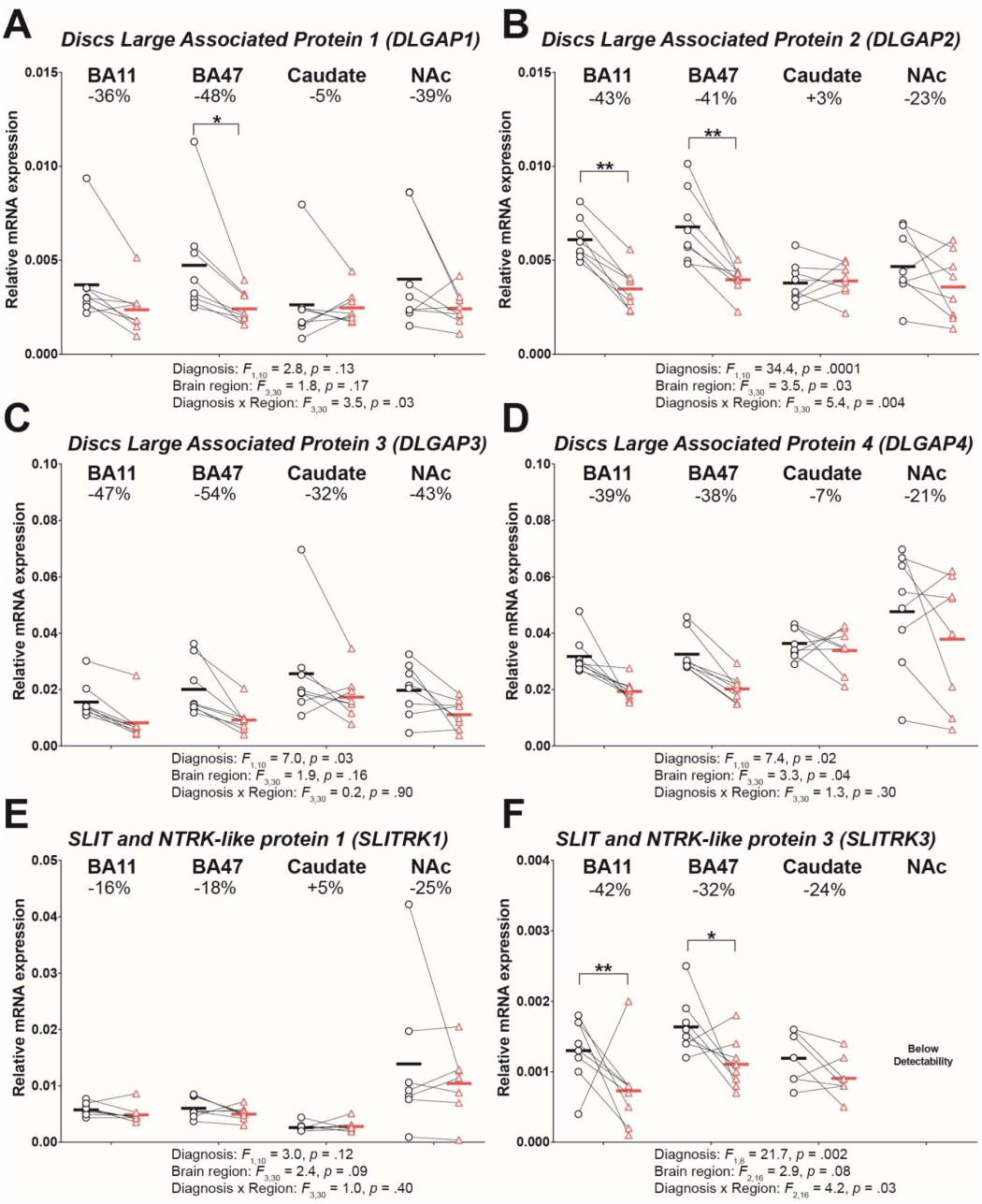

Figure 2-1. Expression of excitatory synaptic structure transcripts in OFC and striatum of OCD subjects and unaffected comparison subjects.

qPCR analysis of excitatory synaptic structure transcripts across two orbitofrontal (BA11 and BA47) and two striatal (caudate and NAc) brain regions in OCD. Unaffected comparison subjects and OCD subjects are represented by black open circles and red open triangles, respectively. A line drawn between a circle and a triangle indicates a matched pair. Horizontal bars indicate group means. Percentages indicate the percentage difference in transcript level of the OCD subject relative to the unaffected comparison subject. Post-hoc significance following significant interactions is indicated by brackets; **p<0.01, *p<0.05.

2.3.2 Effect of OCD diagnosis on expression of transcripts encoding excitatory synaptic receptors and transporters in cortical and striatal regions

We next assessed levels of transcripts encoding glutamate receptors and transporters (Fig.2-2). Expression of the transcript *GRIA1*, which encodes the GluR1 subunit of the AMPA receptor, was lower in OFC and striatum of OCD subjects (Fig.2-2A) [effect of diagnosis ($F_{1,8}$ = 9.0, p = .02); no effect of region ($F_{3,24}$ = 1.0, p = .39) or interaction ($F_{3,24}$ = 1.6, p = .21)]. Similarly, expression of *GRIN2B*, which encodes the NR2B subunit of the NMDA receptor, was lower in OCD subjects (Fig.2-2B) [main effect of diagnosis ($F_{1,8}$ = 6.9, p = .03); no effect of region ($F_{3,24}$ = 1.8, p = .17) or interaction ($F_{3,24}$ = 1.1, p = .36)]. A significant main effect of diagnosis on expression of *SLC1A1*, a glutamate transporter that has been associated with OCD, was also observed ($F_{1,10}$ = 5.0, p = .05) (Fig.2-2C). This transcript also displayed a significant effect of brain region ($F_{3,30}$ = 3.2, p = .04) and an interaction ($F_{3,30}$ = 3.7, p = .02); subsequent pairwise comparisons indicated *SLC1A1* in OCD subjects was lower only in BA47 (-34%: $F_{1,10}$ = 7.9, p = .03), although a trend was also observed in BA11 (-37%: $F_{1,10}$ = 3.9, p = .08). Finally, we measured levels of *SLC17A7,* which encodes the pre-synaptic vesicular glutamate transporter 1 (VGLUT1). Consistent with previous work (Vigneault et al. 2015), *SLC17A7* was undetectable in striatum; however, levels were lower in both OFC regions in OCD subjects [significant effect of diagnosis ($F_{1,10}$ = 12.4, p = .005), no effect of brain region ($F_{1,10}$ = 0.02, p = .89), and no interaction ($F_{1,10}$ = 0.02, p = .89) (Fig.2-2D)].

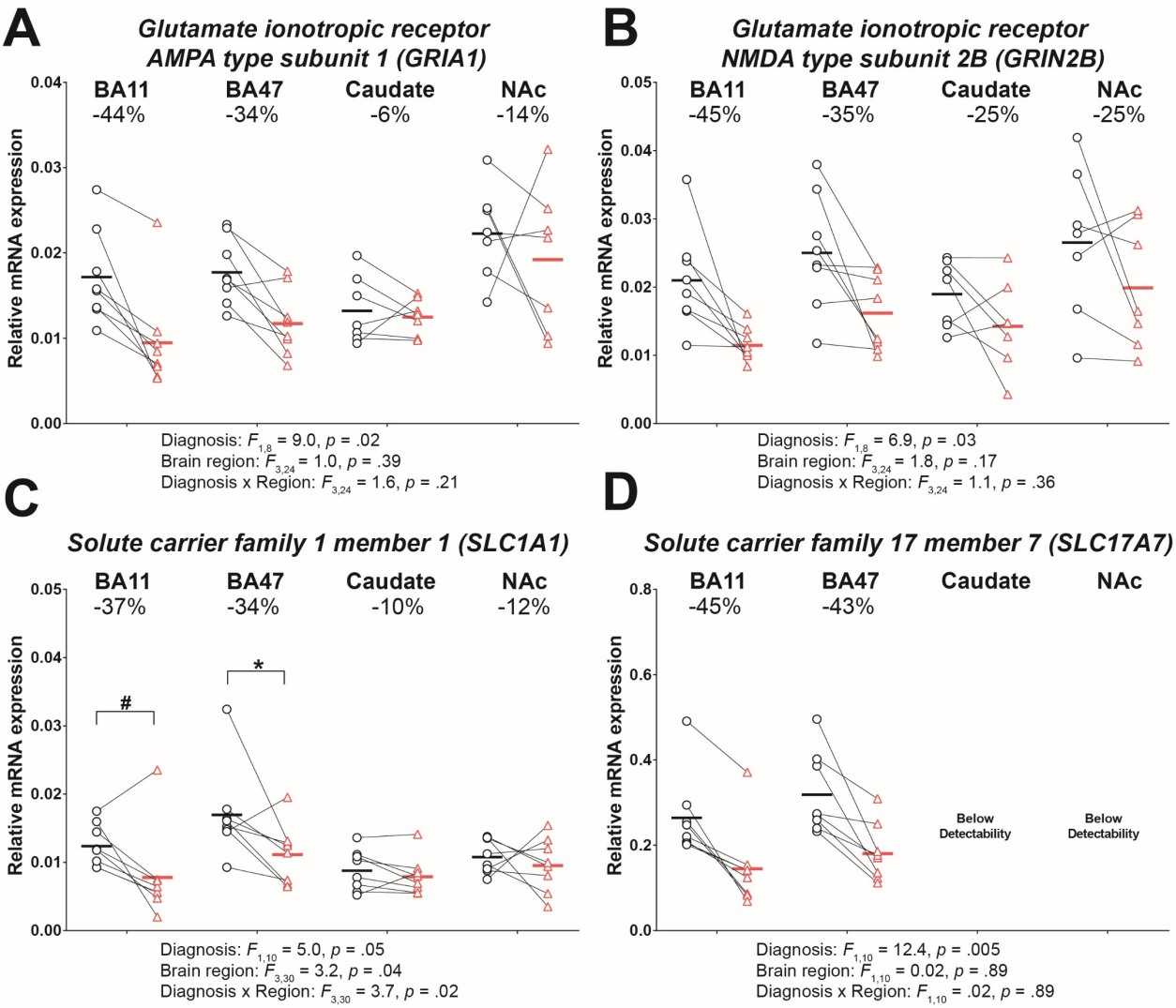

Figure 2-2. Expression of transcripts encoding excitatory synaptic receptors and transcripts in OFC and striatum of OCD subjects and unaffected comparison subjects.

qPCR analysis of transcripts encoding excitatory synaptic receptors and transporters across two orbitofrontal (BA11 and BA47) and two striatal (caudate and NAc) brain regions in OCD. Unaffected comparison subjects and OCD subjects are represented by black open circles and red open triangles, respectively. Lines represent matched pairs. Horizontal bars indicate group means. Percentages indicate the percentage difference in transcript level of the OCD subject relative to the unaffected comparison subject. Post-hoc significance following significant interactions is indicated by brackets; *p<0.05, #p<.1.

2.3.3 Effect of OCD diagnosis on expression of GABA synapse transcripts in cortical and striatal regions

To determine if OCD was associated with alterations in GABAergic transcript levels in OFC and striatum, we first quantified levels of the two major GABA synthesizing enzymes, *GAD1* (Fig.2-3A; GAD_{67}) and *GAD2* (Fig.2-3B; GAD_{65}). ANCOVA revealed a significant effect of diagnosis ($F_{1,10} = 6.9$, $p = .03$) and brain region ($F_{3,30} = 4.3$, $p = .01$) on *GAD1* levels, with an interaction between the two factors ($F_{3,30} = 7.2$, $p = .001$). Post-hoc comparisons revealed that OCD subjects had significantly elevated *GAD1* in BA11 (+99%: $F_{1,10} = 9.5$, $p = .01$), with no other region differing by diagnosis ($p > .05$). In contrast, there was no effect of diagnosis on *GAD2* levels ($F_{1,10} = 2.6$, $p = .14$), although we did observe a significant effect of brain region ($F_{3,30} = 3.9$, $p = .02$) and a trend toward a significant interaction ($F_{3,30} = 2.9$, $p = .052$).

We also examined transcripts encoding parvalbumin and calbindin (*PVALB* and *CALB1*), calcium-binding proteins used as markers of cortical and striatal interneuron subtypes. Although diagnosis had no detectable effect on *PVALB* levels ($F_{1,10} = 2.8$, $p = .13$), an effect of brain region ($F_{2,20} = 5.6$, $p = .01$) and an interaction between region and diagnosis ($F_{2,20} = 4.9$, $p = .02$) were observed [note; *PVALB* expression was too low to detect in the NAc, consistent with previous studies (Bernacer, Prensa, and Gimenez-Amaya 2012)]. Pairwise comparisons suggested increased levels of *PVALB* in BA11 of OCD subjects, although the effect was not significant (+41%: $F_{1,14} = 2.9$, $p = .11$). Similarly, no effect of diagnosis ($F_{1,10} = .84$, $p = .38$) and a significant effect of brain region ($F_{3,30} = 24.7$, $p = .0001$) were observed on *CALB1* levels; however, there was no significant interaction ($F_{3,30} = 1.3$, $p = .27$).

Given the lower levels of transcripts that encode excitatory post-synaptic structural proteins in OCD (Fig.2-1), we also examined *GABARAP*, which encodes a protein involved in GABA

receptor scaffolding (Fig.2-3E). In contrast to the excitatory transcripts, no effect of OCD diagnosis ($F_{1,8}$ = .2.8, p = .13), brain region ($F_{3,24}$ = 2.3, p = .10), or interaction ($F_{3,24}$ = 1.3, p = .30) was observed for *GABARAP*. Levels of *SLC32A1*, which encodes the vesicular inhibitory amino acid transporter, were also not significantly affected by diagnosis (Fig.2-3F; $F_{1,8}$ = .004, p = .95) or brain region ($F_{3,24}$ = 2.0, p = .14), and no interaction was detected ($F_{3,24}$ = 2.2, p = .10).

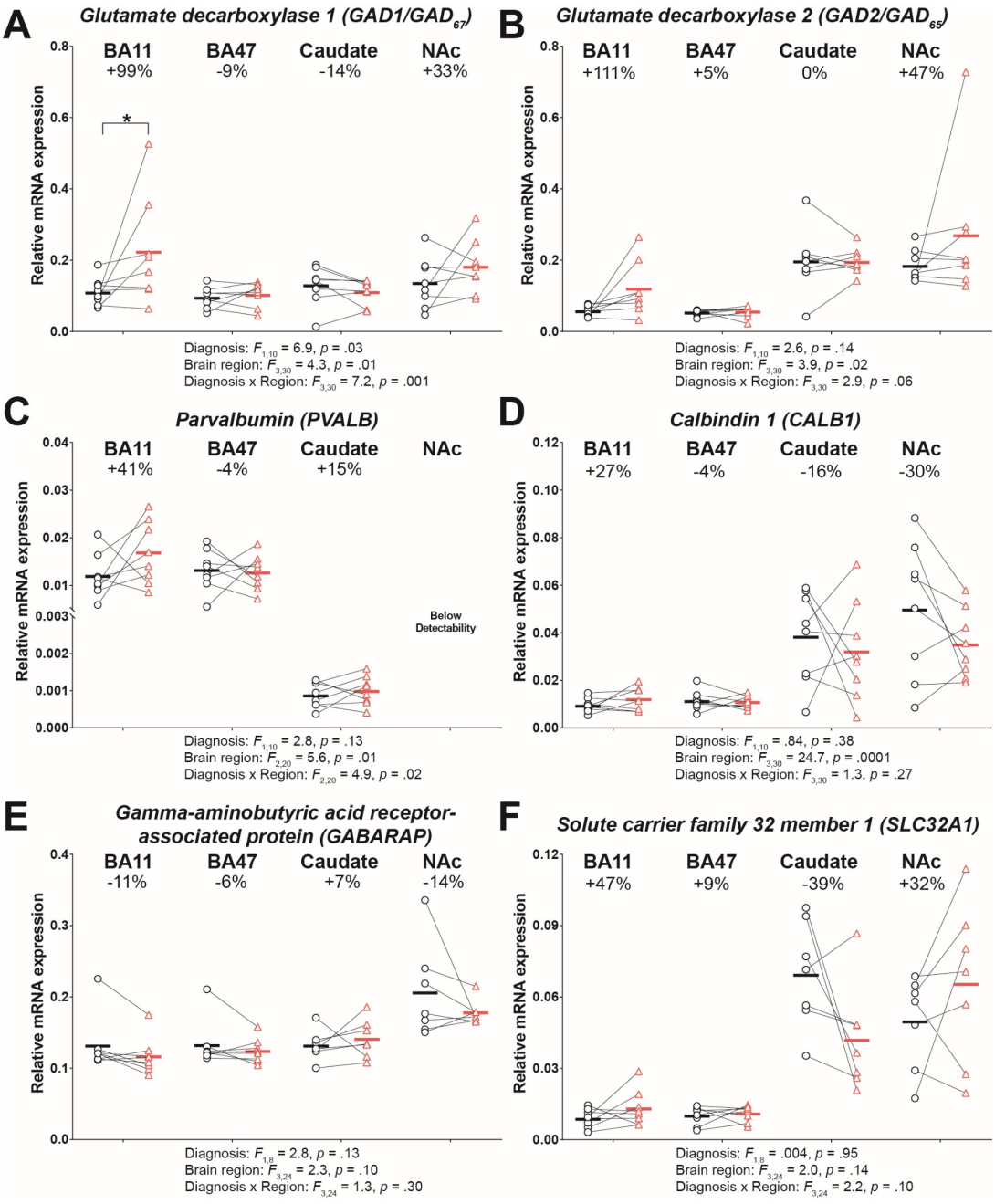

Figure 2-3. Expression of GABA synapse transcripts in OFC and striatum of OCD subjects and unaffected comparison subjects

qPCR analysis of GABA synapse transcripts across two orbitofrontal (BA11 and BA47) and two striatal (caudate and NAc) brain regions in OCD. Unaffected comparison subjects and OCD subjects are represented by black open circles and red open triangles, respectively. Lines represent matched pairs. Horizontal bars indicate group means. Percentages indicate the percentage difference in transcript level of the OCD subject relative to the unaffected comparison subject. Post-hoc significance following significant interactions is indicated by brackets; *p<0.05.

2.3.4 Composite measures of transcript expression across cortical and striatal regions in OCD

To determine the relative contribution of each brain region to the observed changes in transcript levels, we computed composite summary scores from the normalized expression ratios of the transcripts grouped into three categories: excitatory synaptic structure-, excitatory synaptic receptors and transporters-, and GABA synapse-related (Fig.2-4). ANCOVA showed a significant main effect of OCD diagnosis on the excitatory synaptic structure transcript composite measure ($F_{1,10} = 21.2$, $p = .001$; corrected $p = .003$), a trend towards a main effect of region ($F_{3,30} = 2.9$, $p = .052$; corrected $p = .08$), and a significant diagnosis-by-region interaction ($F_{3,30} = 5.2$, $p = .005$; corrected $p = .008$). Pairwise comparisons revealed significantly reduced levels of excitatory synaptic structure transcripts in BA11 ($F_{3,30} = 11.9$, $p = .006$; corrected $p = .02$) and BA47 ($F_{3,30} = 28.1$, $p = .0003$; corrected $p = .002$) of OCD subjects, with no changes in caudate and NAc ($p > .05$) (Fig.2-4A). Similarly, the excitatory synaptic receptor/transporter composite measure showed significant reductions in BA11 and BA47 of OCD subjects, but no changes in caudate or NAc [main effect of diagnosis ($F_{1,8} = 21.2$, $p = .002$; corrected $p = .003$); trend effect of region ($F_{3,24} = 2.5$, $p = .081$; corrected $p = .08$; significant interaction ($F_{3,24} = 4.7$, $p = .01$; corrected $p = .01$); BA11 post-hoc ($F_{1,8} = 34.4$, $p = .0004$; corrected $p = .002$); BA47 post-hoc ($F_{1,8} = 11.4$, $p = .01$; corrected $p = .02$); caudate and NAc ($p > .05$)] (Fig.2-4B). However, the GABA synapse composite measure indicated that GABA-related transcript levels in OCD subjects were elevated in BA11 compared to unaffected comparison subjects, ($F_{1,10} = 11.4$, $p = .007$; corrected $p = .02$), but unchanged in BA47, caudate, and NAc ($p > .05$) [main effect of diagnosis ($F_{1,10} = 6.1$, $p = .03$; corrected $p = .03$); main effect of region ($F_{3,30} = 4.9$, $p = .007$; corrected $p = .02$); significant interaction ($F_{3,30} = 8.7$, $p = .0003$; corrected $p = .0009$)] (Fig.2-4C).

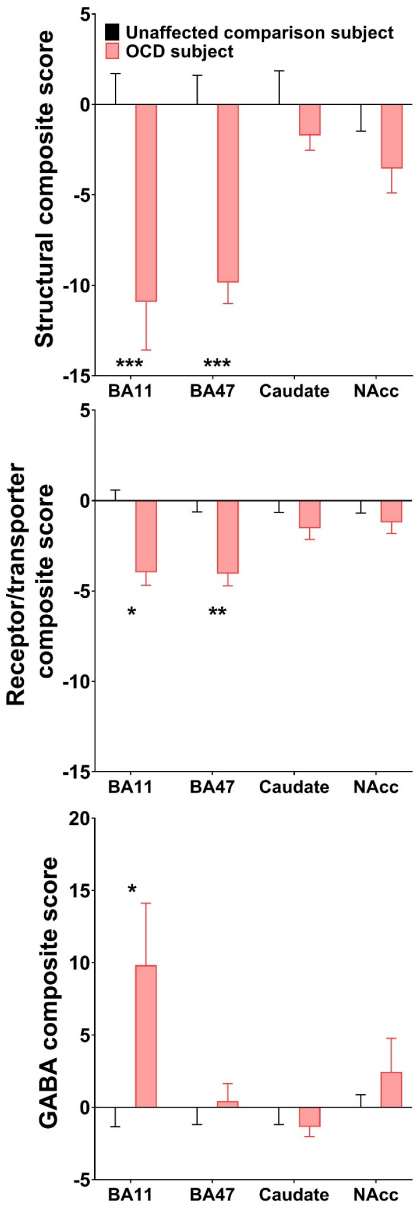

Figure 2-4. Composite measures of excitatory synaptic structure, excitatory synaptic receptors and transporters, and GABA synapse transcripts across cortical and striatal regions in OCD.

(A) In OCD subjects, composite measures of excitatory structural transcripts were lower in BA11 and BA47 relative to unaffected comparison subjects. No differences were observed in either the caudate or NAc. (B) Composite scores of excitatory receptors and transporters were reduced in BA11 and BA47 and unchanged in caudate and NAc in OCD subjects. (C) GABA composite scores were elevated in BA11 and unchanged in BA47, caudate, and NAc of OCD subjects (C). Post-hoc significance following significant nteractions is indicated by brackets; *p<0.05.

2.4 Discussion

Glutamatergic synaptic dysfunction in cortical and striatal brain regions has been suggested as a contributor to the pathophysiology of OCD, but evidence to date has been indirect. Using qPCR in human post-mortem tissue, we now support this hypothesis by demonstrating decreased levels of transcripts encoding excitatory synaptic proteins in OFC and striatal regions in OCD subjects (Figs. 2-1 and 2-2). Composite scores in OCD subjects revealed that these significant reductions in both the excitatory synaptic structure and excitatory synaptic receptors/ transporters transcript groupings were preferentially localized to OFC (BA11 and BA47) and not detected in striatum (caudate and NAc) (Fig.2-4A-B). More subtle increases in GABA synapse transcripts were also identified in OFC, but these were observed selectively in BA11 (Fig.2-3 and Fig.2-4C). Together, these data provide the first evidence of potential molecular dysfunction in brain regions consistently implicated in human imaging studies of OCD (Harrison, Soriano-Mas, Pujol, Ortiz, Lopez-Sola, et al. 2009; Rotge et al. 2009a).

2.4.1 Decreased levels of three key excitatory synaptic structure transcripts are observed in OFC and striatum

Several of the observed down-regulated transcripts have previously been linked to OCD (Pauls et al. 2014; Stewart et al. 2013), including *DLGAP3*. This gene encodes the post-synaptic scaffolding protein most commonly known as SAPAP3, and has been linked to OCD and associated disorders through genetic studies (Bienvenu et al. 2009b; Boardman et al. 2011; Zuchner et al. 2009) [though see (Boardman et al. 2011)]. In human postmortem tissue from OCD subjects, we found that *DLGAP3* expression was significantly decreased across all four cortical

and striatal regions tested (Fig.2-1A-D). This finding is consistent with the fact that *Sapap3* knockout mice, which constitutively lack the *Sapap3* gene, display compulsive behavior, and provides further support for the hypothesis that decreases in SAPAP3 protein are involved in the generation of compulsive behavior in humans (Burguiere et al. 2013; Welch et al. 2007b; Harrison, Soriano-Mas, Pujol, Ortiz, Lopez-Sola, et al. 2009). In addition, the same expression pattern was seen with *DLGAP4*. Interestingly, other *DLGAP* family members showed decreased levels specifically in OFC. Expression of *DGLAP1*, which has recently been identified as the locus of two of the most strongly associated single nucleotide polymorphisms (SNPs) in case-control OCD GWAS (Mattheisen et al. 2015; Stewart et al. 2013), was selectively decreased only in OFC and not striatum (Fig.2-3A); the same pattern was observed for *DLGAP2* (Fig.2-3B). These data raise the possibility that different *DLGAP* family members could differentially impact particular OCD symptom domains based on the regional localization of their alterations in expression.

In addition, in OFC of OCD subjects, we observed a selective reduction in expression of another gene that has been associated with OCD: *SLC1A1* (Fig.2-2C), which encodes the neuronal glutamate transporter EAAT3. *SLC1A1* was first implicated in OCD pathophysiology by two reports identifying genetic variants in two independent patient populations (Arnold et al. 2006; Dickel et al. 2006). Subsequent studies have replicated these findings, although identified variants have not always been consistent(Samuels et al. 2011; Shugart et al. 2009; Stewart et al. 2007). Interestingly, our finding of reduced levels of *SLC1A1* in OFC of OCD subjects relative to unaffected comparison subjects is not aligned with the fact that the most consistently associated SNP in OCD is predicted to result in increased expression of *SLC1A1* (Porton et al. 2013; Zike et al. 2017). To address this discrepancy, future post-mortem brain studies could examine expression

levels of recently-identified *SLC1A1* variants that may serve as negative regulators of SLC1A1/EAAT3 function in cortex and striatum (Porton et al. 2013).

2.4.2 Downregulation of multiple excitatory synaptic transcripts in OFC suggests an upstream causal event

As discussed above, our data can be used to make inferences about the potential role of particular genes in OCD pathology. However, the most striking finding is the simultaneous down-regulation of multiple excitatory synapse-related transcripts in both medial (BA11) and lateral OFC (BA47) (Fig.2-4A-B). Although it is possible that each transcript change is an independently occurring event, this pattern of expression suggests the possibility of an upstream factor leading to abnormal coordinated excitatory synapse gene regulation across the OFC. One potential explanation is altered expression of an upstream "master regulator" gene that influences expression of transcripts associated with post-synaptic excitatory synapse function. Alternatively, due to the diversity of transcripts that were down-regulated, these changes may reflect an overall decrease in number or size of synaptic contacts or dendritic spines in OFC. In turn, this would fit with one of the most consistent findings in structural imaging studies of OCD: a reduction in volume of both left and right OFC (Rotge et al. 2009a; Atmaca et al. 2006; Atmaca et al. 2007a). Precedent for this is observed in other neuropsychiatric illnesses such as schizophrenia, in which dendritic spine loss is one of the greatest indices of gray matter loss (Selemon and Goldman-Rakic 1999; Penzes et al. 2011; Glausier and Lewis 2013).

2.4.3 Synthesis of downregulation of glutamatergic transcripts with existing literature

As discussed above, our findings appear consistent with the structural imaging literature. What becomes more challenging is integrating these data with the existing functional imaging literature demonstrating hyperactivity in OFC at baseline and with symptom provocation in OCD patients (Menzies et al. 2008a). At face value, the results seem contradictory, since one might expect that downregulation of excitatory transcripts in OFC would be consistent with overall decreases in OFC activity. This apparent discrepancy could be explained in several ways. First, there are examples in which knockout of excitatory post-synaptic density proteins leads (potentially counter-intuitively) to both increased neural activity and compulsive grooming behavior: 1) Constitutive knockout of *Sapap3* leads to striatal hyperactivity; 2) Constitutive knockout of *Slitrk5* results in OFC hyperactivity (Shmelkov et al. 2010; Welch et al. 2007b; Burguiere et al. 2013). However, causal links between *Sapap3* and *Slitrk5* down-regulation in specific brain regions and hyperactivity have not yet been demonstrated. Second, our observed decreased levels of excitatory synaptic transcripts could be compensating for changes in neural activity in upstream structures. For example, functional imaging studies demonstrate hyperactivity and increased gray matter volume in the thalamus of OCD subjects (Rotge et al. 2009a). Increased thalamo-cortical drive in OCD patients could therefore be the primary driver of OFC hyperactivity, and lead to compensatory down-regulation of excitatory post-synaptic proteins at thalamo-cortical synapses. In this scenario, OFC hyperactivity could still be observed if this compensation is not sufficient to counteract the increased thalamic drive. If this is the case, we would predict that our observed decrease in excitatory transcript levels in OCD subjects is localized to cortical neurons receiving projections from thalamus, and not neurons in cortical output layers. Thus, our observations from the post-mortem OCD brain lend themselves to directly testable novel

hypotheses regarding OCD pathophysiology. Our data also highlight the importance of moving beyond the targeted set of transcripts tested here, which were mostly selected due to their previous genetic links to OCD and related disorders, and investigating the molecular pathology of OCD on a larger scale–i.e. the transcriptome or proteome.

2.4.4 Potential caveats

When interpreting this study, it is important to note several limitations. First, the sample size is small, with eight pairs of OCD and unaffected comparison subjects. In order to maximize our statistical power to detect differences related to brain region and OCD diagnosis, we have matched our subjects as closely as possible for factors that can affect expression of mRNA (e.g. age, sex, and RIN). No significant effects of these or other post mortem factors were observed in our cohort (Table 2-2). Other limitations include our current inability to rule out the possibility that comorbid diagnoses other than MDD (Fig.A-4; see Table 6) may be affecting mRNA expression due to a lack of statistical power. In particular, this dataset does not allow us to determine if comorbid anxiety disorders in subjects with OCD are contributing to the observed decreases in excitatory synaptic transcript expression. Future studies with a comparator group matched for anxiety disorders will be necessary to make this determination. Similarly, due to lack of power, we are limited in our ability to determine whether medications or other substances contribute to the observed differences in gene expression, although exploratory analyses did not identify any significant impact of antidepressant use, benzodiazepine use, or tobacco use at time of death in OCD subjects (Fig.A-2,A-3,A-5). It is also important to note that the use of targeted qPCR to conserve statistical power in our small sample prevented us from exploring whether subjects with OCD have different levels of expression of alternatively spliced transcripts compared

to unaffected subjects. Although the primary protein coding isoform was always amplified, primer pairs for several transcripts also amplified multiple splice variants (see Table A-4 for details). Our targeted qPCR approach was unable to determine if expression of these transcript variants differs by diagnosis or region. It is therefore possible that the observed excitatory transcript downregulation in orbitofrontal cortex could be accompanied by compensatory upregulation of alternative transcripts not studied here, which could limit the functional impact of the observed transcriptional changes and affect interpretation of our results. This possibility could be addressed in future studies using RNA sequencing (RNAseq). Finally, although some of the effects in Figures 2-1 to 2-3 would not survive Benjamini-Hochberg correction for multiple comparisons due to our limited sample size and power (see Table 7 for uncorrected and corrected *p*-values for all comparisons), this is mitigated by survival of the significant effects of the aggregate analysis following correction (Fig.2-4). Thus, the composite analysis demonstrates that differential expression of transcripts was most prominent in orbitofrontal regions in subjects with OCD.

Despite these potential caveats, this report is, to the authors' knowledge, the first identification of molecular dysfunction in either orbitofrontal or striatal brain regions in OCD. This targeted examination will therefore serve as the foundation for future better-powered studies that will allow us to examine the potential impact of comorbidities, medication status, and disease heterogeneity on expression of excitatory synaptic transcripts.

2.4.5 Acknowledgments

We would first like to thank the subjects and their families for the generous gift of brain donation. Tissue from some subjects was obtained from the NIH NeuroBioBank at the University of Pittsburgh Brain Tissue Donation Program. We would also like to thank Kelly Rogers for her

assistance with subject selection and tissue blocking, and Dr. Sue Johnston for her assistance with clinical assessments of post-mortem subjects. Funding support was provided by the Brain Research Foundation Fay and Frank Seed Grant (S.E.A, S.C.P.)

Table 2-1. Target transcripts and their reported involvement in OCD- and related disorders

[a]Transcript grouping used for calculation of composite measures (see **Methods**)

Gene	Transcript grouping[a]	Encoded protein function	OCD and OCD-related disorder references
DLGAP1	Excitatory structure	Post-synaptic scaffolding	Two SNPs located within *DLGAP1* with strong associations with OCD, though not genome wide significant(26)
DLGAP2	Excitatory structure	Post-synaptic scaffolding	Two SNPs (rs6558484 and rs7014992) associated with reduced white-matter volume in pediatric OCD(52)
DLGAP3	Excitatory structure	Post-synaptic scaffolding	*Dlgap3*(*Sapap3*)-knockout mice display compulsive grooming phenotype (Welch et al. 2007). In humans, *DLGAP3* mutations are associated with pathological grooming/ trichotillomania(44, 46)
DLGAP4	Excitatory structure	Post-synaptic scaffolding	N/A
SLITRK1	Excitatory structure	Transmembrane and signaling protein	Mutations associated with Tourette Syndrome(53) and trichotillomania(46)
SLITRK3	Excitatory structure	Transmembrane and signaling protein	SLITRK3 protein interacts with PTPRD, which harbors the OCD-associated SNP that is closest to genome-wide significance(19)
GRIA1	Excitatory receptors & transporters	Ionotropic AMPA receptor subunit	Two polymorphisms (rs707176 and rs2963944) associated with pediatric OCD(54)
GRIN2B	Excitatory receptors & transporters	Ionotropic NMDA receptor subunit	Positive association between 5072T/G polymorphism and OCD using a family-based design(22)
SLC1A1	Excitatory receptors & transporters	Neuronal glutamate transporter	Multiple variants associated with OCD(21-26)
SLC17A7	Excitatory receptors & transporters	Vesicular glutamate transporter	N/A
GABARAP	GABA synapse	GABA-receptor clustering in membrane	N/A
PVALB	GABA synapse	Calcium binding protein found in inhibitory interneurons	Reduction in transcript expression in DLPFC of OCD subjects and subjects with eating disorders(37)
CALB1	GABA synapse	Calcium binding protein found in inhibitory interneurons	N/A
GAD1	GABA synapse	GABA synthesizing enzyme	Down-regulation of *GAD1* transcript expression in caudate and putamen of Tourette Syndrome subjects(55)
GAD2	GABA synapse	GABA synthesizing enzyme	Significant association of two polymorphisms (rs8190748 and rs992990) in early-onset OCD(56)

Table 2-2. Summary of demographic and postmortem characteristics of human subjects.

Demographic and postmortem characteristics for 8 subjects with OCD and 8 unaffected comparison subjects. PMI: post-mortem interval. ATOD: at time of death. SD: standard deviation.

	COMPARISON SUBJECTS	**OCD SUBJECTS**	***STATISTICS***
Number of subjects (*n*)	8	8	
Sex (F/M)	4/4	4/4	
Mean age (±SD)	43.6 (14.9)	45.3 (14.9)	t_{14} =0.2, *p = 0.83*
Range	20-65	20-69	
PMI (±SD)	16.1 (5.1)	18.2 (7.8)	t_{14} =0.6, *p = 0.54*
Brain pH (±SD)	6.6 (0.2)	6.7 (0.2)	t_{14} =1.6, *p = 0.13*
RNA ratio	1.6 (0.2)	1.6 (0.2)	t_{14} =0.3, *p = 0.75*
RNA integrity number	7.8 (0.6)	7.9 (0.5)	t_{14} =0.2, *p = 0.87*
Suicide, *n* (%)	0 (0%)	3 (38%)	
Antidepressants ATOD, *n* (%)	0 (0%)	5 (63%)	

3.0 Functional analysis of orbitofrontal cortex and central striatal activity during compulsive behavior and following treatment

3.1 Introduction

Obsessive-compulsive disorder (OCD) is a chronic and debilitating psychiatric illness that affects between 2-3% of individuals worldwide. The World Health Organization (WHO) recently listed OCD as a leading cause of illness related disability (Ayuso-Mateos 2006), and it is the fourth most common psychiatric illness (Bloch et al. 2006). Adding to its disease burden, OCD is a chronic disorder that often begins in adolescence or early adulthood (Evans, Lewis, and Iobst 2004; Fitzgerald et al. 2011b). While its pathophysiology is still unknown, imaging studies consistently identify hyperactivity in key cortical and striatal brain regions– including OFC and caudate nucleus– in both pediatric (Fitzgerald et al. 2011b) and adult (Fitzgerald et al. 2011b; Menzies et al. 2008b) OCD patients. Additionally, not only are individual nodes within fronto-striatal circuitry hyperactive, some studies have shown increased functional connectivity between OFC and striatum, suggesting enhanced synchronization between these regions (Nakamae et al. 2014; Sakai et al. 2011; Harrison, Soriano-Mas, Pujol, Ortiz, Lopez-Sola, et al. 2009). Because of its consistent dysregulation, this orbitofronto-striatal network has been theorized to be an "OCD circuit" (Graybiel and Rauch 2000), and continues to be one of the most empirically well-supported circuit models in psychiatry (Gillan et al. 2015; Menzies et al. 2008b). Further supporting the role for this specific cortico-striatal circuit are data demonstrating that successful reduction in symptoms following treatment with the first-line pharmacotherapy of selective serotonin re-uptake inhibitors (SSRIs) is correlated with a reduction in hyperactivity in both the OFC and caudate nucleus of

OCD patients (Saxena et al. 1999; Benkelfat et al. 1990; Swedo et al. 1989). However, it is important to note that SSRI treatment response is quite poor in most subjects with OCD, with only between 10-15% of patients fully remitting following a full treatment course. These data highlight the need to investigate mechanisms by which SSRIs are acting and the specific scenarios in which they are working or failing.

Despite strong correlational evidence for functional alterations in cortical and striatal brain regions in OCD, a paucity of data exists demonstrating how these functional abnormalities may be generated, and how (if at all) they relate to compulsive behavior. In order to begin to answer this question, I have utilized a model system, the *Sapap3*-knockout (*Sapap3*-KO), that displays excellent validity for investigation of OCD-relevant behaviors according to established preclinical criteria (Chadman, Yang, and Crawley 2009). First, *Sapap3*-KO mice have good face validity, in that they display a compulsive grooming phenotype that, similar to what is observed in humans, persists even in the face of negative consequences as measured by the development of facial lesions (Welch et al. 2007b). Second, the *Sapap3*-KO model has good construct validity, with the compulsive behavioral phenotype being localized to the medial striatum (Welch et al. 2007b), as well as striatal hyperactivity (Burguiere et al. 2013). Importantly, cortico-striatal dysfunction is recapitulated in the model, with stimulation of lateral OFC (lOFC) inputs to the central striatum reducing the compulsive behavior as well as the striatal hyperactivity, likely through the entrainment of striatal fast spiking interneurons (FSIs) (Burguiere et al. 2013). Finally, the model also displays predictive validity, as treatment with the SSRI fluoxetine was capable of reducing compulsive grooming (Welch et al. 2007b), though the mechanism behind this reduction has not yet been explored.

Here, we propose that in *Sapap3*-KO mice central striatal hyperactivity is the result of a reduction of input from layer 5 lOFC pyramidal cells to the central striatum specifically at the onset of a grooming bout. Further, we predict that the SSRI fluoxetine will normalize the hyperactivity observed in the central striatum at grooming onset in *Sapap3*-KO mice and this be reflected by a reduction in the overall number of striatal SPNs activated during grooming. Completion of these experiments will shed new light on the circuit and network level generation of compulsive behavior.

3.2 Methods

3.2.1 Animals

All procedures were carried out in accordance with the guidelines for the care and use of laboratory animals from the NIH and with approval from the University of Pittsburgh Institutional Animal Care and Use Committee (IACUC). *Sapap3*-knockout (*Sapap3*-KO) and wildtype littermates were generated through breeding using *Sapap3* heterozygous mutants (*Sapap3*$^{+/-}$). Mice were maintained on a 100% C57BL/6 background. Male and female *Sapap3*-KO and wildtype littermates were used for all experiments. Mice in all cohorts were approximately 4-6 months old at the time of initial surgery. For lOFC experiments, 9 *Sapap3*-KO and 8 *Sapap3*-WT mice were used. For experiments in the central striatum, 11 *Sapap3*-KO and 8 *Sapap3*-WT mice were used (a subset of these containing 5 *Sapap3*-KO and 5 WT mice matched across days for fluoxetine experiments). For experiments using channelrhodopsin to stimulate cell bodies in the central striatum, wildtype C57BL/6 mice were used.

3.2.2 Stereotactic surgery

For all surgeries, mice were anesthetized using 5% isoflurane mixed with oxygen and maintained on 1-2% isoflurane for the duration of surgery. Mice were placed on a small-animal stereotactic instrument (Kopf Instruments) and secured using ear bars and a bite bar. Hair was removed from the dorsal surface of the head with hair clippers and the incision area was scrubbed with a betadine solution. A large incision was then made exposing the dorsal portion of the skull. All measurements were made relative to an interpolated bregma. Viral injections were performed using a fixed needle Hamilton syringe (Cole-Parmer Scientific, Vernon Hills IL, USA) connected to sterile polyethylene tubing affixed to a metal cannula and a Harvard Apparatus Pump 11 Elite Syringe Pump (Harvard Apparatus, Holliston MA, USA). Implanted lenses or ferrules were secured in place with one or two 0.45mm skull screws placed just in front of the lambdoid suture. Following completion of each surgery, mice were injected with sub cutaneous (s.c.) carprofen (10% w/v in 0.9% saline) and administered topical antibiotic ointment (TAO) and lidocaine around the headcap. Mice were then placed on a heating pad and given DietGel (ClearH_2O, Portland ME, USA) and monitored until they were fully recovered from anesthesia. Mice were administered carprofen s.c. and received lidocaine and TAO treatments for 3 days post-surgery. For all surgical procedures mice were kept group housed with littermates unless conspecific fighting was noted, in which case the aggressive mouse was isolated for the duration of the experiment.

3.2.2.1 Calcium imaging surgical methods

In calcium imaging experiments, all wildtype and *Sapap3*-KO mice underwent a series of two procedures, conducted according to (Resendez et al. 2016) with several minor changes. For experiments in the lOFC, 800nl of a virus encoding GCaMP6f under the synapsin promotor

(AAV5-synapsin-GCaMP6f-WPRE-SV40, titer $1.82x10^{12}$; Penn Vector Core) was injected into the lOFC (AP: +2.6, ML: -1.2, DV: -1.65) of mice. Immediately after injection of virus into the lOFC, a 500µm, 6mm length gradient refractive index lens (ProView GRIN lens, Inscopix Pala Alto, CA USA) was lowered just dorsal to the viral injection target (AP: +2.6, ML: -1.2, DV: -1.55) to allow for visualization of cells in the target region.

For experiments in the central striatum, 800nl of a virus encoding GCaMP6m under the synapsin promotor (AAV9-synapsin-GCaMP6m-WPRE-SV40, addgene) was injected into the central striatum (AP: +0.65, ML: -1.8, DV: -2.9 & -3.0) of mice. Injections were done in a two-step manner, with 400nl of virus injected at DV -2.9 and 400nl of virus injected at DV -3.0. Immediately after injection of virus into the central striatum, a 500µm, 6mm length gradient refractive index lens (ProView GRIN lens, Inscopix Pala Alto, CA USA) was lowered just dorsal to the viral injection target (AP: +0.65, ML: -1.8, DV: -2.85) to allow for visualization of cells in the target region. Acrylic dental cement (Lang Dental, Wheeling IL, USA) was then used to secure the lens in place and seal the entire lens during the virus incubation period (4-6 weeks).

For simultaneous optogenetic terminal stimulation and calcium imaging of the central striatum, 350nl of a virus encoding the redshifted opsin Chrimson under the synapsin promotor (AAV9-synapsin-ChrimsonR-tdT, addgene, titer: $2.23x10^{13}$) was first injected into the lOFC (AP: +2.7, ML: -1.55, DV: -1.65). Immediately after injection of Chrimson, a second skull window was drilled above the central striatum. As in our previous central striatal experiments, 800nl of a virus encoding GCaMP6m under the synapsin promotor (AAV9-synapsin-GCaMP6m-WPRE-SV40, addgene) was injected into the central striatum (AP: +0.65, ML: -1.8, DV: -2.9 & -3.0) and a 500µm, 6mm length gradient refractive index lens (ProView GRIN lens, Inscopix Pala Alto, CA USA) was lowered just dorsal to the viral injection target (AP: +0.65, ML: -1.8, DV: -2.85).

After 4-6 weeks for viral incubation, a second procedure was performed during which mice in each experiment were again anesthetized with isoflurane and secured to a stereotactic apparatus using ear cuffs. Using a Dremel, excess dental cement was carefully removed exposing the ProView GRIN lens. The top of the ProView lens was then cleaned with compressed air and lens paper, removing all dental cement dust. A magnetic microscope baseplate (Part ID:1050-002192, Inscopix) was then attached to the miniaturized microscope (nVistaHD 2.0 epifluorescence microscope or nVoke 1.0 epifluorescence microscope, Inscopix) and lowered into place above the GRIN lens with the 475nm blue LED gain and power set to their maximum. The optimal field of view was then determined by focusing on visible cells or other gross landmarks (blood vessels). Once an optimal field of view was obtained, the baseplate was cemented in place and a plastic Microscope Baseplate Cover (Part ID:1050-002193; Inscopix) was attached to prevent debris from blocking the lens.

3.2.2.2 Optogenetic activation of central striatum surgical methods

Wildtype C57BL/6 mice were injected bilaterally with either 500nl of a virus (University of North Carolina Vector Core Facility, viral titer ~$3.1x10^{12}$) encoding channelrhodopsin (AAV2-hsyn-ChR2-eYFP) or eYFP (AAV2-hysn-eYFP) into the central striatum (AP: +0.65, ML: -1.9, DV: -3.0). Immediately after bilateral injections, polished ceramic ferrules were placed over the viral injection holes (AP: +0.65, ML: -1.9) and lowered slowly into position above the viral injection target (DV: -2.65). A layer of Loctite (Loctite, Westlake OH, USA) and several layers of dental cement were then used to secure the two ferrules in place and mice were allowed to recover for 4 weeks of viral incubation.

3.2.3 Drug preparation and administration

(±)Fluoxetine hydrochloride (Fluoxetine) was obtained through the NIMH Chemical Synthesis and Drug Supply Program.

3.2.3.1 lOFC fluoxetine administration

For lOFC imaging experiments, fluoxetine was administered via drinking water according to established methods (Ahmari et al. 2013). Briefly, bottles were placed in each cage and drinking was monitored for 3 consecutive days. Based on the average daily consumption and the average weight of the mice in each cage, 18 mg/kg of fluoxetine hydrochloride was mixed with autoclaved drinking water and stored in black bottles to prevent degradation. Drinking was continually monitored weekly, and doses were adjusted as-needed to maintain an average dose of 18 mg/kg fluoxetine per cage. On average, each cage was given 40 mg fluoxetine / 250 ml of drinking water. Bottles were changed every 4 days to avoid any degradation of the fluoxetine. Body weight was monitored weekly. After 4 weeks of administration, fluoxetine was removed from cages and mice were given a two-week washout from the drug to monitor whether grooming behavior and neural activity differences returned to baseline levels.

3.2.3.2 Central striatum fluoxetine administration

For central striatum imaging, fluoxetine was administered intraperitoneally (i.p.) according to previous reports which report a reduction in *Sapap3*-KO grooming following treatment (Welch et al. 2007a). Fluoxetine hydrochloride (5 mg/kg) in a 0.9% saline solution (10 ml/kg) was injected i.p. daily for 7 days to WT and *Sapap3*-KO mice. Fluoxetine injections occurred between 4:00PM and 6:00PM daily while behavioral testing occurred beginning at 9:00AM on testing days. After 7

days of injections, mice were given a two-week washout from fluoxetine to monitor whether grooming behavior and neural activity differences returned to baseline levels.

3.2.4 Behavioral apparatus and assessment of grooming behavior

A custom-built behavioral apparatus was constructed for the accurate simultaneous assessment of spontaneous (e.g. grooming) behavior and neural activity (Fig.3-1A) via *in vivo* calcium imaging. A clear plexiglass sheet was suspended over a behavioral acquisition camera (Point Grey Blackfly, FLIR Integrated Imaging Solutions). A clear acrylic chamber (8”x8”x12”) was placed above the camera such that a mouse could be visualized at every angle. Behavioral acquisition was conducted at 40 Hz using SpinView (Point Grey) software and detailed frame information was sent directly to a central data acquisition box (LabJack U3-LV, Labjack Corporation, Lakewood CO USA). A randomly flashing (30s ITI) LED visible in the behavioral video controlled by custom scripts via an Arduino (Arduino Leonardo, Somerville MA, USA) and sending TTL pulses to the LabJack was used for alignment of behavior and calcium data.

Following acquisition, video was converted and compressed (maintaining accurate frame rate information) into .MP4 format using the open source software HandBrake. Videos were then imported into Noldus The Observer XT (Noldus, Leesburg VA, USA) and grooming behavior was scored frame by frame. Grooming behavior was scored according to previous reports (Kalueff et al. 2016) by an observer blind to experimental condition (genotype and drug treatment). A mouse was considered to be grooming if it engaged in any of the following behaviors (Fig.3-1B) 1) Facial grooming, when a mouse touches its face, whiskers, or head with its forepaws. 2) Body grooming, when a mouse licks its flank or its ventral surface. 3) Hind leg scratching, when a mouse uses one of its hind legs to scratch its flank. The beginning of a grooming bout was defined as the frame

when a mouse made a movement to begin grooming (e.g. a face grooming bout began the frame a mouse lifted its paw off the ground to touch its face). The end of a grooming bout was defined as the frame when a mouse ceased grooming (e.g. a body grooming bout ended when a mouse moved its snout from its flank). Grooming bout starts separated by less than one second were collapsed into the previous bout. Thus, the minimum amount of time possible between grooming bouts for all experiments was one second.

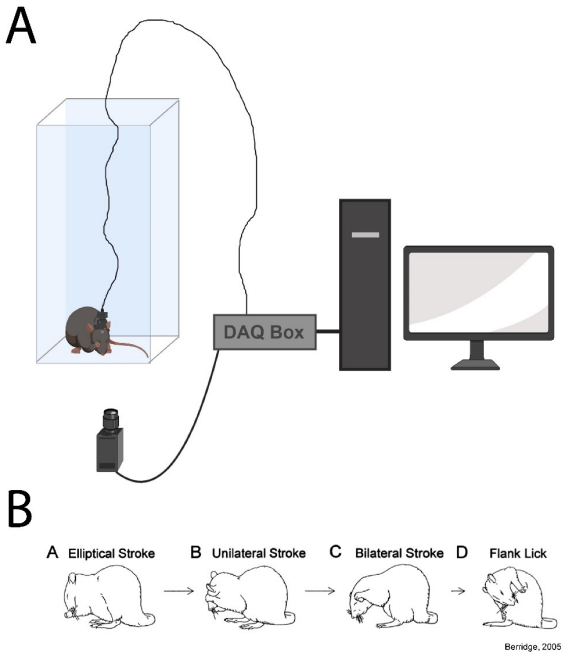

Figure 3-1. Pictoral example of grooming behavior and experimental setup

(**A**) Unfettered ability to engage in naturalistic behavior and the ability to accurately code this behavior was critical for completion of these experiments. In order to achieve this, mice were placed into a clear acrylic chamber with the microscope attached. Behavioral video was recorded from below and behavioral and calcium data was sent to a central data acquisition system. (**B**) Grooming behaviors were coded frame by frame at 40 Hz, according to established methods (modified from (Kalueff et al. 2016)).

3.2.5 *In vivo* calcium imaging in freely moving mice

After at least 1 week of recovery from baseplate surgery, mice were habituated to the attachment of the microscope. In order to attach the microscope securely to the baseplate, mice were lightly scruffed and the miniature nVistaHD 2.0 microscope was connected to the magnetic baseplate and secured with a set screw. During habituation, optimal focus, field of view, and LED power and gain settings were determined visually by assessing the presence of clearly defined putative neurons. A caliper was used to accurately measure the precise microscope focus such that multiple imaging sessions were conducted with the same field of view. In addition to habituation to the microscope, mice were also placed into the acrylic chamber under low light conditions for a period of 5-10 minutes once daily for three days prior to imaging.

Following habituation, mice were given a 40 minute baseline behavior and imaging session. Under low light the microscope was attached and mice were placed into a temporary holding cage. Mice were given 3-5 minutes after attachment of the scope for recovery from scruffing and to allow any rapid photobleaching to occur. After this period, mice were carefully placed into the clear acrylic chamber. LabJack data acquisition was then begun, immediately followed by behavioral SpinView recordings, and finally nVistaHD software began recording compressed greyscale tiff images at 20 Hz. As with the behavioral frame acquisition, individual calcium frame information was also sent to the LabJack for subsequent alignment of behavior and calcium data. For all mice, analog gain of the image sensor was set between 1 and 4 while the 470 nm LED power was set between 10 to 30% transmission range. These settings were kept consistent for each mouse throughout all subsequent imaging sessions.

3.2.6 Calcium imaging data processing

All imaging pre-processing was performed using Mosaic software (version 1.2.0, Inscopix) via custom Matlab (MATHWORKS, Natick MA, USA) scripts. Videos were spatially downsampled by a binning factor of 4 (16x spatial downsample) and temporally downsampled by a binning factor of 2 (down to 10 frames per second). Lateral brain motion was corrected using the registration engine TurboReg (Ghosh et al. 2011), which uses a single reference frame to match the XY positions of each frame throughout the video. Motion corrected 10 Hz video of raw calcium activity was then saved as a .TIFF and used for cell segmentation.

Using custom Matlab scripts, the motion corrected .TIFF video was then processed using the Constrained Non-negative Matrix Factorization approach (CNMFe), which has been optimized to isolate signals from individual putative neurons from microendoscopic imaging (Zhou et al. 2018). The CNMF method is able to simultaneously denoise, deconvolve, and demix imaging data (Pnevmatikakis et al. 2016) and represents an improvement over previously used algorithms based on principle component analysis (Zhou et al. 2018). The primary improvement comes from accurate estimation and subtraction of both local and global background fluorescence signal, providing better separation of densely packed cells and cleaner overall calcium signal from individual putative cells. Putative neurons were identified and manually sorted by an observer blind to genotype according to previously established criteria (Resendez et al. 2016). For the data presented in this dissertation, I report the non-denoised temporal traces (referred to as the "raw" trace in CNMFe) without any deconvolution. For each individual cell, the raw fluorescence trace was Z-scored to the average fluorescence and standard deviation of that same trace. Thus, fluorescence units presented here are referred to as "Z-scored fluorescence".

3.2.7 Calcium imaging analysis

Custom Matlab (MATHWORKS) scripts were used to conduct analysis of grooming-related calcium activity. Grooming behavior (state events) was exported as timestamps (grooming start and grooming stop) and aligned to Ca^{2+} time by recording 5 consecutive LED pulses (point events). The offset of Noldus behavior time to nVista Ca^{2+} time was then subtracted off leaving the same number of frames for both the behavior and Ca^{2+} fluorescence. Grooming timestamps were then transferred to a binary/continuous trace of the same length and sampling rate (10 Hz) as each Ca^{2+} trace via logical indexing (grooming = 1, not-grooming = 0). Timestamps for behavior are converted to the closest matching frame in the calcium recording (maximum error of one frame or ± 100ms at 10 Hz). Calcium activity could then be aligned to the start and end of a grooming bout, or the transition point between grooming bouts (≤ 1s between a grooming bout ending and a grooming bout beginning).

3.2.7.1 Unbiased event-related activity classification

In order to perform unbiased classification of an individual cells responsiveness (activated, inhibited, or unaffected) to a behavioral event (e.g. grooming onset) we adapted a strategy used in (Jimenez et al. 2018) using custom Matlab (MATHWORKS) scripts. First, each individual cell's raw Ca^{2+} was aligned to the onset of each grooming bout (Fig.3-2A). These traces were then averaged across all bouts within a given mouse (Fig.3-2B). For each individual cell, raw Ca^{2+} traces 10 seconds prior to grooming onset and 10 seconds after grooming onset (200 total samples at 10 Hz, 100ms per sample) were shuffled in time for each sample (200x) removing any temporal information that was previously in each trace but maintaining the variance within each grooming bout (Fig.3-2C). This shuffle was then performed 1000 times per cell to obtain a null distribution

of grooming associated Ca^{2+} activity. A cell was considered responsive to grooming onset if its Z-normalized Ca^{2+} fluorescence amplitude between -0.5s before grooming onset to 3s after grooming onset exceeded a 1 standard deviation threshold from the null distribution (Fig.3-2D).

Individual Ca^{2+} traces classified as activated or inhibited could then be averaged across genotype and directly compared within and across sessions, providing an assessment of how cells encoding grooming were different as a factor of genotype or drug treatment.

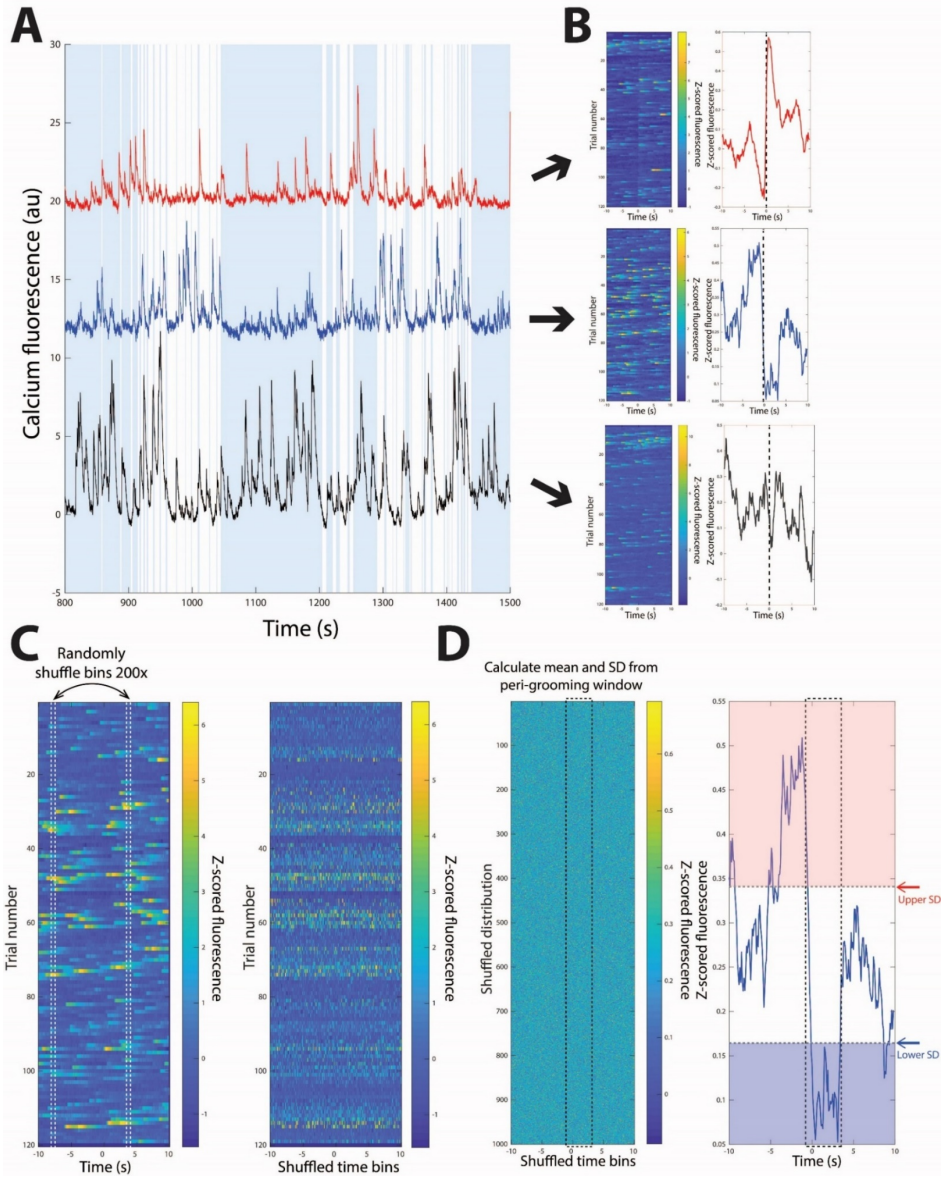

Figure 3-2. Schematic illustrating cell classification strategy.

Individual raw Ca^{2+} traces from three representative putative neurons were aligned to grooming (**A**) and averaged across all grooming bouts (**B**) in a given behavioral session. For each cell (representative example of the middle blue cell), each bin was randomly shuffled 200x (**C**, left) resulting in a shuffled trace with the same variance as the raw data (**C**, right). For each individual cell, this shuffle was then performed 1000 times, resulting in a null Ca^{2+} distribution (**D**, left). Ca^{2+} fluorescence amplitude of the average trace across grooming trials (**D**, right) was then compared to the null distribution, and cells that exceeded ±1 SD of the null distribution were classified as event modulated.

3.2.7.2 Accurate cell matching across sessions

Putative neurons were matched using a probabilistic modeling method detailed in (Sheintuch et al. 2017). The cell matching occurred across two sessions and was performed using the following steps. First, centroid location for all cells were projected onto a single image. Slight rotation and translation difference between sessions were adjusted to achieve maximal cross-correlation between sessions. Probablistic modeling was then employed to determine which model (centroid distance vs spatial correlation) was optimal for each set of data. For all data, the spatial correlation model yielded the best results and was thus used to match cells across sessions. For final alignment, the spatial correlation (not the joint model) was used, and correlation values for nearest neighbors was set at individually for each animal depending on the intersection of the two models.

3.2.7.3 Optogenetic activation of central striatal SPNs

For direct manipulation of SPNs in the central striatum WT mice we bilaterally activated the central striatum using channelrhodopsin (Boyden et al. 2005; Fenno, Yizhar, and Deisseroth 2011; Zhang, Wang, et al. 2007). Mice were habituated to experimenter handling for 1 week prior to 3 days of habituation to being plugged in to bilateral fiber optic adapter cables. During habituation, mice were plugged in and placed into a clear plexiglass chamber (8”x8”x12”) for 5 minutes under low light conditions. Immediately prior to the experimental day, both optical fibers were adjusted such that 5 mW of laser power was output at the tip of the fiber. Mice were connected again to bilateral fibers and placed into the same chamber attached to a bilateral commutator. Behavior was tracked via a camera (PointGrey) below the arena.

After a minute in the chamber, a pseudorandomized stimulation paradigm began controlled by custom Arduino (Arduino Leonardo, Somerville MA, USA) scripts (Fig.3-10B). Mice received

10s of constant 473 nm light stimulation with an average interpulse interval of 30s (range 25s to 35s). After 51 pulses of stimulation (35 minutes), the experiment terminated.

3.2.7.4 Optogenetic activation of lOFC terminals in central striatum

Simultaneous imaging and optogenetic experiments were carried out in the same manner as described in **3.2.5 Calcium imaging in freely moving mice**, with several minor changes. Stimulation of lOFC terminals was achieved through the delivery of 600nm amber light delivered through the objective lens as GCaMP-positive cells are simultaneously being excited with 460nm blue light (Stamatakis et al. 2018). After mice were placed into the chamber and calcium imaging began, the 600 nm optogenetic LED (OG-LED) was turned on. OG-LED stimulation consisted of 15 pulse trains of 20 Hz stimulation for 20 s. Each 20 Hz train was followed by a 30 s interval of no stimulation. Each session lasted 15 minutes in total.

3.2.8 Statistical analysis

Statistical analysis was carried out using custom Matlab scripts (MATHWORKS) or GraphPad Prism 8.0 (GraphPad Software, San Diego CA, USA). Throughout this dissertation results in text are reported as mean ± standard deviation (SD) and data presented on figures are mean ± standard error of measurement (SEM) unless otherwise noted.

3.2.8.1 Statistical analysis of grooming behavior

Baseline grooming behavior was analyzed using two-tailed independent samples *t*-tests. For the analysis of behavior following fluoxetine administration, a two-way repeated measures analysis of variance (ANOVA) was used. Main effects and interaction terms are reported

throughout, and in cases of significant interactions, post-hoc comparisons were made using Sidak's multiple comparison correction. A corrected alpha was set to 0.05.

3.2.8.2 Statistical analysis of calcium imaging data

In order to evaluate the effect of genotype and treatment on grooming evoked Ca^{2+} fluorescence averaged across individual cells, unpaired two-tailed *t*-tests were conducted at each time bin (100 ms). Due to our high *N* with dozens to hundreds of cells in each condition, a conservative Bonferroni correction was performed ($\alpha = \frac{0.05}{m}$). The critical *p* value ($\alpha = 0.05$) was divided by the total number of time bins (each bin = 100ms) to be compared (m), resulting in adjusted critical values between 0.000025 and 0.00005, depending on the exact comparison.

For comparison of proportions of classified cells during baseline imaging sessions, two-tailed independent samples *t*-tests were used. To assess the effect of fluoxetine treatment on the proportions of classified cells, two-way repeated measures ANOVA were used. When a significant interaction between genotype and drug treatment was observed, post-hoc tests were conducted using Sidak's multiple comparisons test. A corrected alpha was set to 0.05.

For nVoke activation of central striatal cells, the response for each cell to 20s of OG-LED stimulation was averaged across presentations (15 total presentations). This average was then compared with an unpaired *t*-test to the periods immediately preceding (10s before) and following (10s after) stimulation. A cell was determined to be significantly modulated if the $p \leq 5x10^{-45}$.

3.2.8.3 Statistical analysis of optogenetic data

In order to evaluate whether optogenetic stimulation of central striatal SPNs increased the probability that mice would engage in grooming-like behaviors, we conducted a two-way

ANOVA. Grooming probability data were first binned into 500ms increments (5 seconds before the onset of the laser to 20 seconds after laser onset), and all 50 bins were compared between eYFP and ChR2 mice. Post-hoc comparisons were made using the stringent Bonferroni multiple comparison test (corrected critical *p*-value of 0.001).

In order to evaluate whether optogenetic activation of lOFC terminals in the central striatum was capable of altering grooming probability in WT and KO mice, we conducted a one-way repeated measures ANOVA comparing grooming probability during a pre-stimulation period to a period during stimulation and post-stimulation. Post-hoc comparisons were made using Sidak's multiple comparisons test.

3.3 Results

3.3.1 *Sapap3*-knockout mice display compulsive grooming

Consistent with prior reports that relative to WT littermates, *Sapap3*-KO mice overgroom (Welch et al. 2007a), we observe that the compulsive phenotype is maintained following microendoscope implantation into the lOFC and attachment of the 2 gram miniature microscope (Fig.3-3A). Relative to WT counterparts, *Sapap3*-KO mice (purple bars) displayed increases in overall time spent grooming (Fig. 3-3B; $t(15) = 3.564$, $p = 0.0028$), total number of grooming bouts (Fig. 3-3C; $t(15) = 3.759$, $p = 0.0019$), and the number of transitions between grooming subtype per individual grooming bout, a measure of grooming microstructure organization (Fig. 3-3D; $t(15) = 3.840$, $p = 0.0016$).

We observe a qualitatively similar pattern of behavior in mice with GCaMP6m virus injections and implantations into the central striatum (Fig.3-3E). Relative to WT mice, *Sapap3*-KO mice (orange bars) spent more time grooming (Fig.3-3F; $t(18) = 3.508$, $p = 0.0025$), engaged in more individual grooming bouts (Fig3-3G; $t(18) = 2.556$, $p = 0.0199$), and made more transitions per bout (Fig.3-3H; $t(18) = 2.413$, $p = 0.0267$) relative to WT littermates.

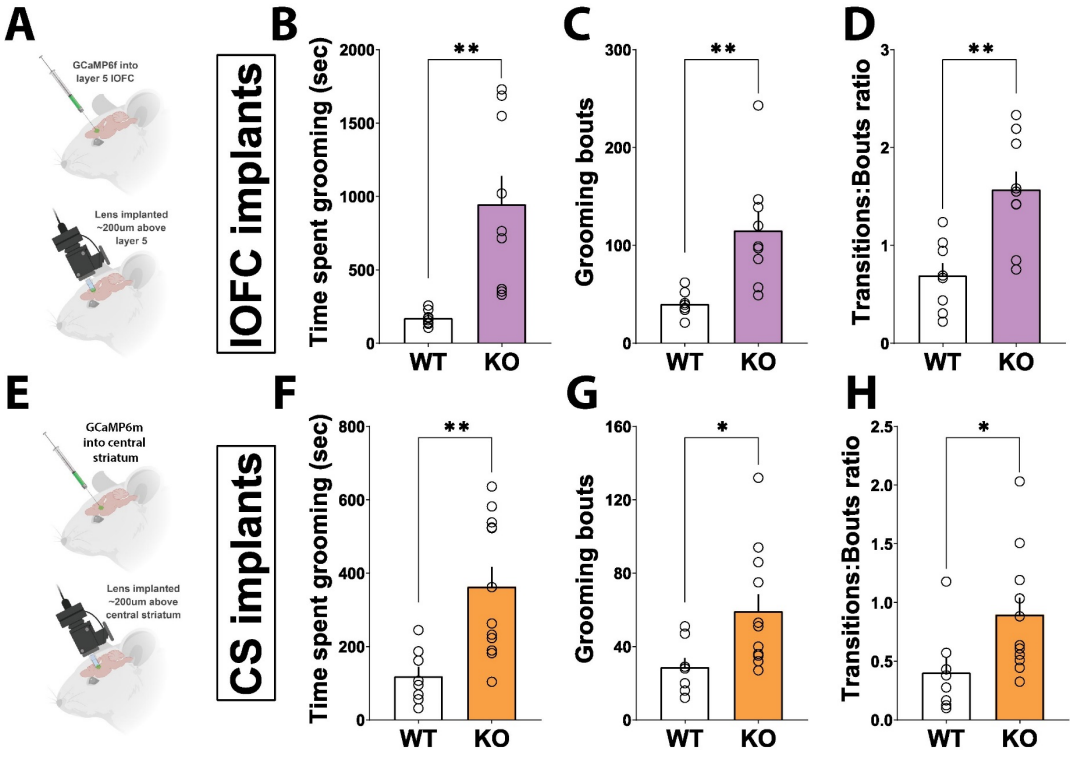

Figure 3-3. *Sapap3*-KO mice display compulsive grooming phenotype with miniature microscope attached.

(**A**) *Sapap3*-KO mice implanted with lenses in the lOFC (purple bars) spend more time during a 40 minute session grooming, (**B**) engage in more individual grooming bouts, and (**C**) make more transitions between grooming subtypes per individual grooming bout compared to WT littermate controls (**$p \leq .01$, * $p \leq .05$, $n = 8$ WT and 9 *Sapap3*-KO mice in lOFC, change to report stats in legend and means in text).

3.3.2 lOFC activity is reduced at grooming onset in *Sapap3*-KO mice

In order to evaluate whether lOFC activity in response to grooming was different in WTs and KOs, we injected GCaMP6f into the lOFC and placed a lens just above layer 5 of lOFC (Fig. 3-4A). Qualitative examination of heat plots across all cells in all mice (WT: 718 cells, average cells/mouse = 90 ± 41. KO: 1123 cells, 125 ± 30 average cells/mouse) appears to suggest more variability in response to grooming onset in WT mice relative to KOs (Fig.3-4B). In order to qualitatively evaluate the change in we examined differences in z-scored calcium fluorescence in the peri-grooming period (500ms before to 3000ms after grooming onset). Interestingly, we found that z-score calcium fluorescence during the peri-grooming period was significantly lower in KO mice relative to WT mice (Fig.3-4C; WT: 0.040 ± 0.4176 vs KO: 0.0075 ± 0.2623, $p = 0.020$ two-tail *t*-test) suggesting that activity in the lOFC is reduced at groom onset in KOs relative to WTs. This reduction appears to be specific to the onset of grooming and not present at baseline, as no changes in non-grooming calcium event rates were detected (data not shown). Indeed, when a mouse engaged in a grooming bout, we observed a significant increase in calcium event rate in WT mice calculated as a percentage change from non-grooming event rate with no change in KO mouse event rate during grooming (Fig.3-4D; WT: +22.28 ± 21.61%, KO: +1.667 ± 17.55%, $p = 0.0465$ two-tail *t*-test). Together, these data suggest that at baseline layer 5 lOFC pyramidal neurons are hypoactive in KOs relative to WTs at the onset of grooming.

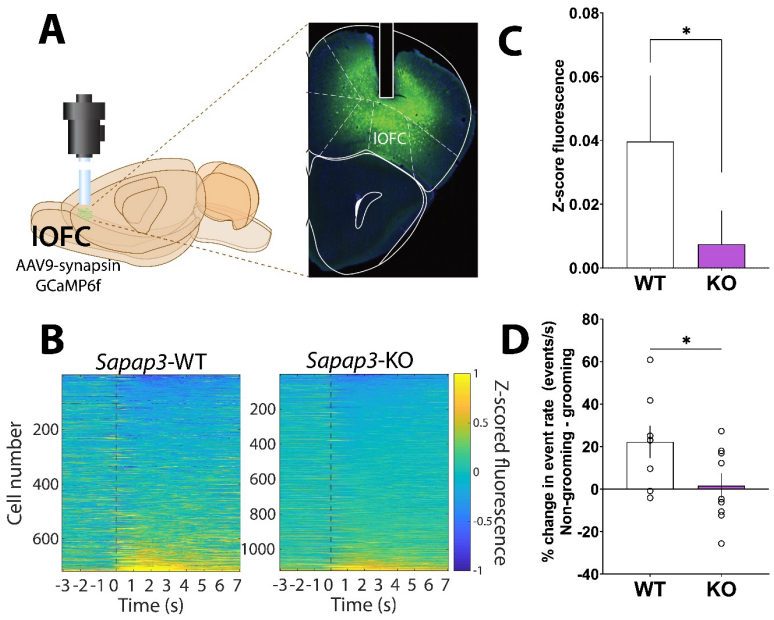

Figure 3-4. Grooming-onset associated activity is reduced in *Sapap3*-KO mice relative to WTs

(**A**) Representative histological image and surgery schematic showing GCaMP6f injection and expression as well as lens placement for imaging of layer 5 lOFC pyramidal neurons. (**B**) Heatplots of all cells aligned to the onset of a grooming bout in a WT (left) and *Sapap3*-KO mice (right). Cells are sorted by average peri-grooming fluorescence. (**C**) Z-score fluorescence during the peri-grooming period across all cells in WT and *Sapap3*-KO mice ($t(1025) = 2.340$, $p = 0.020$). (**D**) Percentage change in calcium event rate (event/s) from non-grooming rates to grooming rates ($t(15) = 2.170$, $p = 0.0465$). *$p \leq .05$, $n = 718$ WT cells and $n = 1123$ *Sapap3*-KO cells.

3.3.3 *Sapap3*-knockout mice have increased numbers of lOFC neurons activated at grooming onset relative to WT mice

Observing that overall lOFC activity was reduced at grooming onset in KO mice, we next set out to examine what might be contributing to this reduction. Given our single cell resolution, we classified putative pyramidal cells as either activated, inhibited, or unaffected by grooming (Jimenez et al. 2018). Comparing only units with significant increases in activity at grooming onset, we observed that, similar to overall lOFC output, activated cell amplitude in the KOs was reduced relative to WTs (Fig.3-5A top). Interestingly, the amplitude of significantly grooming

inhibited units was also blunted in KO mice compared to WT mice, which is inconsistent with the overall reduction in lOFC output we observed on average (Fig.3-4B).

In addition to evaluating amplitude differences, we can also test whether the number of cells categorized as significantly grooming modulated is also significantly changed. Based on our finding of reduced overall lOFC activity in KO mice, we predicted that significantly less cells would be classified as activated in WTs relative to KOs. Surprisingly, we found that there was no difference in the percentage of cells activated during grooming in WTs compared to KOs (Fig.3-5C; WT: 10 ± 7% vs KO: 12 ± 7%, $p = 0.5549$). Instead, we observed a significant increase in the percentage of cells that are inhibited during grooming onset in KOs relative to WTs (KO 17 ± 9% vs WT: 6 ± 6%, $p = 0.0086$). Thus, these data suggest that an overall reduction in lOFC activity is associated with an increase in the number of cells that are significantly inhibited during grooming in KO mice relative to WT mice. This may mean that downstream structures, including the striatum, are receiving reduced glutamatergic input from layer 5 lOFC pyramidal cells.

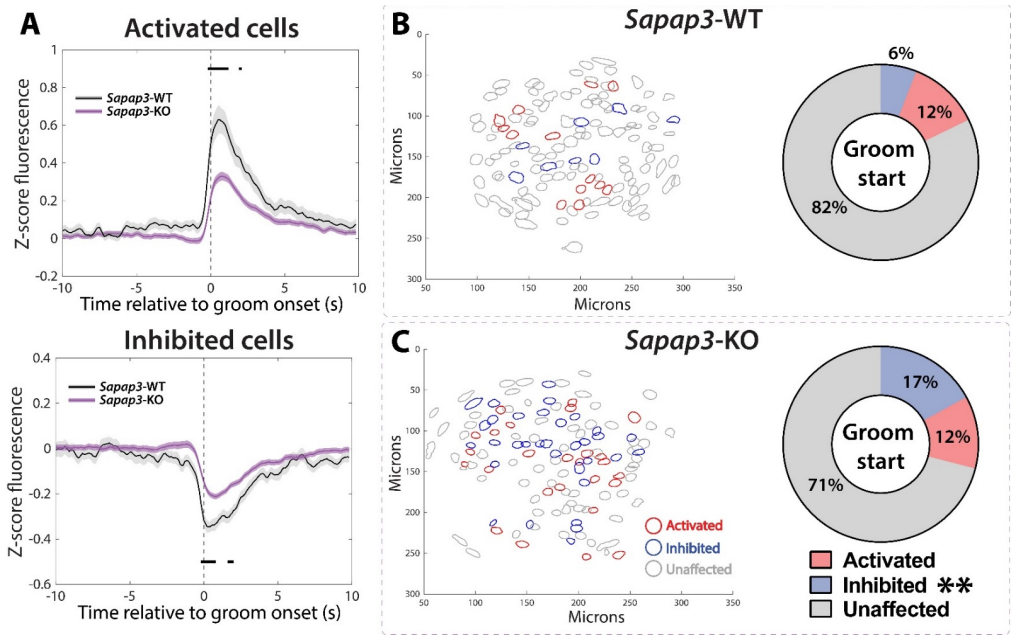

Figure 3-5. *Sapap3*-KO mice have more cells inhibited during grooming relative to WT mice.

(**A**) *Sapap3*-KO mice have reduced amplitude of cells activated during grooming (top; all significant $t \geq 5.20$, $p \leq 0.000046$) and cells inhibited during grooming (bottom; all significant $t \geq 4.191$, $p \leq 0.000041$) relative to WT mice. (**B**) Representative contour image of putative lOFC pyramidal neurons in a WT mouse (left) and the average proportion of cells responsive or non-responsive at grooming start (right). (**C**) Representative contour image of putative lOFC pyramidal neurons in a *Sapap3*-KO mouse (left) and the average proportion of cells activated ($t(15) = 0.6039$, $p = 0.5549$), inhibited ($t(15) = 3.020$, $p = 0.0086$), or non-responsive at grooming start (right) black bars indicate bins where $p \leq 0.00005$, $^{**}p \leq .01$, $n = 8$ WT and 9 *Sapap3*-KO mice).

It is important to note that the observed increase in the percent of inhibited cells identified at grooming onset in *Sapap3*-KO mice was not simply driven by the disparity in the number of grooming bouts KO and WT mice engage in. When the number of bouts was restricted to the mean of the WTs (40 randomly chosen grooming bouts), there was still a significant increase in the percentage of groom-start inhibited units in the KO mice relative to WT mice (Fig.3-6A; KO: 15.75 ± 9.18% vs WT: 5.75 ± 5.50%, $p = 0.0363$). Further, no changes were observed in WT cell classification, and no changes in the percentage of activated cells were observed as well ($p \geq 0.05$), with the absolute values of the averages being nearly identical to our previous analysis (Fig.3-5B).

Additionally, there was no correlation in KO mice between grooming bout number and the percentage of inhibited cells detected (Fig.3-6B; $R = 0.08$, $p = 0.84$). These data indicate that the increase in groom-onset inhibited cells observed in KOs is not simply an artefact of the genotype difference in grooming bouts.

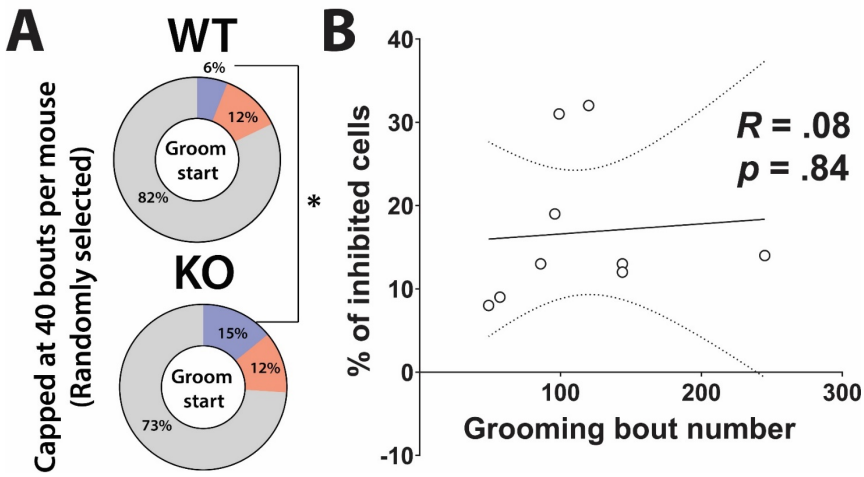

Figure 3-6. Groom-onset inhibited cell increase is not solely driven by increased bout number.

(**A**) Capping the number of grooming bouts (40 total bouts) for cell classification in KO mice still produces a significant elevation compared to groom-onset inhibited cells in WT mice ($t(15) = 2.299$, $p = 0.0363$). (**B**) No correlation between the percentage of inhibited cells and the number of grooming bouts in KOs ($R = 0.08$, $p = 0.84$) *$p \leq 0.05$, $n = 8$ WT and 9 KO mice.

3.3.4 Central striatal activity is increased at grooming onset

A major downstream target of layer 5 lOFC pyramidal neurons is the central striatum (Corbit et al. 2019). Given that cortical projection neurons synapse preferentially onto striatal fast spiking interneurons (Bennett and Bolam 1994; Berke 2011), and lOFC projections to central striatum have previously been shown to entrain striatal FSIs in *Sapap3*-KO mice (Burguiere et al. 2013), we predicted that central striatal activity would be transiently increased at grooming onset in KO mice compared to WT mice due to a lack of inhibitory tone from FSIs. In order to answer

this question, we recorded calcium signals from putative SPNs in the central striatum using GCaMP6m driven by a synapsin promotor (Fig.3-7A). When we analyzed activity across all putative SPNs in all mice, we found that, as predicted, central striatal activity around grooming onset was elevated significantly in KO mice compared to WT mice (Fig. 3-7B; significant epochs indicated by black bar). This transient increase in fluorescence in KO mice appears to be specific to the onset of grooming, as overall calcium event rates during non-grooming times across the session was not significantly different between WTs and KOs (Fig.3-7C left; WT: 0.1013 ± 0.021 vs, KO: 0.1128 ± 0.025 events/s). By contrast, event rates during grooming were significantly elevated in KO mice relative to WT mice (Fig.3-7C right; WT: 0.1071 ± 0.021 vs KO: 0.1381 ± 0.033 events/s). Further, we calculated the percentage change in calcium event rate from pre-grooming (-5 to 0s before grooming) immediately post-grooming (0 to 5s post groom) and found that KOs had a significantly elevated percentage change in calcium event rate compared to WTs (Fig.3-7D; WT: 6.623 ± 11.67% vs KO 19.02 ± 12.10%, two-tail *t*-test).

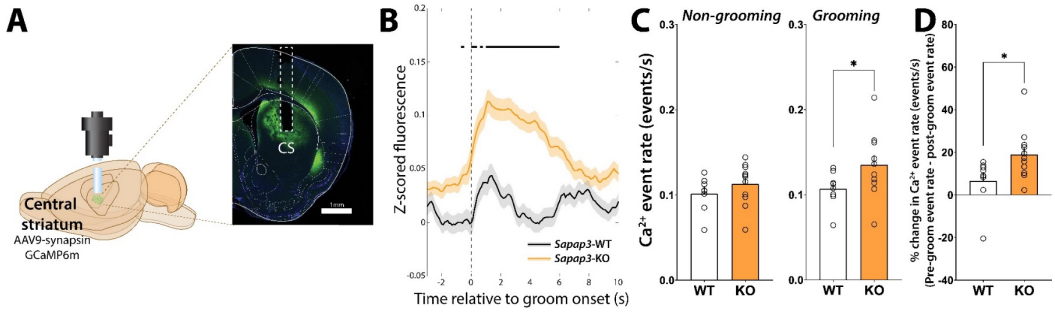

Figure 3-7. Central striatum is hyperactive at grooming onset in *Sapap3*-KO mice

(**A**) Schematized illustration of viral injection and lens placement into central striatum. Histological image of lens placement at GCaMP6m expression. (**B**) Z-scored calcium fluorescence at grooming onset (dashed line) in WT and *Sapap3*-KO mice (all significant $t(2577) \geq 4.1651$, $p \leq 0.0000321$, two-tail *t*-test). (**C** left) Calcium event rate during non-grooming time ($t(17) = 1.065$, $p = 0.3019$, two-tail *t* test) and during grooming times (**C**, right; $t(17) = 2.314$, $p = 0.0334$, two-tail *t*-test) in WT and *Sapap3*-KO mice. (**D**) Percentage change from pre-grooming calcium event rates to post-grooming calcium event rates (5s before and 5s after groom onset) in WT and *Sapap3*-KO mice ($t(17) = 2.237$, $p = 0.0390$, two-tail *t*-test). Bars indicate significance at $p \leq 0.00005$, $*p \leq 0.05$. $n = 8$ WT and 11 *Sapap3*-KO mice.

3.3.5 More SPNs are recruited at grooming onset in *Sapap3*-KO mice

Given our observation of overall increased central striatal activity in KO mice at grooming onset relative to WT mice, we wanted to investigate how such an increase may be generated. One possibility is that the amplitude of individual spiny projection neurons activated during grooming is increased in KO mice compared to WTs. Interestingly, we observe that this doesn't appear to be the case, with no significant differences in activated cell amplitude observed in the peri-grooming period between WTs and KOs (Fig. 3-8A; all epochs $t(356) \leq 3.6022$, all $p \geq 0.000360$). Similarly, hyperactivity could be manifest by a reduction in the amplitude of significantly inhibited units. We also do not observe this to be the case, with no difference in amplitude observed at any epoch around grooming onset (Fig. 3-8C; all epochs all $t(187) \leq 1.8394$, all $p \geq 0.0036$).

Interestingly, when we examined the numbers of activated and inhibited cells in each genotype, it was apparent that compared to WT mice (Fig.3-8B WT representative contour image) KO mice had many more putative SPNs that were transiently activated at grooming onset (Fig.3-8D KO representative contour image). Looking at all cells across all mice (Fig.3-8B right, we find a significant increase in the percentage of cells activated in KO mice (19.63 ± 5.80% activated) compared to WT mice (9.34 ± 3.02% inhibited, two-tail *t*-test). No changes were observed in the percentage of significantly inhibited during grooming in WTs compared to KOs (WT: 5.30 ± 3.04% vs KO: 8.80 ± 4.40%, two-tail *t*-test) Together, these data suggest that hyperactivity in the central striatum of KO mice is manifest through an increase in the numbers of cells activated during

grooming, not by changes in amplitude of individual units that are significantly modulated by the behavior.

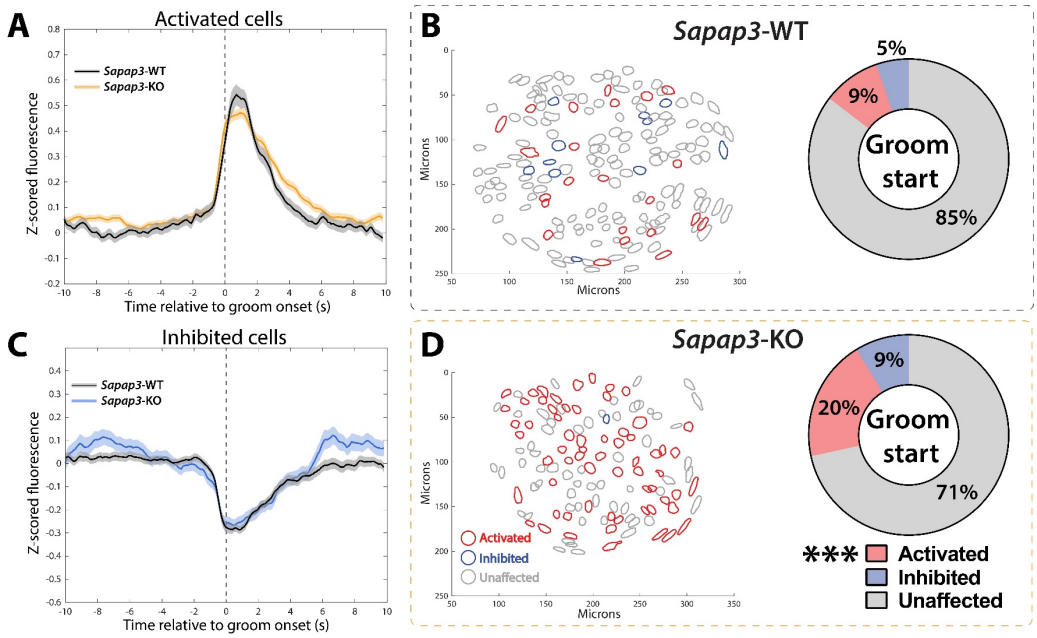

Figure 3-8. Greater percentage of SPNs are active at groom onset in *Sapap3*-KO mice

(**A**) Average amplitude of significantly groom onset activated units in WT and *Sapap3*-KO mice (all $t(356) \leq 3.6022$, all $p \geq 0.000360$). (**C**) Average amplitude of significantly groom onset inhibited units in WT and *Sapap3*-KO mice (all $t(187) \leq 1.8394$, all $p \geq 0.0036$). (**B-D**) contour images of representative WT (top) and *Sapap3*-KO (bottom) mouse during a baseline grooming session. Average percentage of cells identified as activated ($t(17) = 4.577$, $p = 0.0003$, two-tail *t*-test), inhibited ($t(17) = 1.927$, $p = 0.0708$, two tail *t*-test), or unaffected in WT and *Sapap3*-mice. ***$p \leq 0.001$.

As in the lOFC, we wanted to ensure the observed increase in activated cells was not simply due to the basal genotype difference in the number of grooming bouts engaged in. In order to do this, we limited the number of KO grooming bouts to the average of the WTs (30 randomly selected grooming bouts) and examined whether this altered the percentages of grooming-modulated cells (Fig.3-9A). As in the lOFC, we did not observe any significant change in the percentages of cells classified as grooming onset activated, inhibited, or unaffected in KO mice when restricting the number of bouts to 30 (all $t(10) > 1.542$, $p > 0.05$, paired *t*-test). As was the case when we considered all bouts, a significant difference was observed in the percentage of grooming-onset

activated cells in KOs restricted to 30 bouts and WT mice (Fig.3-9A; WT: 9.4 ± 3.02% activated vs. KO: 16.43 ± 6.53 activated, $p = 0.0113$, two-tail *t*-test). Further, no significant correlation was observed between grooming bout number and the percentage of activated cells identified in KO mice (Fig.3-9B; $R = 0.07$, $p = 0.83$, two-tailed Pearson *R*). Together, these data suggest that the increase in the percentage of cells activated during grooming in KO mice is a biological phenomenon and not an artefact of an increase in grooming bouts.

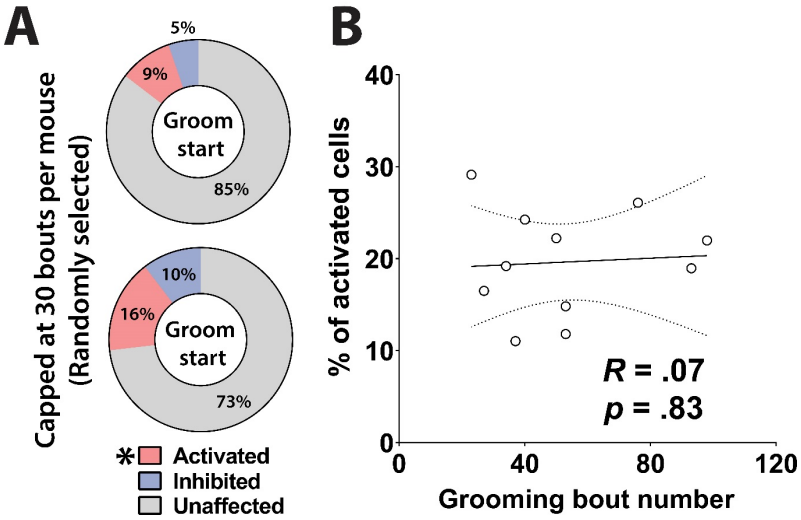

Figure 3-9. Groom-onset activated SPN increase is not an artefact of bout number

(**A**) Percentages of cells activated ($t(17) = 4.577$, $p = 0.0003$, two-tail *t*-test), inhibited ($t(17) = 1.927$, $p = 0.07$, two-tail *t*-test), and unaffected at grooming onset in WT and *Sapap3*-KO mice. (**B**) Correlation between grooming bout number and the percentage of activated cells in *Sapap3*-KO mice ($R = 0.07$, $p = 0.83$, Pearson's *R*). *$p \leq 0.05$.

3.3.6 Optogenetic activation of central striatal SPNs produces grooming-like behavior in WT mice

Our data thus far suggest that a transient increase in central striatal activity, produced by an overall increase in the number of activated SPNs, occurs at the onset of compulsive grooming in KO mice. In order to evaluate whether we could recapitulate grooming behavior via direct activation of central striatal cell bodies, we injected WT mice bilaterally with AAV5-synapsin-

ChR2 or an eYFP control virus and implanted fibers just dorsal to viral injections (Fig. 3-10A-B). Optogenetic stimulation of CS cells was delivered for 10s in a pseudorandom fashion (constant 473nm stimulation), with an average interpulse interval of 30s (Fig. 3-10C). When we plotted the probability that a mouse would groom at a given time bin (500ms bins) and examined the peri-stimulus period, we observed a robust increase in the probability that ChR2 mice would engage in a grooming-related movement (flank-licking, elliptical stroke movement, see Fig.3-1A) only during active stimulation (Fig. 3-10C; all $t(650) \geq 3.961$, $p \leq 0.0041$, Bonferroni's multiple comparisons test). By contrast, there was no change in the probability of engaging in a grooming-like movement during laser stimulation in eYFP mice. Examining only ChR2+ mice (Fig.3-10D) indicates that most mice displayed a robust increase in grooming-related movement probability immediately at the onset of stimulation on most laser pulse trials.

Importantly, the increase in grooming-related movement probability occurred immediately at the onset of laser stimulation in ChR2 mice, mirroring our finding of a transient increase in CS activity at the onset of grooming in KO mice. These data suggest that driving activity of CS cells is sufficient to produce grooming-related behaviors in WT mice.

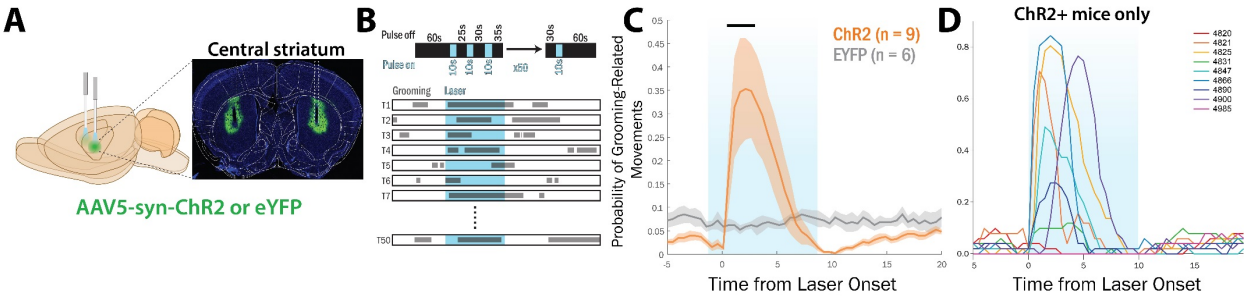

Figure 3-10. Optogenetic activation of the central striatum produces grooming-related movements

(**A**) Mice were bilaterally injected with either AAV5-syn-eYFP (n = 6) or AAV5-syn-ChR2 (n = 9) and implanted with fiber optic ferrules just above injection site in the central striatum. Representative histological image of virus and fiber placements (right). (**B**) Schematic illustration of stimulation paradigm and subsequent behavioral analysis strategy. Laser on times indicated in blue (**C**). Probability of engaging in a grooming-related movement in ChR2 and eYFP mice in response to laser onset (shaded blue) (main effect$_{virus}$: $F(1,13) = 0.3280$, $p = 0.5766$, main effect$_{stimulation\ time}$: $F(49,637) = 3.589$, $p = 0.0001$, interaction$_{virus\ x\ stimulation\ time}$: $F(49, 637) = 4.189$, $p = 0.0001$) (**D**) Individual ChR2+ mouse probability of engaging in a grooming related movement in response to laser stimulation (shaded blue). Black bar indicates $p \leq .001$ with Bonferroni correction).

3.3.7 Fluoxetine treatment reduces compulsive grooming in *Sapap3*-KO mice

Fluoxetine (Prozac) is the first line treatment for OCD, though its effects *in vivo* on the physiology of neurons in either the lOFC or striatum, two of the most commonly linked regions to OCD, are mostly unknown. Previously, it has been demonstrated that a week of fluoxetine administration was capable of reducing compulsive grooming behavior in *Sapap3*-KO mice, though the mechanism of this reduction remains unclear (Welch et al. 2007b). Behaviorally, we see that fluoxetine is indeed capable of reducing compulsive grooming in mice with miniature microscopes attached. After 4 weeks of 20 mg/kg fluoxetine treatment in drinking water, lOFC implanted KO mice spent significantly less time grooming ($t(14) = 4.491$, $p = 0.001$, Sidak's test), engaged in less grooming bouts ($t(14) = 6.758$, $p = 0.0001$, Sidak's test), without any change in the number of transitions made between grooming subtypes per bout ($t(14) = 1.976$, $p =$

0.1317, Sidak's test) relative to WT mice (Fig.3-11A-C). These data suggest that chronic administration of fluoxetine was capable of reducing compulsive behavior in KO mice without affecting WT behavior (all $t \leq 1.791$, all $p \geq 0.1809$).

Sub-chronic (7 days) administration of 5 mg/kg fluoxetine i.p., which has previously been validated in KO mice (Welch et al. 2007b), produced qualitatively very similar reductions in grooming to 4-week treatment in drinking water (Fig.3-11D-G. Compared to WT mice, KO mice spent significantly less time grooming ($t(8) = 5.584$, $p = 0.0010$, Sidak's test), engaged in less grooming bouts ($t(8) = 2.633$, $p = 0.0592$, Sidak's test), and a significant reduction in transitions:bouts ratio ($t(8) = 2.917$, $p = 0.0384$, Sidak's test). Again, WT behavior was unaffected by fluoxetine administration (all $t(8) \leq 1.030$, $p \geq 0.5551$). Combined, our data suggest that two different fluoxetine doses and treatment regimens result in qualitatively similar reductions in compulsive grooming in KO mice.

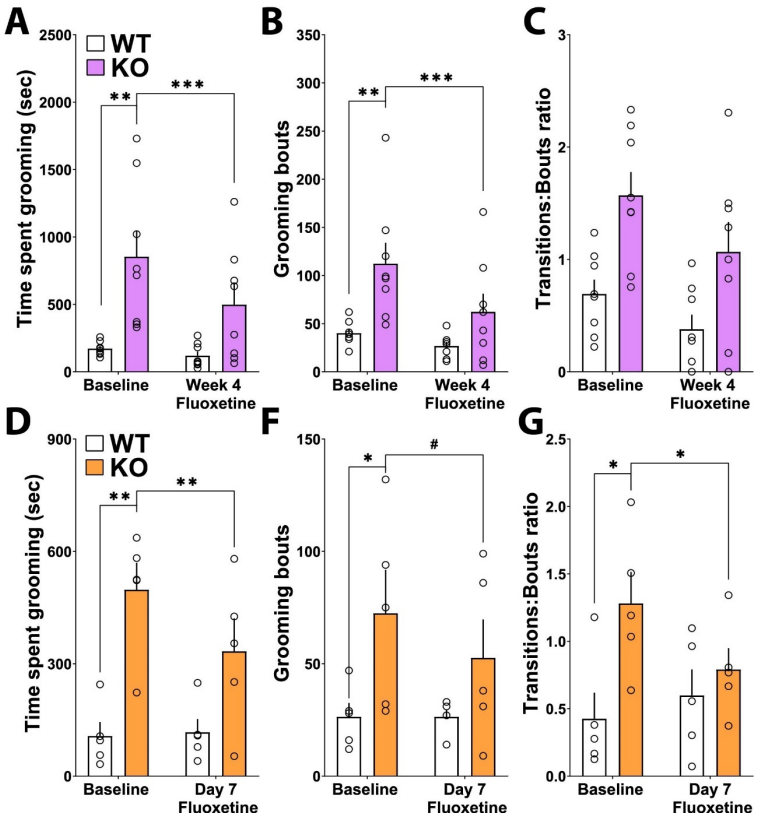

Figure 3-11. Fluoxetine reduces compulsive grooming in *Sapap3*-KO mice

(**A**) Effects of 4 weeks fluoxetine treatment in lOFC implanted mice on time spent grooming (main effect$_{genotype}$: $F(1,14) = 10.33$, $p = 0.0063$, main effect$_{treatment}$: $F(1,14) = 13.29$, $p = 0.0026$, interaction$_{genotype\ x\ treatment}$: $F(1,14) = 7.318$, $p = 0.0171$) (**B**) number of grooming bouts engaged in (main effect$_{genotype}$: $F(1,14) = 7.127$, $p = 0.0183$, main effect$_{treatment}$: $F(1,14) = 36.54$, $p = 0.0001$, interaction$_{genotype\ x\ treatment}$: $F(1,14) = 12.33$, $p = 0.0035$) and (**C**) transition:bouts ratio (main effect$_{genotype}$: $F(1,14) = 15.02$, $p = 0.0017$, main effect$_{treatment}$: $F(1,14) = 5.151$, $p = 0.0396$, interaction$_{genotype\ x\ treatment}$: $F(1,14) = 0.2758$, $p = 0.6077$). (**D**) Effects of 7 days fluoxetine treatment in CS implanted mice on time spent grooming grooming (main effect$_{genotype}$: $F(1,8) = 12.55$, $p = 0.0076$, main effect$_{treatment}$: $F(1,8) = 13.71$, $p = 0.0060$, interaction$_{genotype\ x\ treatment}$: $F(1,14) = 17.59$, $p = 0.0030$) (**E**) number of grooming bouts engaged in (main effect$_{genotype}$: $F(1,8) = 3.941$, $p = 0.0824$, main effect$_{treatment}$: $F(1,8) = 3.465$, $p = 0.0997$, interaction$_{genotype\ x\ treatment}$: $F(1,8) = 3.465$, $p = 0.0997$) and (**F**) transitions:bouts ratio (main effect$_{genotype}$: $F(1,8) = 4.343$, $p = 0.0707$, main effect$_{treatment}$: $F(1,8) = 1.781$, $p = 0.2188$, interaction$_{genotype\ x\ treatment}$: $F(1,8) = 7.793$, $p = 0.0235$). ***$p < 0.001$, **$p < 0.01$, **$p < 0.05$.

3.3.8 Neurons are accurately matched across days

Putative pyramidal neurons in lOFC and SPNs in the central striatum were aligned across sessions using the recently developed CellReg algorithm (Sheintuch et al. 2017). Overall alignment across sessions was quite accurate, with stringent spatial correlations cutoffs set individually for each mouse (average $R = 0.78$). This yielded an average in all mice of 59% of cells tracked across sessions (Fig.3-12B). Model accuracy was assessed by examining the intersection of the model estimating the probability nearby cells were the same ($prob_{same}$) and the model estimating nearby cells were different ($prob_{different}$). No differences were identified across genotypes in lOFC implanted mice in the accuracy of cell matching ($p > 0.05$), and the $Prob_{same}$ average was above 0.85 for both groups (Fig.3-12C). Similarly, no changes were observed in central striatal imaged mice on the accuracy of cell matching ($p \geq 0.05$) and the $probability_{same}$ average across genotypes was above 0.90 (Fig.3-12D). These data suggest that on average across all mice in both regions, cell matching across sessions (4 weeks in the lOFC and one week in the CS) was both highly accurate and highly specific.

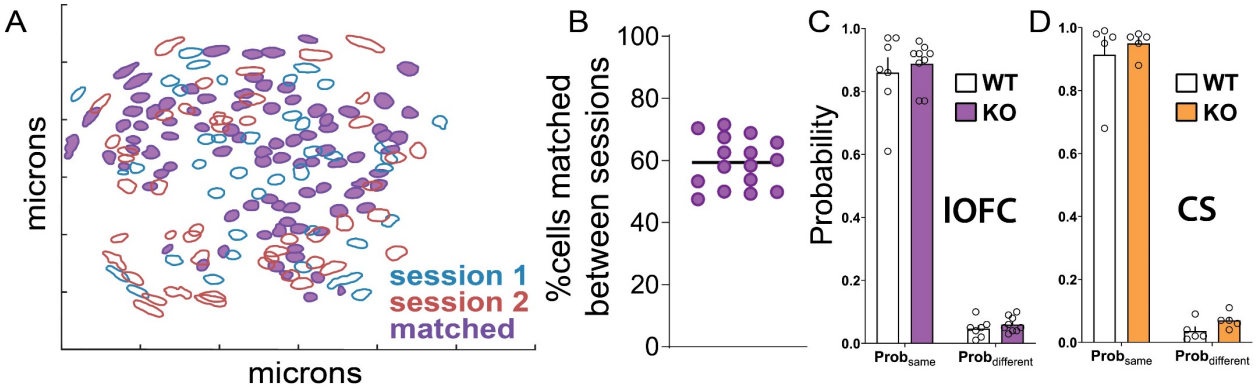

Figure 3-12. Putative neurons are accurately matched across two sessions.

(**A**) Representative contour image from two sessions (blue and red) recording calcium signals of putative lOFC pyramidal neurons. Cells matched across session colored in purple. (**B**) Percentage of cells successfully matched across sessions for lOFC implanted mice (n = 16, $mean_{cells}$ = 59.32%, $range_{cells}$ = 47.5% to 71.5%). (**C**) No differences in genotype for the probability that cells would be classified as the same unit across sessions in lOFC ($prob_{same}$ WT mean = 0.86 ±.13; $prob_{diff}$ WT mean = 0.047 ±.029; $prob_{same}$ KO mean = 0.88 ±.07; $prob_{diff}$ KO mean = 0.06 ±.02). (**D**) No differences in genotype for the probability that cells would be classified as the same unit across sessions in central striatum ($prob_{same}$ WT mean = 0.91 ±.13; $prob_{diff}$ WT mean = 0.036 ±.032; $prob_{same}$ KO mean = 0.95 ±.041; $prob_{diff}$ KO mean = 0.07 ±.025).

3.3.9 Fluoxetine reduces the number of inhibited cells in *Sapap3*-KO mice

We next investigated whether chronic administration of fluoxetine in drinking water was capable of reducing the neural correlate of compulsive grooming, chiefly the increase in the percentage of cells inhibited in the lOFC at grooming onset in KO mice. Using our accurate cell matching across 4 weeks of fluoxetine treatment (Fig.3-13A-B) we are able to assess how cells change their response to the onset of grooming. On average, after 4 weeks of fluoxetine KO mice had significantly fewer grooming-onset inhibited units compared to their baseline session (Fig.3-13C; $KO_{baseline}$: 17 ± 9% vs. $KO_{week\ 4\ FLX}$: 9 ± 7% inhibited, $t(15) = 4.012$, $p = 0.0023$, Sidak's test). By contrast, no changes were observed in the percentage of cells activated at grooming onset in KO mice after fluoxetine treatment ($KO_{baseline}$: 12 ± 7% vs. $KO_{week\ 4\ FLX}$: 11 ± 5% activated, $t(15)$

= 0.5287, $p = 0.8438$, Sidak's test). Fluoxetine had no significant effect on the percentages of cells modulated by grooming onset in WT mice (all $t(15) \leq 0.5551$, $p \geq 0.8294$, Sidak's test). Comparing the amplitude of inhibited cell signal between cells identified as inhibited during the baseline session, and the amplitude from those same cells 4 weeks later reveals a significant increase in the average signal in KO mice (Fig.3-13D; all $t(220) = 4.4214$, $p = 0.0000154$, two-tail *t*-test).

We next sought to assess how this reduction in amplitude was generated by examining how the classification of individual cells changed as a function of fluoxetine treatment. Interestingly, a similar proportion of cells in both WTs and KOs that were classified as activated during the baseline session became unaffected after 4 weeks of fluoxetine treatment (Fig.3-13F; WT: 6.17 ± 2.85% vs. KO: 8.09 ± 6.21%, $t(26) = 0.7505$, $p = 0.7081$, Sidak's test). By comparison, a significantly greater percentage of cells in KO mice changed their classification from inhibited at baseline to unaffected after fluoxetine treatment (WT: 4.76 ± 4.20% vs. KO: 13.02 ± 4.67%, $t(26) = 3.234$, $p = 0.0066$, Sidak's test). While overall cells in both genotypes exhibited diverse responses to 4 weeks of fluoxetine treatment (Fig.3-13G), of all 9 possible outcomes for a cell the only significant difference between WTs and KOs was an increase in the percentage of cells that changed from inhibited at baseline to unaffected after fluoxetine (all other $p \geq 0.22$). Together, these data suggest that fluoxetine may be acting on specific ensembles of cells that reduced their activity at grooming onset in KO mice and attenuating this reduction, possibly leading to an overall increase in lOFC activity at grooming onset.

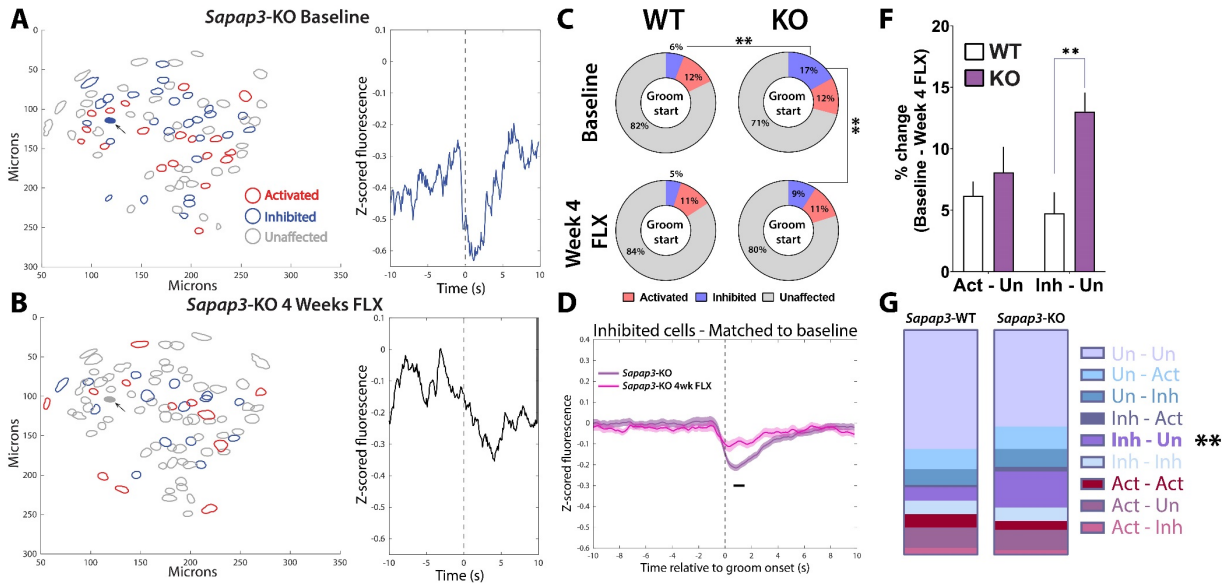

Figure 3-13. Fluoxetine reduces the percentage of cells inhibited during grooming in *Sapap3*-KO mice.

(**A-B**) Representative contour image of a *Sapap3*-KO mouse at baseline and after 4 weeks of fluoxetine treatment. Example trace averaged across grooming bouts of a strongly inhibited cell at baseline (right) and after 4 weeks of fluoxetine where the cell is categories as unaffected (cell indicated by black arrow). (**C**) Effect of 4 weeks fluoxetine on inhibited cell percentages in KOs and WTs (main effect$_{genotype}$: $F(1,15) = 6.916$, $p = 0.0189$. main effect$_{treatment}$: $F(1,15) = 9.963$, $p = 0.0065$. interaction$_{genotype\ x\ treatment}$: $F(1,15) = 5.516$, $p = 0.033$, 2-way repeated measures ANOVA). No effect of either gentype or treatment on activated cell percentages (all $F(1,15) \leq 0.2205$, all $p \geq 0.6454$). (**D**) Change in amplitude of cells previously identifed as inhibited at baseline in *Sapap3*-KO mice after 4 weeks of fluoxetine treatment (all $t(220) = 4.4214$, $p = 0.0000154$, two-tail *t*-test) in response to grooming onset (dashed line). (**E**) Effect of fluoxetine on the overall change from baseline in the percentage of inhibited cells detected in WT and KO mice ($t(13) = 2.412$, $p = 0.040$, two-tailed *t*-test). (**F**) Effect of fluoxetine on the overall change from baseline in the percentage of activated cells detected in WT and KO mice ($t(13) = 0.4924$, $p = 0.6306$, two-tailed *t*-test). (**G**) Breakdown of cell classification changes following fluoxetine in WT and KO mice, change from inhibited$_{baseline}$ to unaffected$_{week\ 4}$ ($t(13) = 3.494$, $p = 0.0040$. all other possibilities $p \geq 0.05$). Black bar indicates $p \leq 0.00005$, $^{**}p < 0.01$, $^{*}p < 0.05$.

3.3.10 Fluoxetine reduces the percentage of SPNs activated during grooming in *Sapap3*-KO mice

Given the reduction in the number of putative lOFC pyramidal cells inhibited at grooming onset in KO mice after 4 weeks of fluoxetine administration, we next wanted to evaluate whether this produced an increased drive to the central striatum and perhaps an overall reduction in the number of cells activated at the onset of compulsive behavior. Through our accurate cell matching, we are able to assess how individual SPNs change their responsiveness after fluoxetine treatment. Qualitatively, we observe that in KO mice there appears to be a reduction in the number of cells that are classified as activated after 7 days of fluoxetine treatment (Fig.3-14A-B), with cells that were activated at baseline no longer displaying a transient increase in activity at grooming onset following fluoxetine treatment. We also find that after 7 days of fluoxetine treatment (Fig.3-14C), there is a reduction in the percentage of grooming-onset activated SPNs in KO mice relative to their baseline ($KO_{baseline}$: 26.13 ± 5.76% vs. $KO_{day\ 7\ FLX}$: 15.32 ± 8.97%, $t(8) = 3.016$, $p = 0.033$ Sidak's multiple comparisons test) with no significant change in WT mice ($WT_{baseline}$: 9.92 ± 4.36% vs. $WT_{day\ 7\ FLX}$: 6.57 ± 3.80%, $t(8) = 0.933$, $p = 0.612$, Sidak's multiple comparisons test). No changes were observed following fluoxetine treatment in the percentages of cells classified as inhibited (all $t \leq 0.69$, $p \geq 0.76$). Further, we found that compared to WT mice (Fig.3-14D), KO mice had a significantly greater proportion of cells change from activated at baseline to unaffected after 7 days of fluoxetine treatment relative to WT mice (WT: 9.27 ± 4.43% vs. KO: 19.2 ± 7.21%, $t(8) = 2.62$, $p = 0.031$, unpaired *t*-test) as well as a trend toward an increase in the percentage of cells that shifted from activated to inhibited (WT: 0.227 ± 0.508% vs. KO 1.86 ± 1.66%, $t(8) = 2.11$, $p = 0.068$, unpaired *t*-test). It is worth noting that there was also a significant increase in the percentage of cells that changed classification from unaffected to inhibited in KO mice after 7 days

of fluoxetine relative to WTs (WT: 4.57 ± 2.82 vs. KO: 10.9 ± 4.30%, $t(8) = 2.77$, $p = 0.024$, unpaired *t*-test), suggesting that perhaps a shift away from a compulsive network of activated units occurred. Finally, we found that the percentage change in calcium event rates from pre- to post-grooming was reduced in KO mice after 7 days of fluoxetine treatment (Fig.3-14E; $KO_{baseline}$: 26.95 ± 11.99 vs. $KO_{day\ 7\ FLX}$: 10.30 ± 5.12%, $t(8) = 2.92$, $p = 0.045$, Sidak's multiple comparison test). No changes were observed in WT mice ($WT_{baseline}$: 15.24 ± 6.72% vs. $WT_{day\ 7\ FLX}$: 7.74 ± 9.92%). These data suggest that fluoxetine may be effective at reducing overall striatal hyperactivity by reducing ensembles of grooming-onset activated units in *Sapap3*-KO mice.

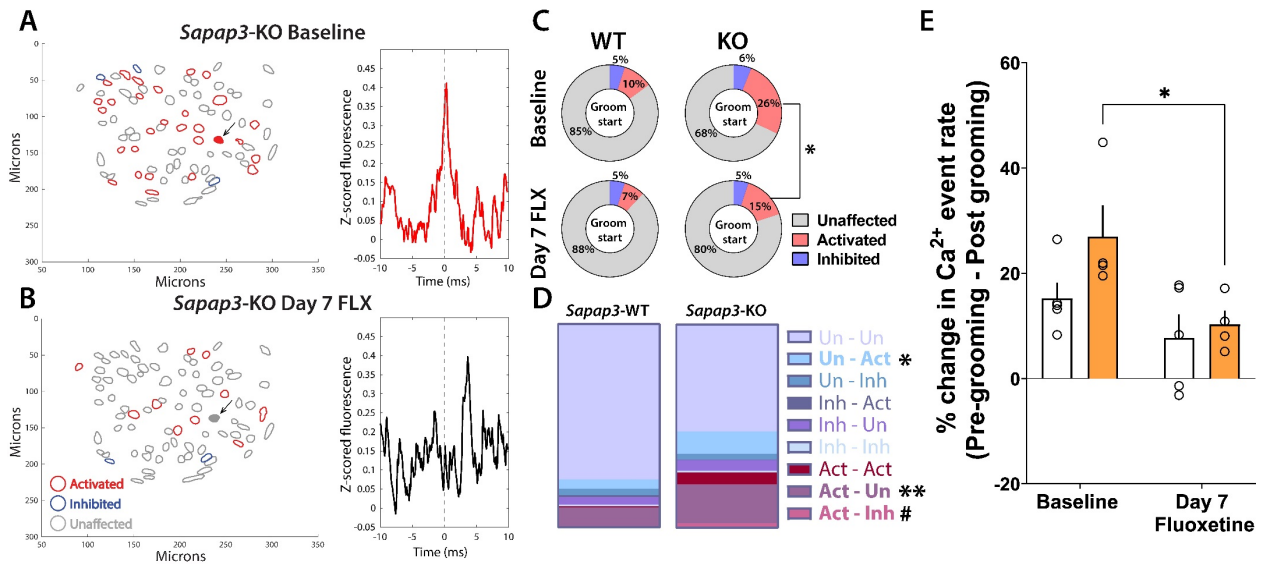

Figure 3-14. Fluoxetine reduces central striatal hyperactivity in *Sapap3*-KO mice

(**A**) (left) Representative contour image of a *Sapap3*-KO mouse contour image at baseline colored to indicate cell classification during grooming (right) Average calcium fluorescence across grooming trials of a single activated cell indicated by black arrow. (**B**) (left) Representative contour image of the same *Sapap3*-KO mouse contour image following 7 days of fluoxetine treatment (right) Average calcium fluorescence across grooming trials of the same cell post-fluoxetine treatment, indicating it is no longer classified as activated. (**C**) Effect of fluoxetine on the percentage of grooming-onset activated cells in WT and *Sapap3*-KOs (main effect$_{genotype}$: $F(1,8) = 18.8$, $p = 0.0025$; main effect$_{treatment}$: $F(1,8) = 7.8$, $p = 0.0235$; interaction$_{genotype\ x\ treatment}$: $F(1,8) = 2.167$, $p = 0.1792$, two-way repeated measures ANOVA). No effect of genotype or treatment on the percentage of grooming-onset inhibited units (all $F(1,8) \leq 0.3836$, $p \geq 0.5529$, two-way repeated measures ANOVA). (**D**) Breakdown of cell classification changes following fluoxetine in WT and KO mice, change from unaffected$_{baseline}$ to activated$_{day\ 7\ FLX}$: ($t(8) = 2.77$, $p = 0.024$, unpaired *t*-test); from activated$_{baseline}$ to unaffected$_{day\ 7\ FLX}$: ($t(8) = 2.62$, $p = 0.031$, unpaired *t*-test); and from activated$_{baseline}$ to inhibited$_{day\ 7\ FLX}$: ($t(8) = 2.11$, $p = 0.068$, unpaired *t*-test). (**E**) Percentage change in calcium event rate from the pre-grooming period (-5 to 0s before grooming onset) to post grooming (0 to 5s after grooming onset) in WT and *Sapap3*-KO mice (main effect$_{genotype}$: $F(1,8) = 2.527$, $p = 0.1559$; main effect$_{treatment}$: $F(1,8) = 9.923$, $p = 0.0162$; $F(1,8) = 3.228$, $p = 0.044$, two-way repeated measures ANOVA). **$p \leq 0.01$, *$p \leq 0.05$, #$p \leq 0.1$.

3.3.11 lOFC terminal stimulation may reduce grooming in *Sapap3*-KO mice

Our data thus far suggest that at baseline, KO mice have reduced input to the central striatum, which may result in disinhibition of SPNs due to a lack of excitation of striatal FSIs, as

has been previously suggested (Burguiere et al. 2013). After fluoxetine treatment we observe an increase in lOFC activity and a reduction in central striatal activity. We next wanted to test whether optogenetically increasing lOFC input specifically to the central striatum would result in decreased grooming in KO mice and an increase in the number of inhibited SPNs. We found that activation of lOFC terminals in the central striatum of WT and KO mice was sufficient to modulate SPN activity (Fig.3-15A). In each mouse we detected a small percentage of cells that were both activated and transiently inhibited at the onset of terminal stimulation (Fig.3-15B). Interestingly, when we looked across all mice (Fig.3-15C), we did not detect any differences in the percentage of cells that were activated (WT: 4 ± 3.27% vs. KO 3.5 ± 3.42%, $t(6) = 0.212$, $p = 0.8394$, unpaired *t*-test) or inhibited (WT: 2.75 ± 2.5% vs. KO: 1.25 ± 0.5%, $t(6) = 1.18$, $p = 0.2839$, unpaired *t*-test) by terminal activation. We next sought to examine whether lOFC terminal stimulation altered grooming behavior in WT and KO mice (Fig.3-15D). When we examined the probability a mouse would be engaged in a grooming bout, we found that as expected KO grooming probability was higher overall than WT grooming probability. Further, KO mice appeared to show a slight reduction in the probability of grooming during lOFC terminal stimulation (reduction from 0.22 probability to 0.15). No such change during the stimulation period was detected in the WT mice, with grooming probability remaining a constant 0.07. When we averaged grooming probabilities in KO mice across pre-stimulation (-20 to 0s), during stimulation (0 to 20s), and post-stimulation (20 to 40s), we found a significant reduction in grooming probability in KO mice during stimulation (Fig.3-15E; KO_{off}: 0.229 ± 0.261 vs. KO_{on}: 0.176 ± 0.230, $t(6) = 4.17$, $p = 0.012$, Sidak's multiple comparison test). These data provide preliminary evidence that selectively enhancing lOFC input to the central striatum in KO mice might transiently reduce compulsive behavior.

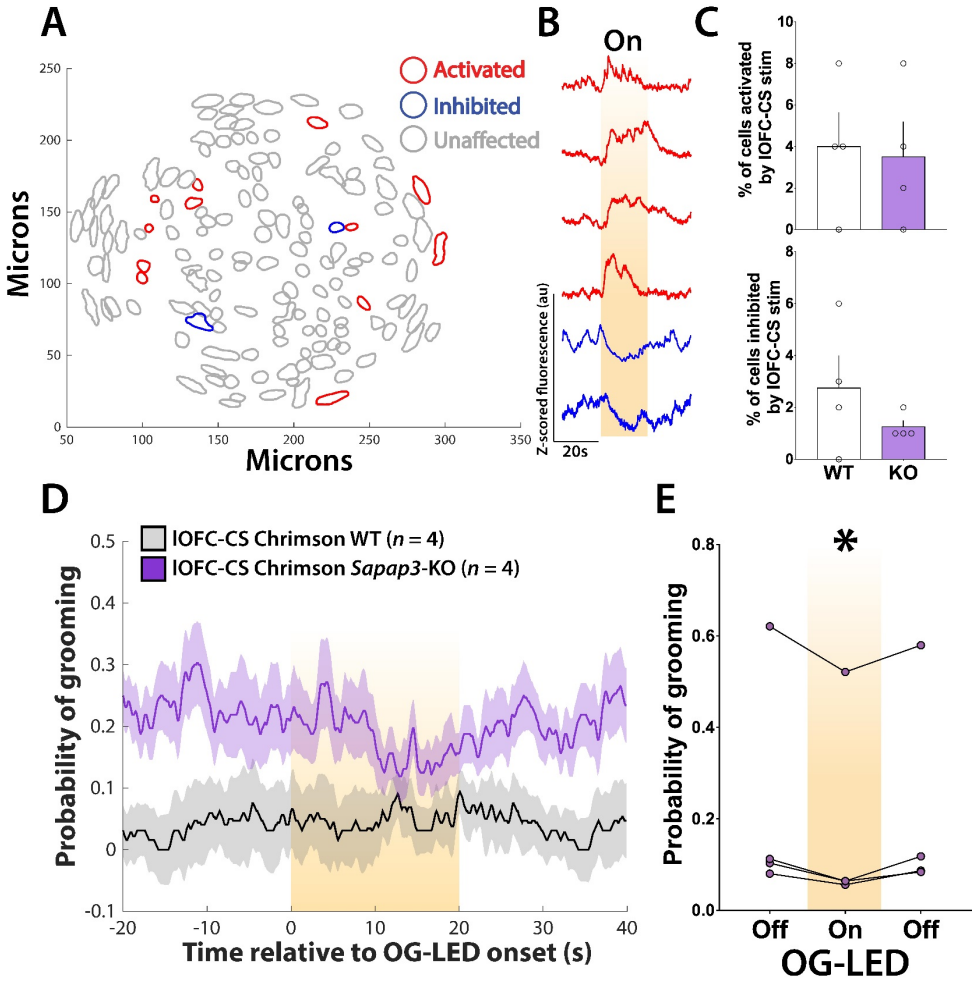

Figure 3-15. lOFC terminal stimulation in *Sapap3*-KO mice may reduce compulsive behavior

(**A**) Contour image of a putative SPNs in the central striatum indicating neurons activated (red), inhibited (blue), or unaffected by optogenetic stimulation of lOFC terminals via Chrimson. (**B**) Four neurons from the mouse in (A) that were activated by terminal stimulation (amber light) noted in red. Two neurons inhibited during stimulation noted in blue. (**C**) Percentage of cells activated ($t(6) = 0.212$, $p = 0.8394$, unpaired *t*-test) and inhibited ($t(6) = 1.18$, $p = 0.2839$, unpaired *t*-test) by terminal stimulation in WT (white) and *Sapap3*-KO mice (purple). (**D**) Probability of grooming across all WT and *Sapap3*-KO mice expressing Chrimson in lOFC terminals projecting to the central striatum. (**E**) Probability of grooming during 20s of terminal stimulation (On) versus pre-stimulation (-20 to 0s) and post-stimulation (20 to 40s) periods (main effect$_{stimulation}$: $F(2,6) = 9.58$, $p = 0.014$, one-way repeated measures ANOVA).

3.4 Discussion

Cortico-striatal circuits have long been implicated in OCD pathophysiology, however how activity patterns in key cortical and striatal brain regions give rise to compulsive behavior remains poorly understood. In the present study, we find that neurons in lOFC are less active in response to grooming onset in *Sapap3*-KO mice relative to WT mice. Further, we demonstrate that amplitudes of individual lOFC neurons that are modulated during grooming (both neurons activated and inhibited at groom onset) are reduced in KO mice, and that they have substantially more grooming-inhibited units observed than WTs. We also examined activity associated with compulsive behavior in major target of lOFC projections, the central striatum (Corbit et al. 2019; Burguiere et al. 2013). Interestingly, in the central striatum we observe an overall increase in activity at grooming onset in KO mice relative to WTs, with an overall increase in the proportion of cells activated at grooming onset. We also demonstrate that transiently increasing central striatal SPN activity via ChR2 could produce grooming-related movements and that specifically stimulating lOFC terminals in the central striatum may reduce compulsive grooming in KO mice. Together, these results shed new light on how compulsive behaviors may be generated in the brain.

While the OFC is among the most frequent regions associated with OCD via neuroimaging studies (Fitzgerald et al. 2011b; Menzies et al. 2008b; Rotge et al. 2009a; Zhang et al. 2016; Chamberlain et al. 2008), our understanding of its *in vivo* participation in compulsive behaviors is limited. Canonically, the OFC is associated with behavioral flexibility associated with changes in action value (Balleine, Leung, and Ostlund 2011) and has previously been demonstrated to be critically involved in the ability for rodents to switch from goal-directed to habitual behavior (Gremel and Costa 2013), a switch hypothesized to be at the core of OCD symptomatology (Graybiel and Rauch 2000). Interestingly, a reduction in lOFC to dorsomedial striatum terminal

activity has been demonstrated to be necessary for development of habitual behavior (Gremel et al. 2016). This finding is broadly consistent with our observation of reduced lOFC activity at the onset compulsive grooming behavior, which suggests that in KO mice a decrease in behavior-related lOFC activity might lead to a lack of ability to flexibly adapt behavior away from a self-injurious compulsive behavior. Assessment of *in vivo* lOFC activity in *Sapap3*-KO mice has been mixed, with one study suggesting no change in baseline activity between WTs and KOs (Burguiere et al. 2013) and another demonstrating subtle alterations in LFP oscillations (Lei et al. 2019). However, neither study evaluated lOFC activity during spontaneous compulsive behavior. Despite this, our findings of reduced grooming-onset activity in the lOFC are consistent with the observation that optogenetic activation of lOFC cell bodies or their terminals in the central striatum reduced compulsive grooming behavior in a conditioned grooming paradigm in *Sapap3*-KO mice (Burguiere et al. 2013). Overall, our data are strongly suggestive of reduced lOFC drive to the central striatum.

Striatal hyperactivity is associated both with OCD and compulsive behaviors in patient populations (Fitzgerald et al. 2011b; Harrison, Soriano-Mas, Pujol, Ortiz, Lopez-Sola, et al. 2009; Menzies et al. 2008b) as well as in mouse models (Ade et al. 2016; Ahmari et al. 2013; Burguiere et al. 2013; Shmelkov et al. 2010). Our observations expand on these findings by positing that increased striatal activity is specific to compulsive behavior onset, and may be the result of an increase in recruitment and subsequent activation of specific SPN ensembles at grooming onset rather than changes in the amplitude of individual SPNs – an important distinction when considering the effect of striatal output on downstream structures. Indeed, an overall increase in striatal gain has been associated with habit formation (O'Hare et al. 2016) and also with compulsive

behavior in *Sapap3*-KO mice (Ade et al. 2016). However, it is worth noting that these studies were conducted in the dorsolateral striatum, and not the central striatum.

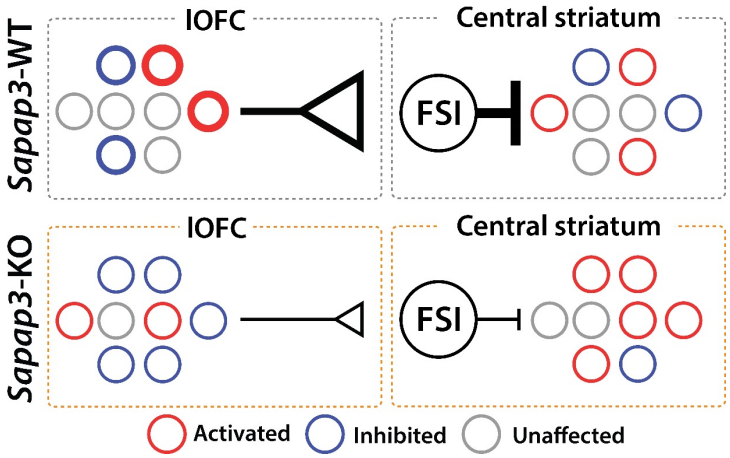

Figure 3-16. Schematic synthesizing findings in lOFC and central striatum at baseline.

In the lOFC, overall activity at grooming onset is reduced in KO mice relative to WTs, likely due to an increase in the proportion of cells that are inhibited. This leads to reduced drive to central striatal FSIs. Reduced excitatory drive of central striatal FSIs in KOs disinhibits local SPNs, resulting in a greater proportion of SPNs activated during grooming and an increase in overall striatal drive (thickness of lines and rings corresponds to amplitude of signal).

On the surface, it may seem that our finding of a grooming-onset associated reduction in lOFC activity is at odds with our observation of increased central striatal activity in *Sapap3*-KO mice relative to WTs, given its nature as a direct glutamatergic projection. However, a key prediction of this model is that lOFC inputs synapse preferentially on striatal parvalbumin positive fast spiking interneurons (FSIs), which monosynaptically inhibit nearby SPNs (Gittis et al. 2010; Koos and Tepper 1999; Tepper et al. 2010), over SPNs (Fig.3-16). Previously a bias toward inhibition of FSIs over SPNs has been demonstrated in other cortico-striatal projections (Mallet et al. 2005; Ramanathan et al. 2002). Although these observations haven't been made specifically in the lOFC to central striatum cortico-striatal projection, support for the existence of this same phenomenon comes from causal experiments demonstrating that when lOFC cell bodies or their terminals in *Sapap3*-KO are activated via optogenetics, an entrainment of central striatal FSIs

occurs and a concomitant reduction in SPN hyperactivity is observed (Burguiere et al. 2013). Given their substantial inhibition of many local SPNs (Gittis et al. 2010; Koos and Tepper 1999), FSIs are well suited to mediate cortical input to the central striatum and regulate overall striatal gain, which has been demonstrated across a variety of circuits and behaviors and is thought to be critical for striatal information processing (Lee et al. 2017; Gage et al. 2010; Berke 2011, 2008). Critically, the impact of striatal FSIs on SPN activity has been demonstrated to be greatest during choice execution (Gage et al. 2010), providing a potential substrate for grooming-onset associated differences in striatal activity in WTs and KOs.

Striatal FSIs may also be involved in mediating the treatment response to fluoxetine we observed in the present set of experiments. Previously, it was demonstrated that fluoxetine could reduce the compulsive grooming phenotype in *Sapap3*-KO mice, but the mechanism by which this occurred was not identified (Welch et al. 2007b). Our studies suggest that a reduction in central striatal activity and decrease in the proportion of grooming-onset activated SPNs occurs on the same time scale as the reduction in compulsive behavior. Consistent with potential FSI involvement in the mechanisms of fluoxetine, FSIs have been reported to be directly excited by serotonin through actions on 5-HT_2 receptors (Blomeley and Bracci 2009). Further, after fluoxetine exposure there is enhanced integration of gamma frequency inputs onto FSIs that translates to a greater probability of FSI spiking (Athilingam et al. 2017). Importantly, fluoxetine itself is capable of directly activating cortical FSIs, which share many physiological and anatomical properties to cortical FSIs (Berke 2011), in a 5-HT_2 receptor dependent manner (Blomeley and Bracci 2009). Unpublished data suggest a similar phenomenon occurs in striatal FSIs, with fluoxetine (100 μM) enhancing FSI firing rate at a series of current steps (Fig.A7). Thus, it seems plausible that the reduction in the number of activated central striatal SPNs we

observe *in vivo* following fluoxetine treatment may be driven by two simultaneously occurring changes: 1) an overall increase in lOFC drive, and 2) direct actions of fluoxetine to increase the excitability and depolarize striatal FSIs, thereby reducing recruitment of nearby SPNs at grooming onset. Future experiments should evaluate the precise activity patterns of FSIs during compulsive behavior in *Sapap3*-KO mice, and whether their activity is necessary for the therapeutic response to fluoxetine.

Taken together, our findings provide novel insights into how compulsive behavior may be generated, focusing on two brain regions most often associated with OCD pathophysiology, the OFC and striatum. These experiments generate many testable hypotheses that can further elucidate the microcircuitry responsible for the generation of compulsive behavior.

4.0 Dissecting the role of genetically distinct striatal cell types on compulsive grooming behavior

4.1 Introduction

Obsessive compulsive disorder (OCD) is a chronic and debilitating psychiatric illness that affects between 1-3% of people worldwide. While the precise pathogenesis of OCD is still unknown, structural and functional imaging studies conducted in OCD patients repeatedly implicate dysfunction in cortico-striatal circuits necessary for regulating action selection (Rotge et al. 2009a; Rauch, Savage, Alpert, Fischman, et al. 1997; Saxena, Bota, and Brody 2001; Maia, Cooney, and Peterson 2008). Convergent findings from rodent research has provided a causal link that hyperactivity broadly within these circuits (specifically between the orbitofrontal cortex (OFC) and striatum) can contribute to compulsive behavior (Ahmari et al. 2013; Burguiere et al. 2013).

These findings and others have led to the development of hypotheses positing imbalance between the parallel "direct" and "indirect" pathways into and out of the basal ganglia in OCD (Pauls et al. 2014; Maia, Cooney, and Peterson 2008), similar to what has been suggested in canonical disorders of the basal ganglia, such as Huntington's and Parkinson's disease (Wichmann and DeLong 1996). While it is difficult to conceptualize how an imbalance in nonmotor direct/indirect pathways may manifest in OCD patients, it has been proposed that excess direct pathway activity may result in a positive feedback loop where obsessive thoughts lock into a specific sensorimotor pattern that is difficult to interrupt (Maia, Cooney, and Peterson 2008). The advent of tools to precisely assess direct and indirect pathway function in rodent models has shed

new light on the function of striatal dopamine D1-receptor expressing direct-pathway projecting (D1-SPN) and dopamine D2-receptor expressing indirect-pathway projecting (D2-SPN) neurons in modulating Parkinsonian states (Kravitz et al. 2010; Mastro et al. 2017), and more recently on how these cell types might act in concert *in vivo* during Parkinsonian conditions and following treatment with $_{L}$-DOPA (Parker et al. 2018). Critically, these two populations of SPNs are subject to feed forward inhibition mediated by parvalbumin (PV)- positive fast spiking interneurons (FSIs) (Berke 2011; Gage et al. 2010; Owen, Berke, and Kreitzer 2018), and thereby tune SPN activity to task-relevant events (O'Hare et al. 2016; Lee et al. 2017).

However, the investigation of direct and indirect pathway balance *in vivo* in affective cortico-striatal loops and how they might contribute to compulsive behavior has not yet been explored. Early pharmacological work examining the contribution of direct pathway activation via D1-receptor specific drugs suggests that D1 agonists are capable of producing excessive grooming (Molloy and Waddington 1987; Page and Terry 1997; Starr and Starr 1986a) in rodents, while D2-receptor antagonists have been reported to be effective augmentation strategies to selective serotonin reuptake inhibitors (SSRI) in OCD (Bloch et al. 2006). Consistent with this evidence, a recent study using *ex vivo* calcium imaging to examine direct and indirect pathway balance in *Sapap3*-knockout (*Sapap3*-KO) mice, which display an SSRI-sensitive OCD-like compulsive grooming phenotype (Welch et al. 2007a) as well as cortico-striatal abnormalities (Corbit et al. 2019; Welch et al. 2007a; Burguiere et al. 2013; Chen et al. 2011; Wan et al. 2014; Wan, Feng, and Calakos 2011), identified a bias toward direct pathway activation (Ade et al. 2016). FSIs have also been implicated in the *Sapap3* phenotype, as stimulation of lOFC terminals in the central striatum may entrain FSIs (Burguiere et al. 2013) and restore normal feed-forward inhibition. These data suggest a potentially complex interplay in the striatal microcircuit during compulsive

behavior. In the present set of experiments, we attempt to examine the contribution of D1- and D2-SPNs, as well as striatal FSIs to compulsive grooming behavior in *Sapap3*-KO mice.

4.2 Methods

4.2.1 Animals

All procedures were carried out in accordance with the guidelines for the care and use of laboratory animals from the NIH and with approval from the University of Pittsburgh Institutional Animal Care and Use Committee (IACUC). *Sapap3*-knockout (*Sapap3*-KO) and wildtype littermates expressing the cre-recombinase (cre) transgene were generated by breeding *Sapap3* heterozygous mutants (*Sapap3*$^{+/-}$) with heterozygous D1-cre mice (D1-cre$^{+/-}$) or heterozygous PV-cre mice (PV-cre$^{+/-}$). Subsequent *Sapap3*$^{+/-}$::cre$^{+/-}$ (either D1-cre$^{+/-}$ or PV-cre$^{+/-}$) were mated with a *Sapap3*$^{+/-}$ mouse, allowing for the generation of cre positive *Sapap3*-WT mice (*Sapap3*$^{+/+}$:: cre$^{+/-}$) and cre positive *Sapap3*-KO mice (*Sapap3*$^{-/-}$:: cre$^{+/-}$). Mice were maintained on a 100% C57BL/6 background. Male and female *Sapap3*-KO and wildtype littermates were used for all experiments. Mice in all cohorts were approximately 4-6 months old at the time of initial surgery.

4.2.2 Stereotactic surgery

For all surgeries, mice were anesthetized using 5% isoflurane mixed with oxygen and maintained on 1-2% isoflurane for the duration of surgery. Mice were placed on a small-animal stereotactic instrument (Kopf Instruments) and secured using ear bars and a bite bar. Hair was

removed from the dorsal surface of the head with hair clippers and the incision area was scrubbed with a betadine solution. A large incision was then made exposing the dorsal portion of the skull. All measurements were made relative to an interpolated bregma. Viral injections were performed using a fixed needle Hamilton syringe (Cole-Parmer Scientific, Vernon Hills IL, USA) connected to sterile polyethylene tubing affixed to a metal cannula and a Harvard Apparatus Pump 11 Elite Syringe Pump (Harvard Apparatus, Holliston MA, USA). Implanted lenses or ferrules were secured in place with one or two 0.45mm skull screws placed just in front of the lambdoid suture. Following completion of each surgery, mice were injected with sub cutaneous (s.c.) carprofen (10% w/v in 0.9% saline) and administered topical antibiotic ointment (TAO) and lidocaine around the headcap. Mice were then placed on a heating pad and given DietGel (ClearH_2O, Portland ME, USA) and monitored until they were fully recovered from anesthesia. Mice were administered carprofen s.c. and received lidocaine and TAO treatments for 3 days post-surgery. For all surgical procedures mice were kept group housed with littermates unless conspecific fighting was noted, in which case the aggressive mouse was isolated for the duration of the experiment.

4.2.2.1 *In vivo* microendoscopy surgical methods

For experiments in the central striatum in D1-cre / *Sapap3* mice as well as PV-cre / *Sapap3* mice, 800nl of a virus encoding cre-dependent GCaMP6m (AAV9-Syn-Flex-GCaMP6m-WPRE-SV40, titer 2.55 x10^{12}) was injected into the central striatum (AP: +0.65, ML: -1.8, DV: -2.9 & -3.0) of mice. Injections were done in a two-step manner, with 400nl of virus injected at DV -2.9 and 400nl of virus injected at DV -3.0. For D1-cre / *Sapap3* experiments, immediately after injection of virus into the central striatum, a 500µm, 6mm length gradient refractive index lens (ProView GRIN lens, Inscopix Pala Alto, CA USA) was lowered just dorsal to the viral injection target (AP: +0.65, ML: -1.8, DV: -2.85) to allow for visualization of cells in the target region. For

PV-cre / *Sapap3* experiments, a 1mm diameter, 4mm long GRIN lens was lowered into the central striatum immediately following viral injection. For experiments using a D2-promotor driven GCaMP6m (AAV8-D2SP-GCaMP6m, gift from Deisseroth lab) reported to have specific expression in D2-SPNs (Zalocusky et al. 2016) was injected into the central striatum of WT and KO mice (two step injection, as above). A 500µm, 6mm length gradient refractive index lens (ProView GRIN lens, Inscopix Pala Alto, CA USA) was then lowered just dorsal to the viral injection target (AP: +0.65, ML: -1.8, DV: -2.85). For all GRIN lens implants, acrylic dental cement (Lang Dental, Wheeling IL, USA) was used to secure the lens in place and seal the entire lens during the virus incubation period (4-6 weeks).

For surgeries imaging striatopallidal projecting D2-SPNs with retrograde GCaMP7, 400nl of AAV-hsyn-GCaMP7 (titer 1.85 $x10^{13}$) was injected into the external segment of the globus pallidus (GPe; AP: 0.0, ML: -2.0, DV: -3.5). After 4-6 weeks for viral incubation, a second procedure was performed during which mice in each experiment were again anesthetized with isoflurane and secured to a stereotactic apparatus using ear cuffs. Using a Dremel, excess dental cement was carefully removed exposing the ProView GRIN lens. The top of the ProView lens was then cleaned with compressed air and lens paper, removing all dental cement dust. A magnetic microscope baseplate (Part ID:1050-002192, Inscopix) was then attached to the miniaturized microscope (nVistaHD 2.0 epifluorescence microscope, Inscopix) and lowered into place above the GRIN lens with the 475nm blue LED gain and power set to their maximum. The optimal field of view was then determined by focusing on visible cells or other gross landmarks (blood vessels). Once an optimal field of view was obtained, the baseplate was cemented in place and a plastic Microscope Baseplate Cover (Part ID:1050-002193; Inscopix) was attached to prevent debris from blocking the lens.

4.2.3 Drug preparation and administration

(±)Fluoxetine hydrochloride (Fluoxetine) was obtained through the NIMH Chemical Synthesis and Drug Supply Program. Fluoxetine was administered intraperitoneally (i.p.) according to previous reports which report a reduction in *Sapap3*-KO grooming following treatment (Welch et al. 2007a). Fluoxetine hydrochloride (5 mg/kg) in a 0.9% saline solution (10 ml/kg) was injected i.p. daily for 7 days to WT and *Sapap3*-KO mice. Fluoxetine injections occurred between 4:00PM and 6:00PM daily while behavioral testing occurred beginning at 9:00AM on testing days. After 7 days of injections, mice were given a two-week washout from fluoxetine to monitor whether grooming behavior and neural activity differences returned to baseline levels.

4.2.4 Behavioral apparatus and assessment of grooming behavior

A custom-built behavioral apparatus was constructed for the accurate simultaneous assessment of spontaneous (e.g. grooming) behavior and neural activity (Fig.3-1A) via *in vivo* calcium imaging. A clear plexiglass sheet was suspended over a behavioral acquisition camera (Point Grey Blackfly, FLIR Integrated Imaging Solutions). A clear acrylic chamber (8”x8”x12”) was placed above the camera such that a mouse could be visualized at every angle. Behavioral acquisition was conducted at 40 Hz using SpinView (Point Grey) software and detailed frame information was sent directly to a central data acquisition box (LabJack U3-LV, Labjack Corporation, Lakewood CO USA). A randomly flashing (30s ITI) LED visible in the behavioral video controlled by custom scripts via an Arduino (Arduino Leonardo, Somerville MA, USA) and sending TTL pulses to the LabJack was used for alignment of behavior and calcium data.

Following acquisition, video was converted and compressed (maintaining accurate frame rate information) into .MP4 format using the open source software HandBrake. Videos were then imported into Noldus The Observer XT (Noldus, Leesburg VA, USA) and grooming behavior was scored frame by frame. Grooming behavior was scored according to previous reports (Kalueff et al. 2016) by an observer blind to experimental condition (genotype and drug treatment). A mouse was considered to be grooming if it engaged in any of the following behaviors (Fig.3-1B) 1) Facial grooming, when a mouse touches its face, whiskers, or head with its forepaws. 2) Body grooming, when a mouse licks its flank or its ventral surface. 3) Hind leg scratching, when a mouse uses one of its hind legs to scratch its flank. The beginning of a grooming bout was defined as the frame when a mouse made a movement to begin grooming (e.g. a face grooming bout began the frame a mouse lifted its paw off the ground to touch its face). The end of a grooming bout was defined as the frame when a mouse ceased grooming (e.g. a body grooming bout ended when a mouse moved its snout from its flank). Grooming bout starts separated by less than one second were collapsed into the previous bout. Thus, the minimum amount of time possible between grooming bouts for all experiments was one second.

4.2.5 *In vivo* calcium imaging in freely moving mice

After at least 1 week of recovery from baseplate surgery, mice were habituated to the attachment of the microscope. In order to attach the microscope securely to the baseplate, mice were lightly scruffed and the miniature nVistaHD 2.0 microscope was connected to the magnetic baseplate and secured with a set screw. During habituation, optimal focus, field of view, and LED power and gain settings were determined visually by assessing the presence of clearly defined putative neurons. A caliper was used to accurately measure the precise microscope focus such that

multiple imaging sessions were conducted with the same field of view. In addition to habituation to the microscope, mice were also placed into the acrylic chamber under low light conditions for a period of 5-10 minutes once daily for three days prior to imaging.

Following habituation, mice were given a 40-minute baseline behavior and imaging session. Under low light the microscope was attached and mice were placed into a temporary holding cage. Mice were given 3-5 minutes after attachment of the scope for recovery from scruffing and to allow any rapid photobleaching to occur. After this period, mice were carefully placed into the clear acrylic chamber. LabJack data acquisition was then begun, immediately followed by behavioral SpinView recordings, and finally nVistaHD software began recording compressed greyscale tiff images at 20 Hz. As with the behavioral frame acquisition, individual calcium frame information was also sent to the LabJack for subsequent alignment of behavior and calcium data. For all mice, analog gain of the image sensor was set between 1 and 4 while the 470 nm LED power was set between 10 to 30% transmission range. These settings were kept consistent for each mouse throughout all subsequent imaging sessions.

4.2.6 Calcium imaging analysis

Custom Matlab (MATHWORKS) scripts were used to conduct analysis of grooming-related calcium activity. Grooming behavior (state events) was exported as timestamps (grooming start and grooming stop) and aligned to Ca^{2+} time by recording 5 consecutive LED pulses (point events). The offset of Noldus behavior time to nVista Ca^{2+} time was then subtracted off leaving the same number of frames for both the behavior and Ca^{2+} fluorescence. Grooming timestamps were then transferred to a binary/continuous trace of the same length and sampling rate (10 Hz) as each Ca^{2+} trace via logical indexing (grooming = 1, not-grooming = 0). Timestamps for behavior

are converted to the closest matching frame in the calcium recording (maximum error of one frame or ± 100ms at 10 Hz). Calcium activity could then be aligned to the start and end of a grooming bout, or the transition point between grooming bouts (≤ 1s between a grooming bout ending and a grooming bout beginning).

4.2.6.1 Unbiased event-related activity classification

In order to perform unbiased classification of an individual cells responsiveness (activated, inhibited, or unaffected) to a behavioral event (e.g. grooming onset) we adapted a strategy used in (Jimenez et al. 2018) using custom Matlab (MATHWORKS) scripts. First, each individual cell's raw Ca^{2+} was aligned to the onset of each grooming bout (Fig.3-2A). These traces were then averaged across all bouts within a given mouse (Fig.3-2B). For each individual cell, raw Ca^{2+} traces 10 seconds prior to grooming onset and 10 seconds after grooming onset (200 total samples at 10 Hz, 100ms per sample) were shuffled in time for each sample (200x) removing any temporal information that was previously in each trace but maintaining the variance within each grooming bout (Fig.3-2C). This shuffle was then performed 1000 times per cell to obtain a null distribution of grooming associated Ca^{2+} activity. A cell was considered responsive to grooming onset if its Z-normalized Ca^{2+} fluorescence amplitude between -0.5s before grooming onset to 3s after grooming onset exceeded a 1 standard deviation threshold from the null distribution (Fig.3-2D).

Individual Ca^{2+} traces classified as activated or inhibited could then be averaged across genotype and directly compared within and across sessions, providing an assessment of how cells encoding grooming were different as a factor of genotype or drug treatment.

4.2.7 Statistical analysis

Statistical analysis was carried out using custom Matlab scripts (MATHWORKS) or GraphPad Prism 8.0 (GraphPad Software, San Diego CA, USA). Throughout this dissertation results in text are reported as mean ± standard deviation (SD) and data presented on figures are mean ± standard error of measurement (SEM) unless otherwise noted.

4.2.7.1 Statistical analysis of grooming behavior

Baseline grooming behavior was analyzed using two-tailed independent samples *t*-tests. For the analysis of behavior following fluoxetine administration, a two-way repeated measures analysis of variance (ANOVA) was used. Main effects and interaction terms are reported throughout, and in cases of significant interactions, post-hoc comparisons were made using Sidak's multiple comparison correction. A corrected alpha was set to 0.05.

4.2.7.2 Statistical analysis of calcium activity

In order to evaluate the effect of genotype and treatment on grooming evoked Ca^{2+} fluorescence averaged across individual cells, unpaired two-tailed *t*-tests were conducted at each time bin (100 ms). Due to our high *N* with dozens to hundreds of cells in each condition, a conservative Bonferroni correction was performed ($\alpha = \frac{0.05}{m}$). The critical *p* value (α = 0.05) was divided by the total number of time bins (each bin = 100ms) to be compared (*m*), resulting in adjusted critical values between 0.000025 and 0.00005, depending on the exact comparison.

For comparison of proportions of classified cells during baseline imaging sessions, two-tailed independent samples *t*-tests were used. To assess the effect of fluoxetine treatment on the proportions of classified cells, two-way repeated measures ANOVA were used. When a significant

interaction between genotype and drug treatment was observed, post-hoc tests were conducted using Sidak's multiple comparisons test. A corrected alpha was set to 0.05.

4.3 Results

4.3.1 D1-SPN activity is increased post-grooming onset in *Sapap3*-KO mice

In order to evaluate whether central striatal D1-SPN activity at grooming onset differs between double transgenic D1-cre/*Sapap3* WT and KO mice, we expressed a cre-mediated GCaMP6m and implanted a GRIN lens just dorsal to our viral injection target (Fig.4-1a). As expected, we found that KO mice spent significantly more time grooming (WT: 179.2 ± 86.99s vs KO: 790 ± 550.5s, unpaired *t*-test) and engaged in significantly more grooming bouts (WT: 38.38 ± 14.97 bouts vs KO: 92.33 ± 48.62 bouts, unpaired *t*-test) than WT littermates (Fig.4-1b). Grooming-onset evoked calcium activity in D1-SPNs was significantly elevated in the period immediately post-grooming in *Sapap3*-KO mice relative to WT mice (Fig.4-1c; all significant time bins $t(2189) \geq 2.109$, $p \leq 0.0351$, Sidak's post-hoc test). Not only was calcium activity elevated in WTs relative to KOs at groom onset, but KO mice displayed a significant increase in calcium event rate during the period immediately following grooming compared to the period preceding grooming (Fig.4-1d; KO pre-grooming: 0.0801 ± 0.0359 events/s vs KO post-grooming: 0.0934 ± 0.03597 events/s, $t(11) = 3.068$, $p = 0.0213$, Sidak's multiple comparisons test) whereas WT mice had no significant change in calcium event rate (WT pre-grooming: 0.1013 ± 0.0259 events/s vs WT post-grooming: 0.1006 ± 0.0305 events/s, $t(11) = 0.1551$, $p = 0.9855$, Sidak's multiple comparisons test). Relative to WTs, the percentage change in D1-SPN event rates from a pre-

grooming period was significantly elevated (WT: 0.7583 ± 6.575% vs KO: 19.51 ± 18.99%, $t(12) = 2.621$, $p = 0.0223$, unpaired t-test). Together, these data suggest that D1-SPN activity in KO mice is elevated while they engage in compulsive grooming behavior.

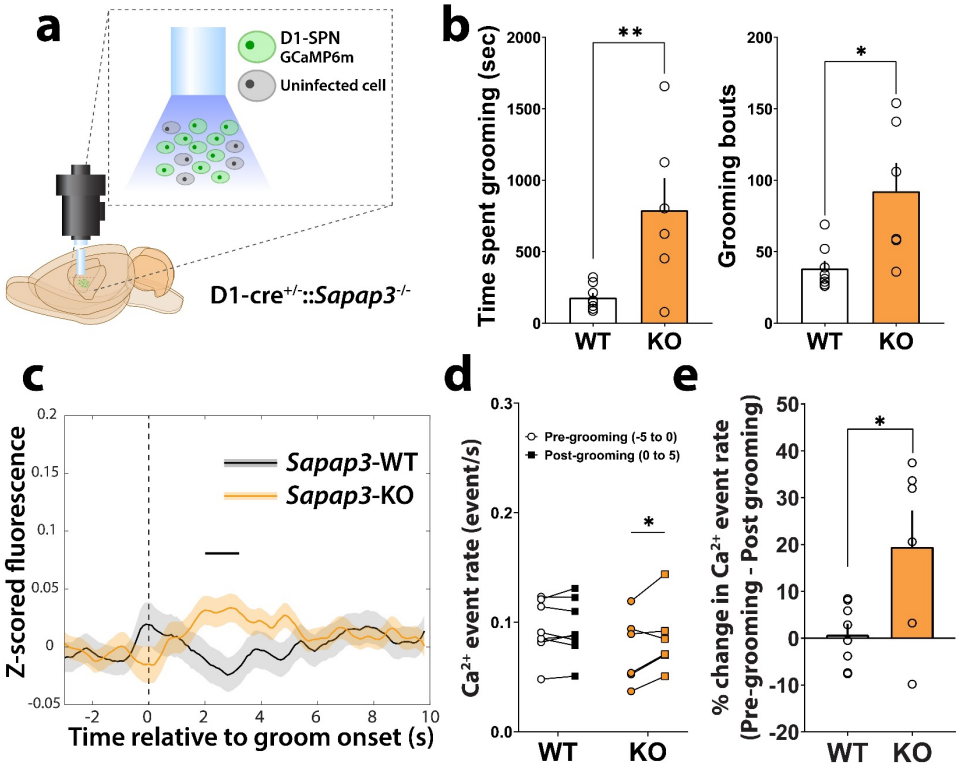

Figure 4-1. D1-SPNs are hyperactive *in vivo* following grooming onset.

(**a**) Schematic of cre-mediated GCaMP6m expression in D1-SPNs of WT and *Sapap3*-KO mice. (**b**) Time spent grooming ($t(12) = 3.130$, $p = 0.0087$, unpaired t-test) and number of grooming bouts ($t(12) = 2.991$, $p = 0.0113$, unpaired t-test) in WT and *Sapap3*-KO mice. (**c**) Grooming-onset associated calcium fluorescence in WT and *Sapap3*-KO mice (main effect$_{genotype}$: $F(1,11) = 0.02031$, $p = 0.8892$, main effect$_{time}$: $F(198, 2178) = 0.6943$, $p = 0.9995$, interaction$_{genotype\ x\ time}$: $F(198,2178) = 1.841$, $p = 0.0001$, two-way repeated measures ANOVA). (**d**) Calcium event rate (event/s) during the period immediately preceeding grooming (-5s to 0s) and immediately following grooming (0s to 5s) in WT and *Sapap3*-KO mice (main effect$_{genotype}$: $F(1,11) = 0.6470$, $p = 0.04382$, main effect$_{time}$: $F(1,11) = 4.604$, $p = 0.055$, main effect$_{genotype\ x\ time}$: $F(1,11) = 5.553$, $p = 0.0380$, two-way repeated measures ANOVA). (**e**) Percent change in calcium event rate (pre-grooming – post-grooming) in WT and *Sapap3*-KO mice ($t(12) = 2.621$, $p = 0.0223$). $n = 7$ WT mice and 6 *Sapap3*-KO mice. $^{**}p < 0.01$, $^{*}p < 0.05$.

4.3.2 Changes in activity and recruitment of D1-SPNs as a function of timing of grooming sequence

With the overall change in calcium fluorescence in D1-SPNs observed predominantly following grooming bout onset, we next sought to examine whether the event-associated activity of significantly modulated D1-SPNs was different at various peri-grooming bout periods (Fig.4-2). We first examined calcium fluorescence in D1-SPNs during the immediate pre-grooming (-0.5s prior to grooming onset) to immediate post grooming (2s post-grooming) period (Fig.4-2a-c). Interestingly, we found that Z-scored fluorescence of significantly activated D1-SPNs during this period was lower in KO mice relative to WT mice (Fig.4-2a; all significant $t \geq -5.153$, $p \leq 0.0000405$, unpaired *t*-test). There was no difference in amplitude of groom-onset inhibited units between WT and KO D1-SPNs (Fig.4-2b; all $t(119) \geq 3.9867$, $p \geq 0.000116$, unpaired *t*-test). Relative to WTs (Fig.4-2c), KO mice had a significantly greater percentage of cells inhibited at grooming onset compared to WT mice (WT: 5.857 ± 2.27% vs KO: 9.667 ± 3.07%, unpaired *t*-test), with no changes in the percentages of activated D1-SPNs (WT: 11.286 ± 7.30% vs KO: 11.17 ± 4.62%, unpaired *t*-test).

Given our finding of an increase in calcium fluorescence in D1-SPNs during grooming rather than locked to grooming onset (Fig.4-2c), we evaluated whether there were differences in modulated grooming within a post-grooming (+0.5 to 4s) window in WT and KOs. Interestingly, we observed that while the amplitude of WT activated D1-SPNs was attenuated during this period (Fig4-2d) relative to their activity at grooming onset (Fig.4-2a), this was not the case in KO mice. This reduction equated in no difference in amplitude of D1-SPNs in the post-grooming onset period in WTs and KOs (all $t(98) \leq 0.8718$, $p \geq 0.000148$, unpaired *t*-tests). Amplitude of significantly inhibited D1-SPNs (Fig.4-2e) was also unchanged in this post-grooming window (all

$t(56) = 4.1566$, $p = 0.000112$, unpaired t-tests). While there were no differences in D1-SPN amplitude in this post-grooming period, we found that there were significant shifts in the percentages of modulated cells in WTs and KOs (Fig.4-2f). We found that the percentage of D1-SPNs activated during grooming was increased in KO mice relative to WTs (WT: 6.29 ± 3.64% vs. KO: 14.33 ± 8.48%, unpaired t-test) while there was no longer a difference in the percentage of grooming inhibited D1-SPNs (WT: 6.57 ± 3.05% vs. KO: 4.50 ± 3.27%, unpaired t-test). These data indicate that at grooming onset, D1-SPN activity is reduced in KO mice relative to WT mice, but that during grooming D1-SPN activity remains elevated while WT activity returns to baseline.

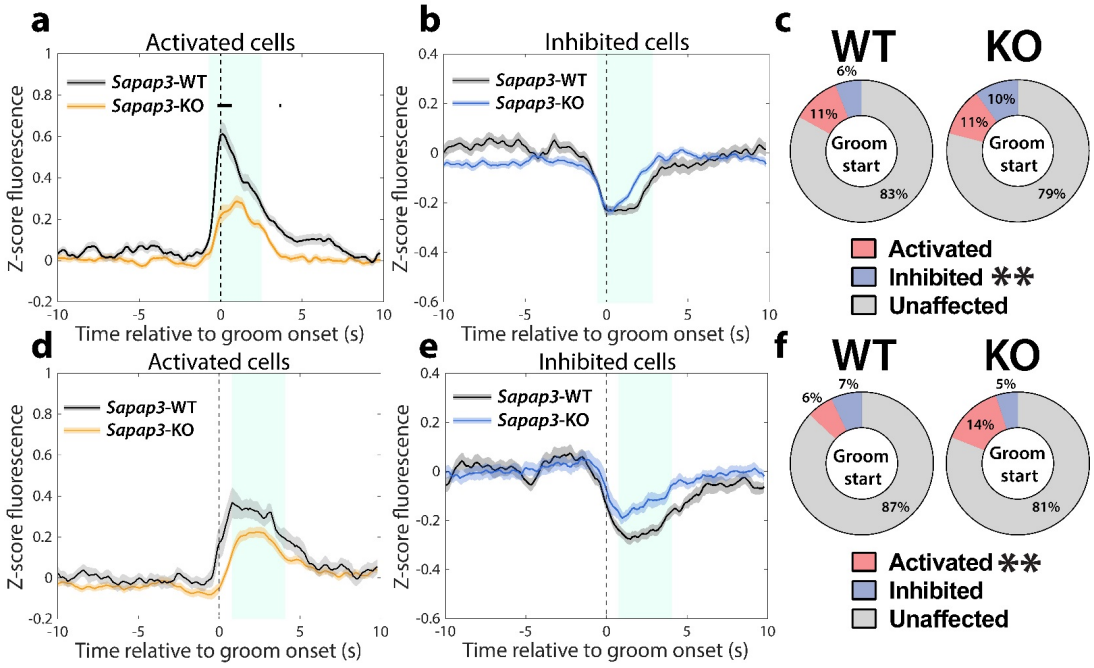

Figure 4-2. *Sapap3*-KO mice have sustained activity of D1-SPNs during grooming

(**a**) Z-scored fluorescence of significantly activated D1-SPNs in the pre-grooming (-0.5s) to immediate post-grooming (2s) period (green shading) in WT and *Sapap3*-KO mice (all significant $t \geq -5.153$, $p \leq 0.0000405$, unpaired *t*-test). (**b**) Z-scored fluorescence of significantly inhibited D1-SPNs in the pre-grooming to immediate post-grooming period in WT and *Sapap3*-KO mice (all $t(119) \geq 3.9867$, $p \geq 0.000116$, unpaired *t*-test). (**c**) Percentages of significantly modulated D1-SPNs at grooming onset in WT and *Sapap3*-KO mice (activated cells: $t(11) = 0.034$, $p = 0.973$; inhibited cells: $t(11) = 2.568$, $p = 0.026$, unpaired *t*-tests). (**d**) Post-grooming (green shading, +0.5s to 2s post-grooming) activated D1-SPN amplitude (all $t(98) \leq 0.8718$, $p \geq 0.000148$, unpaired *t*-tests) and (**e**) inactivated D1-SPN amplitude (all $t(56) = 4.1566$, $p = 0.000112$, unpaired *t*-tests) in WT and *Sapap3*-KO mice. (**f**) Percentages of significantly modulated D1-SPNs post-grooming onset in WT and *Sapap3*-KO mice (activated cells: $t(11) = 2.29$, $p = 0.042$; inhibited cells: $t(11) = 1.18$, $p = 0.262$, unpaired *t*-tests). $n = 7$ WT and 6 *Sapap3*-KO mice. Bar indicates $p < 0.00005$, $^{**}p < 0.01$

4.3.3 Fluoxetine reduces overall increase in D1-SPN activity

We have previously demonstrated that 7 days of fluoxetine treatment, the first line pharmacotherapy for OCD, was capable of reducing overall striatal in KO mice, though its effects on subtypes of SPNs is unknown. We first found that fluoxetine reduced the amount of time KO

mice spent grooming (KO baseline: 790.2 ± 550.5s vs KO Day 7 FLX: 516.6 ± 424.3s, $t(11) = 3.757$, $p = 0.0063$, Sidak's multiple comparisons test) and the number of grooming bouts engaged in (KO baseline: 92.33 ± 48.62 buts vs. KO Day 7 FLX 55.83 ± 31.86 bouts, $t(11) = 2.648$, $p = 0.0448$, Sidak's multiple comparisons test) relative to WT mice (Fig.4-3a-b). Interestingly, we found that 7 days of fluoxetine was capable of preventing an the previously observed increase in D1-SPN calcium event rate (Fig.4-3c) associated with the onset of grooming in KO mice (KO pre-grooming: 0.118 ± 0.036 events/s vs KO post-grooming: 0.126 ± 0.041 events/s, $t(11) = 0.7731$, $p = 0.7038$, Sidak's multiple comparisons test) with no changes in WTs ($p \geq 0.05$). Compared to baseline, where KO mice exhibited a substantial increase in D1-SPN calcium event rates at grooming onset (Fig.4-3d), fluoxetine elicited a trend-level reduction in post-grooming calcium event rates in KO mice (KO baseline: 21.899 ± 20.469% vs. KO Day 7 FLX: 6.165 ± 20.799%, $t(11) = 2.281$, $p = 0.0851$, Sidak's multiple comparison test). No significant effect of fluoxetine on calcium event rate change was observed in WT mice ($p \geq 0.05$). These data indicate that, similar to what is observed in all central striatal SPNs, fluoxetine is capable of reducing increased D1-SPN activity in KO mice.

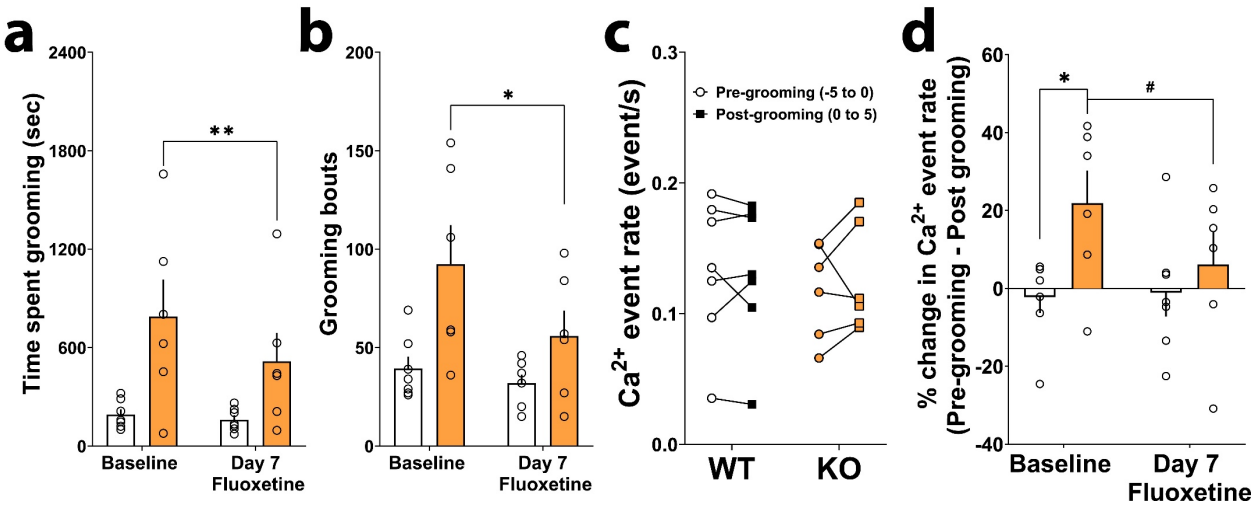

Figure 4-3. Fluoxetine reduces D1-SPN hyperactivity during grooming in KO mice.

(**a**) Time spent grooming in WT and *Sapap3*-KO mice (main effect$_{genotype}$: $F(1,11) = 6.988$, $p = 0.0288$, main effect$_{treatment}$: $F(1,11) = 9.469$, $p = 0.0105$, interaction$_{genotype\ x\ treatment}$: $F(1,11) = 5.940$, $p = 0.0330$, two-way repeated measures ANOVA) (**b**) Number of grooming bouts in WT and *Sapap3*-KO mice (main effect$_{genotype}$: $F(1,11) = 8.121$, $p = 0.0158$, main effect$_{treatment}$: $F(1,11) = 5.467$, $p = 0.0393$, interaction$_{genotype\ x\ treatment}$: $F(1,11) = 2.395$, $p = 0.1500$, two-way repeated measures ANOVA). (**c**) Calcium event rate (event/s) during the period immediately preceeding grooming (-5s to 0s) and immediately following grooming (0s to 5s) in WT and *Sapap3*-KO mice (main effect$_{genotype}$: $F(1,11) = 0.1683$, $p = 0.06895$, main effect$_{time}$: $F(1,11) = 0.1975$, $p = 0.6655$, interaction$_{genotype\ x\ time}$: $F(1,11) = 0.4754$, $p = 0.5043$, two-way repeated measures ANOVA). (**d**) Percentage change in calcium event rate between pre-grooming and post-grooming periods in WT and KO mice (main effect$_{genotype}$: $F(1,11) = 3.551$, $p = 0.0862$, main effect$_{treatment}$: $F(1,11) = 2.431$, $p = 0.1473$, interaction$_{genotype\ x\ treatment}$: $F(1,11) = 5.198$, $p = 0.0139$, two-way repeated measures ANOVA). $n = 7$ WT and 6 *Sapap3*-KO mice, $^{**}p<0.01$, $^{*}p<0.05$,$\#p<0.1$.

4.3.4 D2-SPN imaging *in vivo*

Several methods were utilized to assess the activity of D2-SPNs *in vivo* during compulsive behavior with very limited success. One attempt was made using a virus that would express GCaMP6m under the D2-receptor promotor (AAV8-D2SP-GCaMP6m), which was previously used successfully to image D2-SPNs in the nucleus accumbens of rats using fiber photometry (Zalocusky et al. 2016). While we found this virus to be specific for D2-SPNs in mice, the intensity

of the activity *in vivo* was not sufficient to quantify either via fiber photometry or single photon microendoscopy as described in this thesis (data not shown).

In parallel, we tried a second approach, relying on the segregation in downstream targets of D1- and D2-SPN in the non-ventral striatum. Specifically, inhibitory dorsal striatum D2-SPNs project almost exclusively to the globus pallidus external segment (GPe), allowing us to use a retrogradely trafficked GCaMP in order to visualize GPe-projecting D2-SPNs (Fig.4-4a-top). Unfortunately, despite good viral targeting in the GPe of multiple mice both with and without lens implants (Fig.4-4a-bottom), we were unable to detect calcium *in vivo* and subsequent analysis of the tissue revealed no retrogradely infected D2-SPN cell bodies across the entire striatum (Fig.4-4b, depicted image of mouse with no lens implantation). It is unclear why no retrograde transport was detected in the striatum (despite transport being detected in other GPe projecting regions (data not shown)), though it suspected that tropism of current generation retrograde-AAVs may not allow specific pathways to be targeted, despite the anatomical connections being able to be mapped using traditional retrograde methods (e.g. cholera toxin) (personal correspondence M.R. Bruchas & G.D. Stuber). Given these difficulties, future experiments will utilize an inefficient double-transgenic strategy similar to what was used in our experiments characterizing D1-SPNs, utilizing

mice that express cre-recombinase in adenosine 2a (A2A)-positive striatopallidal projecting spiny projection neurons (Tecuapetla et al. 2014).

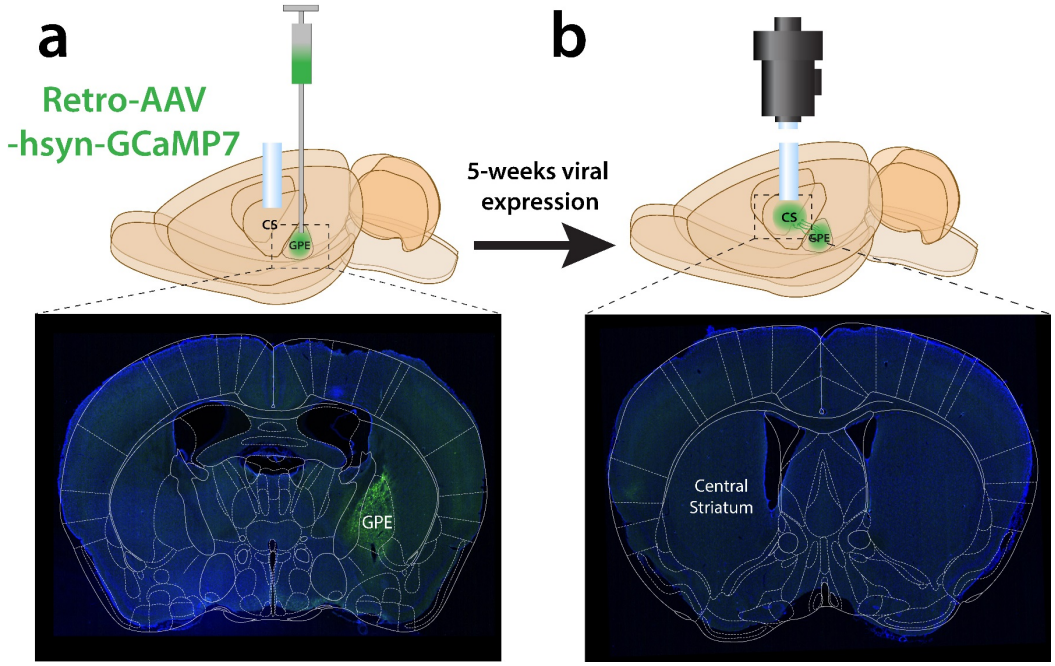

Figure 4-4. Absence of retrograde-GCaMP7 transport in the striatum

(**a**) (top) Depiction of retrograde-AAV strategy to infect GPe-projecting central striatal neurons. (bottom) Representative image of a GPe injection of retrograde-GCaMP7 (green) showing infection of GPe neurons. (**b**) (top) After 5 weeks of viral expression, GCaMP7 should be retrogradely transported to cell bodies upstream of the GPe, including D2-SPNs in the central striatum. (bottom) Absence of retrograde-GCaMP7 labeling across the striatum after 5 weeks of viral expression (blue = DAPI).

4.3.5 Central striatal FSI activity is not different at grooming onset

One possible explanation for sustained activation of D1-SPNs in KO mice during grooming would be a difference in the activity of striatal fast-spiking interneurons, which mediate feed-forward inhibition onto neighboring SPNs (Berke 2011; Owen, Berke, and Kreitzer 2018), in relation to compulsive grooming onset. In order to investigate this possibility, we injected a cre-mediated GCaMP6m into the central striatum of a one double-transgenic PV-cre/*Sapap3*-WT and

one PV-cre/*Sapap3*-KO mouse. Because only between 1-3% of striatal cells are FSIs, we implanted a larger diameter GRIN lens (1mm) to maximize our ability to image such a sparse cell population (Fig.4-5a). As expected, we found few putative FSIs in our field of view (Fig.4-5b), observing 8 cells in a WT mouse and 12 cells in a KO mouse (Fig.4-5b-top). These approximate numbers are in line with what would be expected in the literature (1-3% of all cells) given a 1mm diameter lens (~300-500 cells visible) in the medial portion of the striatum (Parker et al. 2018). Further, we found that compared to SPNs (obtained in experiments conducted in Chapter 3), putative FSIs exhibited characteristic broader and higher amplitude waveforms (Fig.4-5b-bottom), typical of higher firing neurons expressing GCaMP (Gritton et al. 2019).

We found no difference in the calcium event rates of neurons obtained from one WT and one KO mouse during non-grooming times (Fig.4-5c; WT: 0.036 ± 0.027 events/s vs. KO 0.044 ± 0.045 events/s) or during grooming (WT: 0.080 ± 0.053 events/s vs. KO: 0.095 ± 0.083 events/s), though overall FSIs in both genotypes increased their activity during grooming (main effect$_{time}$: $F(1,16) = 7.609$, $p = 0.0140$, two-way repeated measures ANOVA). We next evaluated normalized calcium fluorescence at grooming onset in a WT and KO mouse in response to grooming onset and found no difference in Z-normalized calcium fluorescence in FSIs in WTs and KOs (Fig.4-5d; all $t(18) \leq 1.72$, $p \geq 0.102$, unpaired *t*-tests). While we are underpowered to draw firm conclusions only analyzing a small number of putative FSIs in a single WT and KO mouse, preliminarily it appears that there are no differences in the calcium activity of FSIs during grooming behavior by genotype.

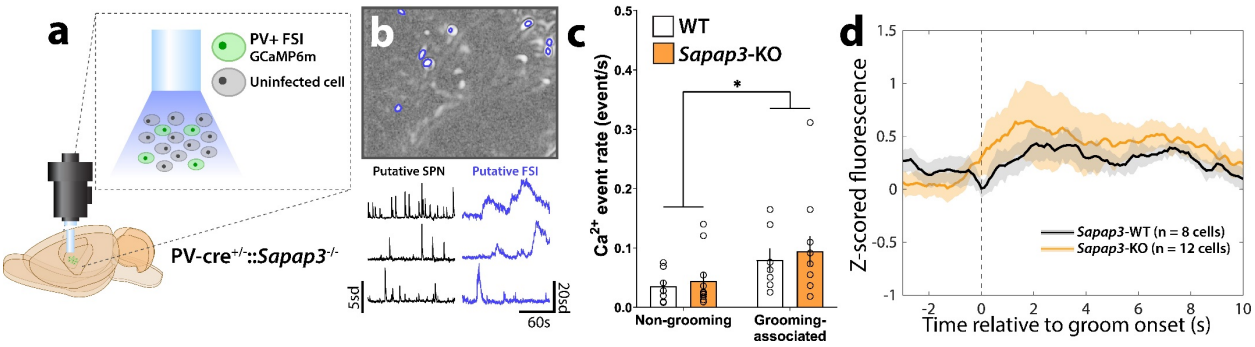

Figure 4-5. Preliminary evidence that *in vivo* activity of central striatal FSIs in a *Sapap3*-KO mouse is normal

(**a**) Schematic representing the cre-mediated strategy for imaging a sparse population PV+ putative central striatal FSIs in WT and KO mice (**b**) (top) Representative maximim projection image of all pixels recorded in a 30 minute grooming session. Contour image of identified putative FSIs overlayed in blue. (bottom) Representative traces of putative SPNs (Chapter 3) demonstrating characteristic narrow waveforms and lower amplitude (black). Representative traces of putative FSIs demonstrating wider and higher amplitude waveforms (blue). Calcium event rates during non-grooming and grooming times in a single WT (n = 8 cells) and single KO (n = 12 cells) mouse (main effect$_{genotype}$: $F(1,16) = 0.271$, $p = 0.6099$; main effect$_{time}$: $F(1,16) = 7.609$, $p = 0.0140$; interaction$_{genotype\ x\ time}$: $F(1,16) = 0.040$, $p = 0.8435$, two-way repeated measures ANOVA). Z-scored calcium fluorescence in FSIs recorded from a WT and KO mouse aligned to grooming onset (all $t(18) \leq 1.72$, $p \geq 0.102$, unpaired t-tests). *$p<0.05$.

4.4 Discussion

In the present set of experiments, we tested the hypothesis that central striatal hyperactivity observed *in vivo* in *Sapap3*-KO mice at the onset of compulsive grooming (Chapter 3) was driven by hyperactivity in direct-pathway projecting D1-SPNs. Consistent with this hypothesis, we observed an increase in D1-SPN calcium event rates during compulsive grooming behavior and an increase in D1-SPN calcium fluorescence (Fig.4-1). However, this increase was not identified immediately at grooming onset, rather post-grooming onset while the mouse was engaged in the compulsive behavior (Fig.4-2) and was associated with an increase in the percentage activated D1-SPNs. Treatment with the SSRI fluoxetine (Prozac), the first-line pharmacotherapy for OCD, also significantly reduced both compulsive grooming behavior as well as the hyperactivity observed

during the compulsive behavior (Fig.4-3). Together these data are the first *in vivo* evidence of how genetically distinct striatal neurons (D1-SPNs) are regulating compulsive behavior, and hint at a complex role for the striatal microcircuit.

Since the 1980s, cortico-basal ganglia circuits have been implicated in OCD through neuroimaging studies (Baxter et al. 1996; Breiter and Rauch 1996; Harrison, Pujol, Cardoner, Deus, Alonso, Lopez-Sola, et al. 2013; Harrison, Soriano-Mas, Pujol, Ortiz, Lopez-Sola, et al. 2009; Insel and Winslow 1992; Milad and Rauch 2007; Nakao et al. 2005; Rauch et al. 1994a; Rotge et al. 2009a; Saxena et al. 1998). These specific circuits, sometimes referred to as the "OCD circuit" because of its well-replicated nature (Graybiel and Rauch 2000), are comprised of projections from frontal cortical regions to the dorsal striatum (caudate nucleus and putamen), and have most often been demonstrated to be hyperactive both at baseline and following symptom provocation (for a thorough review, see (Menzies et al. 2008b) and (Maia, Cooney, and Peterson 2008)). This hyperactivity has been hypothesized to be the result of a bias toward activation of the direct pathway through the basal ganglia, which results in an overall disinhibition of cortical motor programs that might contribute to repetitive behaviors (e.g. compulsions) (Maia, Cooney, and Peterson 2008). The first major divergence in the direct pathway and its parallel counterpart, the indirect pathway, occurs in the striatum where direct pathway projecting neurons express the dopamine D1 receptor and indirect pathway neurons express the dopamine D2 receptor. Our data for the first time describe how direct pathway D1-SPNs are engaged during a compulsive behavior that persists in the fact of significant negative consequences, including the development of raw skin lesions (Welch et al. 2007a).

Consistent with our findings, early work demonstrated that agonism of the D1 receptor was sufficient to produce repetitive grooming behavior (Page and Terry 1997; Starr and Starr 1986a,

1986b) and that genetically stimulating D1 neurons was sufficient to produce other repetitive behaviors (Campbell et al. 1999). Similarly, here we demonstrate that D1-SPN activity is increased during the production of compulsive behavior. Interestingly, we observed that D1-SPN activity was increased throughout the compulsive grooming sequence, not transiently at the onset of a grooming bout. These data are supported by findings that suggest D1-SPN activity is critical for the ongoing performance of a learned behavioral sequence (Tecuapetla et al. 2016), and that as a sequence progressess, there is a shift between D1-SPN activity occurring at the onset of the behavioral sequence to occurring during the sequence (Jin, Tecuapetla, and Costa 2014). In this framework, we can think of compulsive grooming behavior as a well-learned, habitual behavioral sequence. If this is true, we would expect strengthening at specific cortico-striatal synapses onto D1-SPNs. Recent work demonstrates the central striatum receives strong cortical input from supplementary motor region M2 (M2), and that this projection is strengthened in *Sapap3*-KO mice relative to WT mice (Corbit et al. 2019). These data are supported by findings that sustained activity of D1-SPNs during sequence learning is mediated through excitatory synaptic input from M2 (Rothwell et al. 2015).

Despite the fact that we were unable to directly study indirect pathway projecting D2-SPNs *in vivo* in WTs and *Sapap3*-KOs due to technical challenges, we can use this same framework to infer how D2-SPNs may be involved in encoding compulsive grooming. Although the classic model of the direct and indirect pathway predict antagonistic control of motor behaviors (DeLong 1990; Wichmann and DeLong 1996; Graybiel 2000; Kravitz et al. 2010), more recent data suggests concurrent activity of direct and indirect pathway neurons during behavioral sequences (Cui et al. 2013; Jin and Costa 2010; Jin, Tecuapetla, and Costa 2014; Tecuapetla et al. 2016). Specifically, D2-SPNs are active during initiation of (possibly even earlier than D1-SPNs)

a sequenced behavior and their activity decreases during behavioral execution (Jin, Tecuapetla, and Costa 2014), and this reduction in activity is necessary for accurate sequence completion (Rothwell et al. 2015). A prediction could be generated based on these findings that, in *Sapap3*-KO mice, increased D2-SPN activity at the onset of grooming is observed relative to WT mice, resulting in the interruption of previously ongoing behaviors and the switch to a compulsive behavior. It is likely that both the proposed increase in KO D2-SPN activity during compulsive behavior, as well as the empirically noted sustained increase D1-SPN activity after the onset of compulsive behavior may be generated through changes in the function of striatal FSIs. Indeed, dysfunction of striatal FSIs have been previously noted in *Sapap3*-KO mice (Burguiere et al. 2015; Corbit et al. 2019). Given that striatal FSIs preferentially inhibit D1- over D2-SPNs (Gittis et al. 2010), we might predict that FSI activation at grooming onset is reduced in KO mice relative to WTs. However, in the present set of experiments (Fig.4-5) we did not observe this to be the case, although many more animals will be necessary to draw firm conclusions.

5.0 General discussion

5.1 Summary of findings

Glutamatergic dysfunction in cortico-striatal circuits has been hypothesized as a potential contributor to OCD pathophysiology for the better part of a decade (Bloch and Pittenger 2010; Pauls 2010; Pittenger, Bloch, and Williams 2011). To date, no direct assessment of this hypothesis has been conducted, and the functional consequences of potential dysfunction are mostly unknown. Gaining traction into this question is particularly critical, as relative to other major neuropsychiatric illnesses such as major depressive disorder (MDD) and schizophrenia for which substantial progress has been made identifying mechanistically distinct pharmacological treatment strategies, OCD pharmacotherapy still relies on treatments affecting monoaminergic systems whose link to pathogenesis has been all but disproven (Pittenger and Bloch 2014).

Chapter 2 describes the first post-mortem examination of transcriptional dysregulation in the OFC and striatum of OCD subjects and focuses on excitatory and inhibitory transcripts, the two main neurotransmitters used in cortico-striatal circuits (Haber 2016). Recent work from various groups has implicated synaptic glutamatergic dysfunction at the genetic level in OCD ((OCGAS) 2018; Pauls et al. 2014; Stewart et al. 2013) as well as in rodent models of compulsive behavior (Shmelkov et al. 2010; Welch et al. 2007a). Using tissue obtained from two regions of OFC (BA11 and BA47) and two striatal brain regions (caudate nucleus and nucleus accumbens) in OCD subjects and matched healthy comparison subjects, we assessed the expression of many of these candidate transcripts. We find that, contrary to our predictions, the majority of excitatory synaptic transcripts are reduced selectively in the OFC of OCD subjects relative to healthy

comparison subjects. Several transcripts, including *DLGAP3* (also known as *SAPAP3*) were reduced across cortical and striatal brain regions, suggesting their involvement in multiple segments of the cortico-striatal loop. This finding is of particular interest, as *Sapap3*-knockout mice display a compulsive behavioral phenotype (Welch et al. 2007a) as well as cortico-striatal circuit deficits (Chen et al. 2011; Wan et al. 2014; Wan, Feng, and Calakos 2011) that involve specific projections from the lateral OFC (lOFC) to the central striatum (Burguiere et al. 2013). These mice present a unique opportunity to investigate the functional consequences of a reduction in *Sapap3*, which is enriched at cortico-striatal synapses (Welch et al. 2007a), similar to what we observed in OCD subjects.

In Chapter 3, we utilize *Sapap3*-KO mice to investigate how reduced *Sapap3* contributes to altered *in vivo* activity in the OFC and central striatum, the regions directly implicated in the compulsive grooming phenotype (Burguiere et al. 2013; Welch et al. 2007a). Using *in vivo* miniature microscopy, we find that, in the OFC, *Sapap3*-KO mice have reduced lOFC activity at the onset of compulsive behavior and that this is due to an increase in the percentage of cells that are inhibited during grooming onset. Further, we demonstrate that *Sapap3*-KO mice display central striatal hyperactivity transiently at the onset of compulsive behavior. This hyperactivity was not driven by an increase in the amplitude of individual central striatal SPNs activated during grooming onset, but rather by an increase in the recruitment of a greater percentage of SPNs relative to WT mice. Both the increase in the percentage of cells inhibited during grooming onset in the lOFC as well as the increase in the percentage of activated SPNs in *Sapap3*-KO mice were reversed by treatment with the first line pharmacotherapy, fluoxetine. In addition, we demonstrate that direct activation of central striatal SPNs was sufficient to cause grooming-related movements,

suggestive of a causal role for increased activated SPN number in compulsive behavior, and that selective activation of lOFC terminals in the central striatum may reduce compulsive grooming.

Chapter 4 focuses on preliminary experiments assessing the activity of specific genetically distinct cell types in the central striatum during *Sapap3*-KO compulsive grooming. For 20 years OCD has been hypothesized to be the result of an imbalance in the direct and indirect pathway through the basal ganglia (Saxena and Rauch 2000; Maia, Cooney, and Peterson 2008; Pauls et al. 2014; Ahmari 2016). In these experiments, we attempt to record activity from the cell type where the direct and indirect pathways first diverge, dopamine D1-receptor expressing and dopamine D2-receptor expressing SPNs (Kravitz et al. 2010), respectively. We also present preliminary data recording from parvalbumin positive fast spiking interneurons (FSIs), which critically modulate the activity of SPNs (Berke 2011). We find that, consistent with models positing a bias toward direct pathway activation promoting compulsive behavior and with *ex vivo* findings (Ade et al. 2016), that *Sapap3*-KO mice display increased activity in D1-SPNs that persists through the compulsive grooming sequence relative to WT mice. Fluoxetine administration again normalized this increase in activity. Finally, we provide preliminary evidence suggesting that central striatal FSI activity is normal in *Sapap3*-KO mice and speculate as to the role of D2-SPNs in compulsive behavior.

Rather than simply rehash discussion points and conclusions from previous chapters, in the following sections I will attempt to synthesize our findings across species and discuss their implications for our understanding of OCD and OCD-related disorder pathophysiology as well as treatment strategies. I will also discuss limitations of the present experiments as well as future directions.

5.2 Linking reduced excitatory synaptic transcript expression to cortico-striatal activity changes

The constellation of changes that we observed in excitatory synaptic transcripts and excitatory synaptic receptors in the OFC and striatum are difficult to map directly on to changes in activity levels *in vivo*, primarily due to the fact that our findings are likely only an isolated snapshot of the molecular disruption that is occurring at a very specific window in time (at time of death) (see **5.8 Future directions**). It is perhaps more informative to consider changes in specific transcripts for which the basic science literature has causally investigated the function of their protein product on neural activity in cortical and striatal brain regions.

One such transcript, *SLC1A1*, which encodes the neuronal glutamate transporter EAAT3, was reduced in the OFC but not the striatum of OCD subjects relative to unaffected comparison subjects. EAAT3 is expressed both peri- and post-synaptically (Nieoullon et al. 2006; Underhill et al. 2014) where it serves several roles, primarily taking up glutamate from the synapse (Otis et al. 2004). Genetic association of *SLC1A1* and OCD is one of the strongest and most well-replicated links in all of psychiatry (Pauls et al. 2014), though no single SNP has reached genome-wide significance ((OCGAS) 2018; Stewart et al. 2013). Expression of *SLC1A1* and its isoforms has been found across the frontal cortex as well as the striatum in humans (Porton et al. 2013). Interestingly, reduced expression of *SLC1A1* in lymphocytes obtained from OCD subjects compared to controls was detected (a finding that was sensitive to fluoxetine treatment), and the most commonly associated SNP within *SLC1A1* predicts reduced expression in brain tissue (Porton et al. 2013; Wendland et al. 2009). Together, these data might suggest insufficient glutamate buffering at the synapse, which could contribute to cortico-striatal hyperactivity. However, it is worth considering that the majority of preclinical evidence suggests *SLC1A1*s role

in mediating repetitive behavior is through its actions in either the striatum, where we detect no change in *SLC1A1* expression, or subcortically within dopaminergic neurons (Delgado-Acevedo et al. 2018; Zike et al. 2017), which have not yet been evaluated in post-mortem tissue. *SLC1A1* may still contribute to cortical and striatal hyperactivity even if its expression is unchanged within striatal neurons perhaps through alterations within the thalamus, as SNPs in *SLC1A1* have been associated with changes in thalamic volume in OCD subjects (Wu et al. 2013). Reductions in thalamocortical *SLC1A1* expression in OFC could lead to hyperactivity that is then translated downstream to the striatum and perpetuated throughout the cortico-striato-thalamo-cortical (CSTC) loop. Finally, it is worth considering that several isoforms of *SLC1A1* have been found to be negative regulators of EAAT3 transporter function (Porton et al. 2013). As our primers were designed to amplify pan-*SLC1A1*, it is possible that these transcripts are included in this measure and would result in opposing effects on excitatory transmission in the OFC and the striatum.

We also examined the expression of several *SLITRK* transcripts that encode transmembrane proteins known as SLITRKs which aid in neurite outgrowth and both glutamatergic and GABAergic synapse development (Takahashi and Craig 2013; Takahashi et al. 2012). Several SLITRK family members have been linked to OCD and related disorders, with rare variants in *SLITRK1* being linked to Tourette's syndrome (Abelson, Kwan, et al. 2005). Interestingly, in our study we did not detect any differences in *SLITRK1* expression in any brain region studied. These data suggest that *SLITRK1* may not be involved in OCD pathophysiology, a finding supported by data suggesting that *SLITRK1*-null mice lack behavioral phenotypes associated with compulsive behavior and do not appear to have any cortico-striatal abnormalities (Katayama et al. 2010). By contrast, we did observe an OFC specific reduction in another *SLITRK* family member, *SLITRK3*. *SLITRK3* expression was recently implicated in OCD as it interacts with the PTPRD (protein

tyrosine phosphatase, receptor type D) protein at excitatory synapses ((OCGAS) 2018). Although levels of a third SLITRK family member, *SLITRK5*, were too low to detect in our experiments, we can consider data from *Slitrk5* global knockout mice for how cortico-striatal activity may be altered. In addition to displaying compulsive grooming behavior, *Slitrk5*-KO mice display cortico-striatal alterations, including reductions in the expression of striatal glutamate receptors, reminiscent of what we observe in our experiments (reductions of *GRIA1* and *GRIN2B* in both OFC and striatum) (Shmelkov et al. 2010). Although these changes in receptor expression were striatal specific in *Slitrk5*-KOs, an increase in neuronal activity as measured by immediate early gene activation (FosB) were observed within the OFC and not striatum. One possible explanation for this discrepancy is that there may be differential activation of direct and indirect pathway-projecting neurons in the striatum in *Slitrk5*-KO mice, and that simply looking at FosB across all striatal neuron subtypes may obscure pathway specific changes. Further, Shmelkov and colleagues (2010) only examined FosB expression in a restricted area of the dorsolateral striatum which gets limited input directly from OFC (Corbit et al. 2019; Oh et al. 2014). Although the exact molecular mechanism is not clear, data strongly suggest that reductions in *SLITRK* expressions in cortical and striatal brain regions could contribute to cortico-striatal activity changes in OCD.

Finally, prior to our experiments, direct links between *DLGAP3* and OCD were weak. While multiple genomic regions of DLGAP family member encoding *DLGAP1* have emerged as potentially linked to OCD via two GWAS studies (though no single locus has reached genome-wide significance) ((OCGAS) 2018; Stewart et al. 2013), *DLGAP3* has only been tangentially related, with associations made in a subset of OCD patients with grooming disorders (Bienvenu et al. 2009a). More recent evidence has linked rare variants of *DLGAP3* to OCD in a sample of subjects with a comorbid grooming disorder (Trichotillomania) (Zuchner et al. 2009). This

association with grooming disorders in humans perhaps should not be a surprise, given that *Sapap3*-knockout mice display a compulsive grooming behavior that leads to the development of skin lesions (Welch et al. 2007a). Given that DLGAP protein family members are critical for trafficking glutamate receptors (specifically AMPA and NMDA receptors) to excitatory synapses (Rasmussen, Rasmussen, and Silahtaroglu 2017), alterations in excitatory neurotransmission in cortico-striatal circuits are expected.

Indeed, multiple studies have demonstrated dysfunctional cortico-striatal signaling in *ex vivo* preparations from *Sapap3*-KOs; however, most of these studies suggest a reduction in striatal activity mediated through changes in AMPA and NMDA composition at cortico-striatal (but not thalamo-striatal) synapses in the dorsolateral striatum (Chen et al. 2011; Wan et al. 2014; Wan, Feng, and Calakos 2011; Welch et al. 2007a). This is in stark contrast to our findings of increased striatal activity, mediated by an increased recruitment of striatal SPNs at the onset of grooming in *Sapap3*-KO mice. Several possible explanations for this discrepancy exist. First, findings from *ex vivo* preparations may not readily translate *in vivo* within the same circuits, due to a litany of factors, including changes in physiological conditions and alterations in connectivity even when care is taken to preserve the precise circuit being studied. In an *ex vivo* preparation it is not possible to maintain all relevant CSTC connections, rendering accurate assessment of activity within these loops impossible. A substantial and related difference between most *ex vivo* reports and our *in vivo* findings is also the age of *Sapap3*-KO when the experiments were conducted. Studies demonstrating reduced excitatory synaptic transmission at cortico-striatal synapses as well as increased silent synapses were all conducted in 17-25 day old *Sapap3*-KO mice, well before when the compulsive phenotype emerges (post-natal day (PND) 56-60; (Corbit et al. 2019)) and prior to occurrence of many plastic synaptic developmental changes. An inverse disconnect was recently

demonstrated in mutant mice lacking the post-synaptic density protein *Shank3*, with reductions in cortico-striatal activity identified in *Shank3*-KOs at adulthood (Peca et al. 2011) but markedly increased activity found early (< PND 30) in development (Peixoto et al. 2016).

Indeed, when similar *ex vivo* electrophysiological recordings were conducted in adult *Sapap3*-KO mice of phenotypic age, circuit selective changes suggesting striatal hyperactivity emerged (Corbit et al. 2019). These data are complemented nicely by *in vivo* electrophysiological observations of baseline hyperactivity in the central striatum of 3-9 month old WT and *Sapap3*-KO mice, which coincide nicely with our findings of grooming onset-specific increases in striatal hyperactivity (Burguiere et al. 2013). Together, these data suggest that *Sapap3*-KO mice recapitulate a critical and well-replicated observation from OCD patients: cortico-striatal dysfunction. With this in mind, it is useful to develop a neuropsychological model for how this dysfunction may relate to the canonical OCD symptoms of obsessions and compulsions.

5.3 Action chunking: A parsimonious explanation for striatal dysfunction in *Sapap3*-KO mice

One of the more intriguing findings in this thesis is our observation that D1-SPNs are hyperactive during grooming behavior in *Sapap3*-KO mice relative to WT mice (Fig.5-1a), although this activity was not time-locked precisely to the start of a grooming bout. Rather it persisted during the execution of the compulsive behavior. This sort of increase in direct pathway activation during compulsive behavior has long been hypothesized to underlie OCD symptoms (Saxena and Rauch 2000; Maia, Cooney, and Peterson 2008). Interestingly, this activation during execution of compulsive behavior is in contrast to our finding of a transient increase at grooming

onset in overall striatal activity at grooming onset (Fig.5-1c), suggesting that the other predominant cell type within the striatum, D2-SPNs, might be mediating this phenomenon (Fig.5-1b). Given that classic models of the direct and indirect pathway through the basal ganglia would not predict that such an increase in indirect pathway projecting D2-SPNs could lead to compulsive behavior (Kravitz et al. 2010), we need to find a conceptual framework that fits our findings.

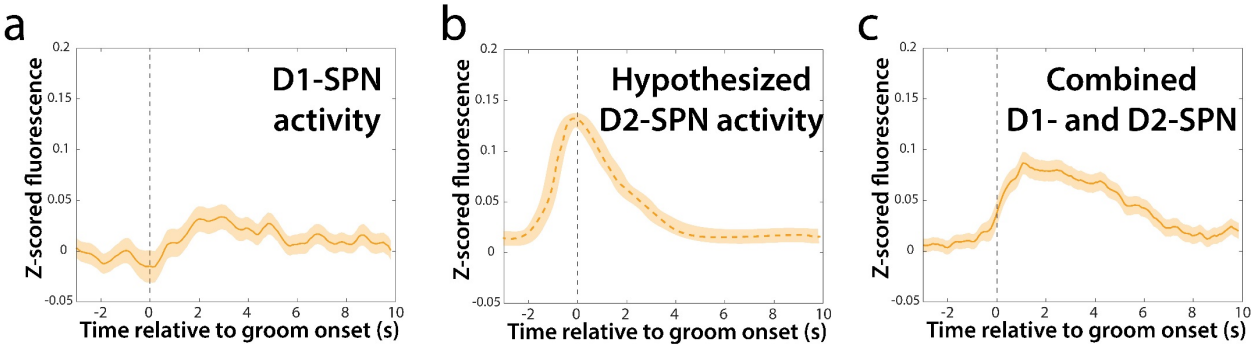

Figure 5-1. Hypothesized contribution of D1- and D2-SPNs to striatal hyperactivity

(**a**) Activity of D1-SPNs during grooming onset display a pattern of increased calcium fluorescence during compulsive grooming rather than at grooming onset. (**b**) Hypothesized transient increase in calcium fluorescence at and just before grooming onset followed by a reduction in activity in D2-SPNs. (**c**) Calcium fluorescence from combined putative D1- and D2-SPNs in the central striatum, characterized by a transient increase in fluorescence at grooming onset and a slow decay during the execution of the compulsive behavior.

An attractive conceptual model that could explain our findings is that compulsive grooming behavior in *Sapap3*-KOs represent concatenated action sequences, as has been reported to occur when a behavior becomes habitual in both rodents and in humans (Graybiel 1998b; Jin, Tecuapetla, and Costa 2014; Wymbs et al. 2012). Critically, this concatenation of learned action sequences, or "chunking", requires cortico-striatal circuitry (Graybiel 1995). This conceptual framework has previously been proposed to underlie OCD symptoms by numerous groups, and nicely bridges the cognitive component of OCD (obsessions) with the repetitive actions (compulsions) through dysfunction in parallel motor and cognitive cortico-basal ganglia loops (Graybiel and Rauch 2000). Our data of an overall increase in striatal activity at the onset of compulsive grooming sequence

(as well as offset; Fig.A-8), combined with data that per individual grooming sequence mice make more transitions between different types of grooming behavior per bout suggest that *Sapap3*-KO mice are engaging in chunking multiple segments of the compulsive sequence. Critically, wildtype mice do not display the same level of grooming onset activity, and engage in single grooming bouts with significantly fewer transitions. These data are consistent with findings that under normal conditions in wildtype mice central striatal activity is not associated with the onset of individual grooming movements (e.g. face grooming or body grooming in isolation), but is rather only found at the onset of syntactic grooming chains (Aldridge and Berridge 1998; Aldridge, Berridge, and Rosen 2004), which are sequences of concatenated grooming events conducted infrequently in normal mice (Kalueff et al. 2016). Perhaps the aberrant activity in the *Sapap3*-KO striatum signals the improper onset of a syntactic grooming chain, which qualitatively might be similar to an individual with OCD engaging in compulsive handwashing, a normative sequence of behavior that has become hijacked. An important consideration with this working hypothesis is that typically action chunking and habitual behavior is associated with activity in the dorsolateral striatum (Graybiel 1998b; Smith and Graybiel 2013a; Smith and Graybiel 2013c; Smith and Graybiel 2016), not the central striatum which appears dysfunctional in *Sapap3*-KO mice both in our studies and in those conducted by others (Burguiere et al. 2013). However, it is worth noting that onset and offset-related activity has also been detected in other striatal subregions upon acquisition of a habit (Howe et al. 2011) and are characteristically found in downstream basal ganglia structures that receive input from across the dorsal and ventral striatum, not just the dorsolateral portion (Jin and Costa 2010). Further, dorsolateral striatum dysfunction is well documented *ex vivo* in *Sapap3*-KO mice, and a similar bias toward D1-SPN signaling has been identified (Ade et al. 2016; Chen et al. 2011; Wan et al. 2014; Wan, Feng, and Calakos 2011;

Welch et al. 2007a). These data suggest the intriguing possibility that the *Sapap3*-KO striatum may be predisposed to developing habitual-like processing strategies, including chunking of normative behavioral patterns such as grooming. However, more work must be done to assess whether *Sapap3*-KO mice are more prone to developing canonical habitual behavior (Balleine and O'Doherty 2010), and whether it is in any way related to the compulsive grooming phenotype.

5.4 The role of D1- and D2-SPNs in action chunking

Our data showing ongoing hyperactivity in direct (D1-SPN) pathway projecting SPNs and the hypothesized role of indirect pathway (D2-SPN) projecting neurons during compulsive grooming are also broadly consistent with the existing literature on the distinct role of these pathways in the concatenation of behavioral sequences. Recent work from Dr. Rui Costa's lab demonstrates that when mice perform a well-learned series of sequential actions, not all that dissimilar from the typical grooming sequence, populations of both D1- and D2-SPNs in the dorsal striatum are active at the start of the sequence (Jin, Tecuapetla, and Costa 2014). This is in line with our data that in both genotypes a percentage of D1-SPNs are active at the onset of a grooming bout. Interestingly, Jin and colleagues (2014) demonstrated that mice performed a well-learned sequence, a significantly greater proportion of D1-SPNs displayed increased activity that persisted through the execution of the sequence compared to D2-SPNs. These data are consistent with our observation that during execution of the compulsive behavior there is a significant increase in the percentage of active D1-SPNs in *Sapap3*-KO mice relative to WTs. By contrast, in (Jin, Tecuapetla, and Costa 2014) D2-SPN activity was elevated only at the start of the learned behavioral sequence and inhibited during the execution of the behavior, with D2-SPN activity

preceding D1-SPN activity. These data suggest that, during well learned action sequences, such as a syntactic grooming chain, D2-SPNs will be preferentially active at the onset of the sequence in *Sapap3*-KO mice relative to WT mice. In a different sequence learning task, it was recently demonstrated that a similar phenomenon occurs, with sustained activity of D1-SPNs and quiescent activity of D2-SPNs necessary for accurate sequence completion (Rothwell et al. 2015). Interestingly, in this task it was found that behavioral training was associated with strengthening of the synapse from supplementary motor area M2 (M2) to D1-SPNs. This same cortico-striatal projection (though not specific to D1- or D2-SPNs) was recently identified as strengthened in *Sapap3*-KO mice relative to WT mice (Corbit et al. 2019), providing a potential substrate for central striatal hyperactivity and chunking of action sequences.

Of course, the activity of D1- and D2-SPNs are not occurring in isolation, and changes across the frontocortical-striatal-thalamo-cortical loops have been consistently observed in OCD (Pauls et al. 2014; Maia, Cooney, and Peterson 2008; Menzies et al. 2008b). An outstanding question is, how are cortical regions that project to the central striatum behaving during sequences of compulsive grooming? Interestingly, in the lOFC, a major source of input to the central striatum (Corbit et al. 2019; Oh et al. 2014), we observe hypoactivity at the onset of compulsive behavior in *Sapap3*-KO mice relative to WT mice. These data coincide with observations in OCD patients that avoidance habit formation was associated with hypoactivation of the OFC and hyperactivation of the caudate nucleus (Gillan et al. 2015; Gillan et al. 2014a). One possible mechanism by which hypoactivation of OFC could be occurring is through feedback through the cortico-basal ganglia loop. It was recently demonstrated that activation of striatal D2-SPNs, while overall reducing cortical activity, transiently excited a subpopulation of superficial cortical neurons (Oldenburg and Sabatini 2015). As the majority of layer 1 cortical neurons are inhibitory interneurons (Larkum

2013), it is possible that *in vivo* activation of D2-SPNs may result in a reduction in cortical activity as the compulsive behavioral sequence unfolds. Importantly, Oldenburg and colleagues (2015) found no such population of neurons were found following stimulation of D1-SPNs, suggesting that while negative feedback might affect D2-SPNs, D1-SPN activity would remain elevated throughout the behavioral sequence, similar to what we observe during compulsive behavior, and what has been reported by others during well-learned action sequences (Jin, Tecuapetla, and Costa 2014; Rothwell et al. 2015; Cui et al. 2013).

Taken together, these data suggest a complex interplay between direct and indirect pathway projecting striatal neurons in regulating compulsive behavior. Overall, they support a role for a bias toward direct pathway activation in individuals with OCD, though they suggest a substantial role for the indirect pathway as well. Obtaining *in vivo* data from D2-SPNs as well as other striatal neuron subtypes during compulsive behavior will be necessary for a comprehensive interpretation.

5.5 Fast spiking interneurons: A critical and vulnerable cell type

While only comprising between 1-3% of all striatal cells, striatal fast-spiking neurons (FSIs) are hypothesized to exert feed-forward inhibition onto networks of nearby SPNs (Berke 2011). Though this property of FSIs has been difficult to observe *in vivo*, a recent study did demonstrate that optogenetically reducing FSI activity was capable of disinhibiting nearby SPNs (Owen, Berke, and Kreitzer 2018). Although our extremely preliminary data obtained from only a single *Sapap3*-KO and WT mouse suggest no difference in activity of central striatal FSIs during compulsive behavior, previous reports suggest functional changes that implicate them in both the compulsive behavioral phenotype as well as the treatment response to fluoxetine. In one report,

Burguiere and colleagues (2013) demonstrated that optogenetic stimulation of lOFC terminals in the central striatum of *Sapap3*-KO mice was capable of entraining striatal FSIs and resulted in a subsequent reduction in SPN activity. These data suggest that there is a deficit in feed-forward inhibition in *Sapap3*-KO mice, which may serve to produce and maintain the hyperactive state of central striatal SPNs discussed previously. While changes in markers of FSIs, such as the calcium binding protein parvalbumin (PV), have not been identified in OCD (including in our studies, see **Chapter 2**), it is worth noting that in an OCD-related disorder characterized by repetitive behavior, Tourette's syndrome, expression of PV in the striatum is reduced relative to healthy comparison subjects (Kalanithi et al. 2005; Kataoka et al. 2010). A causal link between PV expression and repetitive behavior was recently made, with ablation of striatal FSIs (resulting in a 40% reduction) causing elevated grooming and anxiety-like behavior, though only following stress paradigms (Xu, Li, and Pittenger 2016). A recent report out of our laboratory suggests the picture is also more complicated than these previous heavy-hammer approaches suggest, with input to central striatal FSIs in *Sapap3*-KO and WT mice differing as a function of specific cortical inputs (lOFC and M2) (Corbit et al. 2019). Regardless, ample data suggest that striatal FSI dysfunction may be relevant to repetitive and compulsive behavior.

We have also raised the intriguing possibility that striatal FSIs may serve as a novel target for treatment of OCD and compulsive behaviors, which the field desperately needs (Pittenger and Bloch 2014). Consistent with previous studies suggesting that serotonin as well as SSRIs can increase the excitability of FSIs (Zhong and Yan 2011; Athilingam et al. 2017; Blomeley and Bracci 2009), we observe that fluoxetine can reduce the grooming-associated activity of all putative central striatal SPNs, as well as of D1-SPNs specifically, on the same time scale as the reduction in compulsive behavior. While glutamatergic agents such as ketamine and memantine

are beginning to show promise for the treatment of OCD and related disorders (Hirschtritt, Bloch, and Mathews 2017; Rodriguez et al. 2015; Rodriguez et al. 2016), these compounds have significant drawbacks often in the form of adverse side effects (Kirby 2015) that necessitate the development of more specific compounds with similar therapeutic efficacy (Zanos et al. 2015). One possibility raised from our studies would be that rather than decreasing glutamatergic tone via glutamate receptor antagonists, potentially directly targeting FSIs would serve as a more specific therapy. This could potentially be achieved through activation of the 5-HT_2 class of receptors, which are expressed on FSIs and mediate the depolarizing effects of fluoxetine (Zhong and Yan 2011; Athilingam et al. 2017). Preclinically, specific 5-HT_{2C} receptor agonists have been used to reduce compulsive eating in a rodent model, and in our hands the same compound reduces grooming in *Sapap3*-KO mice (Fig.A-9). Future experiments will evaluate whether these compounds selectively modulate striatal FSIs *in vivo*.

5.6 Limitations & Future directions

Throughout we have discussed some logical immediate follow-up experiments that would paint a more complete picture of the role of excitatory synaptic dysfunction in cortical and striatal brain regions in OCD. Rather than re-iterate those same experiments here, we will instead focus on future experiments born out of the questions and models discussed above.

5.6.1 Human post-mortem experiments

Our post-mortem experiments provide a glimpse of potential excitatory synaptic dysfunction in cortical and striatal regions in OCD, but also raise a considerable amount of questions that must be addressed in future experiments. First, what is the scope of the dysfunction? An unbiased RNA-sequencing experiment of these same subjects and regions is already completed, and data analysis is beginning. With a complete picture of the transcriptome, it will be much easier to infer how activity in both the cortex and the striatum might be changed in OCD subjects relative to healthy comparison subjects. These experiments will also shed light on novel molecular pathways that may be involved separate from synaptic dysfunction. We are extremely interested into moving closer to function, as transcript changes do not always correlate with alterations in functional protein. We already have preliminary large scale proteomic data focusing on a curated list of synaptic proteins from a single cortical and single striatal brain region from our OCD subjects and matched comparisons. Given the magnitude of change we observe at the transcript level, we expect to see similar proteomic changes in both the OFC and striatum.

Another interesting question is to evaluate the extent of the decreased expression we observed in excitatory synaptic transcripts. The similarity in expression levels within the OFC regions examined suggests that perhaps these reductions in expression would be found in other regions that participate in other cortico-basal ganglia loops. Further, it would be useful to examine a cortical region not typically associated with cortico-striatal signaling, such as a primary sensory area (e.g. V1) (Haber 2016). In this case I would not expect to see the same changes in excitatory synaptic gene expression that we observed in the OFC. Overall, our post-mortem experiment serves as excellent hypothesis generating data, both for future studies in post-mortem tissue as well as studies in rodents.

5.6.2 Translational rodent experiments

Future experiments in *Sapap3*-KO mice will seek to further investigate the circuit and specific cellular mechanisms underlying compulsive behavior. A major limitation of the present experiments pertains to investigating the effects of fluoxetine on circuit function. It will be critical to include vehicle treated control groups for future experiments, as interpretation of neural activity after fluoxetine treatment may simply represent activity changes that might occur over time or following repeated injections. Current datasets all include two-week washout days (data not yet analyzed), where imaging was conducted two weeks after the final fluoxetine administration, which should help clarify whether our effects are due to drug or the aforementioned confounding factors. Our current data strongly suggest that cells in the central striatum control grooming or grooming related movements, but it is still unclear the causal role they play in the compulsive grooming phenotype shown by *Sapap3*-KO mice. In order to directly test their role, complementary inhibitory experiments in *Sapap3*-KO mice using an inhibitory opsin such as halorhodopsin expressed in striatal neurons must be conducted. However, these experiments are quite challenging without a closed-loop stimulation paradigm that would allow for stimulation immediately at the onset (or even prior to onset) of compulsive behavior. Current experiments are evaluating whether data from an accelerometer attached to the miniature microscope can be accurately decoded on-line to provide rapid and precise information about whether an animal is grooming. While our data suggest that lOFC input to the central striatum of *Sapap3*-KO mice is reduced at the onset of grooming, recently published data from our lab suggests that there is increased input from M2. Additionally, ChR2 stimulation of M2 terminals in the central striatum of WT mice causes an increase in grooming probability relative to control virus (Fig.A-10). Future experiments will use a variety of strategies, including using transsynaptic viruses that will allow

for cre-mediated transgene expression in cells that project to central striatum from isolated cortical regions in order to explore the precise role of lOFC versus M2 in compulsive grooming in *Sapap3*-KO mice.

We have also suggested that, based on activity patterns observed during compulsive behavior in the lOFC and striatum, *Sapap3*-KO mice may be prone to developing habitual behavior. This hypothesis should be directly tested using conventional operant devaluation or contingency degradation experiments. Our hypothesis for these experiments would be that *Sapap3*-KO mice might shift from using a goal-directed response strategy to a habitual one earlier in training, and that this dysfunction may be associated with elevated central striatal activity (as opposed to dorsolateral striatal activity). Another active area of investigation is how *Sapap3*-KOs perform on sequence learning tasks where the roles of D1- and D2-SPNs have recently been elucidated (Cui et al. 2013; Jin, Tecuapetla, and Costa 2014; Rothwell et al. 2015). Based on the data presented here, we might predict that *Sapap3*-KOs would have a bias toward more sequence starts but less completions, similar to their fragmented and uncompleted grooming chains.

Finally, given the goals set out in the introduction of this dissertation, a future experiment that would be broadly interesting would be to attempt to investigate the causal effects of modifying multiple transcripts in a single mouse model. While monogenic knockouts are excellent for isolating the effects of a single gene or protein on a circuit of interest (Picciotto and Wickman 1998), the reality is that most neuropsychiatric diseases are likely caused by multiple genetic insults, each of small effect size ((OCGAS) 2018; Bloch and Pittenger 2010). Just as optogenetics has revolutionized our ability to associate specific circuits and cells, as we utilized in this dissertation, with particular behavioral phenotypes, the CRISPR-cas9 system may dramatically improve our ability to precisely target specific molecular pathways (Sadhu et al. 2018). Disrupting

multiple genes (e.g. multiple genes encoding for excitatory synaptic proteins) at once would allow for a more accurate model of specific pathological phenotypes, though it has the potential to make interpretation of these changes more challenging.

5.7 Conclusions

In summary, this dissertation provides the first evidence that OCD subjects have altered expression of glutamatergic synaptic transcripts in regions consistently linked to OCD via structural and functional neuroimaging studies (the OFC and the striatum). Taking a translational approach, we also investigated how compulsive behavior was encoded in homologous brain regions (lateral OFC and the central striatum) of a mouse globally lacking one of these critical excitatory synaptic transcripts (*Sapap3*). These data lend support to hypotheses positing that compulsive behavior may be the result of imbalance in the direct and indirect pathway through the basal ganglia and demonstrate how a first-line pharmacological treatment for OCD may be normalizing this balance. Altogether, these data lay the groundwork for future investigations of the cellular, molecular, and circuit mechanisms underlying the generation of compulsive behavior.

Appendix A Chapter 2, 3 & 4 Supplemental details

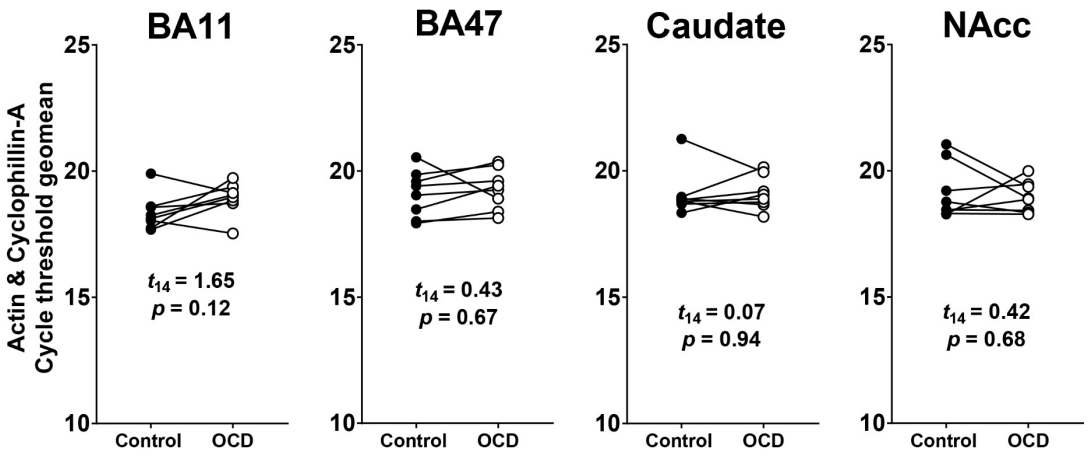

Figure A-1. Stable expression of two housekeeping genes, *ACTB* and *PPIA*, in OCD and unaffected comparison subjects.

No significant differences were observed across all 4 brain regions in the geometric mean of the cycle threshold values for two housekeeping genes: *ACTB* (encoding β-actin) and *PPIA* (encoding cyclophilin-A).

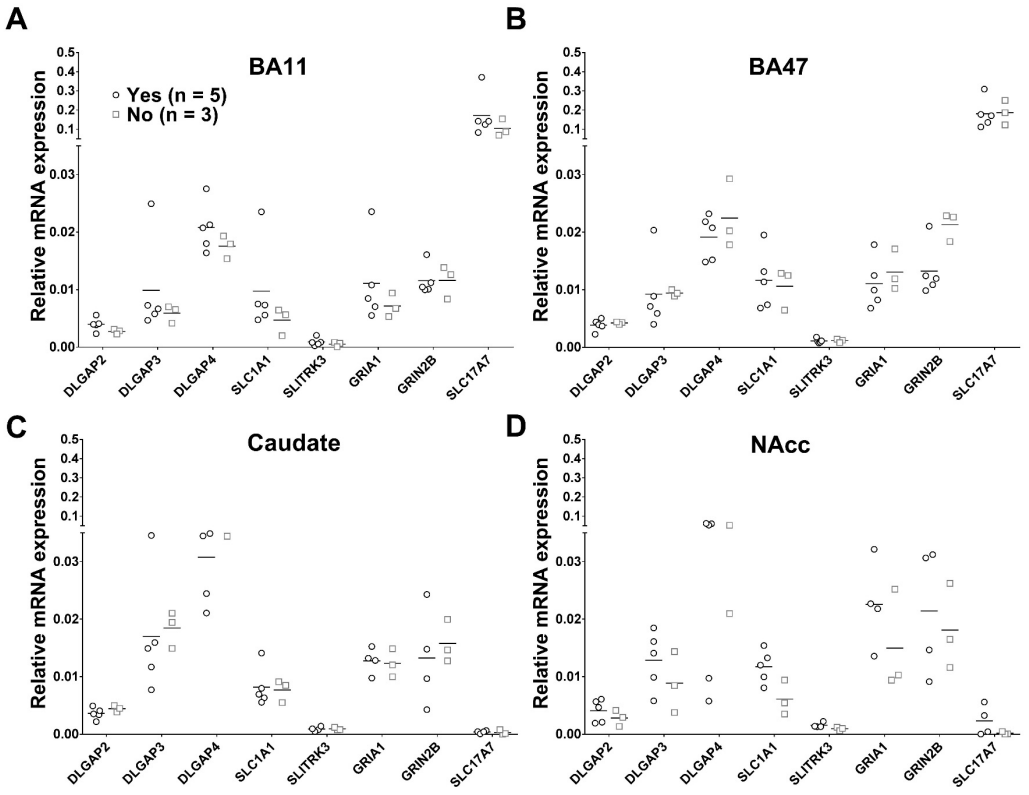

Figure A-2. No effect of antidepressant medications at time of death on expression of significantly altered transcripts in OCD subjects.

No significant differences in expression of 8 transcripts that were differentially affected by OCD diagnosis were observed between OCD subjects on (n = 5) and off (n = 3) antidepressants at time of death within BA11 (**A**), BA47 (**B**), caudate (**C**), or NAc (**D**). All $t_6 < 2.8$ and all $p > 0.22$.

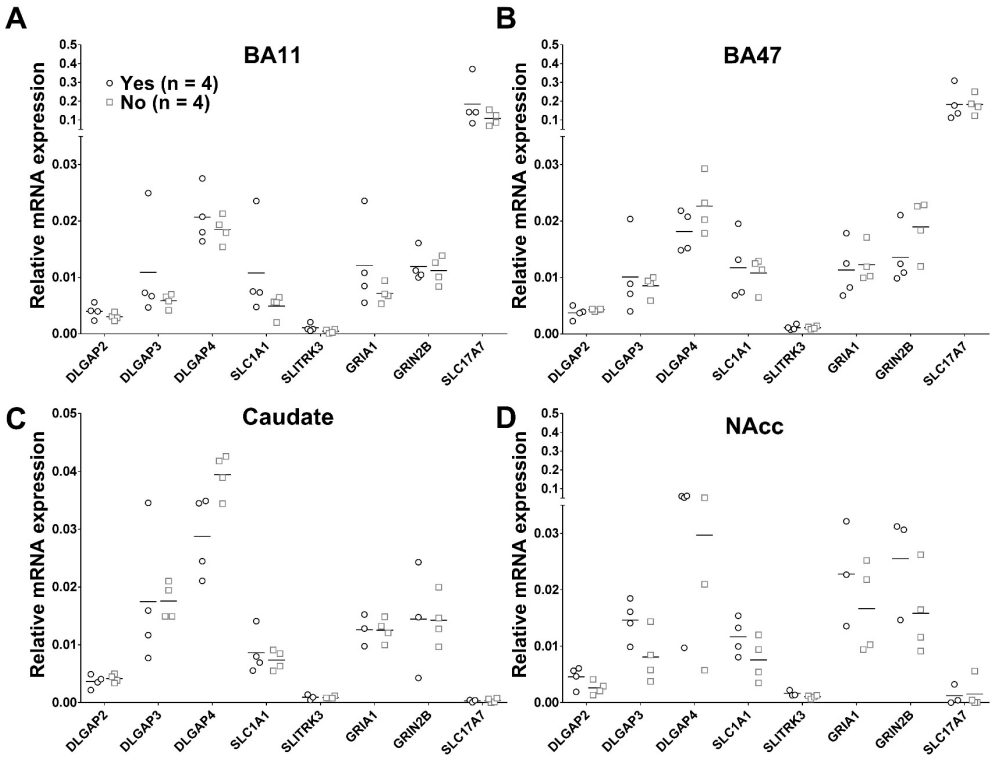

Figure A-3. No effect of benzodiazepines at time of death on expression of significantly altered transcripts in OCD subjects.

No significant differences in expression of 8 transcripts that were differentially affected by OCD diagnosis were observed between OCD subjects on (n = 4) and off (n = 4) benzodiazepines at time of death within BA11 (**A**), BA47 (**B**), caudate (**C**), or NAc (**D**). All $t_6 < 2.7$ and all $p > 0.23$.

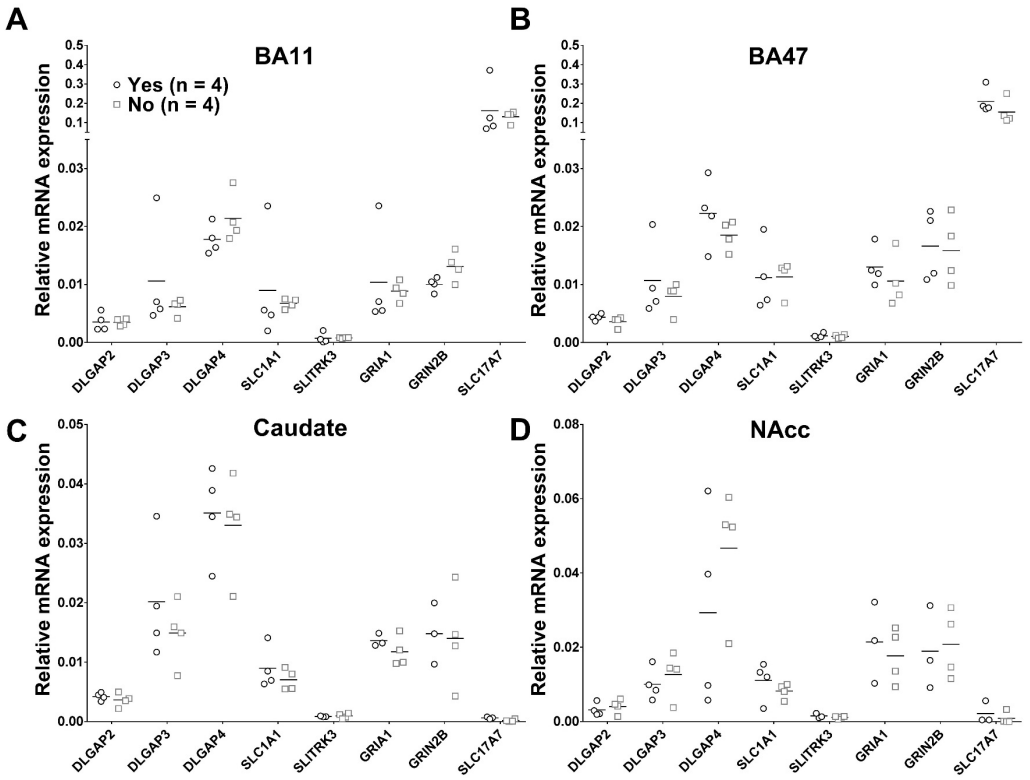

Figure A-4. No effect of comorbid major depressive disorder (MDD) diagnosis on expression of significantly altered transcripts in OCD subjects.

No significant differences in expression of 8 transcripts that were differentially affected by OCD diagnosis were observed between OCD subjects with an MDD diagnosis ($n = 4$) and those without an MDD diagnosis ($n = 4$) within BA11 (**A**), BA47 (**B**), caudate (**C**), or NAc (**D**). All $t_6 < 2.2$ and all $p > 0.44$.

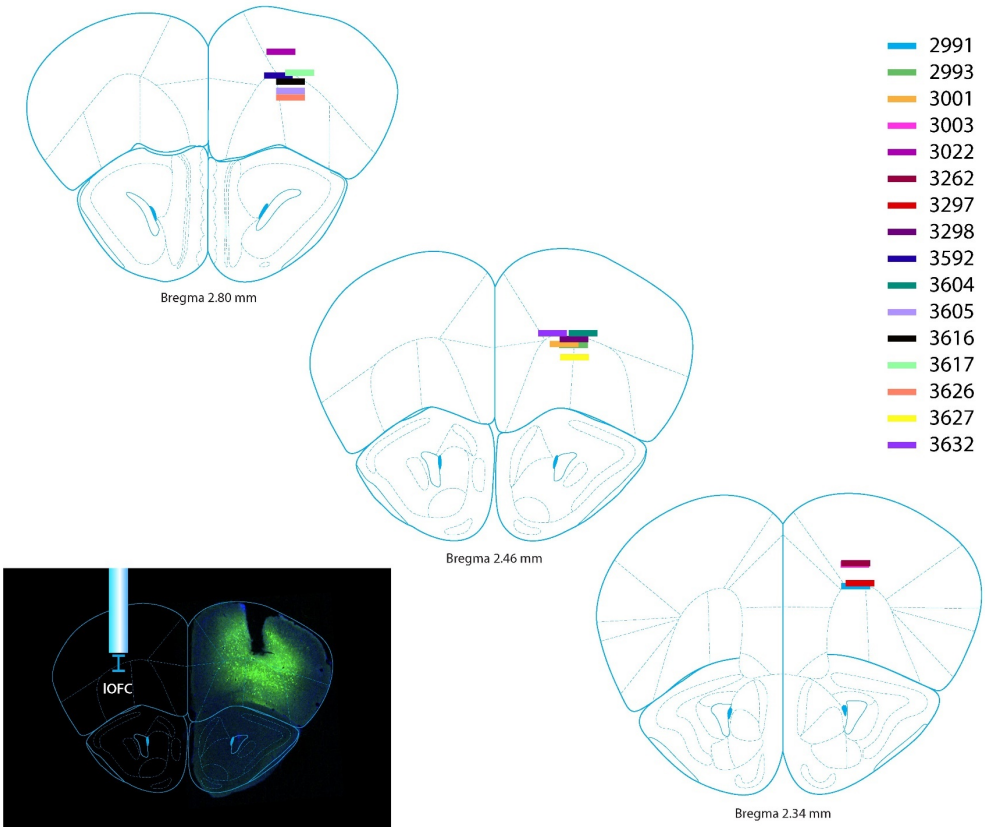

Figure A-5. Histological verification of lens placement in lOFC

Each line indicates the estimated location of bottom of the 200 μm focal distance below the 0.5 mm diameter lens (inset image).

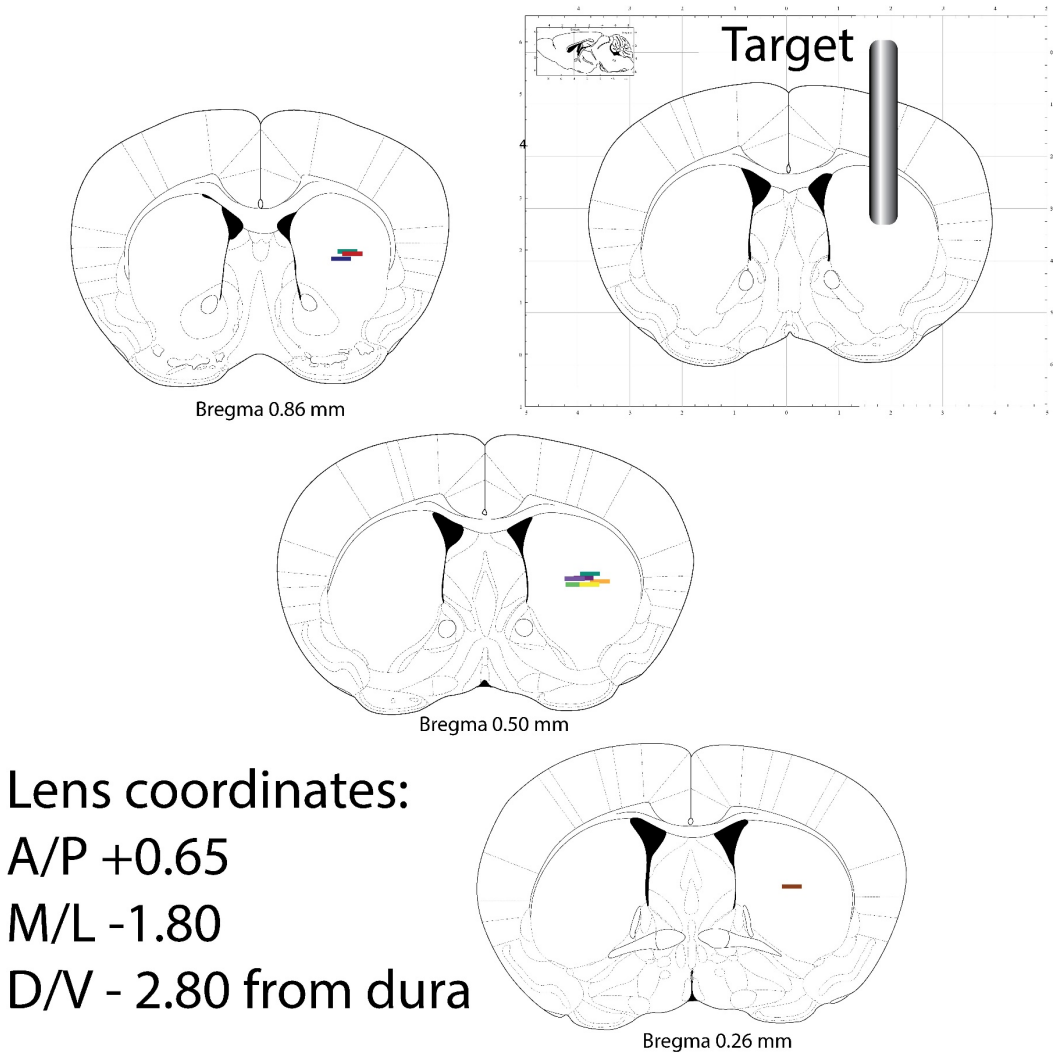

Figure A-6. Histological verification of lens implants into central striatum

Each line indicates the estimated location of bottom of the 200 µm focal distance below the 0.5 mm diameter lens (inset image). 10 total WT and *Sapap3*-KO mice used in the fluoxetine study.

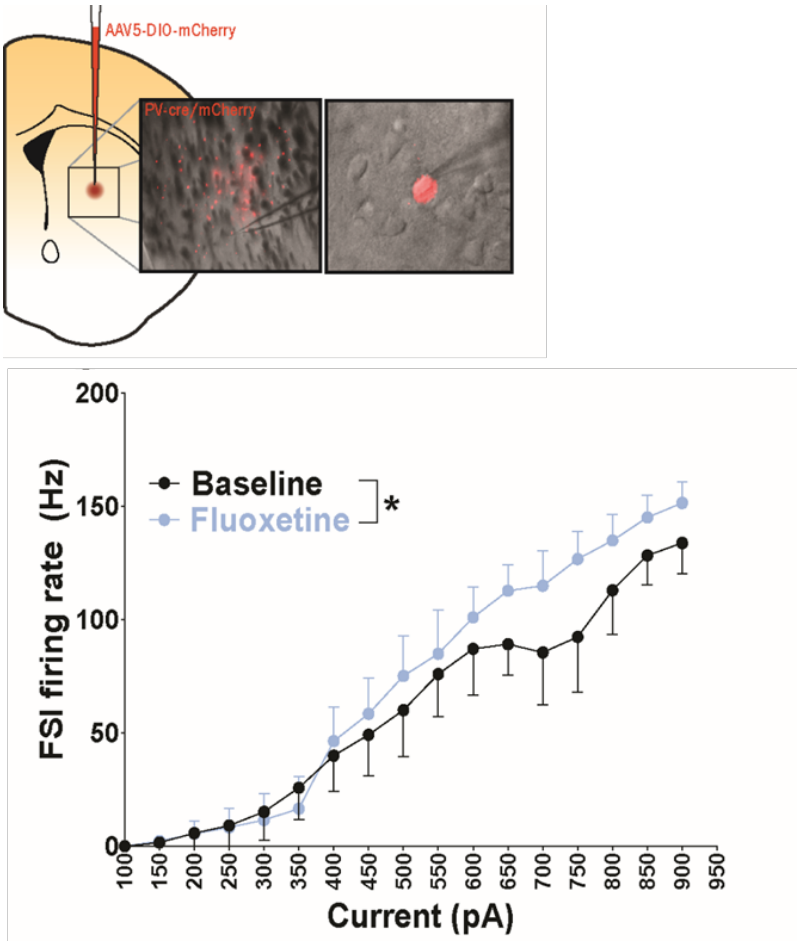

Figure A-7. Effect of fluoxetine on central striatal FSI activity in *Sapap3*-KO mice

(top) Image depicting mCherry reporter expression from PV-cre / *Sapap3*-KO mouse injected with a cre-mediated reporter virus. (bottom) *Ex vivo* voltage clamp recording of central striatal FSI firing rates at baseline at a variety of current steps, and after application of 100 μM fluoxetine.

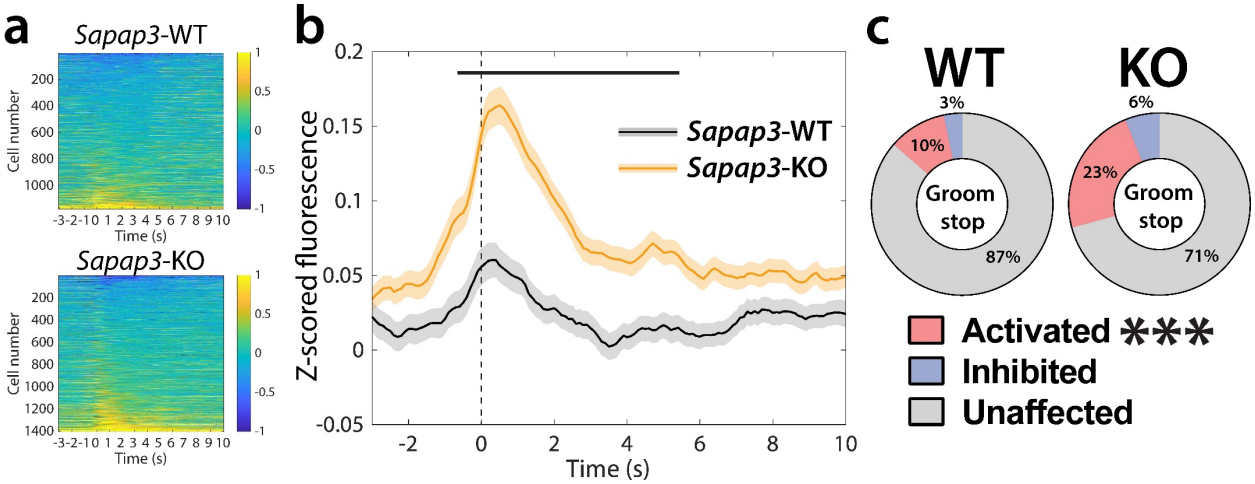

Figure A-8. Central striatal activity aligned to grooming-stop in WT and *Sapap3*-KO mice

(**a**) Heatplots for all cells in WT (top) and *Sapap3*-KO mice (bottom). Each row represents an individual SPNs response to all grooming bout stops, sorted by average fluorescence in the peri-grooming window (-0.5s to 3s). (**b**) Grooming-stop aligned calcium fluorescence across all SPNs in each genotype (all significant $t(2577) \geq 4.28$, $p \leq 0.000019$, unpaired *t*-test). (**c**) Percentage of groom-stop activated ($t(17) = 4.748$, $p = 0.0002$, unpaired *t*-test) and groom-stop inhibited ($t(17) = 1.954$, $p = 0.067$, unpaired *t*-test) SPNs in WT and *Sapap3*-KO mice.

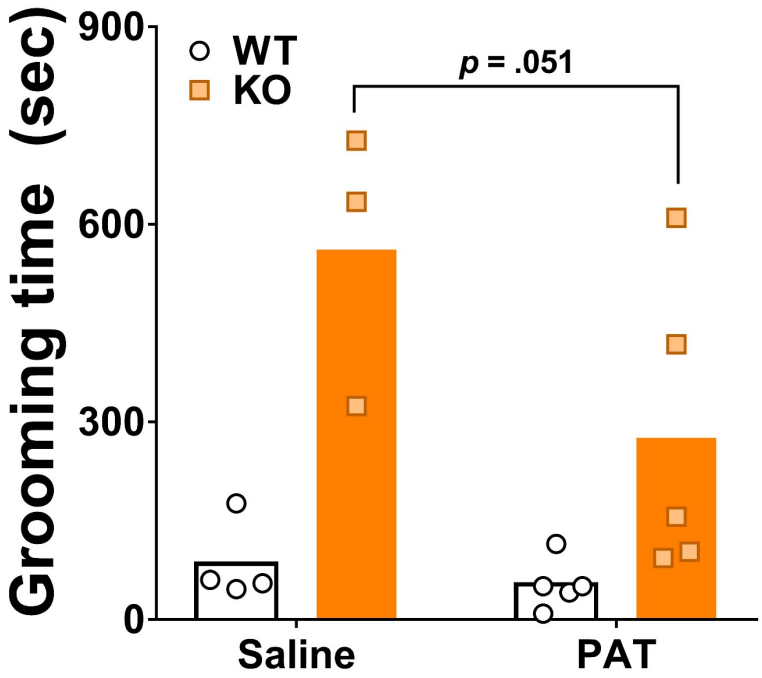

Figure A-9. Effect of 5-HT$_{2C}$ receptor agonist on compulsive grooming in WT and *Sapap3*-KO mice.

Effect of subchronic (5 day) treatment with the 5-HT$_{2C}$ receptor agonist (1R,3S)-(−)-trans-1-phenyl-3-dimethylamino-1,2,3,4-tetrahydronaphthalene (PAT) on grooming in WT and *Sapap3*-KO mice ($t(13) = 2.511$, $p = 0.0514$, Sidak's multiple comparisons test).

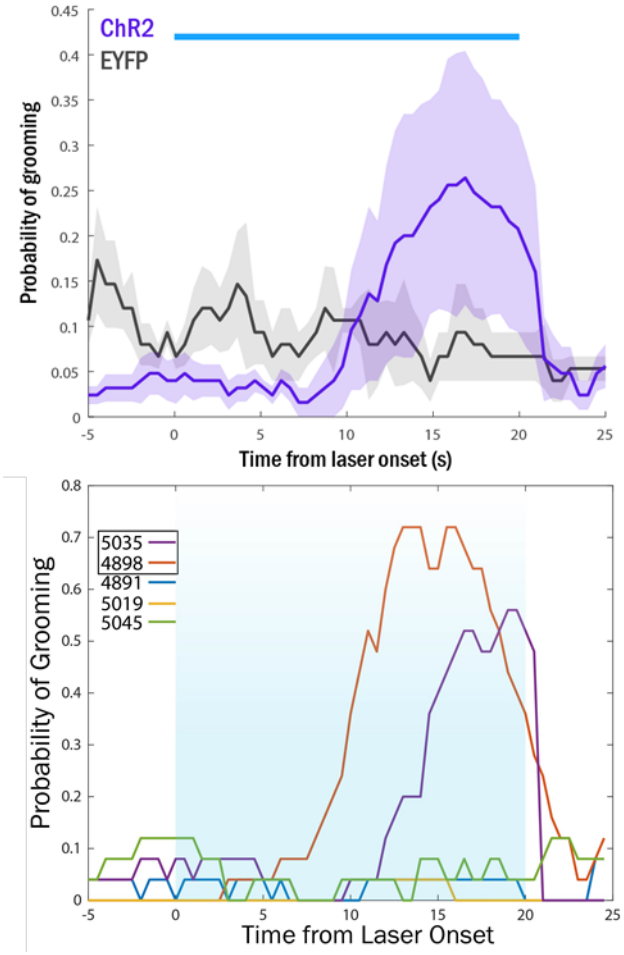

Figure A-10. Effect of M2 terminal stimulation in central striatum of wildtype mice.

(top) Average response of M2 terminal activation (blue bar; 20Hz 473nm wavelength stimulation for 20s) in ChR2-positive and eYFP-positive WT mice. (bottom) Individual ChR2-positive mice demonstrates heterogeneity in response to M2 terminal activation, with 2/5 mice displaying a robust but delayed increase in grooming.

Table A-1. Oligonucleotide sequences of forward and reverse primers used for each transcript in this study.

Oligonucleotide sequence length was between 18 and 23 bases for each primer. Primers were designed using NCBI Primer-Blast and synthesized by Integrated DNA technologies (IDT; Coralville, Iowa, USA). Transcript variants (indicated by the letter V) were considered detectable if the primer sequence and target sequence template was a 100% match[1]. Genes with no characterized transcript variants are indicated by[2].

Gene	*Forward Primer*	*Reverse Primer*	*Amplicon size*	*Transcript variants detectable*[1]	*Accession Number*
ACTB	ACGGTGAAGGTGACAGCA	TTAGGATGGCAAGGGACTTC	92	*None*[2]	NM_001101
PPIA	GCAGACAAGGTCCCAAAG	GAAGTCACCACCCTGACAC	126	*V1, V2*	NM_021130
DLGAP1	GAAACAGATGGATCCTCTTGACA	ACAGCAGGACTGAATGCAGAA	71	*V1, V3, V7*	NM_004746
DLGAP2	CAGCCATACCCAAGGTCAGA	CACCCCGACAGAGTGGTATT	87	*V3*	NM_001346810
DLGAP3	CAGCACACAACTTCTCCTGTC	GCTGTTGGCCTTGAGTTGC	187	*None*[2]	NM_001080418
DLGAP4	GCCCCCAAAAGGAAACTGTC	TCACATCGATCGCTTTGGGT	100	*V1*	NM_014902
SLC1A1	TTTGGACTTGTCATTGGAAA	TATGATCTTCCCAGCAATCA	150	*None*[2]	NM_004170
SLITRK1	CAACAGAAGCCGCGGAAAAC	GAGGGTTTGCAGCGTAGTACA	102	*V1*	NM_052910
SLITRK3	CTCCCTTGGTGCGCGATTT	AGCGCCAGGTCGTGTATAAG	96	*V2*	NM_014926
GRIA1	GGGTCTGCCCTGAGAAATCC	GTCCTTGGAATCACCTCCCC	132	*V1, V3, V7, V10*	NM_000827
GRIN2B	GGCCTTCTTTGCTGTCATCT	GGAAAGGGGGTGAGAAGTCAT	140	*None*[2]	NM_000834
GABARAP	AGAAGAGCATCCGTTCGAGA	TTCTACTATCACCGGCACCC	85	*None*[2]	NM_007278
PVALB	CTGCTGGAGACAAAGATGG	GTTCAGGGCAGAGAGGTG	114	*V1, V2*	NM_002854
CALB1	AATGATCGTTCTGGGTCAGC	GCCAATCTCCCACTCAACAT	177	*V1, V2*	NM_004929
GAD1	CTGGCTGTACGTCTGGTG	GCGAGTCACAGAGATTGGT	104	*None*[2]	NM_000817
GAD2	GTGGCAACCTGTTCTTCC	ATTTGGGTTTAGAGAGACAACAC	81	*V1, V2*	NM_000818
SLC32A1	TTCAGGAATCTAAACTCTCATCTT	CTTATTCACCACGAGCACA	85	*None*[2]	NM_080552
SLC17A7	AGCTGGGATCCAGAGACTGT	CCGAAAACTCTGTTGGCTGC	116	*None*[2]	NM_020309

Table A-2. Detailed information on data analyzed for each transcript across subject pairs and regions.

For most transcripts and subject pairs, all 8 subjects were analyzed (empty squares). Two transcripts (*SLITRK3* and *PVALB*) did not have detectable levels of transcript expression in the NAc of all subjects, and *SLC17A7* expression was too low to be detected in both the caudate and NAc of all subjects; these values could therefore not be included in the analysis (indicated by grey crosshatch). In addition, a single subject pair (pair 8) had low RNA yield for 6 transcripts (indicated by orange shading).

Supplemental Table 2: Detailed information on data analyzed for each transcript across subject pairs and regions.

	Pair 1				Pair 2				Pair 3				Pair 4			
Transcript	BA11	BA47	Caudate	NAcc	BA11	BA47	Caudate	NAcc	BA11	BA47	Caudate	NAcc	BA11	BA47	Caudate	NAcc
DLGAP1																
DLGAP2																
DLGAP3																
DLGAP4																
SLC1A1																
SLITRK1																
SLITRK3																
GRIA1																
GRIN2B																
GABARAP																
PVALB																
CALB1																
GAD1																
GAD2																
SLC32A1																
SLC17A7																
	Pair 5				**Pair 6**				**Pair 7**				**Pair 8**			
Transcript	BA11	BA47	Caudate	NAcc	BA11	BA47	Caudate	NAcc	BA11	BA47	Caudate	NAcc	BA11	BA47	Caudate	NAcc
DLGAP1																
DLGAP2																
DLGAP3																
DLGAP4																
SLC1A1																
SLITRK1																
SLITRK3																
GRIA1																
GRIN2B																
GABARAP																
PVALB																
CALB1																
GAD1																
GAD2																
SLC32A1																
SLC17A7																

	indicates no data for this transcript from this pair of subjects
	indicates low expression for this transcript in specific brain region

Table A-3. Expanded demographic information for all subjects

Demographic characteristics for all subjects (n = 8 per diagnostic group), including comorbidities. **a:** PMI (post-mortem interval) in hours. **b:** RIN (RNA integrity) measured by Agilent Genomics Bioanalyzer 2100. **c:** MOD (manner of death). **d:** COD (cause of death), ASVCD (arrhythmogenic right ventricular dysplasia). **e:** Comorbidities: OCPD (obsessive-compulsive personality disorder), MDD (major depressive disorder), BPD (bipolar disorder), GAD (generalized anxiety disorder), PD (panic disorder), PTSD (post-traumatic stress disorder).

											Comorbid Diagnoses					
Pair	Case #	OCD Diagnosis	Sex	Age	Race	PMI[a]	RIN[b]	MOD[c]	COD[d]	Tobacco ATOD	OCPD	MDD	BPD	GAD	PD	PTSD
1	1159	Unaffected comparison	M	51	W	16.7	7.6	Natural	ASCVD	N	-	-	-	-	-	-
	1413	OCD	M	52	W	17.4	8.0	Suicide	Fluvoxamine OD	N	Yes	Yes	-	-	-	-
2	1293	Unaffected comparison	F	65	W	18.5	7.0	Accidental	Trauma	N	-	-	-	-	-	-
	1424	OCD	F	69	W	10.5	7.1	Natural	Dilated cardiomyopathy	N	Yes	-	-	-	-	-
3	13032	Unaffected comparison	M	52	W	9	8.2	Natural	Pulmonary embolism	Y	-	-	-	-	-	-
	1435	OCD	M	52	W	7.9	8.0	Natural	ASCVD	N	-	-	-	-	-	-
4	1092	Unaffected comparison	F	40	B	16.6	8.0	Natural	Mitral valve prolapse	N	-	-	-	-	-	-
	1505	OCD	F	42	W	23.5	8.2	Natural	ARVP	N	-	-	-	-	Yes	Yes
5	1543	Unaffected comparison	F	45	W	17.9	7.4	Natural	Subarachnoid hemorrhage	Y	-	-	-	-	-	-
	1785	OCD	F	50	W	29.8	7.3	Suicide	Drowning	Y	-	-	Yes	-	-	-
6	1391	Unaffected comparison	F	51	W	7.8	7.1	Natural	ASCVD	Y	-	-	-	-	-	-
	13051	OCD	F	47	W	10.8	7.6	Natural	ASCVD	Y	Yes	-	-	-	Yes	Yes
7	1083	Unaffected comparison	M	20	W	19.9	8.8	Accidental	Trauma	Y	-	-	-	-	-	-
	13022	OCD	M	20	W	24.4	8.2	Suicide	Hydrogen sulfide poisoning	Y	-	Yes	-	-	-	-
8	13237	Unaffected comparison	M	25	O	22.3	8.2	Accidental	Trauma	Y	-	-	-	-	-	-
	13173	OCD	M	30	W	21	8.6	Accidental	Combined drug overdose	N	-	Yes	-	Yes	-	-

Table A-4. Detailed uncorrected and corrected *p*-values using the Benjamini-Hochberg adjustment for false discovery rate.

	Main effect of diagnosis			Main effect of brain region			Diagnosis by brain region interaction			Uncorrected				B-H correction			
Gene	F value	Uncorrected P	Corrected P	F value	Uncorrected P	Corrected P	F value	Uncorrected P	Corrected P	Post-hoc BA11	Post-hoc BA47	Post-hoc Caudate	Post-hoc NAcc	Post-hoc BA11	Post-hoc BA47	Post-hoc Caudate	Post-hoc NAcc
DLGAP1	F1,10 = 2.8	0.1300	0.1600	F3,30 = 1.8	0.1700	0.1943	F3,30 = 3.5	0.0300	0.0800	0.1460	0.0468	0.8624	0.1122	0.2294	0.1287	0.8624	0.1899
DLGAP2	F1,10 = 34.4	0.0001	0.0016	F3,30 = 3.5	0.0300	0.0914	F3,30 = 5.4	0.0040	0.0320	0.0004	0.0026	0.4717	0.1010	0.0044	0.0191	0.5765	0.1852
SLITRK3	F1,8 = 21.7	0.0020	0.0160	F2,16 = 2.9	0.0800	0.1600	F2,16 = 4.2	0.0300	0.0800	0.0004	0.0230	0.1680		0.0044	0.1012	0.2464	
DLGAP3	F1,10 = 7.0	0.0300	0.0600	F3,30 = 1.9	0.1600	0.1943	F3,30 = 0.2	0.9000	0.9000								
DLGAP4	F1,10 = 7.4	0.0200	0.0600	F3,30 = 3.3	0.0400	0.0914	F3,30 = 1.3	0.3000	0.4000								
SLITRK1	F1,8 = 3.0	0.1200	0.1600	F3,24 = 2.4	0.0900	0.1600	F3,24 = 1.0	0.4000	0.4571								
GRIA1	F1,8 = 9.0	0.0200	0.0600	F3,24 = 1.0	0.3900	0.4160	F3,24 = 1.6	0.2100	0.3733								
GRIN2B	F1,8 = 6.9	0.0300	0.0600	F3,24 = 1.8	0.1700	0.1943	F3,24 = 1.1	0.3600	0.4431								
SLC1A1	F1,10 = 5.0	0.0500	0.0889	F3,30 = 3.2	0.0400	0.0914	F3,30 = 3.7	0.0200	0.0800	0.0757	0.0337	0.7060	0.3133	0.1514	0.1236	0.8121	0.4308
SLC17A7	F1,10 = 12.4	0.0050	0.0267	F1,10 = 0.02	0.8900	0.8900	F1,10 = 0.02	0.8900	0.9000								
GAD1	F1,10 = 6.9	0.0300	0.0600	F3,30 = 4.3	0.0100	0.0533	F3,30 = 7.2	0.0010	0.0160	0.0115	0.0693	0.8489	0.0532	0.0633	0.1514	0.8624	0.1300
GAD2	F1,10 = 2.6	0.1400	0.1600	F3,30 = 3.9	0.0200	0.0800	F3,30 = 2.9	0.0520	0.1189								
PVALB	F1,10 = 2.8	0.1300	0.1600	F2,20 = 5.6	0.0100	0.0533	F2,20 = 4.9	0.0200	0.0800	0.1134	0.7383	0.4256		0.1287	0.8121	0.5508	
CALB1	F1,10 = .84	0.3800	0.4053	F3,30 = 24.7	0.0001	0.0016	F3,30 = 1.3	0.2700	0.4000								
GABARAP	F1,8 = .2.8	0.1300	0.1600	F3,24 = 2.3	0.1000	0.1600	F3,24 = 1.3	0.3000	0.4000								
SLC32A1	F1,8 = .004	0.9500	0.9500	F3,24 = 2.0	0.1400	0.1943	F3,24 = 2.2	0.1000	0.2000								
	Main effect of diagnosis			Main effect of brain region			Diagnosis by brain region interaction			Uncorrected				B-H correction			
Gene	F value	Uncorrected P	Corrected P	F value	Uncorrected P	Corrected P	F value	Uncorrected P	Corrected P	Post-hoc BA11	Post-hoc BA47	Post-hoc Caudate	Post-hoc NAcc	Post-hoc BA11	Post-hoc BA47	Post-hoc Caudate	Post-hoc NAcc
Synaptic	F1,10 = 21.2	0.0010	0.0027	F3,30 = 2.9	0.0520	0.0780	F3,30 = 5.2	0.0050	0.0075	0.0062	0.0003	0.7894	0.1034	0.0213	0.0024	0.7894	0.2122
Receptor	F1,8 = 21.2	0.0018	0.0027	F3,24 = 2.5	0.0814	0.0814	F3,24 = 4.7	0.0103	0.0103	0.0004	0.0097	0.2607	0.1878	0.0024	0.0233	0.3476	0.2817
GABA	F1,10 = 6.1	0.0335	0.0335	F3,30 = 4.9	0.0071	0.0213	F3,30 = 8.7	0.0003	0.0009	0.0071	0.3597	0.3437	0.1635	0.0213	0.3924	0.3924	0.2803

Appendix B Using Optogenetics to Dissect the Neural Circuits Underlying OCD and Related Disorders

Using Optogenetics to Dissect the Neural Circuits Underlying

OCD and Related Disorders

Current Treatment Options in Psychiatry (2015) 2:297-311

Sean C Piantadosi[a,b] & Susanne E Ahmari, MD, PhD[a,b,c]

[a]450 Technology Drive, Room 227, Department of Psychiatry, University of Pittsburgh, Pittsburgh, PA 15219, USA; Phone 412-624-3183; Fax 412-624-5280

[b]Center for Neuroscience, University of Pittsburgh, Pittsburgh PA, USA

[c]Center for the Neural Basis of Cognition, Pittsburgh, PA, USA

B.1 Summary

Clinical and preclinical studies have uncovered substantial evidence that dysfunction in cortico-striatal-thalamo-cortical (CSTC) loops central to the selection of action strategies may underlie OCD symptoms. In human OCD, data suggest that the balance between selection of habitual versus goal-directed action strategies is disrupted, with concomitant hyperactivation of CSTC regions associated with these strategies. Preclinical lesion and inactivation studies of homologous CSTC regions in rodents have shed light on how sub-regions of the frontal cortex and striatum can have dissociable effects on the exhibition of goal-directed or habitual behavior. However, these traditional methods lack the precision necessary to dissect the exact projections and cell types underlying these behaviors. It is essential to uncover this information to begin to determine how disruption in these circuits may lead to disease pathology. Here we summarize several recent studies that utilize optogenetics, a technique that allows stimulation or inhibition of specific neural projections and cell types using light, to further understand the contribution of CSTC activity to both action selection and the OCD-relevant behavior of perseverative grooming. Based on these experiments and findings in human OCD patients, we argue that OCD symptoms may not only be associated with an enhancement of habitual behavior, but also with aberrant recruitment of goal-directed neural circuits. We also discuss the current status of translating optogenetic technology to primates, as well as how findings in rodents may help inform treatment of patients suffering from OCD and related disorders.

B.2 Introduction

Maladaptive repetitive actions and thoughts are key features of many neuropsychiatric illnesses, including autism (McDougle et al. 1995), substance abuse disorders (Everitt and Robbins 2005), Tourette's syndrome (*Diagnostic and statistical manual of mental disorders, (DSM-5®)* 2013), and eating disorders (Smith and Robbins 2013). The burden of these symptoms is perhaps most clearly highlighted in obsessive compulsive disorder (OCD), a chronic and severe mental illness affecting 2-3% of people worldwide and identified as a leading cause of illness-related disability by the World Health Organization (Kessler et al. 2005). Recently separated from anxiety disorders in the DSM-5 based on proposed differences in neural substrates, subtypes of OCD are unified by the commonality of repetitive behaviors and/or thoughts that severely impair functioning. Several theories exist that may explain the pathophysiologic processes leading to compulsive behavior. Importantly, these proposed models posit dysfunction in distinct brain regions that comprise cortico-striato-thalamo-cortical (CSTC) loops, which are thought to be responsible for controlling action selection and behavioral inhibition (Valentin, Dickinson, and O'Doherty 2007). Specific cortical and striatal regions within each loop have been linked to the development of either goal-directed or habitual behavior. In rodent studies, compulsive behavior has been linked to a progressive shift from recruitment of goal-directed systems to habit-related systems (Everitt and Robbins 2005, 2013), which has led to the proposal of the habit hypothesis of OCD (Graybiel and Rauch 2000). However, the habit theory may not account for a key facet of compulsions in OCD - the intense urge to act (Denys 2014), which is indicative of a behavior that is still goal-directed. Similar to models within the framework of addiction (Sjoerds et al. 2014), we propose that compulsive behaviors observed in OCD contain a substantial motivational and goal-directed component.

Here we will summarize evidence from both human and preclinical animal studies linking dysfunctional CSTC activity to repetitive behaviors, and discuss potential implications of these findings for treatment. We will also highlight recent studies that investigate whether directly altering activity in discrete CSTC loops can change action strategies and affect compulsive behaviors. Based on convergent findings from animal and human OCD studies, we propose that compulsive behaviors may be induced either through increased habit system activity or enhanced recruitment of goal-directed systems.

B.2.1 Neuroimaging studies highlight abnormalities in CSTC loops in OCD

While the pathogenesis of OCD is still unknown, structural and functional neuroimaging studies have identified alterations in CSTC regions that are major players in the development of both goal-directed behaviors and habits in OCD patients compared to unaffected controls. Three general CSTC loops are believed to be important for controlling different neurocognitive functions and are comprised of different interconnected brain regions (Milad and Rauch 2012b). These include the sensorimotor loop, which controls motor and response inhibition via lateral OFC (lOFC) projections to the putamen, the cognitive loop, which regulates working memory via connections between dorsolateral PFC (dlPFC) and the caudate nucleus, and the affective loop, which directs reward processing through interactions between the anterior cingulate cortex (ACC), the medial OFC (mOFC), and the ventral striatum (Di Martino et al. 2008; Posner et al. 2014). For each loop, information from the striatum is passed through the basal ganglia and ultimately conveyed back to the cortex via thalamic relays (Milad and Rauch 2012b; Di Martino et al. 2008).

Multiple lines of evidence suggest dysfunction in many of these regions– most of which contribute to producing goal-directed and habitual behavior– in OCD.

Functional magnetic resonance imaging (fMRI) studies highlight a role for both frontocortical structures (such as the OFC and ACC) and the striatum in OCD. Resting state studies suggest that, compared to healthy controls, OCD subjects have increased activity within both OFC and ACC (Baxter et al. 1987; Swedo et al. 1989), as well as the caudate (dorsal striatum) (Nordahl et al. 1989). OFC and caudate hyperactivity and ACC activity are further accentuated during symptom provocation, suggesting a potential casual role for these nuclei in the generation or expression of OCD symptoms (Rauch et al. 1994b; Adler et al. 2000b). Successful treatment of symptoms correlates with reduced activity in both caudate and OFC, regions associated with goal-directed action strategies (Valentin, Dickinson, and O'Doherty 2007), as measured by positron emission tomography and magnetic resonance spectroscopy (Abelson, Curtis, et al. 2005; Rauch et al. 2002; Rosenberg et al. 2000). In addition to elevated resting state activity, abnormal functional connectivity between these regions has also been observed. In particular, some (but not all, see (Posner et al. 2014)) data suggest increased functional connectivity between the ventral striatum/nucleus accumbens and medial OFC (mOFC) (Harrison, Soriano-Mas, Pujol, Ortiz, López-Solà, et al. 2009; Fitzgerald et al. 2011b; Hou et al. 2012), a finding that is predictive of illness severity (Harrison, Pujol, Cardoner, Deus, Alonso, López-Solà, et al. 2013). These functional imaging studies provide evidence that activity in regions involved in the development of both goal-directed and habitual behaviors is abnormal in OCD.

Though structural imaging studies have also suggested alterations in the caudate in both adults (Robinson et al. 1995; Scarone et al. 1992) and children (Rosenberg et al. 1997) with OCD, the directionality of change has not been consistent. In addition, increases in ventral striatal gray

matter are observed in OCD subjects compared to controls and subjects with other anxiety disorders, implicating the ventral striatum in the formation of repetitive behavior rather than generalized anxiety (Menzies et al. 2008b). Structural differences have also been detected in fronto-cortical regions. Decreased ACC volume has been reported in OCD patients (Menzies et al. 2008b; Radua et al. 2010), and alterations in OFC grey matter volume in adult OCD have been observed (Radua et al. 2010; Rotge et al. 2009b; Atmaca et al. 2007b) (though it is unclear if these changes are compensatory (Radua and Mataix-Cols 2009)). In addition to changes in gray matter density, abnormalities in white matter integrity have been identified using diffusion tensor imaging in corpus callosum, anterior limb of the internal capsule, and cingulum bundle. As with the aforementioned neurochemical and fMRI findings, decreases in white matter integrity within the left striatum of OCD patients could be reversed with chronic pharmacotherapy (Fan et al. 2012), suggesting that these changes may be central to the pathophysiology of the disorder. Although less consistent than functional imaging studies, structural MRI studies therefore identify alterations in OCD subjects within many of same brain regions which are responsible for the development of goal-directed and habitual behavior.

Further evidence of CSTC dysfunction in OCD comes from invasive neurosurgical techniques used in treatment refractory OCD patients. It is estimated that 10-20% of patients with OCD do not respond to traditional pharmacological and psychological therapy (Husted and Shapira 2004; Rodman et al. 2012; Greenberg et al. 2010; Denys et al. 2010). Some of these individuals may benefit from treatments that directly target dysfunctional circuitry, including deep brain stimulation (DBS). DBS uses constant high-frequency electrical stimulation in targeted brain regions, and although the mechanism of action is unknown, some theories suggest that it is efficacious due to normalization of hyperactivity (Abelson, Curtis, et al. 2005). Currently, one of

the most frequently studied DBS targets with substantial efficacy for OCD treatment is the ventral capsule/ventral striatum (VC/VS), with 25% of patients achieving remission after a year of stimulation (Greenberg et al. 2010; Greenberg, Rauch, and Haber 2010; Denys et al. 2010). VC/VS DBS normalized intraregion hyperactivity and reduced the increased functional activity observed between striatum and frontal cortex (Figee, Luigjes, et al. 2013; Figee, Wielaard, et al. 2013). Again, this highlights the possible role of dysfunctional goal-directed behavior in OCD, since the VS is implicated in the prediction and evaluation of reward value, a necessary component of successful goal-directed action (Everitt and Robbins 2005). Together, these data highlight the involvement of regions that regulate habitual and goal directed behavior in the pathophysiology of OCD, and provide hypotheses that can be tested utilizing new circuit-based interventions in animal models.

B.2.2 Disruptions in habitual and goal directed behavior in OCD

Several recent studies in OCD patients have supported the hypothesis that compulsions stem from abnormal goal directed versus habitual striatal-mediated action strategies. First, in an instrumental conditioning paradigm, both OCD patients and controls learned to correctly discriminate between two visual stimuli at the same rate (Gillan et al. 2011). However, following devaluation of one of the two stimuli, OCD patients continued to respond to the devalued reward, reminiscent of rodents with DMS lesions (Yin, Knowlton, and Balleine 2005) (see animal model section below). Similarly, in an aversive conditioning paradigm, where correct discrimination of two visual stimuli leads to avoidance of a shock, no learning differences were detected (Gillan et al. 2014b). However, following overtraining and devaluation, OCD patients continued to avoid the devalued stimulus, despite the fact that they were consciously aware that it no longer predicted the

shock. Using a modified version of the same task, researchers recently linked this increased habit formation back to CSTC circuits, finding increased activation of the caudate (DMS) in patients whose behavior had become habitual, and increased activation of the mOFC in all OCD subjects (Gillan et al. 2015). Together these data suggest a shift in balance from goal directed to habitual action selection strategy in OCD. However, it is worth noting that the degree of shock avoidance did not correlate with compulsion symptom severity (as measured by YBOCS compulsion subscale), suggesting the bias toward habitual strategy may not be relevant to OCD symptomatology. Further, OCD patients reported an increased urge to respond despite devaluation, suggesting that enhanced responding may still be goal-directed (Gillan et al. 2015; Gillan et al. 2014b). These findings are broadly consistent with one current theory of drug addiction proposed by Sjoerds and colleagues (Sjoerds et al. 2014), in which compulsive drug seeking can be conceptualized as a maladaptive motivational habit with a substantial goal directed component. Taken together with the identification of hyperactivity in regions linked to goal-directed behavior (the mOFC and caudate) by Gillan et al. (Gillan et al. 2015), it is possible that compulsivity in OCD may arise, at least for avoidance habits, from aberrant goal-directed recruitment.

Several other lines of evidence support a potential enhancement of the goal-directed action system in OCD. In experiments in which implicit (habitual) learning is examined, enhanced utilization of regions of the goal directed system, including the OFC, is observed in OCD patients compared to controls (Rauch, Savage, Alpert, Dougherty, et al. 1997; Rauch et al. 2007b). When explicit learning or processing is introduced during the implicit task (thereby activating goal-directed circuitry), the performance of OCD patients compared to controls is impaired (Deckersbach et al. 2002; Joel et al. 2005). A parsimonious explanation for these seemingly contradictory behavioral results, in which some data suggest an over-reliance on habit systems at

the expense of goal-directed systems (Gillan et al. 2011), while others indicate a strengthening of goal-directed actions in OCD (Deckersbach et al. 2002; Joel et al. 2005), has recently been summarized by Gruner and colleagues (Gruner et al. 2015). However, the exact circuit level mechanisms regulating the inappropriate recruitment of either behavioral strategy are still not clear. Until recently, correlations between systems level disruptions in cortico-striatal-thalamic-cortical (CSTC) circuits and relevant behavioral abnormalities in OCD have provided the best available insight into the underlying neurobiology of OCD, since manipulation of specific neural circuits is still not possible in humans. Researchers have therefore now turned to animal models to address questions of causality.

B.2.3 Circuits mediating goal directed and habitual behavior

To dissect the circuit mechanisms underlying the recruitment of goal-directed versus habitual behaviors, elegant studies have been performed in rodent models. This work has been essential to our understanding of drug addiction, which has been conceptualized as a disorder in which there is a gradual shift from recruitment of goal-directed systems to habit systems (Everitt and Robbins 2005). According to classic theory, the formation of habits arises when action-outcome driven (A-O) behaviors lead to learned stimulus-response (S-R) associations (Adams 2007; Balleine and Dickinson 1992). Habitual behavior in normal animals (S-R driven) is typically induced by overtraining an animal during an operant task (e.g. pressing a lever for a reward). When the reward is then subsequently devalued through aversive conditioning, overtrained animals continue to respond despite the change in outcome, while normally trained animals respond less for the devalued outcome, indicative that the behavior remains goal-directed and flexible (Yin, Knowlton, and Balleine 2006). The neural basis for this change in strategy appears to lie in a shift

from associative CSTC circuits to sensorimotor circuits, in analogous structures to those that are dysfunctional in OCD. Specifically, habitual responding can be induced via lesion of dorsomedial striatum (DMS: caudate in primates) (Yin, Knowlton, and Balleine 2005, 2004). In contrast, disruption of the dorsolateral striatum (DLS: putamen in primates) promotes goal-directed behavior, even after overtraining and outcome devaluation (Yin and Knowlton 2006; Yin, Knowlton, and Balleine 2004). Furthermore, substantial plasticity in these regions has been observed via *in vivo* recordings during habit formation. For example, during learning of a maze task, DLS activity rapidly shifts to a task-bracketing pattern during training, in which activity is high during both the beginning and end of a maze run (Thorn et al. 2010). This "chunking" pattern is believed to allow for more rapid and efficient neural processing during habitual behavior (Graybiel 2008). By contrast, activity in DMS is initially high at decision points during training and gradually decreases throughout overtraining, consistent with its role in action-outcome learning (Thorn et al. 2010).

Less is known about upstream mediators that may regulate the shift between goal directed and habitual action strategies. Lesion and inactivation studies suggest that two adjacent frontal cortical regions, the prelimbic (PL) and infralimbic (IL) cortices, may be important for regulating the switch between behavioral strategies. When activity of IL (akin to primate BA25) is inhibited, an animal's behavior becomes goal directed ((Coutureau and Killcross 2003): inactivation, (Killcross and Coutureau 2003): lesion). In contrast, when activity of PL (akin to primate BA32, part of anterior cingulate cortex) is disrupted, an animal's behavior becomes less goal-directed (Killcross and Coutureau 2003; Balleine and Dickinson 1998). In addition to these regions, lesions of the lateral OFC in the monkey disrupt the ability to form action-outcome associations

(Rudebeck and Murray 2011), indicating that OFC is also crucial for goal-directed decision making.

B.2.4 Development of optogenetics for investigation of complex behavior

Although animal models have provided great insight into the brain regions mediating goal-directed vs habitual behavior, until recently they were limited by the inability to manipulate specific cell-types in particular neural circuits. This limitation has recently been surmounted by the development of optogenetics, a technique that leverages light-sensitive ion channels, known as *opsins*, for the precise activation and inhibition of neural circuits of interest. Although opsins were first isolated from microbial organisms approximately 40 years ago (Oesterhelt and Stoeckenius 1971; Matsuno-Yagi and Mukohata 1977), their utility for manipulating cellular activity has only recently been harnessed (Boyden et al. 2005). In the first wave of studies, two major opsins were used to bidirectionally alter cellular activity: 1) *channelrhodopsin* (ChR2), a cation channel that depolarizes cells in response to blue light (Boyden et al. 2005; Nagel et al. 2002); and *halorhodopsin* (NpHR), a chloride pump that hyperpolarizes cells in response to yellow light (Zhang, Aravanis, et al. 2007; Zhang, Wang, et al. 2007). As first reported in the seminal paper from Boyden and colleagues in 2005 (Boyden et al. 2005), the expression of these light sensitive ion channels in mammalian neurons combined with local light delivery (Aravanis et al. 2007; Arenkiel et al. 2007) allows for control of membrane excitability with millisecond temporal precision; this is significantly faster and more precise than traditional pharmacological methods. Significant efforts have since focused on expansion of the opsin family to improve kinetics, enhance photocurrents, limit toxicity, and broaden the range of usable light wavelengths. This has led to the creation of many valuable reagents, such as C1V1 (Erbguth et al. 2012) and ReaChR

(Lin et al. 2013), which are red-shifted excitatory opsins; *archaerhodopsin* (ArchT), an outward driven proton pump that more efficiently hyperpolarizes cell membranes and therefore yields larger photocurrents compared to NpHR (Han et al. 2011); and more potent forms of ChR2, such as ChETA with improved kinetics (Gunaydin et al. 2010), ChR2-TC that allows for lower intensity light stimulation (Berndt et al. 2011), and step function opsins (SFO) with which single light pulses can stably alter membrane potential (Berndt et al. 2009).

In addition to unrivaled temporal resolution, optogenetics provides unique advantages over traditional pharmacological and electrical stimulation, including spatial resolution and targeting to genetically distinct cell populations via stereotactic injection of viral vectors under the control of cell-type specific promoters (Mattis et al. 2012). Additional specificity can be gained using combinatorial genetic approaches that include virally expressing opsins only in cells with genetically encoded cre-recombinase, a strategy which has now been successfully used many times to manipulate small populations of cells during behavioral tasks (Tsai et al. 2009; Witten et al. 2010; Fenno, Yizhar, and Deisseroth 2011). Furthermore, optogenetic methods allow for the dissection of microcircuits on a scale not previously possible. Following injection of an opsin-encoding virus (either promoter or cre-dependent) into a region of interest, infected cells will express the channel or pump throughout the cell membrane, including at the axon terminals. Implanting a light source into the terminal region allows for precise manipulation of very specific projections within a microcircuit rather than pan-activation of cell bodies that project to multiple target sites (see Fig.B-1 and (Tye and Deisseroth 2012) for detailed description). As we will highlight later in this review, this technique can be used to tease apart the contribution of subregion-specific projections to complex behaviors.

B.2.5 Optogenetic manipulation of habit and goal directed circuits

Over the past 5 years, optogenetics has been utilized to more precisely define the circuits that control goal directed versus habitual behavior according to traditional lesion and inactivation studies, as well as to determine how activity of these circuits may contribute to OCD-relevant behavior. In 2013, Gremel & Costa established a behavioral paradigm to better understand the mechanisms underlying the shift from goal directed to habitual actions. To test whether separate neural ensembles within CSTC circuits control goal directed versus habitual behavior, or whether two types of action strategies are encoded by identical ensembles, they constructed a novel behavioral task in which animals performed an identical action (a lever press) using either a goal directed (random ratio) or habitual (random interval) strategy. As predicted based on prior studies, lesions to DMS resulted in habitual behavior in both conditions, while lesions to DLS led to goal directed behavior. Lesioning lOFC had the same effect as a DMS lesion–i.e. producing habitual responding. These data suggest that the lOFC and DMS are critical for encoding changes in outcome value. In order to test the necessity and sufficiency of lOFC activation in encoding outcome value, the authors next conducted chemogenetic loss of function (Alexander et al. 2009; Pei, Dong, and Roth 2010) and optogenetic gain of function studies. After injection of a virus encoding the inhibitory designer receptor exclusively activated by designer drug (DREADD) ($hM4D_i$) into the lOFC and subsequent inhibition via administration of its ligand clozapine-N-oxide (CNO), mice behaved in a habitual manner, similarly to performance following an OFC lesion. Based on these findings, the authors hypothesized that activation of OFC projection neurons would enhance goal directed behavior. Bilateral activation of lOFC cell bodies via optical stimulation had no effect when the reward was still valued in the random ratio condition. Instead, it drastically increased lever pressing when the reward was devalued, resulting in levels of pressing

similar to non-devalued rats, which the authors interpreted as an enhancement of goal directed behavior. These data support previous studies suggesting that goal directed behavior is controlled by the DMS, while habitual behavior is subserved by the DLS (Yin, Knowlton, and Balleine 2005; Dezfouli and Balleine 2012). Furthermore, they confirm the role of the OFC in encoding value and goal directed behavior (Valentin, Dickinson, and O'Doherty 2007; Damasio, Tranel, and Damasio 1990).

Optogenetics has also been used to investigate the contribution of affective/prefrontal circuits to the shift from goal directed to habitual behavior. These experiments focused on manipulating the infralimbic PFC (IL), which directly projects to the DMS (Killcross and Coutureau 2003; Balleine and Dickinson 1998) and may indirectly project to the DLS via the ventral striatum or the amygdala (Hurley et al. 1991). A dual pattern of connections to the sensorimotor network (DLS; promoting habitual behavior) and to regions that promote goal directed behavior (DMS) suggests that the IL may exert executive control over habit formation. To assess the real-time impact of IL activity on habit formation, Smith and colleagues (2012) selectively expressed halorhodopsin (NpHR3) bilaterally in IL pyramidal cells. Based on tones, rats then learned to predict which arm of a T-maze contained one of two food rewards. After overtraining, rats received home-cage devaluation of one of the rewards through conditioned taste aversion. After devaluation, control rats continued to run to the devalued arm, suggesting this behavior had become habitual. In contrast, rats that received optical inhibition of the IL immediately after devaluation generally ran to the non-devalued arm, suggesting that IL inhibition blocked habit expression. Consistent with literature suggesting that once a habit is broken it is often replaced with another habit, all rats that received devaluation began to run consistently to the non-devalued reward in response to the devalued tone. These responses increased over time in

both groups, suggestive of new habit formation. Strikingly, when IL optical inhibition was performed 2 weeks post-devaluation, the rats immediately ran back to the devalued arm. This suggests that, as with initial habit formation, the IL was responsible for the establishment of the new habit. These data support the idea that inhibition of the IL restores previously learned action strategies once a new habit is ingrained (Killcross and Coutureau 2003). Consistent with this interpretation, while *in vivo* activity in the DLS exhibited characteristic task bracketing during the middle of acquisition of this T-maze task (Thorn et al. 2010; Graybiel 1998a), activity in the IL only became task bracketed very late in overtraining, when habits become crystallized (Smith and Graybiel 2013b). To test the significance of IL task bracketing during overtraining, rats received bilateral injection of NpHR3 in the IL and underwent T-maze training in an independent study (Smith et al. 2012). Optical inhibition of IL pyramidal neurons was conducted selectively during overtraining, when task-bracketing activity appeared during recording. As predicted, habit formation was blocked in rats with IL perturbation during overtraining (Smith and Graybiel 2013b). Together, these data suggest that IL activity has a role in both the formation and the expression of habits. Recent computational work in humans corroborates these findings, implicating the inferior lateral PFC (ilPFC) and frontopolar cortex (FPC) as potential arbitrators of the switch from goal-directed to habitual behavior through connections with the putamen (Lee, Shimojo, and O'Doherty 2014).

B.2.6 Optogenetic manipulation of circuits underlying compulsive behavior

Two recent optogenetic studies have begun to explore the relationship of the hyperactivity of CSTC pathways observed in human OCD to the development and resolution of perseverative behavior. An experiment conducted by Burguiere and colleagues (2013) used a transgenic mouse

model of OCD-like behavior based on deletion of *Sapap3* (SAP90/PSD95-associated protein 3), which is found in the post-synaptic density of glutamatergic synapses and interacts with PSD95 and other scaffolding proteins (Takeuchi et al. 1997). Genetic variants of SAPAP3 have been linked to OCD and grooming disorders, such as trichotillomania and skin-picking ((Bienvenu et al. 2009a; Züchner et al. 2009) correspondingly), and *Sapap3* knockout (KO) mice exhibit OCD-related behaviors including compulsive over-grooming and increased anxiety (Welch et al. 2007b). In this study, an aversive conditioning paradigm was used to train mice to associate a tone with delivery of a drop of water on their head. As training progressed, both wild-type and SAPAP3 KOs successfully learned that the tone predicted the water drop, and groomed in response to the tone. However, wild-type mice began to inhibit this response late in training, only grooming after the water drop was presented. In contrast, *Sapap3* KOs were unable to inhibit the response to the tone, and instead continued to groom after tone presentation throughout training (Burguiere et al. 2013); this was reminiscent of the findings from the conditioning experiments in OCD patients described above. The authors then characterized the neural underpinnings of this impaired behavioral inhibition, finding that the deficit was correlated with elevated striatal activity in *Sapap3* KOs. Supporting the hypothesis that this increased activity of striatal medium spiny neurons (MSNs) resulted from a loss of striatal inhibitory interneurons, they observed that *Sapap3* KOs had fewer parvalbumin-positive (PV+) interneurons in the centromedial striatum (CMS). In an attempt to correct for this deficit, they then performed selective ChR2-mediated optogenetic stimulation of projections from lOFC to CMS. This intervention both reversed the deficit in behavioral inhibition and the increased striatal activity, presumably via enhancing the responsiveness of the remaining PV-positive interneurons and restoring normal feed-forward inhibition. These experiments

provided support for the idea that lOFC regulates the inhibition of conditioned responses, and linked hyperactivity in striatum to compulsive behavior.

In a complementary set of studies, our lab used optogenetics to test whether inducing hyperactivity in CSTC circuits in wild-type mice directly leads to abnormal repetitive behaviors. Focusing on the subregions that have been implicated in goal-directed behavior and anxiety, we selectively expressed ChR2 in excitatory projections from mOFC to ventromedial striatum (VMS). Although acute optogenetic stimulation did not lead to OCD-related behavioral changes, brief but repeated stimulation of mOFC-VMS projections led to a significant increase in perseverative grooming over the course of 5-6 days (Ahmari et al. 2013). Strikingly, this increase in grooming was persistent for up to 2 weeks after cessation of the optogenetic stimulation. Together, these findings suggested the development of pathologic plasticity at mOFC-VMS. In support of this concept, we demonstrated a progressive increase in evoked firing rate of VMS neurons over 5 days of stimulation using *in vivo* recording. Lending support to the idea that these plastic changes may have relevance to pathologic processes involved in OCD, both the increased grooming behavior and the increase in evoked firing were normalized by chronic SSRI administration. Our data suggest that brief but repeated hyperstimulation of regions implicated in both goal-directed behavior (mOFC and medial striatum) and limbic/anxiety circuits (VMS) can lead to perseverative behavior that may be relevant to OCD. These data therefore support the hypothesis that hyperactivity in goal-directed circuits can lead to the development of abnormal repetitive behaviors. Future studies will seek to synthesize these two sets of findings, which together suggest there may be two paths to producing perseverative behavior– i.e. through dysfunction of either habit systems or goal-directed/limbic systems.

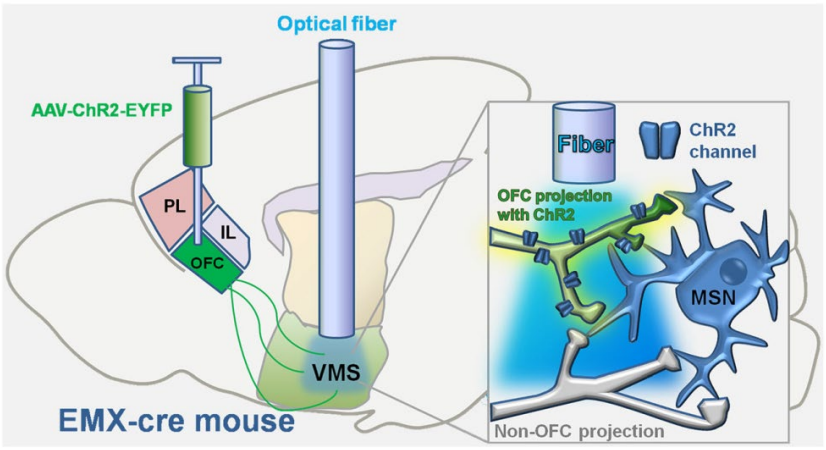

Figure B-1. Projection-specific expression and activation of excitatory opsin (ChR2) to dissect OCD-related circuitry.

Presynaptic neurons within the OFC of EMX-cre mice are transduced with ChR2-EYFP. An optical fiber is implanted into the target region (VMS) and blue light (473 nm wavelength) is delivered to excite infected projection neurons. (Inset)Blue light stimulation selectively activates OFC projection neurons infected with ChR2, resulting in depolarization of post-synaptic medium spiny neurons (MSNs) selectively connected to OFC. Uninfected projection neurons from the OFC or from other regions are unaffected by optical stimulation.

B.3 Summary and conclusions

Over the past 5 years, optogenetic experiments have led to rapid progress in dissecting the functional relationship between CSTC circuits and the development of OCD-relevant behaviors in animal models. Chief among these findings are the importance of different prefrontal and striatal subregions in the control of goal-directed versus habitual behavior, and the direct test of the hypothesis that hyperactivity in OFC and striatal circuitry is involved in OCD-relevant behavioral phenotypes in normal and pathological animals (Gremel and Costa 2013; Ahmari et al. 2013; Burguiere et al. 2013). These findings provide a causal link to some of the most well replicated findings in human OCD imaging studies, demonstrating OFC hyperactivity and altered functional

connectivity between OFC and the medial striatum (Harrison, Pujol, Cardoner, Deus, Alonso, López-Solà, et al. 2013; Menzies et al. 2008b). Interestingly, involvement of the mOFC suggests that an over-reliance on the goal directed system (including the mOFC and medial striatum) may play a role in the development of compulsive behavior (Gruner et al. 2015). These data are particularly interesting in light of recent neuroimaging findings in which increased avoidance habit formation in OCD patients was associated with hyperactivation of mOFC and medial striatum, classically thought of as regions promoting goal directed behavior (Yin, Knowlton, and Balleine 2005; Gillan et al. 2015; Balleine and Dickinson 1998). Future work will determine how other regions outside of the CSTC involved in anxiety and reward, such as the amygdala, ventral hippocampus, and VTA, may be involved in mediating compulsive behavior.

B.4 Future directions and prospective implications for treatment of OCD and related disorders

Optogenetics has allowed for unparalleled precise control in animal model systems over circuits implicated in OCD and known to be involved in goal directed and habitual behavior. Future research will focus on elucidating the molecular mechanisms underlying not only the onset of compulsive and perseverative behaviors, but also their persistence. The striking findings of Burguiere and colleagues (2013) and our group that optogenetic stimulation of disease-relevant neural circuits can alter perseverative behavior raises the attractive possibility of optogenetics as a potential therapeutic tool for OCD and related disorders. However, substantial hurdles exist before this technology can be translated to humans, including synthesizing viruses that are both safe for humans and can effectively target specific cell types. In addition, experiments using optogenetics

in primates to date have had substantial difficulty in generating the striking behavioral effects that are commonly observed in rodent studies (Han et al. 2011; Diester et al. 2011); the reasons for this are unclear, but must be determined before progress can be made towards using the technology in people. Finally, further progress still needs to be made towards development of wireless systems for effective stimulation, though this goal is clearly within reach (Diester et al. 2011). More practically, optogenetics will continue to be utilized as a valuable tool for dissection of circuits known to be dysfunctional in human disease. Indeed, the potential combination of optogenetics and fMRI (Desai et al. 2011) or *in vivo* calcium imaging (Shipley et al. 2014) provide important avenues for enhancing our understanding of how hyperactivity of a single pathway (e.g. OFC to VMS) can impact brain-wide networks. Critically, the information gained from these targeted approaches will inform therapeutics either through the refinement of current technologies, such as DBS and transcranial magnetic stimulation (TMS), or through the development of new technologies, such as closed loop systems that would allow for real-time adjustment of stimulation parameters based on abnormal neural activity patterns (Kent and Grill 2011).

Bibliography

(OCGAS), International Obsessive Compulsive Disorder Foundataion Genetics Collaborative (IOCDF-GC) and OCD Collaborative Genetics Association Studies. 2018. 'Revealing the complex genetic architecture of obsessive-compulsive disorder using meta-analysis', *Mol Psychiatry*, 23: 1181-88.

Abelson, J. F., K. Y. Kwan, B. J. O'Roak, D. Y. Baek, A. A. Stillman, T. M. Morgan, C. A. Mathews, D. L. Pauls, M. R. Rasin, M. Gunel, N. R. Davis, A. G. Ercan-Sencicek, D. H. Guez, J. A. Spertus, J. F. Leckman, L. S. th Dure, R. Kurlan, H. S. Singer, D. L. Gilbert, A. Farhi, A. Louvi, R. P. Lifton, N. Sestan, and M. W. State. 2005. 'Sequence variants in SLITRK1 are associated with Tourette's syndrome', *Science*, 310: 317-20.

Abelson, James L., George C. Curtis, Oren Sagher, Ronald C. Albucher, Mark Harrigan, Stephan F. Taylor, Brian Martis, and Bruno Giordani. 2005. 'Deep brain stimulation for refractory obsessive-compulsive disorder', *Biol Psychiatry*, 57: 510-16.

Adams, C. 2007. 'Variations in the sensitivity of instrumental responding to reinforcer devaluation', *The Quarterly Journal of Experimental Psychology Section B*, 34: 7798.

Ade, K. K., Y. Wan, H. C. Hamann, J. K. O'Hare, W. Guo, A. Quian, S. Kumar, S. Bhagat, R. M. Rodriguiz, W. C. Wetsel, P. J. Conn, K. Dzirasa, K. M. Huber, and N. Calakos. 2016. 'Increased Metabotropic Glutamate Receptor 5 Signaling Underlies Obsessive-Compulsive Disorder-like Behavioral and Striatal Circuit Abnormalities in Mice', *Biol Psychiatry*.

Adler, C. M., P. McDonough-Ryan, K. W. Sax, S. K. Holland, S. Arndt, and S. M. Strakowski. 2000a. 'fMRI of neuronal activation with symptom provocation in unmedicated patients with obsessive compulsive disorder', *J Psychiatr Res*, 34: 317-24.

———. 2000b. 'fMRI of neuronal activation with symptom provocation in unmedicated patients with obsessive compulsive disorder', *Journal of psychiatric research*, 34: 317-24.

Ahmari, S. E. 2016. 'Using mice to model Obsessive Compulsive Disorder: From genes to circuits', *Neuroscience*, 321: 121-37.

Ahmari, S. E., T. Spellman, N. L. Douglass, M. A. Kheirbek, H. B. Simpson, K. Deisseroth, J. A. Gordon, and R. Hen. 2013. 'Repeated cortico-striatal stimulation generates persistent OCD-like behavior', *Science*, 340: 1234-9.

Akerboom, J., T. W. Chen, T. J. Wardill, L. Tian, J. S. Marvin, S. Mutlu, N. C. Calderon, F. Esposti, B. G. Borghuis, X. R. Sun, A. Gordus, M. B. Orger, R. Portugues, F. Engert, J. J. Macklin, A. Filosa, A. Aggarwal, R. A. Kerr, R. Takagi, S. Kracun, E. Shigetomi, B. S. Khakh, H. Baier, L. Lagnado, S. S. Wang, C. I. Bargmann, B. E. Kimmel, V. Jayaraman, K. Svoboda, D. S. Kim, E. R. Schreiter, and L. L. Looger. 2012. 'Optimization of a GCaMP calcium indicator for neural activity imaging', *J Neurosci*, 32: 13819-40.

Aldridge, J. W., and K. C. Berridge. 1998. 'Coding of serial order by neostriatal neurons: a "natural action" approach to movement sequence', *J Neurosci*, 18: 2777-87.

Aldridge, J. W., K. C. Berridge, and A. R. Rosen. 2004. 'Basal ganglia neural mechanisms of natural movement sequences', *Can J Physiol Pharmacol*, 82: 732-9.

Alexander, GE, MR DeLong, and PL Strick. 1986. 'Parallel organization of functionally segregated circuits linking basal ganglia and cortex', *Annu Rev Neurosci*, 9: 357-81.

Alexander, Georgia M., Sarah C. Rogan, Atheir I. Abbas, Blaine N. Armbruster, Ying Pei, John A. Allen, Randal J. Nonneman, John Hartmann, Sheryl S. Moy, Miguel A. Nicolelis, James O. McNamara, and Bryan L. Roth. 2009. 'Remote control of neuronal activity in transgenic mice expressing evolved G protein-coupled receptors', *Neuron*, 63: 27-39.

Alonso, P., M. Gratacos, C. Segalas, G. Escaramis, E. Real, M. Bayes, J. Labad, C. Lopez-Sola, X. Estivill, and J. M. Menchon. 2012. 'Association between the NMDA glutamate receptor GRIN2B gene and obsessive-compulsive disorder', *J Psychiatry Neurosci*, 37: 273-81.

Aravanis, Alexander M., Li-Ping P. Wang, Feng Zhang, Leslie A. Meltzer, Murtaza Z. Mogri, M. B. Schneider, and Karl Deisseroth. 2007. 'An optical neural interface: in vivo control of rodent motor cortex with integrated fiberoptic and optogenetic technology', *Journal of neural engineering*, 4: 56.

Arenkiel, Benjamin R., Joao Peca, Ian G. Davison, Catia Feliciano, Karl Deisseroth, George J. Augustine, Michael D. Ehlers, and Guoping Feng. 2007. 'In vivo light-induced activation of neural circuitry in transgenic mice expressing channelrhodopsin-2', *Neuron*, 54: 205-18.

Arnold, P. D., D. R. Rosenberg, E. Mundo, S. Tharmalingam, J. L. Kennedy, and M. A. Richter. 2004. 'Association of a glutamate (NMDA) subunit receptor gene (GRIN2B) with obsessive-compulsive disorder: a preliminary study', *Psychopharmacology (Berl)*, 174: 530-8.

Arnold, P. D., T. Sicard, E. Burroughs, M. A. Richter, and J. L. Kennedy. 2006. 'Glutamate transporter gene SLC1A1 associated with obsessive-compulsive disorder', *Arch Gen Psychiatry*, 63: 769-76.

Athilingam, J. C., R. Ben-Shalom, C. M. Keeshen, V. S. Sohal, and K. J. Bender. 2017. 'Serotonin enhances excitability and gamma frequency temporal integration in mouse prefrontal fast-spiking interneurons', *Elife*, 6.

Atmaca, M., B. H. Yildirim, B. H. Ozdemir, B. A. Aydin, A. E. Tezcan, and A. S. Ozler. 2006. 'Volumetric MRI assessment of brain regions in patients with refractory obsessive-compulsive disorder', *Prog Neuropsychopharmacol Biol Psychiatry*, 30: 1051-7.

Atmaca, M., H. Yildirim, H. Ozdemir, E. Tezcan, and A. K. Poyraz. 2007a. 'Volumetric MRI study of key brain regions implicated in obsessive-compulsive disorder', *Prog Neuropsychopharmacol Biol Psychiatry*, 31: 46-52.

Atmaca, Murad, Hanefi Yildirim, Huseyin Ozdemir, Ertan Tezcan, and A. K. Poyraz. 2007b. 'Volumetric MRI study of key brain regions implicated in obsessive-compulsive disorder', *Prog Neuropsychopharmacol Biol Psychiatry*, 31: 46-52.

Ayuso-Mateos, Jose Luis. 2006. 'Global burden of obsessive-compulsive disorder in the year 2000', *Global Burden of Disease 2000*.

Balleine, B., and A. Dickinson. 1992. 'Signalling and incentive processes in instrumental reinforcer devaluation', *The Quarterly journal of experimental psychology. B, Comparative and physiological psychology*, 45: 285-301.

Balleine, B. W., and A. Dickinson. 1998. 'Goal-directed instrumental action: contingency and incentive learning and their cortical substrates', *Neuropharmacology*, 37: 407-19.

Balleine, B. W., B. K. Leung, and S. B. Ostlund. 2011. 'The orbitofrontal cortex, predicted value, and choice', *Ann N Y Acad Sci*, 1239: 43-50.

Balleine, B. W., and J. P. O'Doherty. 2010. 'Human and rodent homologies in action control: corticostriatal determinants of goal-directed and habitual action', *Neuropsychopharmacology*, 35: 48-69.

Barr, L. C., W. K. Goodman, and L. H. Price. 1993. 'The serotonin hypothesis of obsessive compulsive disorder', *International Clinical Psychopharmacology*, 8: 79-82.

Baxter, L. R., Jr., S. Saxena, A. L. Brody, R. F. Ackermann, M. Colgan, J. M. Schwartz, Z. Allen-Martinez, J. M. Fuster, and M. E. Phelps. 1996. 'Brain Mediation of Obsessive-Compulsive Disorder Symptoms: Evidence From Functional Brain Imaging Studies in the Human and Nonhuman Primate', *Semin Clin Neuropsychiatry*, 1: 32-47.

Baxter, L. R., Jr., J. M. Schwartz, K. S. Bergman, M. P. Szuba, B. H. Guze, J. C. Mazziotta, A. Alazraki, C. E. Selin, H. K. Ferng, P. Munford, and et al. 1992. 'Caudate glucose metabolic rate changes with both drug and behavior therapy for obsessive-compulsive disorder', *Arch Gen Psychiatry*, 49: 681-9.

Baxter, L. R., Jr., J. M. Schwartz, J. C. Mazziotta, M. E. Phelps, J. J. Pahl, B. H. Guze, and L. Fairbanks. 1988. 'Cerebral glucose metabolic rates in nondepressed patients with obsessive-compulsive disorder', *Am J Psychiatry*, 145: 1560-3.

Baxter, L. R., M. E. Phelps, J. C. Mazziotta, B. H. Guze, J. M. Schwartz, and C. E. Selin. 1987. 'Local cerebral glucose metabolic rates in obsessive-compulsive disorder. A comparison with rates in unipolar depression and in normal controls', *Archives of general psychiatry*, 44: 211-18.

Benjamini Y., Hochberg Y. 1995. 'Controlling the False Discovery Rate: A Practical and Powerful Approach to Multiple Testing. ', *Journal of the Royal Statistical Society. Series B (Methodological)*, 57(1): 289-300.

Benkelfat, C., T. E. Nordahl, W. E. Semple, A. C. King, D. L. Murphy, and R. M. Cohen. 1990. 'Local cerebral glucose metabolic rates in obsessive-compulsive disorder. Patients treated with clomipramine', *Arch Gen Psychiatry*, 47: 840-8.

Bennett, B. D., and J. P. Bolam. 1994. 'Synaptic input and output of parvalbumin-immunoreactive neurons in the neostriatum of the rat', *Neuroscience*, 62: 707-19.

Berke, J. D. 2008. 'Uncoordinated firing rate changes of striatal fast-spiking interneurons during behavioral task performance', *J Neurosci*, 28: 10075-80.

———. 2011. 'Functional properties of striatal fast-spiking interneurons', *Front Syst Neurosci*, 5: 45.

Bernacer, J., L. Prensa, and J. M. Gimenez-Amaya. 2012. 'Distribution of GABAergic interneurons and dopaminergic cells in the functional territories of the human striatum', *PLoS One*, 7: e30504.

Berndt, A., O. Yizhar, L. A. Gunaydin, P. Hegemann, and K. Deisseroth. 2009. 'Bi-stable neural state switches', *Nat Neurosci*, 12: 229-34.

Berndt, André, Philipp Schoenenberger, Joanna Mattis, Kay M. Tye, Karl Deisseroth, Peter Hegemann, and Thomas G. Oertner. 2011. 'High-efficiency channelrhodopsins for fast neuronal stimulation at low light levels', *Proc Natl Acad Sci U S A*, 108: 7595-600.

Bernstein, G. A., A. M. Victor, A. J. Pipal, and K. A. Williams. 2010. 'Comparison of clinical characteristics of pediatric autoimmune neuropsychiatric disorders associated with streptococcal infections and childhood obsessive-compulsive disorder', *J Child Adolesc Psychopharmacol*, 20: 333-40.

Berridge, M. J., M. D. Bootman, and H. L. Roderick. 2003. 'Calcium signalling: dynamics, homeostasis and remodelling', *Nat Rev Mol Cell Biol*, 4: 517-29.

Beucke, J. C., J. Sepulcre, T. Talukdar, C. Linnman, K. Zschenderlein, T. Endrass, C. Kaufmann, and N. Kathmann. 2013. 'Abnormally high degree connectivity of the orbitofrontal cortex in obsessive-compulsive disorder', *JAMA Psychiatry*, 70: 619-29.

Bhattacharyya, S., S. Khanna, K. Chakrabarty, A. Mahadevan, R. Christopher, and S. K. Shankar. 2009. 'Anti-brain autoantibodies and altered excitatory neurotransmitters in obsessive-compulsive disorder', *Neuropsychopharmacology*, 34: 2489-96.

Bienvenu, O. J., Y. Wang, Y. Y. Shugart, J. M. Welch, M. A. Grados, A. J. Fyer, S. L. Rauch, J. T. McCracken, S. A. Rasmussen, D. L. Murphy, B. Cullen, D. Valle, R. Hoehn-Saric, B. D. Greenberg, A. Pinto, J. A. Knowles, J. Piacentini, D. L. Pauls, K. Y. Liang, V. L. Willour, M. Riddle, J. F. Samuels, G. Feng, and G. Nestadt. 2009a. 'Sapap3 and pathological grooming in humans: Results from the OCD collaborative genetics study', *American journal of medical genetics. Part B, Neuropsychiatric genetics : the official publication of the International Society of Psychiatric Genetics*, 150B: 710-20.

———. 2009b. 'Sapap3 and pathological grooming in humans: Results from the OCD collaborative genetics study', *Am J Med Genet B Neuropsychiatr Genet*, 150B: 710-20.

Bloch, M. H., A. Landeros-Weisenberger, B. Kelmendi, V. Coric, M. B. Bracken, and J. F. Leckman. 2006. 'A systematic review: antipsychotic augmentation with treatment refractory obsessive-compulsive disorder', *Mol Psychiatry*, 11: 622-32.

Bloch, M. H., A. Landeros-Weisenberger, M. C. Rosario, C. Pittenger, and J. F. Leckman. 2008. 'Meta-analysis of the symptom structure of obsessive-compulsive disorder', *Am J Psychiatry*, 165: 1532-42.

Bloch, M. H., and C. Pittenger. 2010. 'The Genetics of Obsessive-Compulsive Disorder', *Curr Psychiatry Rev*, 6: 91-103.

Blomeley, C. P., and E. Bracci. 2009. 'Serotonin excites fast-spiking interneurons in the striatum', *Eur J Neurosci*, 29: 1604-14.

Boardman, L., L. van der Merwe, C. Lochner, C. J. Kinnear, S. Seedat, D. J. Stein, J. C. Moolman-Smook, and S. M. Hemmings. 2011. 'Investigating SAPAP3 variants in the etiology of obsessive-compulsive disorder and trichotillomania in the South African white population', *Compr Psychiatry*, 52: 181-7.

Bollini, P., S. Pampallona, G. Tibaldi, B. Kupelnick, and C. Munizza. 1999. 'Effectiveness of antidepressants. Meta-analysis of dose-effect relationships in randomised clinical trials', *Br J Psychiatry*, 174: 297-303.

Bolton, D., F. Rijsdijk, T. G. O'Connor, S. Perrin, and T. C. Eley. 2007. 'Obsessive-compulsive disorder, tics and anxiety in 6-year-old twins', *Psychol Med*, 37: 39-48.

Bourne, S. K., C. A. Eckhardt, S. A. Sheth, and E. N. Eskandar. 2012. 'Mechanisms of deep brain stimulation for obsessive compulsive disorder: effects upon cells and circuits', *Front Integr Neurosci*, 6: 29.

Boyden, Edward S., Feng Zhang, Ernst Bamberg, Georg Nagel, and Karl Deisseroth. 2005. 'Millisecond-timescale, genetically targeted optical control of neural activity', *Nature neuroscience*, 8: 1263-68.

Breiter, H. C., and S. L. Rauch. 1996. 'Functional MRI and the study of OCD: from symptom provocation to cognitive-behavioral probes of cortico-striatal systems and the amygdala', *Neuroimage*, 4: S127-38.

Breiter, H. C., S. L. Rauch, K. K. Kwong, J. R. Baker, R. M. Weisskoff, D. N. Kennedy, A. D. Kendrick, T. L. Davis, A. Jiang, M. S. Cohen, C. E. Stern, J. W. Belliveau, L. Baer, R. L. O'Sullivan, C. R. Savage, M. A. Jenike, and B. R. Rosen. 1996. 'Functional magnetic resonance imaging of symptom provocation in obsessive-compulsive disorder', *Arch Gen Psychiatry*, 53: 595-606.

Burguiere, E., P. Monteiro, G. Feng, and A. M. Graybiel. 2013. 'Optogenetic stimulation of lateral orbitofronto-striatal pathway suppresses compulsive behaviors', *Science*, 340: 1243-6.

Burguiere, E., P. Monteiro, L. Mallet, G. Feng, and A. M. Graybiel. 2015. 'Striatal circuits, habits, and implications for obsessive-compulsive disorder', *Curr Opin Neurobiol*, 30: 59-65.

Buzsaki, G. 2004. 'Large-scale recording of neuronal ensembles', *Nature neuroscience*, 7: 446-51.

Campbell, K. M., L. de Lecea, D. M. Severynse, M. G. Caron, M. J. McGrath, S. B. Sparber, L. Y. Sun, and F. H. Burton. 1999. 'OCD-Like behaviors caused by a neuropotentiating transgene targeted to cortical and limbic D1+ neurons', *J Neurosci*, 19: 5044-53.

Cardin, J. A., M. Carlén, K. Meletis, U. Knoblich, F. Zhang, K. Deisseroth, L. H. Tsai, and C. I. Moore. 2010. 'Targeted optogenetic stimulation and recording of neurons in vivo using cell-type-specific expression of Channelrhodopsin-2', *Nat Protoc*, 5: 247-54.

Casey, B. J., N. Craddock, B. N. Cuthbert, S. E. Hyman, F. S. Lee, and K. J. Ressler. 2013. 'DSM-5 and RDoC: progress in psychiatry research?', *Nat Rev Neurosci*, 14: 810-4.

Chadman, K. K., M. Yang, and J. N. Crawley. 2009. 'Criteria for validating mouse models of psychiatric diseases', *Am J Med Genet B Neuropsychiatr Genet*, 150B: 1-11.

Chakrabarty, K., S. Bhattacharyya, R. Christopher, and S. Khanna. 2005. 'Glutamatergic dysfunction in OCD', *Neuropsychopharmacology*, 30: 1735-40.

Chamberlain, S. R., A. D. Blackwell, N. A. Fineberg, T. W. Robbins, and B. J. Sahakian. 2005. 'The neuropsychology of obsessive compulsive disorder: the importance of failures in cognitive and behavioural inhibition as candidate endophenotypic markers', *Neurosci Biobehav Rev*, 29: 399-419.

Chamberlain, S. R., L. Menzies, A. Hampshire, J. Suckling, N. A. Fineberg, N. del Campo, M. Aitken, K. Craig, A. M. Owen, E. T. Bullmore, T. W. Robbins, and B. J. Sahakian. 2008. 'Orbitofrontal dysfunction in patients with obsessive-compulsive disorder and their unaffected relatives', *Science*, 321: 421-2.

Chen, M., Y. Wan, K. Ade, J. Ting, G. Feng, and N. Calakos. 2011. 'Sapap3 deletion anomalously activates short-term endocannabinoid-mediated synaptic plasticity', *J Neurosci*, 31: 9563-73.

Chen, S. K., P. Tvrdik, E. Peden, S. Cho, S. Wu, G. Spangrude, and M. R. Capecchi. 2010. 'Hematopoietic origin of pathological grooming in Hoxb8 mutant mice', *Cell*, 141: 775-85.

Chen, T. W., T. J. Wardill, Y. Sun, S. R. Pulver, S. L. Renninger, A. Baohan, E. R. Schreiter, R. A. Kerr, M. B. Orger, V. Jayaraman, L. L. Looger, K. Svoboda, and D. S. Kim. 2013. 'Ultrasensitive fluorescent proteins for imaging neuronal activity', *Nature*, 499: 295-300.

Cho, K. K., L. Khibnik, B. D. Philpot, and M. F. Bear. 2009. 'The ratio of NR2A/B NMDA receptor subunits determines the qualities of ocular dominance plasticity in visual cortex', *Proc Natl Acad Sci U S A*, 106: 5377-82.

Cohen, J. Y., S. Haesler, L. Vong, B. B. Lowell, and N. Uchida. 2012. 'Neuron-type-specific signals for reward and punishment in the ventral tegmental area', *Nature*, 482: 85-8.

Corbit, V. L., E. E. Manning, A. H. Gittis, and S. E. Ahmari. 2019. 'Strengthened inputs from secondary motor cortex to striatum in a mouse model of compulsive behavior', *J Neurosci*.

Coutureau, Etienne, and Simon Killcross. 2003. 'Inactivation of the infralimbic prefrontal cortex reinstates goal-directed responding in overtrained rats', *Behav Brain Res*, 146: 167-74.

Cui, G., S. B. Jun, X. Jin, G. Luo, M. D. Pham, D. M. Lovinger, S. S. Vogel, and R. M. Costa. 2014. 'Deep brain optical measurements of cell type-specific neural activity in behaving mice', *Nat Protoc*, 9: 1213-28.

Cui, G., S. B. Jun, X. Jin, M. D. Pham, S. S. Vogel, D. M. Lovinger, and R. M. Costa. 2013. 'Concurrent activation of striatal direct and indirect pathways during action initiation', *Nature*, 494: 238-42.

Damasio, A. R., D. Tranel, and H. Damasio. 1990. 'Individuals with sociopathic behavior caused by frontal damage fail to respond autonomically to social stimuli', *Behav Brain Res*, 41: 81-94.

Deckersbach, Thilo, Cary R. Savage, Tim Curran, Antje Bohne, Sabine Wilhelm, Lee Baer, Michael A. Jenike, and Scott L. Rauch. 2002. 'A study of parallel implicit and explicit information processing in patients with obsessive-compulsive disorder', *Am J Psychiatry*, 159: 1780-82.

Deisseroth, K., and M. J. Schnitzer. 2013. 'Engineering approaches to illuminating brain structure and dynamics', *Neuron*, 80: 568-77.

Delgado-Acevedo, C., S. F. Estay, A. K. Radke, A. Sengupta, A. P. Escobar, F. Henriquez-Belmar, C. A. Reyes, V. Haro-Acuna, E. Utreras, R. Sotomayor-Zarate, A. Cho, J. R. Wendland, A. B. Kulkarni, A. Holmes, D. L. Murphy, A. E. Chavez, and P. R. Moya. 2018. 'Behavioral and synaptic alterations relevant to obsessive-compulsive disorder in mice with increased EAAT3 expression', *Neuropsychopharmacology*.

DeLong, M. R. 1990. 'Primate models of movement disorders of basal ganglia origin', *Trends Neurosci*, 13: 281-5.

Delorme, R., M. O. Krebs, N. Chabane, I. Roy, B. Millet, M. C. Mouren-Simeoni, W. Maier, T. Bourgeron, and M. Leboyer. 2004. 'Frequency and transmission of glutamate receptors GRIK2 and GRIK3 polymorphisms in patients with obsessive compulsive disorder', *NeuroReport*, 15: 699-702.

Denys, D., M. Mantione, M. Figee, P. van den Munckhof, F. Koerselman, H. Westenberg, A. Bosch, and R. Schuurman. 2010. 'Deep brain stimulation of the nucleus accumbens for treatment-refractory obsessive-compulsive disorder', *Arch Gen Psychiatry*, 67: 1061-8.

Denys, Damiaan. 2014. 'Compulsivity and free will', *CNS spectrums*, 19: 8-9.

Desai, M., I. Kahn, U. Knoblich, J. Bernstein, H. Atallah, A. Yang, N. Kopell, R. L. Buckner, A. M. Graybiel, C. I. Moore, and E. S. Boyden. 2011. 'Mapping brain networks in awake mice using combined optical neural control and fMRI', *J Neurophysiol*, 105: 1393-405.

Dezfouli, Amir, and Bernard W. Balleine. 2012. 'Habits, action sequences and reinforcement learning', *Eur J Neurosci*, 35: 1036-51.

Di Martino, A., A. Scheres, D. S. Margulies, A. M. Kelly, L. Q. Uddin, Z. Shehzad, B. Biswal, J. R. Walters, F. X. Castellanos, and M. P. Milham. 2008. 'Functional connectivity of human striatum: a resting state FMRI study', *Cerebral cortex (New York, N.Y. : 1991)*, 18: 2735-47.

Diagnostic and statistical manual of mental disorders, (DSM-5®). 2013. (American Psychiatric Pub).

Dickel, D. E., J. Veenstra-VanderWeele, N. J. Cox, X. Wu, D. J. Fischer, M. Van Etten-Lee, J. A. Himle, B. L. Leventhal, E. H. Cook, Jr., and G. L. Hanna. 2006. 'Association testing of the positional and functional candidate gene SLC1A1/EAAC1 in early-onset obsessive-compulsive disorder', *Arch Gen Psychiatry*, 63: 778-85.

Diester, Ilka, Matthew T. Kaufman, Murtaza Mogri, Ramin Pashaie, Werapong Goo, Ofer Yizhar, Charu Ramakrishnan, Karl Deisseroth, and Krishna V. Shenoy. 2011. 'An optogenetic toolbox designed for primates', *Nat Neurosci*, 14: 387-97.

Dombeck, D. A., A. N. Khabbaz, F. Collman, T. L. Adelman, and D. W. Tank. 2007. 'Imaging large-scale neural activity with cellular resolution in awake, mobile mice', *Neuron*, 56: 43-57.

Donaldson, Z. R., K. M. Nautiyal, S. E. Ahmari, and R. Hen. 2013. 'Genetic approaches for understanding the role of serotonin receptors in mood and behavior', *Curr Opin Neurobiol*, 23: 399-406.

Doyle, A., M. P. McGarry, N. A. Lee, and J. J. Lee. 2012. 'The construction of transgenic and gene knockout/knockin mouse models of human disease', *Transgenic Res*, 21: 327-49.

Du, J. C., T. F. Chiu, K. M. Lee, H. L. Wu, Y. C. Yang, S. Y. Hsu, C. S. Sun, B. Hwang, and J. F. Leckman. 2010. 'Tourette syndrome in children: an updated review', *Pediatr Neonatol*, 51: 255-64.

Dunah, A. W., E. Hueske, M. Wyszynski, C. C. Hoogenraad, J. Jaworski, D. T. Pak, A. Simonetta, G. Liu, and M. Sheng. 2005. 'LAR receptor protein tyrosine phosphatases in the development and maintenance of excitatory synapses', *Nat Neurosci*, 8: 458-67.

Eaton, W. W., S. S. Martins, G. Nestadt, O. J. Bienvenu, D. Clarke, and P. Alexandre. 2008. 'The burden of mental disorders', *Epidemiol Rev*, 30: 1-14.

Erbguth, Karen, Matthias Prigge, Franziska Schneider, Peter Hegemann, and Alexander Gottschalk. 2012. 'Bimodal activation of different neuron classes with the spectrally red-shifted channelrhodopsin chimera C1V1 in Caenorhabditis elegans', *PLoS One*, 7.

Evans, D. W., M. D. Lewis, and E. Iobst. 2004. 'The role of the orbitofrontal cortex in normally developing compulsive-like behaviors and obsessive-compulsive disorder', *Brain Cogn*, 55: 220-34.

Everitt, B. J., and T. W. Robbins. 2005. 'Neural systems of reinforcement for drug addiction: from actions to habits to compulsion', *Nat Neurosci*, 8: 1481-9.

———. 2013. 'From the ventral to the dorsal striatum: devolving views of their roles in drug addiction', *Neurosci Biobehav Rev*, 37: 1946-54.

Fan, Qing, Xu Yan, Jijun Wang, Ying Chen, Xuemei Wang, Chunbo Li, Ling Tan, Chao You, Tianhong Zhang, Sai Zuo, Dongrong Xu, Kemin Chen, Jodie M. Finlayson-Burden, and Zeping Xiao. 2012. 'Abnormalities of white matter microstructure in unmedicated obsessive-compulsive disorder and changes after medication', *PLoS One*, 7.

Fenno, L., O. Yizhar, and K. Deisseroth. 2011. 'The development and application of optogenetics', *Annu Rev Neurosci*, 34: 389-412.

Fernández de la Cruz, L., M. Rydell, B. Runeson, B. M. D'Onofrio, G. Brander, C. Rück, P. Lichtenstein, H. Larsson, and D. Mataix-Cols. 2017. 'Suicide in obsessive-compulsive disorder: a population-based study of 36 788 Swedish patients', *Mol Psychiatry*, 22: 1626-32.

Figee, Martijn, Judy Luigjes, Ruud Smolders, Carlos-Eduardo E. Valencia-Alfonso, Guido van Wingen, Bart de Kwaasteniet, Mariska Mantione, Pieter Ooms, Pelle de Koning, Nienke Vulink, Nina Levar, Lukas Droge, Pepijn van den Munckhof, P. R. Schuurman, Aart Nederveen, Wim van den Brink, Ali Mazaheri, Matthijs Vink, and Damiaan Denys. 2013. 'Deep brain stimulation restores frontostriatal network activity in obsessive-compulsive disorder', *Nat Neurosci*, 16: 386-87.

Figee, Martijn, Ilse Wielaard, Ali Mazaheri, and Damiaan Denys. 2013. 'Neurosurgical targets for compulsivity: what can we learn from acquired brain lesions?', *Neuroscience and biobehavioral reviews*, 37: 328-39.

Fitzgerald, K. D., R. C. Welsh, E. R. Stern, M. Angstadt, G. L. Hanna, J. L. Abelson, and S. F. Taylor. 2011a. 'Developmental alterations of frontal-striatal-thalamic connectivity in obsessive-compulsive disorder', *J Am Acad Child Adolesc Psychiatry*, 50: 938-48 e3.

Fitzgerald, Kate D., Robert C. Welsh, Emily R. Stern, Mike Angstadt, Gregory L. Hanna, James L. Abelson, and Stephan F. Taylor. 2011b. 'Developmental alterations of frontal-striatal-thalamic connectivity in obsessive-compulsive disorder', *Journal of the American Academy of Child and Adolescent Psychiatry*, 50: 938-948000.

Frick, L. R., M. Rapanelli, K. Jindachomthong, P. Grant, J. F. Leckman, S. Swedo, K. Williams, and C. Pittenger. 2018. 'Differential binding of antibodies in PANDAS patients to cholinergic interneurons in the striatum', *Brain Behav Immun*, 69: 304-11.

Gage, G. J., C. R. Stoetzner, A. B. Wiltschko, and J. D. Berke. 2010. 'Selective activation of striatal fast-spiking interneurons during choice execution', *Neuron*, 67: 466-79.

Gallagher, M, RW McMahan, and G Schoenbaum. 1999. 'Orbitofrontal cortex and representation of incentive value in associative learning', *Journal of Neuroscience*, 19: 6610-14.

Geller, D. A. 2006. 'Obsessive-compulsive and spectrum disorders in children and adolescents', *Psychiatr Clin North Am*, 29: 353-70.

Ghosh, K. K., L. D. Burns, E. D. Cocker, A. Nimmerjahn, Y. Ziv, A. E. Gamal, and M. J. Schnitzer. 2011. 'Miniaturized integration of a fluorescence microscope', *Nat Methods*, 8: 871-8.

Gillan, C. M., S. Morein-Zamir, G. P. Urcelay, A. Sule, V. Voon, A. M. Apergis-Schoute, N. A. Fineberg, B. J. Sahakian, and T. W. Robbins. 2014a. 'Enhanced avoidance habits in obsessive-compulsive disorder', *Biol Psychiatry*, 75: 631-8.

Gillan, C. M., M. Papmeyer, S. Morein-Zamir, B. J. Sahakian, N. A. Fineberg, T. W. Robbins, and S. de Wit. 2011. 'Disruption in the balance between goal-directed behavior and habit learning in obsessive-compulsive disorder', *Am J Psychiatry*, 168: 718-26.

Gillan, Claire M., Annemieke M. Apergis-Schoute, Sharon Morein-Zamir, Gonzalo P. Urcelay, Akeem Sule, Naomi A. Fineberg, Barbara J. Sahakian, and Trevor W. Robbins. 2015. 'Functional neuroimaging of avoidance habits in obsessive-compulsive disorder', *The American journal of psychiatry*, 172: 284-93.

Gillan, Claire M., Sharon Morein-Zamir, Gonzalo P. Urcelay, Akeem Sule, Valerie Voon, Annemieke M. Apergis-Schoute, Naomi A. Fineberg, Barbara J. Sahakian, and Trevor W. Robbins. 2014b. 'Enhanced avoidance habits in obsessive-compulsive disorder', *Biol Psychiatry*, 75: 631-38.

Gittis, A. H., A. B. Nelson, M. T. Thwin, J. J. Palop, and A. C. Kreitzer. 2010. 'Distinct roles of GABAergic interneurons in the regulation of striatal output pathways', *J Neurosci*, 30: 2223-34.

Glausier, J. R., and D. A. Lewis. 2013. 'Dendritic spine pathology in schizophrenia', *Neuroscience*, 251: 90-107.

Gonzalez, L. F., F. Henriquez-Belmar, C. Delgado-Acevedo, M. Cisternas-Olmedo, G. Arriagada, R. Sotomayor-Zarate, D. L. Murphy, and P. R. Moya. 2017. 'Neurochemical and behavioral characterization of neuronal glutamate transporter EAAT3 heterozygous mice', *Biol Res*, 50: 29.

Grace, A. A., and B. S. Bunney. 1983. 'Intracellular and extracellular electrophysiology of nigral dopaminergic neurons--1. Identification and characterization', *Neuroscience*, 10: 301-15.

Graybiel, A. M. 1998a. 'The basal ganglia and chunking of action repertoires', *Neurobiology of learning and memory*, 70: 119-36.

———. 1998b. 'The basal ganglia and chunking of action repertoires', *Neurobiol Learn Mem*, 70: 119-36.

———. 2000. 'The basal ganglia', *Curr Biol*, 10: R509-11.

Graybiel, A. M., and S. L. Rauch. 2000. 'Toward a neurobiology of obsessive-compulsive disorder', *Neuron*, 28: 343-47.

Graybiel, AM. 1995. 'Building action repertoires: memory and learning functions of the basal ganglia', *Currents Opinions in Neurobiology*, 5: 733-41.

Graybiel, Ann M. 2008. 'Habits, rituals, and the evaluative brain', *Annual review of neuroscience*, 31: 359-87.

Greenberg, B. D., L. A. Gabriels, D. A. Malone, A. R. Rezai, G. M. Friehs, M. S. Okun, N. A. Shapira, K. D. Foote, P. R. Cosyns, C. S. Kubu, P. F. Malloy, S. P. Salloway, J. E. Giftakis, M. T. Rise, A. G. Machado, K. B. Baker, P. H. Stypulkowski, W. K. Goodman, S. A. Rasmussen, and B. J. Nuttin. 2010. 'Deep brain stimulation of the ventral internal capsule/ventral striatum for obsessive-compulsive disorder: worldwide experience', *Mol Psychiatry*, 15: 64-79.

Greenberg, Benjamin D., Scott L. Rauch, and Suzanne N. Haber. 2010. 'Invasive circuitry-based neurotherapeutics: stereotactic ablation and deep brain stimulation for OCD', *Neuropsychopharmacology*, 35: 317-36.

Greer, J. M., and M. R. Capecchi. 2002. 'Hoxb8 is required for normal grooming behavior in mice', *Neuron*, 33: 23-34.

Gremel, C. M., J. H. Chancey, B. K. Atwood, G. Luo, R. Neve, C. Ramakrishnan, K. Deisseroth, D. M. Lovinger, and R. M. Costa. 2016. 'Endocannabinoid Modulation of Orbitostriatal Circuits Gates Habit Formation', *Neuron*, 90: 1312-24.

Gremel, C. M., and R. M. Costa. 2013. 'Orbitofrontal and striatal circuits dynamically encode the shift between goal-directed and habitual actions', *Nat Commun*, 4: 2264.

Grienberger, C., and A. Konnerth. 2012. 'Imaging calcium in neurons', *Neuron*, 73: 862-85.

Gritton, H. J., W. M. Howe, M. F. Romano, A. G. DiFeliceantonio, M. A. Kramer, V. Saligrama, M. E. Bucklin, D. Zemel, and X. Han. 2019. 'Unique contributions of parvalbumin and cholinergic interneurons in organizing striatal networks during movement', *Nat Neurosci*, 22: 586-97.

Gruner, Patricia, Alan Anticevic, Daeyeol Lee, and Christopher Pittenger. 2015. 'Arbitration between Action Strategies in Obsessive-Compulsive Disorder', *The Neuroscientist : a review journal bringing neurobiology, neurology and psychiatry*.

Gunaydin, L. A., O. Yizhar, A. Berndt, V. S. Sohal, K. Deisseroth, and P. Hegemann. 2010. 'Ultrafast optogenetic control', *Nat Neurosci*, 13: 387-92.

Haber, S. N. 2003. 'The primate basal ganglia: parallel and integrative networks', *J Chem Neuroanat*, 26: 317-30.

———. 2016. 'Corticostriatal circuitry', *Dialogues Clin Neurosci*, 18: 7-21.

Haber, S.N., K. Kunishio, M. Mizobuchi, and E. Lynd-Balta. 1995. 'The orbital and medial prefrontal circuit through the primate basal ganglia', *Journal of Neuroscience*, 15: 4851-67.

Han, Xue, Brian Y. Chow, Huihui Zhou, Nathan C. Klapoetke, Amy Chuong, Reza Rajimehr, Aimei Yang, Michael V. Baratta, Jonathan Winkle, Robert Desimone, and Edward S. Boyden. 2011. 'A high-light sensitivity optical neural silencer: development and application to optogenetic control of non-human primate cortex', *Frontiers in systems neuroscience*, 5: 18.

Hanna, G. L., J. A. Himle, G. C. Curtis, and B. W. Gillespie. 2005. 'A family study of obsessive-compulsive disorder with pediatric probands', *Am J Med Genet B Neuropsychiatr Genet*, 134b: 13-9.

Hanna, G. L., J. Veenstra-VanderWeele, N. J. Cox, M. Boehnke, J. A. Himle, G. C. Curtis, B. L. Leventhal, and E. H. Cook, Jr. 2002. 'Genome-wide linkage analysis of families with obsessive-compulsive disorder ascertained through pediatric probands', *Am J Med Genet*, 114: 541-52.

Harrison, B. J., J. Pujol, N. Cardoner, J. Deus, P. Alonso, M. Lopez-Sola, O. Contreras-Rodriguez, E. Real, C. Segalas, L. Blanco-Hinojo, J. M. Menchon, and C. Soriano-Mas. 2013. 'Brain corticostriatal systems and the major clinical symptom dimensions of obsessive-compulsive disorder', *Biol Psychiatry*, 73: 321-8.

Harrison, B. J., C. Soriano-Mas, J. Pujol, H. Ortiz, M. Lopez-Sola, R. Hernandez-Ribas, J. Deus, P. Alonso, M. Yucel, C. Pantelis, J. M. Menchon, and N. Cardoner. 2009. 'Altered corticostriatal functional connectivity in obsessive-compulsive disorder', *Arch Gen Psychiatry*, 66: 1189-200.

Harrison, Ben J., Jesus Pujol, Narcis Cardoner, Joan Deus, Pino Alonso, Marina López-Solà, Oren Contreras-Rodríguez, Eva Real, Cinto Segalàs, Laura Blanco-Hinojo, José M. Menchon, and Carles Soriano-Mas. 2013. 'Brain corticostriatal systems and the major clinical symptom dimensions of obsessive-compulsive disorder', *Biol Psychiatry*, 73: 321-28.

Harrison, Ben J., Carles Soriano-Mas, Jesus Pujol, Hector Ortiz, Marina López-Solà, Rosa Hernández-Ribas, Joan Deus, Pino Alonso, Murat Yücel, Christos Pantelis, José M. Menchon, and Narcís Cardoner. 2009. 'Altered corticostriatal functional connectivity in obsessive-compulsive disorder', *Archives of general psychiatry*, 66: 1189-200.

Hirschtritt, M. E., M. H. Bloch, and C. A. Mathews. 2017. 'Obsessive-Compulsive Disorder: Advances in Diagnosis and Treatment', *JAMA*, 317: 1358-67.

Hou, Jingming, Wenjing Wu, Yun Lin, Jian Wang, Daiquan Zhou, Junwei Guo, Shanshan Gu, Mei He, Saud Ahmed, Jiani Hu, Wei Qu, and Haitao Li. 2012. 'Localization of cerebral functional deficits in patients with obsessive-compulsive disorder: a resting-state fMRI study', *J Affect Disord*, 138: 313-21.

Howe, M. W., H. E. Atallah, A. McCool, D. J. Gibson, and A. M. Graybiel. 2011. 'Habit learning is associated with major shifts in frequencies of oscillatory activity and synchronized spike firing in striatum', *Proc Natl Acad Sci U S A*, 108: 16801-6.

Hubel, D. H., and T. N. Wiesel. 2009. 'Republication of The Journal of Physiology (1959) 148, 574-591: Receptive fields of single neurones in the cat's striate cortex. 1959', *J Physiol*, 587: 2721-32.

Hurley, K. M., H. Herbert, M. M. Moga, and C. B. Saper. 1991. 'Efferent projections of the infralimbic cortex of the rat', *J Comp Neurol*, 308: 249-76.

Husted, David S., and Nathan A. Shapira. 2004. 'A review of the treatment for refractory obsessive-compulsive disorder: from medicine to deep brain stimulation', *CNS spectrums*, 9: 833-47.

Insel, T. R., and J. T. Winslow. 1992. 'Neurobiology of obsessive compulsive disorder', *Psychiatr Clin North Am*, 15: 813-24.

Jaffe, A. E., A. Deep-Soboslay, R. Tao, D. T. Hauptman, W. H. Kaye, V. Arango, D. R. Weinberger, T. M. Hyde, and J. E. Kleinman. 2014. 'Genetic neuropathology of obsessive psychiatric syndromes', *Transl Psychiatry*, 4: e432.

Jimenez, J. C., K. Su, A. R. Goldberg, V. M. Luna, J. S. Biane, G. Ordek, P. Zhou, S. K. Ong, M. A. Wright, L. Zweifel, L. Paninski, R. Hen, and M. A. Kheirbek. 2018. 'Anxiety Cells in a Hippocampal-Hypothalamic Circuit', *Neuron*, 97: 670-83 e6.

Jin, X., and R. M. Costa. 2010. 'Start/stop signals emerge in nigrostriatal circuits during sequence learning', *Nature*, 466: 457-62.

Jin, X., F. Tecuapetla, and R. M. Costa. 2014. 'Basal ganglia subcircuits distinctively encode the parsing and concatenation of action sequences', *Nat Neurosci*, 17: 423-30.

Joel, Daphna, Orly Zohar, Michal Afek, Haggai Hermesh, Lidia Lerner, Ruth Kuperman, Ruth Gross-Isseroff, Abraham Weizman, and Rivka Inzelberg. 2005. 'Impaired procedural learning in obsessive-compulsive disorder and Parkinson's disease, but not in major depressive disorder', *Behav Brain Res*, 157: 253-63.

Kalanithi, P. S., W. Zheng, Y. Kataoka, M. DiFiglia, H. Grantz, C. B. Saper, M. L. Schwartz, J. F. Leckman, and F. M. Vaccarino. 2005. 'Altered parvalbumin-positive neuron distribution in basal ganglia of individuals with Tourette syndrome', *Proc Natl Acad Sci U S A*, 102: 13307-12.

Kalueff, A. V., A. M. Stewart, C. Song, K. C. Berridge, A. M. Graybiel, and J. C. Fentress. 2016. 'Neurobiology of rodent self-grooming and its value for translational neuroscience', *Nat Rev Neurosci*, 17: 45-59.

Kataoka, Y., P. S. Kalanithi, H. Grantz, M. L. Schwartz, C. Saper, J. F. Leckman, and F. M. Vaccarino. 2010. 'Decreased number of parvalbumin and cholinergic interneurons in the striatum of individuals with Tourette syndrome', *J Comp Neurol*, 518: 277-91.

Katayama, K., K. Yamada, V. G. Ornthanalai, T. Inoue, M. Ota, N. P. Murphy, and J. Aruga. 2010. 'Slitrk1-deficient mice display elevated anxiety-like behavior and noradrenergic abnormalities', *Mol Psychiatry*, 15: 177-84.

Kent, Alexander R., and Warren M. Grill. 2011. 'Instrumentation to record evoked potentials for closed-loop control of deep brain stimulation', *Conference proceedings : ... Annual International Conference of the IEEE Engineering in Medicine and Biology Society. IEEE Engineering in Medicine and Biology Society. Annual Conference*, 2011: 6777-80.

Kessler, Ronald C., Patricia Berglund, Olga Demler, Robert Jin, Kathleen R. Merikangas, and Ellen E. Walters. 2005. 'Lifetime prevalence and age-of-onset distributions of DSM-IV disorders in the National Comorbidity Survey Replication', *Archives of general psychiatry*, 62: 593-602.

Killcross, Simon, and Etienne Coutureau. 2003. 'Coordination of actions and habits in the medial prefrontal cortex of rats', *Cerebral cortex (New York, N.Y. : 1991)*, 13: 400-08.

Kirby, T. 2015. 'Ketamine for depression: the highs and lows', *Lancet Psychiatry*, 2: 783-4.

Kohlrausch, F. B., I. G. Giori, F. B. Melo-Felippe, T. Vieira-Fonseca, L. G. Velarde, J. B. de Salles Andrade, and L. F. Fontenelle. 2016. 'Association of GRIN2B gene polymorphism and Obsessive Compulsive disorder and symptom dimensions: A pilot study', *Psychiatry Res*, 243: 152-5.

Koos, T., and J. M. Tepper. 1999. 'Inhibitory control of neostriatal projection neurons by GABAergic interneurons', *Nat Neurosci*, 2: 467-72.

Koran, L. M. 2000. 'Quality of life in obsessive-compulsive disorder', *Psychiatr Clin North Am*, 23: 509-17.

Koran, L. M., G. L. Hanna, E. Hollander, G. Nestadt, H. B. Simpson, and Association American Psychiatric. 2007. 'Practice guideline for the treatment of patients with obsessive-compulsive disorder', *Am J Psychiatry*, 164: 5-53.

Koran, L. M., S. Pallanti, and L. Quercioli. 2001. 'Sumatriptan, 5-HT(1D) receptors and obsessive-compulsive disorder', *Eur Neuropsychopharmacol*, 11: 169-72.

Koran, L. M., M. L. Thienemann, and R. Davenport. 1996. 'Quality of life for patients with obsessive-compulsive disorder', *Am J Psychiatry*, 153: 783-8.

Kravitz, A. V., B. S. Freeze, P. R. Parker, K. Kay, M. T. Thwin, K. Deisseroth, and A. C. Kreitzer. 2010. 'Regulation of parkinsonian motor behaviours by optogenetic control of basal ganglia circuitry', *Nature*, 466: 622-6.

Kravitz, A. V., S. F. Owen, and A. C. Kreitzer. 2013. 'Optogenetic identification of striatal projection neuron subtypes during in vivo recordings', *Brain Res*, 1511: 21-32.

Larkum, M. E. 2013. 'The yin and yang of cortical layer 1', *Nat Neurosci*, 16: 114-5.

Lee, K., S. M. Holley, J. L. Shobe, N. C. Chong, C. Cepeda, M. S. Levine, and S. C. Masmanidis. 2017. 'Parvalbumin Interneurons Modulate Striatal Output and Enhance Performance during Associative Learning', *Neuron*, 93: 1451-63.e4.

Lee, Sang W., Shinsuke Shimojo, and John P. O'Doherty. 2014. 'Neural computations underlying arbitration between model-based and model-free learning', *Neuron*, 81: 687-99.

Lei, H., J. Lai, X. Sun, Q. Xu, and G. Feng. 2019. 'Lateral orbitofrontal dysfunction in the Sapap3 knockout mouse model of obsessive-compulsive disorder', *J Psychiatry Neurosci*, 44: 120-31.

Licinio, J. 2011. 'Translational Psychiatry: leading the transition from the cesspool of devastation to a place where the grass is really greener', *Transl Psychiatry*, 1: e1.

Lin, J. Y., P. M. Knutsen, A. Muller, D. Kleinfeld, and R. Y. Tsien. 2013. 'ReaChR: a red-shifted variant of channelrhodopsin enables deep transcranial optogenetic excitation', *Nat Neurosci*, 16: 1499-508.

Liu, S., Y. Yin, Y. Liu, Y. Sun, X. Zhang, and X. Ma. 2012. 'Lack of an association between obsessive-compulsive disorder and polymorphisms in the 3' untranslated region of GRIN2B in a Chinese Han population', *Psychiatry Res*, 196: 142-4.

Maia, T. V., R. E. Cooney, and B. S. Peterson. 2008. 'The neural bases of obsessive-compulsive disorder in children and adults', *Dev Psychopathol*, 20: 1251-83.

Mallet, N., C. Le Moine, S. Charpier, and F. Gonon. 2005. 'Feedforward inhibition of projection neurons by fast-spiking GABA interneurons in the rat striatum in vivo', *J Neurosci*, 25: 3857-69.

Mastro, K. J., K. T. Zitelli, A. M. Willard, K. H. Leblanc, A. V. Kravitz, and A. H. Gittis. 2017. 'Cell-specific pallidal intervention induces long-lasting motor recovery in dopamine-depleted mice', *Nat Neurosci*, 20: 815-23.

Matsuno-Yagi, A., and Y. Mukohata. 1977. 'Two possible roles of bacteriorhodopsin; a comparative study of strains of Halobacterium halobium differing in pigmentation', *Biochem Biophys Res Commun*, 78: 237-43.

Mattheisen, M., J. F. Samuels, Y. Wang, B. D. Greenberg, A. J. Fyer, J. T. McCracken, D. A. Geller, D. L. Murphy, J. A. Knowles, M. A. Grados, M. A. Riddle, S. A. Rasmussen, N. C. McLaughlin, E. L. Nurmi, K. D. Askland, H. D. Qin, B. A. Cullen, J. Piacentini, D. L. Pauls, O. J. Bienvenu, S. E. Stewart, K. Y. Liang, F. S. Goes, B. Maher, A. E. Pulver, Y. Y. Shugart, D. Valle, C. Lange, and G. Nestadt. 2015. 'Genome-wide association study in obsessive-compulsive disorder: results from the OCGAS', *Mol Psychiatry*, 20: 337-44.

Mattis, Joanna, Kay M. Tye, Emily A. Ferenczi, Charu Ramakrishnan, Daniel J. O'Shea, Rohit Prakash, Lisa A. Gunaydin, Minsuk Hyun, Lief E. Fenno, Viviana Gradinaru, Ofer Yizhar, and Karl Deisseroth. 2012. 'Principles for applying optogenetic tools derived from direct comparative analysis of microbial opsins', *Nat Methods*, 9: 159-72.

McDougle, C. J., L. E. Kresch, W. K. Goodman, S. T. Naylor, F. R. Volkmar, D. J. Cohen, and L. H. Price. 1995. 'A case-controlled study of repetitive thoughts and behavior in adults with autistic disorder and obsessive-compulsive disorder', *Am J Psychiatry*, 152: 772-77.

Menzies, L., S. R. Chamberlain, A. R. Laird, S. M. Thelen, B. J. Sahakian, and E. T. Bullmore. 2008a. 'Integrating evidence from neuroimaging and neuropsychological studies of obsessive-compulsive disorder: the orbitofronto-striatal model revisited', *Neurosci Biobehav Rev*, 32: 525-49.

Menzies, Lara, Samuel R. Chamberlain, Angela R. Laird, Sarah M. Thelen, Barbara J. Sahakian, and Ed T. Bullmore. 2008b. 'Integrating evidence from neuroimaging and neuropsychological studies of obsessive-compulsive disorder: the orbitofronto-striatal model revisited', *Neuroscience and biobehavioral reviews*, 32: 525-49.

Milad, M. R., and S. L. Rauch. 2007. 'The role of the orbitofrontal cortex in anxiety disorders', *Ann N Y Acad Sci*, 1121: 546-61.

———. 2012a. 'Obsessive-compulsive disorder: beyond segregated cortico-striatal pathways', *Trends Cogn Sci*, 16: 43-51.

Milad, Mohammed R., and Scott L. Rauch. 2012b. 'Obsessive-compulsive disorder: beyond segregated cortico-striatal pathways', *Trends in cognitive sciences*, 16: 43-51.

Molloy, A. G., and J. L. Waddington. 1987. 'Pharmacological characterization in the rat of grooming and other behavioural responses to the D1 dopamine receptor agonist R-SK&F 38393', *J Psychopharmacol*, 1: 177-83.

Moore, G. J., F. P. MacMaster, C. Stewart, and D. R. Rosenberg. 1998. 'Case study: caudate glutamatergic changes with paroxetine therapy for pediatric obsessive-compulsive disorder', *J Am Acad Child Adolesc Psychiatry*, 37: 663-7.

Nagarajan, N., B. W. Jones, P. J. West, R. E. Marc, and M. R. Capecchi. 2018. 'Corticostriatal circuit defects in Hoxb8 mutant mice', *Mol Psychiatry*, 23: 1-10.

Nagel, G., T. Szellas, W. Huhn, S. Kateriya, N. Adeishvili, P. Berthold, D. Ollig, P. Hegemann, and E. Bamberg. 2003. 'Channelrhodopsin-2, a directly light-gated cation-selective membrane channel', *Proc Natl Acad Sci U S A*, 100: 13940-5.

Nagel, Georg, Doris Ollig, Markus Fuhrmann, Suneel Kateriya, Anna M. Musti, Ernst Bamberg, and Peter Hegemann. 2002. 'Channelrhodopsin-1: a light-gated proton channel in green algae', *Science (New York, N.Y.)*, 296: 2395-98.

Nakamae, T., Y. Sakai, Y. Abe, S. Nishida, K. Fukui, K. Yamada, M. Kubota, D. Denys, and J. Narumoto. 2014. 'Altered fronto-striatal fiber topography and connectivity in obsessive-compulsive disorder', *PLoS One*, 9: e112075.

Nakao, T., A. Nakagawa, T. Yoshiura, E. Nakatani, M. Nabeyama, C. Yoshizato, A. Kudoh, K. Tada, K. Yoshioka, M. Kawamoto, O. Togao, and S. Kanba. 2005. 'Brain activation of patients with obsessive-compulsive disorder during neuropsychological and symptom provocation tasks before and after symptom improvement: a functional magnetic resonance imaging study', *Biol Psychiatry*, 57: 901-10.

Nestadt, G., J. Samuels, M. A. Riddle, K. Y. Liang, O. J. Bienvenu, R. Hoehn-Saric, M. Grados, and B. Cullen. 2001. 'The relationship between obsessive-compulsive disorder and anxiety and affective disorders: results from the Johns Hopkins OCD Family Study', *Psychol Med*, 31: 481-7.

Nieoullon, A., B. Canolle, F. Masmejean, B. Guillet, P. Pisano, and S. Lortet. 2006. 'The neuronal excitatory amino acid transporter EAAC1/EAAT3: does it represent a major actor at the brain excitatory synapse?', *J Neurochem*, 98: 1007-18.

Nordahl, T. E., C. Benkelfat, W. E. Semple, M. Gross, A. C. King, and R. M. Cohen. 1989. 'Cerebral glucose metabolic rates in obsessive compulsive disorder', *Neuropsychopharmacology*, 2: 23-28.

O'Hare, J. K., K. K. Ade, T. Sukharnikova, S. D. Van Hooser, M. L. Palmeri, H. H. Yin, and N. Calakos. 2016. 'Pathway-Specific Striatal Substrates for Habitual Behavior', *Neuron*, 89: 472-9.

Oesterhelt, D., and W. Stoeckenius. 1971. 'Rhodopsin-like protein from the purple membrane of Halobacterium halobium', *Nature: New biology*, 233: 149-52.

Oh, S. W., J. A. Harris, L. Ng, B. Winslow, N. Cain, S. Mihalas, Q. Wang, C. Lau, L. Kuan, A. M. Henry, M. T. Mortrud, B. Ouellette, T. N. Nguyen, S. A. Sorensen, C. R. Slaughterbeck, W. Wakeman, Y. Li, D. Feng, A. Ho, E. Nicholas, K. E. Hirokawa, P. Bohn, K. M. Joines, H. Peng, M. J. Hawrylycz, J. W. Phillips, J. G. Hohmann, P. Wohnoutka, C. R. Gerfen, C. Koch, A. Bernard, C. Dang, A. R. Jones, and H. Zeng. 2014. 'A mesoscale connectome of the mouse brain', *Nature*, 508: 207-14.

Oldenburg, I. A., and B. L. Sabatini. 2015. 'Antagonistic but Not Symmetric Regulation of Primary Motor Cortex by Basal Ganglia Direct and Indirect Pathways', *Neuron*, 86: 1174-81.

Otis, T. S., G. Brasnjo, J. A. Dzubay, and M. Pratap. 2004. 'Interactions between glutamate transporters and metabotropic glutamate receptors at excitatory synapses in the cerebellar cortex', *Neurochem Int*, 45: 537-44.

Owen, S. F., J. D. Berke, and A. C. Kreitzer. 2018. 'Fast-Spiking Interneurons Supply Feedforward Control of Bursting, Calcium, and Plasticity for Efficient Learning', *Cell*, 172: 683-95 e15.

Page, S. J., and P. Terry. 1997. 'Conditioned grooming induced by the dopamine D1-like receptor agonist SKF 38393 in rats', *Pharmacol Biochem Behav*, 57: 829-33.

Parker, J. G., J. D. Marshall, B. Ahanonu, Y. W. Wu, T. H. Kim, B. F. Grewe, Y. Zhang, J. Z. Li, J. B. Ding, M. D. Ehlers, and M. J. Schnitzer. 2018. 'Diametric neural ensemble dynamics in parkinsonian and dyskinetic states', *Nature*, 557: 177-82.

Pauls, D. L. 2010. 'The genetics of obsessive-compulsive disorder: a review', *Dialogues Clin Neurosci*, 12: 149-63.

Pauls, D. L., A. Abramovitch, S. L. Rauch, and D. A. Geller. 2014. 'Obsessive-compulsive disorder: an integrative genetic and neurobiological perspective', *Nat Rev Neurosci*, 15: 410-24.

Peca, J., C. Feliciano, J. T. Ting, W. Wang, M. F. Wells, T. N. Venkatraman, C. D. Lascola, Z. Fu, and G. Feng. 2011. 'Shank3 mutant mice display autistic-like behaviours and striatal dysfunction', *Nature*, 472: 437-42.

Pei, Ying, Shuyun Dong, and Bryan L. Roth. 2010. 'Generation of designer receptors exclusively activated by designer drugs (DREADDs) using directed molecular evolution', *Current protocols in neuroscience / editorial board, Jacqueline N. Crawley ... [et al.]*, Chapter 4.

Peixoto, R. T., W. Wang, D. M. Croney, Y. Kozorovitskiy, and B. L. Sabatini. 2016. 'Early hyperactivity and precocious maturation of corticostriatal circuits in Shank3B(-/-) mice', *Nat Neurosci*, 19: 716-24.

Penzes, P., M. E. Cahill, K. A. Jones, J. E. VanLeeuwen, and K. M. Woolfrey. 2011. 'Dendritic spine pathology in neuropsychiatric disorders', *Nat Neurosci*, 14: 285-93.

Perani, D., C. Colombo, S. Bressi, A. Bonfanti, F. Grassi, S. Scarone, L. Bellodi, E. Smeraldi, and F. Fazio. 1995. '[18F]FDG PET study in obsessive-compulsive disorder. A clinical/metabolic correlation study after treatment', *Br J Psychiatry*, 166: 244-50.

Piantadosi, and S. E. Ahmari. 2015. 'Using Optogenetics to Dissect the Neural Circuits Underlying OCD and Related Disorders', *Current Treatment Options in Psychiatry*.

Picciotto, M. R., and K. Wickman. 1998. 'Using knockout and transgenic mice to study neurophysiology and behavior', *Physiol Rev*, 78: 1131-63.

Pigott, T. A., and S. M. Seay. 1999. 'A review of the efficacy of selective serotonin reuptake inhibitors in obsessive-compulsive disorder', *J Clin Psychiatry*, 60: 101-6.

Pittenger, C., and M. H. Bloch. 2014. 'Pharmacological treatment of obsessive-compulsive disorder', *Psychiatr Clin North Am*, 37: 375-91.

Pittenger, C., M. H. Bloch, and K. Williams. 2011. 'Glutamate abnormalities in obsessive compulsive disorder: neurobiology, pathophysiology, and treatment', *Pharmacol Ther*, 132: 314-32.

Pittenger, C., B. Kelmendi, M. Bloch, J. H. Krystal, and V. Coric. 2005. 'Clinical treatment of obsessive compulsive disorder', *Psychiatry (Edgmont)*, 2: 34-43.

Pnevmatikakis, E. A., D. Soudry, Y. Gao, T. A. Machado, J. Merel, D. Pfau, T. Reardon, Y. Mu, C. Lacefield, W. Yang, M. Ahrens, R. Bruno, T. M. Jessell, D. S. Peterka, R. Yuste, and L. Paninski. 2016. 'Simultaneous Denoising, Deconvolution, and Demixing of Calcium Imaging Data', *Neuron*, 89: 285-99.

Porton, B., B. D. Greenberg, K. Askland, L. M. Serra, J. Gesmonde, G. Rudnick, S. A. Rasmussen, and H. T. Kao. 2013. 'Isoforms of the neuronal glutamate transporter gene, SLC1A1/EAAC1, negatively modulate glutamate uptake: relevance to obsessive-compulsive disorder', *Transl Psychiatry*, 3: e259.

Posner, Jonathan, Rachel Marsh, Tiago V. Maia, Bradley S. Peterson, Allison Gruber, and H. B. Simpson. 2014. 'Reduced functional connectivity within the limbic cortico-striato-thalamo-cortical loop in unmedicated adults with obsessive-compulsive disorder', *Human brain mapping*, 35: 2852-60.

Proenca, C. C., K. P. Gao, S. V. Shmelkov, S. Rafii, and F. S. Lee. 2011. 'Slitrks as emerging candidate genes involved in neuropsychiatric disorders', *Trends Neurosci*, 34: 143-53.

Radua, Joaquim, and David Mataix-Cols. 2009. 'Voxel-wise meta-analysis of grey matter changes in obsessive-compulsive disorder', *Br J Psychiatry*, 195: 393-402.

Radua, Joaquim, Odile A. van den Heuvel, Simon Surguladze, and David Mataix-Cols. 2010. 'Meta-analytical comparison of voxel-based morphometry studies in obsessive-compulsive disorder vs other anxiety disorders', *Arch Gen Psychiatry*, 67: 701-11.

Rajendram, R., S. Kronenberg, C. L. Burton, and P. D. Arnold. 2017. 'Glutamate Genetics in Obsessive-Compulsive Disorder: A Review', *J Can Acad Child Adolesc Psychiatry*, 26: 205-13.

Ramanathan, S., J. J. Hanley, J. M. Deniau, and J. P. Bolam. 2002. 'Synaptic convergence of motor and somatosensory cortical afferents onto GABAergic interneurons in the rat striatum', *J Neurosci*, 22: 8158-69.

Rasmussen, A. H., H. B. Rasmussen, and A. Silahtaroglu. 2017. 'The DLGAP family: neuronal expression, function and role in brain disorders', *Mol Brain*, 10: 43.

Rauch, S. L., D. D. Dougherty, D. Malone, A. Rezai, G. Friehs, A. J. Fischman, N. M. Alpert, S. N. Haber, P. H. Stypulkowski, M. T. Rise, S. A. Rasmussen, and B. D. Greenberg. 2006. 'A functional neuroimaging investigation of deep brain stimulation in patients with obsessive-compulsive disorder', *J Neurosurg*, 104: 558-65.

Rauch, S. L., M. A. Jenike, N. M. Alpert, L. Baer, H. C. Breiter, C. R. Savage, and A. J. Fischman. 1994a. 'Regional cerebral blood flow measured during symptom provocation in obsessive-compulsive disorder using oxygen 15-labeled carbon dioxide and positron emission tomography', *Arch Gen Psychiatry*, 51: 62-70.

———. 1994b. 'Regional cerebral blood flow measured during symptom provocation in obsessive-compulsive disorder using oxygen 15-labeled carbon dioxide and positron emission tomography', *Arch Gen Psychiatry*, 51: 62-70.

Rauch, S. L., C. R. Savage, N. M. Alpert, D. Dougherty, A. Kendrick, T. Curran, H. D. Brown, P. Manzo, A. J. Fischman, and M. A. Jenike. 1997. 'Probing striatal function in obsessive-compulsive disorder: a PET study of implicit sequence learning', *The Journal of neuropsychiatry and clinical neurosciences*, 9: 568-73.

Rauch, S. L., C. R. Savage, N. M. Alpert, A. J. Fischman, and M. A. Jenike. 1997. 'The functional neuroanatomy of anxiety: a study of three disorders using positron emission tomography and symptom provocation', *Biol Psychiatry*, 42: 446-52.

Rauch, S. L., L. M. Shin, D. D. Dougherty, N. M. Alpert, A. J. Fischman, and M. A. Jenike. 2002. 'Predictors of fluvoxamine response in contamination-related obsessive compulsive disorder: a PET symptom provocation study', *Neuropsychopharmacology*, 27: 782-91.

Rauch, S. L., M. M. Wedig, C. I. Wright, B. Martis, K. G. McMullin, L. M. Shin, P. A. Cannistraro, and S. Wilhelm. 2007a. 'Functional magnetic resonance imaging study of regional brain activation during implicit sequence learning in obsessive-compulsive disorder', *Biol Psychiatry*, 61: 330-6.

Rauch, Scott L., Michelle M. Wedig, Christopher I. Wright, Brian Martis, Katherine G. McMullin, Lisa M. Shin, Paul A. Cannistraro, and Sabine Wilhelm. 2007b. 'Functional magnetic resonance imaging study of regional brain activation during implicit sequence learning in obsessive-compulsive disorder', *Biol Psychiatry*, 61: 330-36.

Resendez, S. L., J. H. Jennings, R. L. Ung, V. M. Namboodiri, Z. C. Zhou, J. M. Otis, H. Nomura, J. A. McHenry, O. Kosyk, and G. D. Stuber. 2016. 'Visualization of cortical, subcortical and deep brain neural circuit dynamics during naturalistic mammalian behavior with head-mounted microscopes and chronically implanted lenses', *Nat Protoc*, 11: 566-97.

Richter, M. A., D. R. de Jesus, S. Hoppenbrouwers, M. Daigle, J. Deluce, L. N. Ravindran, P. B. Fitzgerald, and Z. J. Daskalakis. 2012. 'Evidence for cortical inhibitory and excitatory dysfunction in obsessive compulsive disorder', *Neuropsychopharmacology*, 37: 1144-51.

Robinson, D., H. Wu, R. A. Munne, M. Ashtari, J. M. Alvir, G. Lerner, A. Koreen, K. Cole, and B. Bogerts. 1995. 'Reduced caudate nucleus volume in obsessive-compulsive disorder', *Arch Gen Psychiatry*, 52: 393-98.

Rodman, A. M., M. R. Milad, T. Deckersbach, J. Im, T. Chou, and D. D. Dougherty. 2012. 'Neuroimaging contributions to novel surgical treatments for intractable obsessive-compulsive disorder', *Expert Rev Neurother*, 12: 219-27.

Rodriguez, C. I., L. S. Kegeles, A. Levinson, R. T. Ogden, X. Mao, M. S. Milak, D. Vermes, S. Xie, L. Hunter, P. Flood, H. Moore, D. C. Shungu, and H. B. Simpson. 2015. 'In vivo effects of ketamine on glutamate-glutamine and gamma-aminobutyric acid in obsessive-compulsive disorder: Proof of concept', *Psychiatry Res*, 233: 141-7.

Rodriguez, C. I., A. Levinson, J. Zwerling, D. Vermes, and H. B. Simpson. 2016. 'Open-Label trial on the effects of memantine in adults with obsessive-compulsive disorder after a single ketamine infusion', *J Clin Psychiatry*, 77: 688-9.

Rosenberg, D. R., M. S. Keshavan, K. M. O'Hearn, E. L. Dick, W. W. Bagwell, A. B. Seymour, D. M. Montrose, J. N. Pierri, and B. Birmaher. 1997. 'Frontostriatal measurement in treatment-naive children with obsessive-compulsive disorder', *Arch Gen Psychiatry*, 54: 824-30.

Rosenberg, D. R., F. P. MacMaster, M. S. Keshavan, K. D. Fitzgerald, C. M. Stewart, and G. J. Moore. 2000. 'Decrease in caudate glutamatergic concentrations in pediatric obsessive-compulsive disorder patients taking paroxetine', *J Am Acad Child Adolesc Psychiatry*, 39: 1096-103.

Rotge, J. Y., D. Guehl, B. Dilharreguy, J. Tignol, B. Bioulac, M. Allard, P. Burbaud, and B. Aouizerate. 2009a. 'Meta-analysis of brain volume changes in obsessive-compulsive disorder', *Biol Psychiatry*, 65: 75-83.

Rotge, Jean-Yves Y., Dominique Guehl, Bixente Dilharreguy, Jean Tignol, Bernard Bioulac, Michele Allard, Pierre Burbaud, and Bruno Aouizerate. 2009b. 'Meta-analysis of brain volume changes in obsessive-compulsive disorder', *Biol Psychiatry*, 65: 75-83.

Rothwell, P. E., S. J. Hayton, G. L. Sun, M. V. Fuccillo, B. K. Lim, and R. C. Malenka. 2015. 'Input- and Output-Specific Regulation of Serial Order Performance by Corticostriatal Circuits', *Neuron*, 88: 345-56.

Rudebeck, Peter H., and Elisabeth A. Murray. 2011. 'Dissociable effects of subtotal lesions within the macaque orbital prefrontal cortex on reward-guided behavior', *J Neurosci*, 31: 10569-78.

Sadhu, M. J., J. S. Bloom, L. Day, J. J. Siegel, S. Kosuri, and L. Kruglyak. 2018. 'Highly parallel genome variant engineering with CRISPR-Cas9', *Nat Genet*, 50: 510-14.

Sakai, Y., J. Narumoto, S. Nishida, T. Nakamae, K. Yamada, T. Nishimura, and K. Fukui. 2011. 'Corticostriatal functional connectivity in non-medicated patients with obsessive-compulsive disorder', *Eur Psychiatry*, 26: 463-9.

Sampaio, A. S., J. Fagerness, J. Crane, M. Leboyer, R. Delorme, D. L. Pauls, and S. E. Stewart. 2011. 'Association between polymorphisms in GRIK2 gene and obsessive-compulsive disorder: a family-based study', *CNS neuroscience & therapeutics*, 17: 141-7.

Samuels, J., Y. Wang, M. A. Riddle, B. D. Greenberg, A. J. Fyer, J. T. McCracken, S. L. Rauch, D. L. Murphy, M. A. Grados, J. A. Knowles, J. Piacentini, B. Cullen, O. J. Bienvenu, 3rd, S. A. Rasmussen, D. Geller, D. L. Pauls, K. Y. Liang, Y. Y. Shugart, and G. Nestadt. 2011. 'Comprehensive family-based association study of the glutamate transporter gene SLC1A1 in obsessive-compulsive disorder', *Am J Med Genet B Neuropsychiatr Genet*, 156B: 472-7.

Saxena, S., R. G. Bota, and A. L. Brody. 2001. 'Brain-behavior relationships in obsessive-compulsive disorder', *Semin Clin Neuropsychiatry*, 6: 82-101.

Saxena, S., A. L. Brody, M. L. Ho, S. Alborzian, M. K. Ho, K. M. Maidment, S. C. Huang, H. M. Wu, S. C. Au, and L. R. Baxter, Jr. 2001. 'Cerebral metabolism in major depression and obsessive-compulsive disorder occurring separately and concurrently', *Biol Psychiatry*, 50: 159-70.

Saxena, S., A. L. Brody, M. L. Ho, N. Zohrabi, K. M. Maidment, and L. R. Baxter, Jr. 2003. 'Differential brain metabolic predictors of response to paroxetine in obsessive-compulsive disorder versus major depression', *Am J Psychiatry*, 160: 522-32.

Saxena, S., A. L. Brody, K. M. Maidment, J. J. Dunkin, M. Colgan, S. Alborzian, M. E. Phelps, and L. R. Baxter, Jr. 1999. 'Localized orbitofrontal and subcortical metabolic changes and predictors of response to paroxetine treatment in obsessive-compulsive disorder', *Neuropsychopharmacology*, 21: 683-93.

Saxena, S., A. L. Brody, J. M. Schwartz, and L. R. Baxter. 1998. 'Neuroimaging and frontal-subcortical circuitry in obsessive-compulsive disorder', *Br J Psychiatry Suppl*: 26-37.

Saxena, S., and S. L. Rauch. 2000. 'Functional neuroimaging and the neuroanatomy of obsessive-compulsive disorder', *Psychiatr Clin North Am*, 23: 563-86.

Scarone, S., C. Colombo, S. Livian, M. Abbruzzese, P. Ronchi, M. Locatelli, G. Scotti, and E. Smeraldi. 1992. 'Increased right caudate nucleus size in obsessive-compulsive disorder: detection with magnetic resonance imaging', *Psychiatry Res*, 45: 115-21.

Schweitzer, B., U. Suter, and V. Taylor. 2002. 'Neural membrane protein 35/Lifeguard is localized at postsynaptic sites and in dendrites', *Brain Res Mol Brain Res*, 107: 47-56.

Selemon, L. D., and P. S. Goldman-Rakic. 1999. 'The reduced neuropil hypothesis: a circuit based model of schizophrenia', *Biol Psychiatry*, 45: 17-25.

Sheintuch, L., A. Rubin, N. Brande-Eilat, N. Geva, N. Sadeh, O. Pinchasof, and Y. Ziv. 2017. 'Tracking the Same Neurons across Multiple Days in Ca(2+) Imaging Data', *Cell Rep*, 21: 1102-15.

Shipley, Frederick B., Christopher M. Clark, Mark J. Alkema, and Andrew M. Leifer. 2014. 'Simultaneous optogenetic manipulation and calcium imaging in freely moving C. elegans', *Front Neural Circuits*, 8: 28.

Shmelkov, S. V., A. Hormigo, D. Jing, C. C. Proenca, K. G. Bath, T. Milde, E. Shmelkov, J. S. Kushner, M. Baljevic, I. Dincheva, A. J. Murphy, D. M. Valenzuela, N. W. Gale, G. D. Yancopoulos, I. Ninan, F. S. Lee, and S. Rafii. 2010. 'Slitrk5 deficiency impairs corticostriatal circuitry and leads to obsessive-compulsive-like behaviors in mice', *Nat Med*, 16: 598-602, 1p following 02.

Shugart, Y. Y., Y. Wang, J. F. Samuels, M. A. Grados, B. D. Greenberg, J. A. Knowles, J. T. McCracken, S. L. Rauch, D. L. Murphy, S. A. Rasmussen, B. Cullen, R. Hoehn-Saric, A. Pinto, A. J. Fyer, J. Piacentini, D. L. Pauls, O. J. Bienvenu, M. A. Riddle, K. Y. Liang, and G. Nestadt. 2009. 'A family-based association study of the glutamate transporter gene SLC1A1 in obsessive-compulsive disorder in 378 families', *Am J Med Genet B Neuropsychiatr Genet*, 150B: 886-92.

Silbersweig, D. A., and S. L. Rauch. 2017. 'Neuroimaging in Psychiatry: A Quarter Century of Progress', *Harvard review of psychiatry*, 25: 195-97.

Simpson, H. B., D. C. Shungu, J. Bender, Jr., X. Mao, X. Xu, M. Slifstein, and L. S. Kegeles. 2012. 'Investigation of cortical glutamate-glutamine and gamma-aminobutyric acid in obsessive-compulsive disorder by proton magnetic resonance spectroscopy', *Neuropsychopharmacology*, 37: 2684-92.

Sjoerds, Zsuzsika, Judy Luigjes, Wim van den Brink, Damiaan Denys, and Murat Yücel. 2014. 'The role of habits and motivation in human drug addiction: a reflection', *Front Psychiatry*, 5: 8.

Smith, Dana G., and Trevor W. Robbins. 2013. 'The neurobiological underpinnings of obesity and binge eating: a rationale for adopting the food addiction model', *Biol Psychiatry*, 73: 804-10.

Smith, K. S., and A. M. Graybiel. 2013a. 'A dual operator view of habitual behavior reflecting cortical and striatal dynamics', *Neuron*, 79: 361-74.

———. 2016. 'Habit formation', *Dialogues Clin Neurosci*, 18: 33-43.

Smith, Kyle S., and Ann M. Graybiel. 2013b. 'A dual operator view of habitual behavior reflecting cortical and striatal dynamics', *Neuron*, 79: 361-74.

———. 2013c. 'Using optogenetics to study habits', *Brain Res*, 1511: 102-14.

Smith, Kyle S., Arti Virkud, Karl Deisseroth, and Ann M. Graybiel. 2012. 'Reversible online control of habitual behavior by optogenetic perturbation of medial prefrontal cortex', *Proc Natl Acad Sci U S A*, 109: 18932-37.

Soares, D. P., and M. Law. 2009. 'Magnetic resonance spectroscopy of the brain: review of metabolites and clinical applications', *Clin Radiol*, 64: 12-21.

Song, M., J. Giza, C. C. Proenca, D. Jing, M. Elliott, I. Dincheva, S. V. Shmelkov, J. Kim, R. Schreiner, S. H. Huang, E. Castren, R. Prekeris, B. L. Hempstead, M. V. Chao, J. B. Dictenberg, S. Rafii, Z. Y. Chen, E. Rodriguez-Boulan, and F. S. Lee. 2015. 'Slitrk5 Mediates BDNF-Dependent TrkB Receptor Trafficking and Signaling', *Dev Cell*, 33: 690-702.

Song, M., C. A. Mathews, S. E. Stewart, S. V. Shmelkov, J. G. Mezey, J. L. Rodriguez-Flores, S. A. Rasmussen, J. C. Britton, Y. S. Oh, J. T. Walkup, F. S. Lee, and C. E. Glatt. 2017. 'Rare Synaptogenesis-Impairing Mutations in SLITRK5 Are Associated with Obsessive Compulsive Disorder', *PLoS One*, 12: e0169994.

Stamatakis, A. M., M. J. Schachter, S. Gulati, K. T. Zitelli, S. Malanowski, A. Tajik, C. Fritz, M. Trulson, and S. L. Otte. 2018. 'Simultaneous Optogenetics and Cellular Resolution Calcium Imaging During Active Behavior Using a Miniaturized Microscope', *Front Neurosci*, 12: 496.

Starr, B. S., and M. S. Starr. 1986a. 'Differential effects of dopamine D1 and D2 agonists and antagonists on velocity of movement, rearing and grooming in the mouse. Implications for the roles of D1 and D2 receptors', *Neuropharmacology*, 25: 455-63.

———. 1986b. 'Grooming in the mouse is stimulated by the dopamine D1 agonist SKF 38393 and by low doses of the D1 antagonist SCH 23390, but is inhibited by dopamine D2 agonists, D2 antagonists and high doses of SCH 23390', *Pharmacol Biochem Behav*, 24: 837-9.

Stern, L., J. Zohar, R. Cohen, and Y. Sasson. 1998. 'Treatment of severe, drug resistant obsessive compulsive disorder with the 5HT1D agonist sumatriptan', *European Neuropsychopharmacology*, 8: 325-8.

Stewart, S. E., J. A. Fagerness, J. Platko, J. W. Smoller, J. M. Scharf, C. Illmann, E. Jenike, N. Chabane, M. Leboyer, R. Delorme, M. A. Jenike, and D. L. Pauls. 2007. 'Association of the SLC1A1 glutamate transporter gene and obsessive-compulsive disorder', *Am J Med Genet B Neuropsychiatr Genet*, 144B: 1027-33.

Stewart, S. E., D. A. Geller, M. Jenike, D. Pauls, D. Shaw, B. Mullin, and S. V. Faraone. 2004. 'Long-term outcome of pediatric obsessive-compulsive disorder: a meta-analysis and qualitative review of the literature', *Acta Psychiatr Scand*, 110: 4-13.

Stewart, S. E., D. Yu, J. M. Scharf, B. M. Neale, J. A. Fagerness, C. A. Mathews, P. D. Arnold, P. D. Evans, E. R. Gamazon, L. K. Davis, L. Osiecki, L. McGrath, S. Haddad, J. Crane, D. Hezel, C. Illman, C. Mayerfeld, A. Konkashbaev, C. Liu, A. Pluzhnikov, A. Tikhomirov, C. K. Edlund, S. L. Rauch, R. Moessner, P. Falkai, W. Maier, S. Ruhrmann, H. J. Grabe, L. Lennertz, M. Wagner, L. Bellodi, M. C. Cavallini, M. A. Richter, E. H. Cook, Jr., J. L. Kennedy, D. Rosenberg, D. J. Stein, S. M. Hemmings, C. Lochner, A. Azzam, D. A. Chavira, E. Fournier, H. Garrido, B. Sheppard, P. Umana, D. L. Murphy, J. R. Wendland, J. Veenstra-VanderWeele, D. Denys, R. Blom, D. Deforce, F. Van Nieuwerburgh, H. G. Westenberg, S. Walitza, K. Egberts, T. Renner, E. C. Miguel, C. Cappi, A. G. Hounie, M. Conceicao do Rosario, A. S. Sampaio, H. Vallada, H. Nicolini, N. Lanzagorta, B. Camarena, R. Delorme, M. Leboyer, C. N. Pato, M. T. Pato, E. Voyiaziakis, P. Heutink, D. C. Cath, D. Posthuma, J. H. Smit, J. Samuels, O. J. Bienvenu, B. Cullen, A. J. Fyer, M. A. Grados, B. D. Greenberg, J. T. McCracken, M. A. Riddle, Y. Wang, V. Coric, J. F. Leckman, M. Bloch, C. Pittenger, V. Eapen, D. W. Black, R. A. Ophoff, E. Strengman, D. Cusi, M. Turiel, F. Frau, F. Macciardi, J. R. Gibbs, M. R. Cookson, A. Singleton, Consortium North American Brain Expression, J. Hardy, U. K. Brain Expression Database, A. T. Crenshaw, M. A. Parkin, D. B. Mirel, D. V. Conti, S. Purcell, G. Nestadt, G. L. Hanna, M. A. Jenike, J. A. Knowles, N. Cox, and D. L. Pauls. 2013. 'Genome-wide association study of obsessive-compulsive disorder', *Mol Psychiatry*, 18: 788-98.

Svoboda, K., and R. Yasuda. 2006. 'Principles of two-photon excitation microscopy and its applications to neuroscience', *Neuron*, 50: 823-39.

Swedo, S. E., M. B. Schapiro, C. L. Grady, D. L. Cheslow, H. L. Leonard, A. Kumar, R. Friedland, S. I. Rapoport, and J. L. Rapoport. 1989. 'Cerebral glucose metabolism in childhood-onset obsessive-compulsive disorder', *Archives of general psychiatry*, 46: 518-23.

Takahashi, H., and A. M. Craig. 2013. 'Protein tyrosine phosphatases PTPdelta, PTPsigma, and LAR: presynaptic hubs for synapse organization', *Trends Neurosci*, 36: 522-34.

Takahashi, H., K. Katayama, K. Sohya, H. Miyamoto, T. Prasad, Y. Matsumoto, M. Ota, H. Yasuda, T. Tsumoto, J. Aruga, and A. M. Craig. 2012. 'Selective control of inhibitory synapse development by Slitrk3-PTPdelta trans-synaptic interaction', *Nat Neurosci*, 15: 389-98, s1-2.

Takeuchi, M., Y. Hata, K. Hirao, A. Toyoda, M. Irie, and Y. Takai. 1997. 'SAPAPs. A family of PSD-95/SAP90-associated proteins localized at postsynaptic density', *J Biol Chem*, 272: 11943-51.

Tambs, K., N. Czajkowsky, E. Roysamb, M. C. Neale, T. Reichborn-Kjennerud, S. H. Aggen, J. R. Harris, R. E. Orstavik, and K. S. Kendler. 2009. 'Structure of genetic and environmental risk factors for dimensional representations of DSM-IV anxiety disorders', *Br J Psychiatry*, 195: 301-7.

Taylor, S. 2011. 'Etiology of obsessions and compulsions: a meta-analysis and narrative review of twin studies', *Clin Psychol Rev*, 31: 1361-72.

Tecuapetla, F., X. Jin, S. Q. Lima, and R. M. Costa. 2016. 'Complementary Contributions of Striatal Projection Pathways to Action Initiation and Execution', *Cell*, 166: 703-15.

Tecuapetla, F., S. Matias, G. P. Dugue, Z. F. Mainen, and R. M. Costa. 2014. 'Balanced activity in basal ganglia projection pathways is critical for contraversive movements', *Nat Commun*, 5: 4315.

Tepper, J. M., F. Tecuapetla, T. Koos, and O. Ibanez-Sandoval. 2010. 'Heterogeneity and diversity of striatal GABAergic interneurons', *Front Neuroanat*, 4: 150.

Thorn, Catherine A., Hisham Atallah, Mark Howe, and Ann M. Graybiel. 2010. 'Differential dynamics of activity changes in dorsolateral and dorsomedial striatal loops during learning', *Neuron*, 66: 781-95.

Tsai, Hsing-Chen C., Feng Zhang, Antoine Adamantidis, Garret D. Stuber, Antonello Bonci, Luis de Lecea, and Karl Deisseroth. 2009. 'Phasic firing in dopaminergic neurons is sufficient for behavioral conditioning', *Science (New York, N.Y.)*, 324: 1080-84.

Tye, K. M., and K. Deisseroth. 2012. 'Optogenetic investigation of neural circuits underlying brain disease in animal models', *Nat Rev Neurosci*, 13: 251-66.

Underhill, S. M., D. S. Wheeler, M. Li, S. D. Watts, S. L. Ingram, and S. G. Amara. 2014. 'Amphetamine modulates excitatory neurotransmission through endocytosis of the glutamate transporter EAAT3 in dopamine neurons', *Neuron*, 83: 404-16.

Valentin, Vivian V., Anthony Dickinson, and John P. O'Doherty. 2007. 'Determining the neural substrates of goal-directed learning in the human brain', *J Neurosci*, 27: 4019-26.

van Grootheest, D. S., D. C. Cath, A. T. Beekman, and D. I. Boomsma. 2005. 'Twin studies on obsessive-compulsive disorder: a review', *Twin Res Hum Genet*, 8: 450-8.

Vandesompele, J., K. De Preter, F. Pattyn, B. Poppe, N. Van Roy, A. De Paepe, and F. Speleman. 2002. 'Accurate normalization of real-time quantitative RT-PCR data by geometric averaging of multiple internal control genes', *Genome Biol*, 3: RESEARCH0034.

Vigneault, E., O. Poirel, M. Riad, J. Prud'homme, S. Dumas, G. Turecki, C. Fasano, N. Mechawar, and S. El Mestikawy. 2015. 'Distribution of vesicular glutamate transporters in the human brain', *Front Neuroanat*, 9: 23.

Vogelstein, J. T., A. M. Packer, T. A. Machado, T. Sippy, B. Babadi, R. Yuste, and L. Paninski. 2010. 'Fast nonnegative deconvolution for spike train inference from population calcium imaging', *J Neurophysiol*, 104: 3691-704.

Wan, Y., K. K. Ade, Z. Caffall, M. Ilcim Ozlu, C. Eroglu, G. Feng, and N. Calakos. 2014. 'Circuit-selective striatal synaptic dysfunction in the Sapap3 knockout mouse model of obsessive-compulsive disorder', *Biol Psychiatry*, 75: 623-30.

Wan, Y., G. Feng, and N. Calakos. 2011. 'Sapap3 deletion causes mGluR5-dependent silencing of AMPAR synapses', *J Neurosci*, 31: 16685-91.

Welch, J. M., J. Lu, R. M. Rodriguiz, N. C. Trotta, J. Peca, J. D. Ding, C. Feliciano, M. Chen, J. P. Adams, J. Luo, S. M. Dudek, R. J. Weinberg, N. Calakos, W. C. Wetsel, and G. Feng. 2007a. 'Cortico-striatal synaptic defects and OCD-like behaviours in Sapap3-mutant mice', *Nature*, 448: 894-900.

Welch, Jeffrey M., Jing Lu, Ramona M. Rodriguiz, Nicholas C. Trotta, Joao Peca, Jin-Dong D. Ding, Catia Feliciano, Meng Chen, J. P. Adams, Jianhong Luo, Serena M. Dudek, Richard J. Weinberg, Nicole Calakos, William C. Wetsel, and Guoping Feng. 2007b. 'Cortico-striatal synaptic defects and OCD-like behaviours in Sapap3-mutant mice', *Nature*, 448: 894-900.

Wendland, J. R., P. R. Moya, K. R. Timpano, A. P. Anavitarte, M. R. Kruse, M. G. Wheaton, R. F. Ren-Patterson, and D. L. Murphy. 2009. 'A haplotype containing quantitative trait loci for SLC1A1 gene expression and its association with obsessive-compulsive disorder', *Arch Gen Psychiatry*, 66: 408-16.

Whiteside, S. P., J. D. Port, and J. S. Abramowitz. 2004. 'A meta-analysis of functional neuroimaging in obsessive-compulsive disorder', *Psychiatry Res*, 132: 69-79.

Whiteside, S. P., J. D. Port, B. J. Deacon, and J. S. Abramowitz. 2006. 'A magnetic resonance spectroscopy investigation of obsessive-compulsive disorder and anxiety', *Psychiatry Res*, 146: 137-47.

Wichmann, T., and M. R. DeLong. 1996. 'Functional and pathophysiological models of the basal ganglia', *Curr Opin Neurobiol*, 6: 751-8.

Witten, Ilana B., Shih-Chun C. Lin, Matthew Brodsky, Rohit Prakash, Ilka Diester, Polina Anikeeva, Viviana Gradinaru, Charu Ramakrishnan, and Karl Deisseroth. 2010. 'Cholinergic interneurons control local circuit activity and cocaine conditioning', *Science (New York, N.Y.)*, 330: 1677-81.

Woo, J., S. K. Kwon, S. Choi, S. Kim, J. R. Lee, A. W. Dunah, M. Sheng, and E. Kim. 2009. 'Trans-synaptic adhesion between NGL-3 and LAR regulates the formation of excitatory synapses', *Nat Neurosci*, 12: 428-37.

Wood, J., and S. E. Ahmari. 2015. 'A Framework for Understanding the Emerging Role of Corticolimbic-Ventral Striatal Networks in OCD-Associated Repetitive Behaviors', *Front Syst Neurosci*, 9: 171.

Wu, K., G. L. Hanna, P. Easter, J. L. Kennedy, D. R. Rosenberg, and P. D. Arnold. 2013. 'Glutamate system genes and brain volume alterations in pediatric obsessive-compulsive disorder: a preliminary study', *Psychiatry Res*, 211: 214-20.

Wymbs, N. F., D. S. Bassett, P. J. Mucha, M. A. Porter, and S. T. Grafton. 2012. 'Differential recruitment of the sensorimotor putamen and frontoparietal cortex during motor chunking in humans', *Neuron*, 74: 936-46.

Xu, M., L. Li, and C. Pittenger. 2016. 'Ablation of fast-spiking interneurons in the dorsal striatum, recapitulating abnormalities seen post-mortem in Tourette syndrome, produces anxiety and elevated grooming', *Neuroscience*, 324: 321-9.

Yin, Henry H., and Barbara J. Knowlton. 2006. 'The role of the basal ganglia in habit formation', *Nature reviews. Neuroscience*, 7: 464-76.

Yin, Henry H., Barbara J. Knowlton, and Bernard W. Balleine. 2004. 'Lesions of dorsolateral striatum preserve outcome expectancy but disrupt habit formation in instrumental learning', *Eur J Neurosci*, 19: 181-89.

———. 2005. 'Blockade of NMDA receptors in the dorsomedial striatum prevents action-outcome learning in instrumental conditioning', *Eur J Neurosci*, 22: 505-12.

———. 2006. 'Inactivation of dorsolateral striatum enhances sensitivity to changes in the action-outcome contingency in instrumental conditioning', *Behav Brain Res*, 166: 189-96.

Zalocusky, K. A., C. Ramakrishnan, T. N. Lerner, T. J. Davidson, B. Knutson, and K. Deisseroth. 2016. 'Nucleus accumbens D2R cells signal prior outcomes and control risky decision-making', *Nature*, 531: 642-6.

Zanos, P., S. C. Piantadosi, H. Q. Wu, H. J. Pribut, M. J. Dell, A. Can, H. R. Snodgrass, C. A. Zarate, Jr., R. Schwarcz, and T. D. Gould. 2015. 'The Prodrug 4-Chlorokynurenine Causes Ketamine-Like Antidepressant Effects, but Not Side Effects, by NMDA/GlycineB-Site Inhibition', *J Pharmacol Exp Ther*, 355: 76-85.

Zhang, Feng, Alexander M. Aravanis, Antoine Adamantidis, Luis de Lecea, and Karl Deisseroth. 2007. 'Circuit-breakers: optical technologies for probing neural signals and systems', *Nature reviews. Neuroscience*, 8: 577-81.

Zhang, Feng, Li-Ping P. Wang, Martin Brauner, Jana F. Liewald, Kenneth Kay, Natalie Watzke, Phillip G. Wood, Ernst Bamberg, Georg Nagel, Alexander Gottschalk, and Karl Deisseroth. 2007. 'Multimodal fast optical interrogation of neural circuitry', *Nature*, 446: 633-39.

Zhang, Z., Q. Fan, Y. Bai, Z. Wang, H. Zhang, and Z. Xiao. 2016. 'Brain Gamma-Aminobutyric Acid (GABA) Concentration of the Prefrontal Lobe in Unmedicated Patients with Obsessive-Compulsive Disorder: A Research of Magnetic Resonance Spectroscopy', *Shanghai Arch Psychiatry*, 28: 263-70.

Zhong, P., and Z. Yan. 2011. 'Differential regulation of the excitability of prefrontal cortical fast-spiking interneurons and pyramidal neurons by serotonin and fluoxetine', *PLoS One*, 6: e16970.

Zhou, P., S. L. Resendez, J. Rodriguez-Romaguera, J. C. Jimenez, S. Q. Neufeld, A. Giovannucci, J. Friedrich, E. A. Pnevmatikakis, G. D. Stuber, R. Hen, M. A. Kheirbek, B. L. Sabatini, R. E. Kass, and L. Paninski. 2018. 'Efficient and accurate extraction of in vivo calcium signals from microendoscopic video data', *Elife*, 7.

Zike, I. D., M. O. Chohan, J. M. Kopelman, E. N. Krasnow, D. Flicker, K. M. Nautiyal, M. Bubser, C. Kellendonk, C. K. Jones, G. Stanwood, K. F. Tanaka, H. Moore, S. E. Ahmari, and J. Veenstra-VanderWeele. 2017. 'OCD candidate gene SLC1A1/EAAT3 impacts basal ganglia-mediated activity and stereotypic behavior', *Proc Natl Acad Sci U S A*, 114: 5719-24.

Zohar, J., E. A. Mueller, T. R. Insel, R. C. Zohar-Kadouch, and D. L. Murphy. 1987. 'Serotonergic responsivity in obsessive-compulsive disorder. Comparison of patients and healthy controls', *Arch Gen Psychiatry*, 44: 946-51.

Zuchner, S., J. R. Wendland, A. E. Ashley-Koch, A. L. Collins, K. N. Tran-Viet, K. Quinn, K. C. Timpano, M. L. Cuccaro, M. A. Pericak-Vance, D. C. Steffens, K. R. Krishnan, G. Feng, and D. L. Murphy. 2009. 'Multiple rare SAPAP3 missense variants in trichotillomania and OCD', *Mol Psychiatry*, 14: 6-9.

Züchner, S., J. R. Wendland, A. E. Ashley-Koch, A. L. Collins, K. N. Tran-Viet, K. Quinn, K. C. Timpano, M. L. Cuccaro, M. A. Pericak-Vance, D. C. Steffens, K. R. Krishnan, G. Feng, and D. L. Murphy. 2009. 'Multiple rare SAPAP3 missense variants in trichotillomania and OCD', *Mol Psychiatry*, 14: 6-9.